# PREPARATION AND CHARACTERIZATION OF THIN FILM AND NANO PHASE BASED MODIFIED ELECTRODES FOR ELECTROCHEMICAL SENSOR APPLICATION

*By*
**MILAN KUMAR DEY**
**(CHEM01201104003)**

**BHABHA ATOMIC RESEARCH CENTRE**

*A thesis submitted to the*
*Board of Studies in Chemical Sciences*
*In partial fulfillment of requirements*
*for the Degree of*
**DOCTOR OF PHILOSOPHY**
*of*
**HOMI BHABHA NATIONAL INSTITUTE**

**December, 2016**

# Homi Bhabha National Institute[1]

## Recommendations of the Viva Voce Committee

As members of the Viva Voce Committee, we certify that we have read the dissertation prepared by **Shri Milan Kumar Dey** entitled "**Preparation and characterization of thin film and nano phase based modified electrodes for electrochemical sensor application**" and recommend that it may be accepted as fulfilling the thesis requirement for the award of Degree of Doctor of Philosophy.

Chairman - **Prof. D. Das** D.Das. **Date:** 07/07/2017

Guide / Convener - **Dr. A. K. Satpati** **Date:** 07/07/2017

Examiner – **Prof. A. K. Srivastava** **Date:** 07/07/2017

Member 1- **Dr. P. A. Hassan** **Date:** 07/07/2017

Member 2- **Dr. R. K. Singhal** R.K. Singhal **Date:** 07/07/2017

Member 3- **Dr. S. N. Achary** S. N. Achy **Date:** 7/7/17

Final approval and acceptance of this thesis is contingent upon the candidate's submission of the final copies of the thesis to HBNI.

I/We hereby certify that I/we have read this thesis prepared under my/our direction and recommend that it may be accepted as fulfilling the thesis requirement.

**Date:** 07/07/2017

**Place: Mumbai**

'<Signature>

**Dr. A. K. Satpati (Guide)**

---

[1] This page is to be included only for final submission after successful completion of viva voce.

# STATEMENT BY AUTHOR

This dissertation has been submitted in partial fulfillment of requirements for an advanced degree at Homi Bhabha National Institute (HBNI) and is deposited in the Library to be made available to borrowers under rules of the HBNI.

Brief quotations from this dissertation are allowable without special permission, provided that accurate acknowledgement of source is made. Requests for permission for extended quotation from or reproduction of this manuscript in whole or in part may be granted by the Competent Authority of HBNI when in his or her judgment the proposed use of the material is in the interests of scholarship. In all other instances, however, permission must be obtained from the author.

Milan Kumar Dey

# DECLARATION

I, hereby declare that the investigation presented in the thesis has been carried out by me. The work is original and has not been submitted earlier as a whole or in part for a degree / diploma at this or any other Institution / University.

Milan Kumar Dey

# List of Publications arising from the thesis

## Journal

1. “Bi-Film on a carbon paste electrode modified with nafion film embedded with multiwall carbon nano tubes for the determination of heavy metals”, Dey, M. K.; Satpati, A. K.; Sahoo, S.; Kameswaran, R.; Reddy, A. V. R.; Mukherjee T., *Anal. Methods*, **2011**, *3*, 2540-2546.

2. “Electrodeposited antimony and antimony–gold nano composite modified carbon paste electrodes for the determination of heavy metal ions”, Dey, M. K.; Satpati, A. K.; Reddy A. V. R., *Anal. Methods*, **2014**, *6*, 5207–5213.

3. “Electrochemical determination of melamine on static mercury drop electrode and on gold nano particle modified carbon paste electrode”, Dey, M. K.; Satpati, A. K.; Reddy A. V. R., *Am. J. Anal. Chem.*, **2014**, *5*, 598-603.

4. “Determination of melamine by a reduced graphene oxide–gold nanoparticle composite carbon paste electrode”, Dey, M. K.; Reddy A. V. R.; Satpati, A. K., *Anal. Lett.*, **2016**, *49(17)*, 2703-2715.

5. “Functionalised carbon nano spheres modified electrode for electrochemical determination of dopamine and uric acid”, Dey, M. K.; Satpati, A. K., *J. Electroanal. Chem.,* **2017**, *787,* 95-102.

6. “Probing adsorptive/desorptive redox processes and detection of Cysteine: A voltammetric and scanning electrochemical microscopy study”, Dey, M. K.; Kumar, S.; Satpati, A. K., *Talanta* (**communicated**).

7. “Fabrication of ultra-microelectrode and its application of in-situ detection of dopamine”, Dey, M. K.; Satpati, A. K. (***Manuscript Under preparation***)

## Conferences

1. “Electrochemical investigations of 2-(o-hydroxyphenyl) benzoxazole on glassy carbon electrode”, Dey, M. K.; Satpati, A. K.; Reddy, A. V. R., DM-ISEAC, February 7-10, **2011**, Thiruvananthapuram, India. Poster Presentation.

2. “Electrochemical investigations of 2-(o-hydroxyphenyl) benzoxazole and melamine on glassy carbon, HMDE and multiwall carbon nano tube modified electrode”, Dey, M. K.; Satpati, A. K.; Reddy, A. V. R., CRSM 2011, IGCAR, July 14-15, **2011**, Kalpakkam, India. Poster Presentation.

3. “Development of carbon and metallic nano particle composite materials for the determination of uranium and other heavy metal ions”, Sahoo, S., Dey, M. K., Satpati, A. K., Reddy, A. V. R., NAC V, January 20-24, **2014**, TSH, Anushaktinagar, BARC, Mumbai, India. Poster Presentation, received best paper award.

4. “Electrochemical property of melamine and its determination using mercury and graphene/gold nano particles composite modified carbon paste electrodes”, Dey, M. K.; Satpati, A. K.; Reddy, A. V. R., DM-ISEAC, February 20-25, **2014**, Amritsar, India. Poster Presentation.

5. “Bismuth and antimony film and nano composite modified electrodes as sensors in voltammetric analysis of heavy metal ions”, Dey, M. K., Satpati, A. K., Reddy, A. V. R., ICONSEA, June 26-28, **2014**, IST, JNTUH, Hyderabad, India. Oral Presentation.

6. “Electrochemical determination of dopamine in human blood serum in presence of uric acid and ascorbic acid using functionalized carbon based electrodes”, Dey, M. K.; Satpati, A. K., CTAC-2015, AERB, May 26-29, **2015**, Anushaktinagar, BARC, India. Oral Presentation.

7. “Carbon based Composite materials for analysis of important biomolecules by electrochemical methods”, Dey, M. K.; Satpati, A. K., ANASAT-2015, September 24-26, **2015**, Munnar, Kerala, India. Poster Presentation.

Milan Kumar Dey

Dedicated to……….

My Family…….

# ACKNOWLEDGEMENTS

First and foremost, I express my deepest gratitude to my guide Dr. A. K. Satpati, Analytical Chemistry Division for his invaluable guidance, continuous support, motivation and encouragements throughout the tenure of my research work. His profound knowledge and logical way of thinking always inspires me.

I also thank Dr. A.V.R. Reddy former head Analytical Chemistry Division for his constant encouragements and supports; I had started the present thesis work under his guideship. I would like to take this opportunity to record my sincere thanks to all the doctoral committee members for their critical review of my work and their valuable comments and suggestions during the progress reviews and pre-synopsis viva-voce. My special thanks to Dr. P. D. Naik, Head of the Division for maintaining a very nice working environment. I thank Shri Srikant Sahoo and all the colleagues in Analytical Chemistry Division for their friendly and co-operative nature which made the journey smooth and comfortable. I express my heartfelt gratitude to some special persons, my teachers, Prof. Ashok Kumar Mukherjee, Prof. S. Maji and late Mrityunjoy Bhattacharrya, who made a great impact in my academic carrier.

Words fail to express my deepest gratitude to my wife who has always been a great friend, and companion in ups and downs of my life. Her unconditional love, continuous faith in me and support has made these past few years an easy ride for me both academically and personally. Special thanks to my parents-in-laws for their love and support.

Finally, I owe my heartfelt gratitude and indebtedness to my parents whose endless love, blessings, moral support and continuous faith in me made me overcome many obstacles in my life and to achieve this goal successfully.

December, 2016 Milan Kumar Dey

ACD, BARC

# CONTENTS

Page No.

SYNOPSIS i-xvii

LIST OF FIGURES xviii-xxvii

LIST OF TABLES xxviii-xxix

CHAPTER I: INTRODUCTION

- I.1. Analytical Chemistry 1
- I.2. Electroanalytical Chemistry 2
  - I.2.1. Electroanalytical techniques 2
  - I.2.2. Classification of Electroanalytical techniques 3
  - I.2.3. Voltammetric techniques 7
  - I.2.4. Chronoamperometry 19
- I.3. Pathways of electrode process 21
- I.4. Types of electron transfer 24
- I.5. Sensors and applications 26
- I.6. Experimental setup for the voltammetric sensors 28
- I.7. Objective of the present work 33
- I.8. Scope of the present work 34

CHAPTER II: EXPERIMENTAL

- II. 1. Introduction 36
- II. 2. Reagents and Solutions 36
- II. 3. Instrumentation 37
- II. 4. Carbon paste electrode (CPE) as working electrode 40
  - II. 4. 1. A brief background of the Carbon Paste Electrode 41
  - II. 4. 2. Constituents of Carbon Paste 41

II. 4. 3. Classification of Carbon Paste Electrode 43

II. 4. 4. Practical aspects of preparation of bare CPE 50

II. 4. 5. Typical properties and specifics of CPEs in electrochemical measurements 51

II. 4. 6. Preparation of the bare Carbon Paste Electrode 52

II. 5. Graphene oxide (GO) and Reduced Graphene Oxide (RGO) 54

II. 5. 1. Introduction on the preparation of GO by Chemical oxidation method 56

II. 5. 2. Methods for reduction of GO 58

II. 5. 3. Synthesis of RGO 59

II. 6. Different characterization techniques used in this work 60

II. 7. Electrochemical Techniques used in the present investigation 61

II. 8. Determination of electrochemical surface area of the electrodes 61

II. 9. Analytical Treatment of the recorded data 61

II. 10. Electrochemical Impedance study for the electrochemical characterization of modified electrode 64

II. 11. Scanning Electrochemical Microscopy 70

II. 12. Modified electrodes used in the study 78

**CHAPTER III: MODIFIED CARBON PASTE ELECTRODE AS ELECTROCHEMICAL SENSOR FOR HEAVY METAL IONS**

Introduction 79

**Chapter III. 1. Bismuth film on carbon paste electrode modified with nafion film embedded multiwalled carbon nanotubes for the determination of heavy metals. 82-102**

III. 1. 1. Abstract 82

III. 1. 2. Brief account on Bi film and its composites with nafion and MWCNT as electrode modifier 82

III. 1. 3. Modification of CPE 84

III. 1. 3. 1. Deposition of Bi film on CPE 84

III. 1. 3. 2. Modification of CPE by Nafion and Bi film composite 86

III. 1. 3. 3. Modification of CPE by nafion-MWCNT- bismuth film composite 86

III. 1. 4. Results and Discussions 87

III. 1. 4. 1. Scanning electron microscopy (SEM) on the surface of BFCPE and CNTMBFE 90

III. 1. 4. 2. Effect of the deposition potential on analyte deposition 91

III. 1. 4. 3. Comparison of sensitivity of the electrodes 92

III. 1. 4. 4. Determination of Cu 94

III. 1. 4. 5. Effect of surfactants on the measurements 96

III. 1. 4. 6. Study of interferences 99

III. 1. 4. 7. Analytical treatment of the recorded data 100

III. 1. 4. 8. Sample Analysis 101

III. 1. 5. Conclusion 102

**Chapter III. 2. Antimony and antimony-gold nano composite modified carbon paste electrodes for the determination of heavy metal ions 103-121**

III. 2. 1. Abstract 103

III. 2. 2. A brief account of antimony film and its composite with gold as sensing platforms for heavy metal ions 103

III. 2. 3. Fabrication of modified electrodes 105

III. 2. 4. Results and Discussions 106

III. 2. 4. 1. Morphological study using SEM and EDS 106

III. 2. 4. 2. Effect of the thickness of the Sb film on the analytical response of the modified electrode 110

III. 2. 4. 3. Effect of pH on the stripping peak of Sb films deposited over the surface of carbon paste electrode 111

III. 2. 4. 4. Analytical responses for Cd and Pb 114

III. 2. 4. 5. Analytical response for Cu 116

III. 2. 4. 6. Determination of Hg 117

III. 2. 4. 7. Analytical treatment of the recorded data 118

III. 2. 4. 8. Recovery test and sample analysis 119

III. 2. 5. Conclusion 121

## CHAPTER IV: ENGINEERED NANOMATERIAL BASED ELECTROCHEMICAL SENSORS FOR BIOMOLECULES

Introduction 122

**Chapter IV. 1. Investigation of electrochemical properties of melamine and development of methods for its determination in milk samples. 124-152**

IV. 1. 1. Abstract 124

IV. 1. 2. Introduction to melamine 124

IV. 1. 3. Toxicity of melamine 125

IV. 1. 4. A brief account on the analysis of melamine 128

IV. 1. A. Investigation of redox properties of melamine with static mercury drop electrode. 130

IV. 1. A. 1. Reduction behavior of melamine 130

IV. 1. A. 2. Interaction of melamine with $Cu^{2+}$ as a tool to determine its concentration using SMDE 133

IV. 1. B. Determination of melamine by a RGO-AuNPs composite modified CPE 136

IV. 1. B. 1. Why RGO-AuNPs composite? 136

IV. 1. B. 2. Preparation of RGO-AuNPs composite modified CPE 136

IV. 1. B. 3. Characterization of the composite 137

IV. 1. B. 4. Electrochemical performance of the modified electrode 139

IV. 1. B. 5. Effect of melamine on the voltammetric response of oxidation of ferrocyanide 141

IV. 1. B. 6. SECM study to characterize adsorption of Melamine on the electrode 142

IV. 1. B. 7. Interferences 144

IV. 1. B. 8. Recovery test and validation 146

IV. 1. C. Determination of Melamine from its direct oxidation 148

IV. 1. C. 1. Preparation and characterization of AuNPs modified CPE 149

IV. 1. C. 2. Analytical response for the oxidation of melamine 150

IV. 1. C. 3. Effect of interfering species 151

IV. 1. C. 4. Sample recovery test 152

IV. 1. D. Conclusion 152

**Chapter IV. 2. Electrochemical determination of dopamine and uric acid using functionalized carbon nano spheres modified electrode 153-179**

IV. 2. 1. Brief introduction of Dopamine and Uric acid 153

IV. 2. 2. A brief account on sensing Dopamine and Uric acid 155

IV. 2. 3. Abstract of the present work 156

IV. 2. 4. Preparation of functionalized carbon nano spheres and its paste electrode 156

IV. 2. 5. Characterization of functionalized carbon nano spheres 157

IV. 2. 6. Results and Discussions 161

IV. 2. 6. 1. Basic experimental conditions 161

IV. 2. 6. 2. Optimization of loading of FCNSs in the electrode 161

IV. 2. 6. 3. pH dependent cyclic voltammetric response of DA, UA and AA on FCNSPE 162

IV. 2. 6. 4. Optimization of accumulation potential and accumulation time 165

IV. 2. 6. 5. Analytical response of the electrode for DA, UA and AA and evaluation of important analytical parameters 166

IV. 2. 6. 6. Result of interference study 170

IV. 2. 6. 7. Comparison of analytical performance with reported literatures 170

IV. 2. 6. 8. Interaction of molecules over the modified electrode 171

IV. 2. 6. 9. Electrochemical Impedance Spectroscopy (EIS) on FCNSPE 172

IV. 2. 6. 10. Spike recovery test and application of the method in real blood serum analysis 175

IV. 2. 7. Conclusion 178

**Chapter IV. 3. Investigation of electrochemical properties of L-Cysteine and method development for its determination. 180-197**

IV. 3. 1. Abstract 180

IV. 3. 2. Introduction 180

IV. 3. 3. Fabrication of electrode and experimental conditions 181

IV. 3. 4. Results and Discussions 182

IV. 3. 4. 1. Cyclic voltammetric measurements 182

IV. 3. 4. 2. Electrochemical impedance measurement 189

IV. 3. 4. 3. SECM measurements 190

IV. 3. 4. 4. Analytical determination of CySH 195

IV. 3. 5. Conclusion 197

**Electrochemical investigation of 2-(o-hydroxyphenyl)benzoxazole (BNZ) 198**

**CHAPTER V: SUMMARY AND FURTHER SCOPE 202**

**REFERENCES 204-243**

# Homi Bhabha National Institute

## SYNOPSIS OF Ph. D. THESIS

1. **Name of the Student:** **Shri Milan Kumar Dey**
2. **Name of the Constituent Institution:** **Bhabha Atomic Research Centre**
3. **Enrolment No. :** **CHEM01201104003**
4. **Title of the Thesis:** **Preparation and characterization of thin film and nano phase based modified electrodes for electrochemical sensor application**
5. **Board of Studies:** **Chemical Sciences**

## Preamble

A chemical sensor is defined as a device that provides continuous information about its environment. Ideally, a chemical sensor provides the required chemical response directly related to the quantity of a specific chemical species. All chemical sensors consist of a transducer, which transforms the response into a detectable signal on modern instrumentation, and a chemically selective layer, which isolates the response of the analyte from its immediate environment. They can be classified according to the property to be determined as: electrical, optical, mass or thermal sensors and they are designed to detect and respond to an analyte in the gaseous, liquid or solid state. Compared to optical, mass and thermal sensors, electrochemical sensors are especially attractive because of their remarkable delectability, experimental simplicity and low cost. They have a leading position among the presently available sensors that have reached the commercial stage and which have found a vast range of important applications in the fields of clinical, industrial, environmental and agricultural analyses. In view of this, the present work is focussed on the development of alternate electrode materials based on thin films and nano phase based materials for the determination of toxic heavy metal ions and to understand electrochemical properties of few very important bio-molecules and development of methodologies for their detection. An introduction, instrumentation and the discussion about the results are presented in four chapters of the thesis as detailed below. Consolidated summary of the thesis and future direction of the related research is discussed in Chapter V. The bibliography of all the chapters is presented collectively at the end of the thesis.

## Chapter I: Introduction

This chapter is entitled to give a brief review on electroanalytical chemistry, different electrochemical techniques and their importance and advantages. The chapter also includes general pathways of electrochemical reactions, kinetics and types of electron transfer processes. A brief account on electrochemical sensors is given. Finally objective of the present thesis and outline of the work is provided.

## Chapter II: Experimental

Chapter II describes about the chemicals, reagents, solvents; preparation of solutions and supporting electrolytes for electrochemical experiments. The instrumentation, devices and the electrode systems used are discussed. Special emphasis is given on the practical aspects of preparation of carbon paste electrodes from the graphitic carbon powder. Synthesis procedure of the graphene oxide from graphite powder is described and the procedure of modification of the carbon paste using reduced graphene oxide and carbon nanotubes are presented. Microscopic techniques e.g. Scanning Electron Microscopy, Atomic Force Microscopy and Scanning Electrochemical Microscopy which are used for the characterization of surface of the electrodes are described. A brief account on X- Ray diffraction technique and Energy Dispersive Spectroscopy is given. Electrochemical techniques used to characterize modified electrodes, methods used to determine electrochemical surface area of the electrodes, diffusion coefficient, electron transfer rate constant and analytical treatment to the recorded data are detailed.

## Chapter III: Modified carbon paste electrode as electrochemical sensor for heavy metal ions.

Heavy metallic trace elements have been one of the most detrimental sources of pollution to the environments. Theses also have devastation effect on the ecological balance. Toxic heavy metals have been consistently increasing due to human activities over time. Rapid diffusion of these metal ions in the environments and their deposition in almost all matrices of the food materials is a major concern. Electrochemical methods based on the anodic stripping voltammetry using either mercury drop or the mercury film as the working electrode provides excellent method of the determination of heavy metal ions. However, use of mercury as the working electrode material is a debatable issue considering the toxicity of mercury [1]. Soft metallic thin films capable of pre-concentrating the heavy metal ions are in demand as an alternate to the mercury drop electrode. Bismuth and antimony are chosen for this purpose. Modification of carbon paste electrodes by electrochemically deposited bismuth and antimony films and their composites are discussed in this chapter. Electrochemical properties of these modified electrodes are explored. Sensing ability of these modified electrodes towards the heavy metal ions are discussed and results are compared with that of mercury based electrodes in order to establish the modified carbon paste electrodes as alternate sensing platform. Since two metallic deposition viz, bismuth and antimony is used for the modification of carbon paste electrode and applied for the determination of heavy metal ions, Chapter III is subdivided into two parts; in part 1 fabrication and application of bismuth film is discussed and in part 2 fabrication and application of antimony film is discussed.

### III.1: Bismuth film on carbon paste electrode modified with nafion film embedded multiwall carbon nanotube for the determination of heavy metals.

In this part modification of carbon paste electrode with bismuth film and its composite with nafion and multiwalled carbon nanotube is discussed. Bi film deposition is carried out in acetate buffer solution of pH 4.5 under optimized parameters of deposition potential, deposition time and the bismuth concentration of-0.8 V (SCE), 300 s and in 0.3 mM $Bi(NO_3)_3$ solution respectively. Bi is deposited on bare CPE (BFE) and nafion coated CPE (NCBFE). A substantial enhancement of an order of magnitude in the sensitivity has been observed when carbon paste electrode is modified with nafion coated carbon nanotube on which Bi-film is deposited (CNTMBFE). This enhanced sensitivity is attributed to the increased active surface area and also the enhanced charge transfer processes which increases the deposition processes and so the stripping current. Effect of different surfactants on the stripping peak of the heavy metal ions has been investigated with NCBFE and BFE. Detection limits using Bi-film electrode (BFE) is obtained for Zn, Cd and Pb as 17.3, 16.9, 11.9 μgL$^{-1}$ respectively (Table III.1.a). This electrode is employed for the analysis of aqueous samples and ayurvedic medicines and the results are tabulated in Table III.1.b.

**Table III.1.a.** Detection limits obtained using different electrodes for Zn, Cd and Pb using BFE, NCBFE and CNTBFE.

| **Element** | **BFE (μg L$^{-1}$)** | **NCBFE (μg L$^{-1}$)** | **CNTMBFE (μg L$^{-1}$)** |
|---|---|---|---|
| Zn | 17.3 | 37.1 | 17.7 |
| Cd | 16.9 | 16.2 | 16.5 |
| Pb | 11.9 | 10.9 | 17.6 |

**Table III.1.b.** Analysis result of water samples collected from different places of India using NCBFE for water samples and BFE for solid samples, values under the parenthesis are using HMDE.

| **Sample** | **Zn** | **Pb** | **Cd** |
|---|---|---|---|
| Powai lake (μg L-1) | 160±6.56 (155) | 12±0.44 (13) | ND (1.4) |
| Tap water (μg L-1) | 121±4.96 (150) | 16±0.59(15) | ND (1.0) |
| M7205 (mg Kg-1) | 42±2.18 (44) | 36±1.37 (33) | ND (0.02) |
| M7206 (mg Kg-1) | 30±1.56 (32) | 8.1±0.31(7.6) | ND (0.31) |

## III.2: Antimony and antimony-gold nano composite modified carbon paste electrodes for the determination of heavy metal ions

In this study antimony film (Sb film) is electrodeposited over the carbon paste electrode (CPE) surface for the determination of heavy metal ions like, Cd, Pb and Cu. An analytical method using the Sb fim modified CPE is proposed for the determination of heavy metal ions in ex-situ mode where the deposition of Sb film is performed in 0.02 M HCl solution and the determination of heavy metal ions is performed in sodium acetate media. For the determination Cu the pH of the solution is most crucial and it is optimized at a value of 6. For the determination of Hg, antimony and gold nano composite (Sb/Au nano composite) is deposited together over the carbon paste electrode surface. Modified electrodes are characterised using SEM and EDS measurements. On SEM measurements, Sb/Au nano composite have shown dendrimer morphology. Parameters for the electrodeposition of Sb film and Sb/Au nano composite and the voltammetric determination of heavy metal ions such as Cd, Pb, Cu and Hg are optimized. Detection limits for Cd and Pb using Sb film modified electrode are found as 2.32μgL$^{-1}$ and 26.5μgL$^{-1}$ and for Cu and Hg using Sb/Au composite modified electrode as 9.7μgL$^{-1}$ and 0.052μgL$^{-1}$. Recovery test results in the recovery of the elements within the range of ±10% deviation (Table III.2.a). Finally the method is applied for the determination of Cd, Pb, Cu and Hg in real water samples (Table III.2.b).

**Table III.2.a.** Recovery test results of Hg, Cu, Pb and Cd using the modified electrode.

| **Element** | **Spiked concentration (μg L$^{-1}$)** | **Recovery concentration (μg L$^{-1}$)** | **% of Recovery** |
|---|---|---|---|
| Hg | 5 | 5.03±0.241 | 100.6% |
| Cu | 20 | 21.5±1.14 | 107.5% |
| Pb | 10 | 9.6±0.59 | 96% |
| Cd | 5 | 5.3±0.24 | 106% |

**Table III.2.b.** Analysis results of Cu, Pb, Cd and Hg in two samples collected from two regions of India using the modified electrode (Values in the parenthesis are determined using the inductively coupled plasma atomic emission spectrometry [ICPAES] technique for Cu, Pb and Cd and the total mercury analyser based on atomic absorption technique for Hg).

| **Sample** | **Cu (μg L$^{-1}$)** | **Pb (μg L$^{-1}$)** | **Cd (μg L$^{-1}$)** | **Hg (μg L$^{-1}$)** |
|---|---|---|---|---|
| Powai lake | 26±1.38 (30) | 12±0.74 (10) | Not detected | 0.25±0.012 (0.55) |
| OSCOM | 49±2.59 (63) | 50±3.1 (56) | 10±0.46 (11) | 145±6.96 (134) |

## Chapter IV: Engineered nanomaterial-based electrochemical sensors for biomolecules

The study of electrochemical behaviour of bioactive molecules has become one of the most rapidly developing scientific fields. Biotechnology and biomedical engineering fields have a vested interest in constructing more precise and accurate voltammetric/amperometric biosensors [2]. One rapidly growing area of biosensor design involves incorporation of carbon-based nanomaterials in working electrodes. The sensing of biomolecules including glucose, dopamine, proteins, enzymes, uric acid, DNA, RNA, and $H_2O_2$ traditionally employs enzymes in detection; however, these enzymes denature easily, therefore the enzymeless methods are highly desired. This chapter deals with the inspection of redox properties of few important biomolecules such as melamine, dopamine, uric acid and L-cysteine using enzymeless electrodes and further, development of electrochemical methods for the determination of the concentration of these molecules in different media. The chapter comprises of three parts where in part 1 the electrochemical property of melamine is discussed, in part 2 the electrochemical property of important neurotransmitter, dopamine is discussed and in part 3 the electrode property of cysteine is discussed.

### Chapter IV.1: Investigation of electrochemical properties of melamine and development of methods for its determination in milk samples.

Melamine (2,4,6-Triamino-1,3,5-triazine) is a nitrogen rich compound with around 66% of nitrogen, which has attracted its use as an adulterant in milk and milk products. Melamine is reported to be toxic and damages kidney by formation of needle like crystal when it combines with cyanuric acid. Thus, it has been a concern to determine melamine in milk and milk related samples and in water sample. There are some reports of determination of melamine based on chromatography [3-5] and colorimetry [6,7]; Determination of melamine using electrochemical techniques is becoming popular [8,9]. In the present work, electrochemical properties are investigated using static mercury drop electrode (SMDE) and gold nanoparticles modified carbon paste electrode. Graphene gold nanoparticle composite is prepared and used as the modifier for determination of melamine. The study is presented here in three sections.

#### Section IV.1.A: Investigation of redox properties of melamine with static mercury drop electrode.

With an aim to explore the electrochemical behavior of melamine, which is electrochemically inactive over conventional electrode, the cyclic voltammetry (CV) of the compound is investigated in Britton-Robinson buffer (BR buffer) using SMDE. CV plots have shown a sharp reduction peak at -0.93V at pH 2. The reduction peak shifts towards more negative potential with increase in pH of the buffer and finally merges with the hydrogen evolution peak. Shifting of reduction peak potentials is linear with pH of the buffer with a slope of -0.116 V/pH, the result reflects involvement of double number of proton to that of electron in the reduction process. The reduction process is also found to be diffusion controlled. The reduction peak current increases linearly with concentration of melamine (from 1μM to 0.1mM) in differential pulsed voltammetry study. Detection limit is found to be 0.2 μM (S/N of 3). The interference due to reduction of commonly occurring ion $Zn^{2+}$ at this potential region restricted the use of reduction of melamine as a tool for its determination.

Analytical method is developed for the quantitative determination of melamine by utilising the property of strong interaction with $Cu^{2+}$ with melamine, where the redox property of $Cu^{2+}$ having reversible electrochemical signal is used for monitoring the melamine concentration. The stripping peak due to the oxidation of Cu is observed at around 0 V using SMDE. The original Cu stripping peak current is gradually decreased with the addition of melamine and a new pre-peak at more negative potential to that of the Cu stripping peak appears. A calibration plot is constructed from the decrease in the stripping peak of Cu. The calibration plot follows a linear regression equation as $Ip = 1.55 \times 10^{-8} - 2.37 \times 10^{-3}$ C (C in molar concentration) with a correlation coefficient of 0.998 and standard deviation of $6.15 \times 10^{-10}$. The three sigma detection limit obtained from the linear calibration plot is 0.778 μM. The new peak appeared at −0.09 V is found to increase proportionately with the melamine concentration. The calibration plot followed a linear regression equation as $I_p = -7.05 \times 10^{-12} + 9.71 \times 10^{-4}$ C (C in molar concentration) with correlation coefficient of 0.996 and standard deviation of $2.503 \times 10^{-10}$. The detection limit obtained from the linear calibration plots is 0.773 μM (S/N ratio of 3). But, presence of $Ag^+$ and $Hg^{2+}$ even at nM concentration interfered strongly as the stripping peak potentials of these ions falls very closely to that of $Cu^{2+}$.

### Section IV.1.B: Fabrication of reduced graphene oxide/gold nanoparticles composite modified carbon paste electrodes for the determination of melamine.

Gold nanoparticles (AuNPs) modified surface is an excellent substrate for electrochemical devices due to the enhanced surface to volume ratio and good physical properties. AuNPs modified substrates have been applied in many chemical and biological sensing platforms [10-13]. Reduced graphene oxide is a good choice for fabrication of electrochemical sensor due to their excellent conductivity, wide electrochemically active surface area and ease for functionalization. Due to good electrochemical properties reduced graphene oxide and gold nanoparticle composite materials are in high demand for sensor application. Herein reduced graphene oxide (RGO) and gold nanoparticle (AuNP) composite material is prepared and characterized. A sensitive method for determination of melamine is reported. Graphene oxide (GO) is prepared chemically by modified hummers method [14, 15]. Resulting GO is reduced chemically by 0.1M sodium borohydride to produce RGO. X Ray Diffraction technique is used for characterization of Graphene oxide and reduced graphene oxide. From Atomic Force Microscopy measurement thickness of the graphene sheet is found to be 1nm reflecting stacking of two pristine graphene sheets. RGO is drop casted on CPE and gold nanoparticles are electrochemically deposited on the RGO coated CPE at an optimized potential of -0.3V with an optimized deposition time of 100 sec. The electrochemical signal due to the oxidation of ferrocyanide is used as the probe to determine the melamine concentration. It is observed that the oxidation signal of ferrocyanide is decreased proportionately with the addition of melamine in the test solution. Scanning electrochemical microscopy (SECM) measurement confirms the efficient adsorption of melamine over the RGO/AuNPs substrate. The calibration plot of melamine follows a straight line equation with the slope of 0.0025 A/M and correlation coefficient of 0.997. The detection limit from the calibration plot is obtained as 2.23 μM. No interference due to the presence of commonly occurring ions such as $Hg^{2+}$,$Ag^{+}$ , $K^{+}$, $Na^{+}$ and $Cl^{-}$ at 100 times higher concentration than melamine is observed. Spike recovery tests are performed in both milk and water samples; this results in 112% and 110% recovery for melamine in milk and water sample respectively.

### Section IV.1.C: Determination of melamine on gold nanoparticles (AuNPs) modified carbon paste electrode.

In this section oxidation of melamine using AuNPs modified CPE is discussed. Most of the electrochemical procedures reported are indirect determination, based on the variation of electrochemical signal of other electrochemically active compound in presence of melamine [16, 17]. Response from the direct electron transfer process in melamine is quite poor [18]. Here a method is developed based on the oxidation of melamine on gold nanoparticle modified CPE for the determination of its concentration. Gold has strong interaction with melamine [19-22]. However the oxidation peak due to melamine is not observed on bulk gold electrode. Thus, AuNPs modified electrode is preferred for the investigation with the aim to improve the electrochemical response of melamine, especially its oxidation signal. Carbon paste is used as the substrate due to the advantage of easy renewability on regular applications. Carbon paste electrode is modified with AuNPs by electrodeposition method. Deposits are characterized using SEM. Sizes of most of the deposits are in the range of 100 to 120nm with some occasional smaller deposits of around 30 nm. Melamine is found to get oxidised at 0.15V in phosphate buffer of pH 7. Using square wave voltammetry technique oxidation signal is recorded against the concentration of melamine. Detection limit is found to be 0.43μM. Present method is free from interferences form the metal ions like, $Cu^{2+}$ $Ag^{1+}$, $Pb^{2+}$, $Bi^{3+}$, $U^{6+}$, and $Hg^{2+}$ at 100 fold higher concentration than melamine.

## Chapter IV.2: Electrochemical determination of dopamine and uric acid using functionalized carbon nano spheres modified electrode.

Dopamine (DA) is one of the most important neurotransmitter in our brain. DA has significant role in modulating the brain functions [23]. In presence of lower concentration of DA in human leads to various neurological disorders, Parkinson's disease etc. Higher level of DA leads to the mental disorder due to the abnormal brain function. Uric acid (UA) is another important metabolic product in biological system. An elevated UA concentration in body system may cause renal failure and gout. It may even cause leukaemia and lymphoma at adverse conditions [24]. Therefore determination of concentration of DA and UA in blood, urine and any biological fluids is important. Electrochemical method is one of the important techniques for the determination of DA and UA in biological samples. Ascorbic Acid (AA) is also one more constituent present along with DA and UA. The major challenge is to separate the electrochemical signal peak due to DA, UA and AA, since the electrochemical potential of these three biological molecules are close and it is difficult to generate the separate electrochemical response from the three molecules using conventional electrodes [25]. Among different modifications, carbon-based materials such as activated carbon, carbon nanotubes (CNTs), graphene and nitrogen doped graphene are important materials of modifications, due to their good electrochemical activity and the large active surface area [26-28]. Different nanoparticles in polymeric matrices also have shown good detection sensitivity of the DA and UA [29-35].

In this work we have functionalized the carbon nano spheres (CNSs) by refluxing in acid mixture ($H_2SO_4$:$HNO_3$ = 1:1) and modified electrode is fabricated using the functionalized CNSs (FCNSs). FCNSs are characterized by Fourier Transform Infra Red spectroscopy (FTIR), Raman spectroscopy, AFM and SEM. FTIR data confirms incorporation of carboxylic acid group (-COOH), Hydroxyl group (-OH) and epoxy group. SEM and AFM image shows that the carbon particles retain spherical size even after acid treatment. The electrode fabricated from the FCNSs shows separate electrochemical signals due to the oxidation of DA and UA in phosphate buffer of pH 7, although, the electrode is fairly irresponsive towards AA. The pH variation study indicates the 2 electron 2 proton transfer during oxidation of both UA and AA (Scheme IV.2.a & IV.2.b). Detection limits obtained for DA and UA are 10nM and 42nM respectively. The electrode has shown around 95% - 97% recovery for DA in real blood serum sample. UA has been determined directly in the real blood sample using standard addition method and the concentration of UA calculated is (17 ± 1) μM. Present method is simple, inexpensive and suitable for real application.

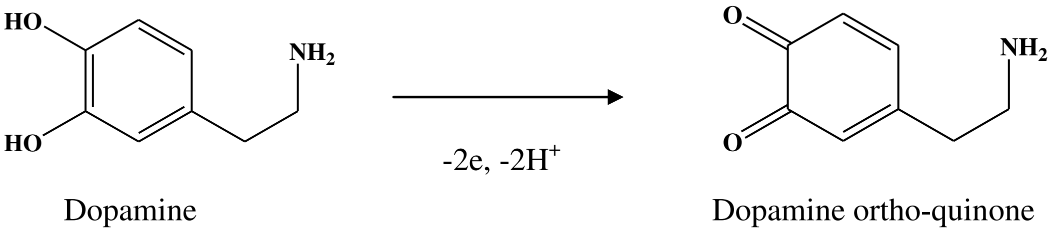

**Scheme IV.2.a:** Oxidation reaction of Dopamine.

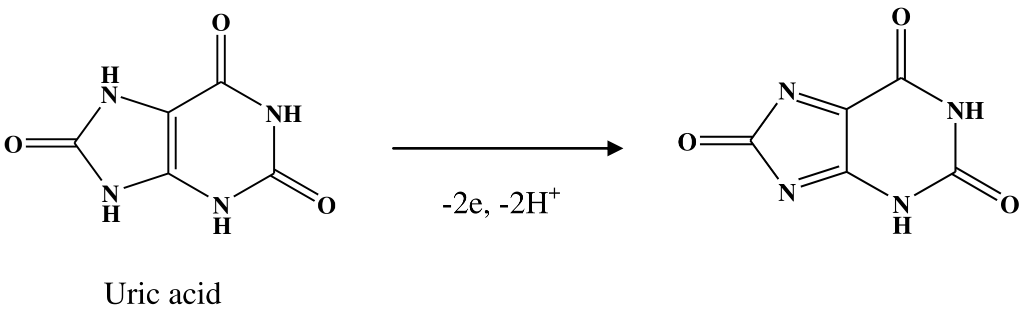

**Scheme IV.2.b:** Oxidation reaction of uric acid.

## Chapter IV.3: Investigation of electrochemical properties of L-Cysteine and method development for its determination.

L-Cysteine (CySH, l-2-amino-3-mercaptopropionic acid) is a biologically important sulfur-containing amino acid which is involved in a variety of important cellular functions, including protein synthesis, detoxification and metabolism [36]. The biological reactions of cysteine are accompanied by SH-SS exchange reactions and the conversion of the disulphide into a dithiol group [37]. In order to understand the electrochemical behaviour of cysteine and its high sensitive determination, this investigation has been taken up. The electrochemical oxidation of CySH on carbon material electrodes, such as graphite, C60 and carbon nanotubes (CNTs) [38-41], has been reported previously. However, these responses are not satisfactory for its determination due to slow heterogeneous electron transfer at electrode. Some improvements have been achieved by modifying the electrode with phthalocyanines, porphyrin and etc. [42-45] but the stability of such modified electrodes is not satisfactory.

In this study glassy carbon electrode (GCE) is modified with gold nanoparticles under optimized condition (-0.8V, 50s, 0.1mM $Au^{3+}$ solution). Due to the presence of sulphur containing thiol group (-SH) CySH shows strong affinity towards gold. Redox properties of the molecule are investigated in phosphate buffer at an optimized pH of 7.5. The molecule is oxidised at 0.7V on the modified electrode (Scheme IV.3.a), resulting Cystine (dimer of Cysteine) ,being electrochemically inactive, actually reduces the electrochemical response of the electrode. Besides that gold oxide produced at such high positive potential added to the reduction of sensitivity of the electrode.

$$2\ \mathrm{CySH} \rightleftarrows \mathrm{CySSCy} + 2e^{-} + 2H^{+}$$

**Scheme IV.3.a**: Oxidation of CySH to produce Cystine (CySSCy).

To regenerate the electrode surface the electrode is exposed to negative potential by scanning the potential in the cathodic direction (0.78V to -1V). Potential scanning in the cathodic direction allows desorption of the Cystine and also reduces the gold oxide to gold. Considering the adsorption desorption phenomena a method based on the differential pulse voltammetric technique (DPV) is developed for the determination of concentration of CySH. Similar to cysteine, the electrochemical property of another important organic molecule benzoxazole has been investigated. In addition to the bio-chemical application benzoxazole has importance as energy storage materials when a composite of benzoxazole with different from carbon is fabricated.

**Chapter V: Summary and further scope.**

In this chapter the entire thesis is summarised. A short discussion is included on the global status of the research topic. Future direction of the research work is also included in this chapter.

# References

[1] Wang, J. *Acc. Chem. Res.* **2002**, *35,* 811-816.

[2] Tiwari, J. N.; Vij, V.; Kemp, K. C.; Kim, K. S. *ACS Nano* **2016**, *10*, 46−80.

[3] Filigenzi, M. S.; Puschner, B.; Aston, L.S.; Poppenga, R.H. *J. Agric. Food Chem.* **2008**, *56*, 7593-7599.

[4] Wang, H.; Liu, Y. Q.; Cao, H.; Yang, H. M.; Liu, X. L.; Yan, L. B. *Chin. J. Anal. Chem.* **2008**, *36*, 273-274.

[5] Andersen, W. C.; Turnipseed, S. B.; Karbiwnyk, C. M.; Clark, S. B.; Madson, M. R.; Gieseker, C. M.; Miller, R. A.; Rummel, N. G.; Reimschuessel, R. *J. Agric. Food Chem.* **2008**, *56*, 4340-4347.

[6] Wei, F.; Lam, R.; Cheng, S.; Lu, S.; Ho, D.; Li, N. *Appl. Phys. Lett.* **2010**, 96, 133702-1-3.

[7] Bera, R. K.; Raj, C. R. *Analyst* **2011**, *136*, 1644-1648.

[8] Kong, Y.; Wei, C.; Wang, Z.; Hou, Z.; Li, H.; Yu, J.; Yuan, J.; Zhao, Y.; Long, J.; Tang, Y.; Gao, M. *Am. J. Anal. Chem.* **2014**, *5*, 258-265.

[9] Akter, H.; Shaikh, A. A.; Chowdhury, T. R.; Rahman, M. S.; Bakshi, P. K.; Ahammad, A. J. S. *ECS Electrochem. Lett.* **2013**, *2*, B13-B15.

[10] Yang, W.; Gooding, J. J.; He, Z.; Li, Q.; Chen, G. *J. Nanosci. Nanotechnol.* **2007***,* 7, 712-716.

[11] Aili, D.; Enander, K.; Rydberg, J.; Nesterenko, I.; Björefors, F.; Baltzer, L.; Liedberg, B. *J. Am. Chem. Soc.* **2008**, *130*, 5780-5788.

[12] Han, M. S.; Lytton-Jean, A. K. R.; Oh, B. K.; Heo, J.; Mirkin, C. A. *Angew. Chem.* **2006**, *118*, 1839-1842.

[13] Zhao, W.; Chiuman, W.; Lam, J. C.; Brook, M. A.; Li, Y. *Chem. Commun.* **2007**, *36*, 3729-3731.

[14] Hummers, W. S.; Offeman, R. E. *J. Am. Chem. Soc.* **1958**, *80*, 1339.

[15] Huang, N. M.; Lim, H. N.; Chia, C. H.; Yarmo, M. A.; Muhamad, M. R. *Int. J. Nanomed.* **2011**, *6*, 3443-3448.

[16] Cao, Q.; Zhao, H.; Zeng, L.; Wang, J.; Wang, R., Qiu, X.; He, Y. *Talanta* **2009**, *80*, 484-488**.**

[17] Liao, C.; Chen, W. Y. R.; Chang, J. L.; Zen, J. M. *Electroanalysis* **2011**, *23*, 573-576.

[18] Zhu, H.; Zhang, S.; Li, M.; Shao, Y.; Zhu, Z. *Chem. Commun* **2010**, *46*, 2259-2261.

[19] Yue, J.; Jiang, X.; Kaneti, Y. V.; Yu, A. *J. Colloid Interface Sci.*, **2012**, *367*, 204-212.

[20] Bai, L. Y.; Dong, C. X.; Zhang, Y. P.; Li, W.; Chen, J. *J. Chin. Chem. Soc.* **2011**, *58*, 846-852.

[21] Zeng, S.; Cai, M.; Liang, H.; Hao, J. *Anal. Methods* **2012**, *4*, 2499-2505.

[22] Chi, H.; Liu, B.; Guan, G.; Zhang, Z.; Han, M. Y. *Analyst* **2010**, *135*, 1070-1075.,

[23] Montague, P. R.; Hyman, S. E.; Cohen, J. D. *Nature* **2004**, *431*, 760-767.

[24] Ndamanisha, J. C.; Guo, L.; *Biosens. Bioelectron.* **2008**, *23*, 1680-1685.

[25] Wang, C.; Yuan, R.; Chai, Y.; Chen, S.; Zhang, Y.; Hu, F.; Zhang, M. *Electrochim. Acta* **2012**, *62*, 109-115.

[26] Xie, S. H.; Liu, Y. Y.; Li, J. Y. *Appl. Phys. Lett.* **2008**, *92*, 243121-1-243121-3.

[27]. Zhang, H.; Gai, P.; Cheng, R.; Wu, L.; Zhang, X.; Chen, J. *Anal. Methods* **2013**, *5*, 3591-3600.

[28] Beitollahi, H.; Hamzavi, M.; Mahani, M. T.; Shanesaz, M.;Maleh, H. K. *Electroanalysis* **2015**, *27*, 524-533.

[29] Lin, X. Q.; Kang G. F.; Lu, L. P. *Bioelectrochemistry* **2007**, *70*, 235–244.

[30] Liu, X. G.; Peng, Y. H.; Qu, X. J.; Ai, S. Y.; Han, R. X.; Zhu, X. B. *J. Electroanal. Chem.* **2011**, *654*, 72–78.

[31] Wang, P.; Li, Y. X.; Huang, X.; Wang, L. *Talanta* **2007**, *73*, 431–437.

[32] Ulubay, S. U.; Dursun, Z. *Talanta* **2010**, *80*, 1461–1466.

[33] Zhang, W. X.; Zheng, J. Z.; Shi, J. G.; Lin, Z. Q.; Huang, Q. T.; Zhang, H. Q.; Wei, C.; Chen, J. H.; Hua, S.; Hao, A. *Anal. Chim. Acta* **2015**, *853*, 285–290.

[34] Zhu, X. H.; Liang, Y.; Zuo, X. X.; Hu, R. P.; Xiao, X.; Nan, J. *Electrochim. Acta* **2014**, *143*, 366–373.

[35] Wang, C.; Li, J.; Shi, K.; Wanga, Q.; Zhao, X.; Xiong, Z.; Zou, X.; Wang, Y. *J. Electroanal. Chem.* **2016**, *770*, 56–61.

[36] Burtis, C. A.; Ashwood, E. R. *Tietz Fundamental of Clinical Chemistry*, 4th ed.; W.S. Saunders company: A Division of Horcount Brace & Company: Philadelphia, PA, USA, **1996**; p. 242.

[37] Kazuharu, S.; Shunitz, T.; Mitsuniko, T. *Bioelectrochem. Bioenerg.* **1991**, *26*, 469–474.

[38] Reynaud, J. A.; Maltoy, B.; Canessan, P. *J. Electroanal. Chem.* **1980**, *114*, 195–211.

[39] Tan, W. T.; Bond, A. M.; Ngooi, S. W.; Lim, E. B.; Goh, J. K. *Anal. Chim. Acta* **2003**, *491*, 181–191.

[40] Zhao, Y. D.; Zhang, W. D.; Cheng, H.; Luo, Q. M. *Sens. Actuat. B* **2003**, *92*, 279–285.

[41] Xu, J.; Wang, Y., Xian, Y.; Jin, L.; Tanaka, K. *Talanta* **2003**, *60*, 1123–1130.

[42] Maree, S.; Nyokong, T. *J. Electroanal. Chem.* **2000**, *492*, 120–127.

[43] Filanovsky, B. *Anal. Chim. Acta* **1999**, *394*, 91–100.

[44] Wang, Z.; Pang, D. *J. Electroanal. Chem.* **1990**, *283*, 349–358.

[45] Zhang, S.; Sun, W.; Zhang, W.; Qi, W. *Anal. Chim. Acta* **1999**, *386*, 21–30.

# LIST OF FIGURES

| Figure No. | Title | Page No. |
|---|---|---|
| Figure I.1.a | Potential excitation signal used for Linear Sweep Voltammetry (LSV). | 9 |
| Figure I.1.b | Typical linear sweep voltammogram for a redox reaction. | 9 |
| Figure I.2.a | Potential excitation signal used for Cyclic Voltammetry (CV). | 10 |
| Figure I.2.b | Typical cyclic voltammogram for a reversible electrochemical system. | 10 |
| Figure I.3.a | Potential excitation signal for a Normal Pulse Voltammetry (NPV). | 14 |
| Figure I.3.b | Voltammogram for NPV. | 14 |
| Figure I.4.a | Two types of potential excitation signal for Differential Pulse Voltammetry (DPV). | 15 |
| Figure I.4.b | Peak shaped voltammogram for DPV. | 15 |
| Figure I.5.a | Potential excitation signal for a Square Wave Voltammetry (SWV). | 17 |
| Figure I.5.b | Voltammogram of SWV. | 17 |
| Figure I.6.a | Potential excitation signal for a Stair Case Voltammetry (SCV). | 19 |
| Figure I.6.b | Voltammogram of SCV. | 19 |
| Figure I.7.a | Potential excitation signal for a single potential step Chronoamperometry (CA). | 20 |
| Figure I.7.b | Formation of concentration gradient with time during CA. | 20 |
| Figure I.7.c | Chronoamperogram. | 20 |
| Figure I.8.a | Potential excitation signal for a double potential step chronoamperometry where final potential input occurs in the reverse direction. | 21 |
| Figure I.8.b | Chronoamperogram for double potential step chronoamperometry where final potential input occurs in the reverse direction. | 21 |
| Figure I.9 | Pathways of general electrode reaction. | 22 |

| | | |
|---|---|---|
| Figure II.1 | Block diagram of potentiostat/galvanostat. | 39 |
| Figure II.2 | Voltammogram of $K_4[Fe(CN)_4]/K_3[Fe(CN)_3]$ couple on CPE, inset: plot of oxidation peak current vs. square root of scan rate. | 53 |
| Figure II.3.a | Diagram showing relationship between alternating current and excitation potential signal at frequency $\omega$. | 66 |
| Figure II.3.b | Vector diagram of impedance, Z and its real and imaginary component. | 66 |
| Figure II.4.a | Equivalent electrical circuit of an electrochemical cell. | 67 |
| Figure II.4.b | Nyquist plot for the corresponding electrochemical system. | 67 |
| Figure II.5 | Block diagram for the instrumentation of a Scanning Electrochemical Microscopy (SECM). | 72 |
| Figure II.6.a | Pictorial representation of interaction of redox active species with ultramicroelectrode during steady state (diffusion limited) behaviour in SECM experiment. | 74 |
| Figure II.6.b | Pictorial representation of interaction of redox active species with ultramicroelectrode in the negative feedback mode of SECM experiment. | 74 |
| Figure II.6.c | Pictorial representation of interaction of redox active species with ultramicroelectrode in the positive feedback mode of SECM experiment. | 74 |
| Figure II.7.a | Tip current-distance curve for negative feedback mode of SECM experiment. | 74 |
| Figure II.7.b | Tip current-distance curve for positive feedback mode of SECM experiment. | 74 |
| Figure II.8.a | Pictorial representation of interaction of redox active species with ultramicroelectrode in the tip generation/substrate collection mode of SECM experiment. | 75 |
| Figure II.8.b | Pictorial representation of interaction of redox active species with ultramicroelectrode in the substrate generation/tip collection mode of SECM experiment. | 75 |
| Figure II.9 | Pictorial representation of interaction of redox active species with ultramicroelectrode in the redox competition mode of SECM experiment. | 76 |

Figure II.10 Pictorial representation of interaction of redox active species with ultramicroelectrode in the direct mode of SECM experiment. 77

Figure III.1 Effect of deposition time of Bi deposition on the stripping peak of Cd, deposition potential was fixed at -0.8 V (SCE). Concentration of $Cd^{2+}$was 30 µg $L^{-1}$. 85

Figure III.2 Pictorial representation of BFCPE, NCBFE-1 and NCBFE-2. 86

Figure III.3.a Anodic stripping voltammograms of Pb, Cd and Zn in sodium acetate solution of pH 6.5 using BFCPE, analyte deposition potential was -1.25V and deposition time was 300 sec (Inset: Response of bare GCE for Zn, Cd and Pb of concentration 150, 90 and 120 µg $L^{-1}$ respectively). 88

Figure III.3.b Calibration plots of peak current vs. concentration for Pb, Cd and Zn using BFCPE. 88

Figure III.4 Differential pulse anodic stripping voltammograms of Pb, Cd and Zn in sodium acetate solution of pH 6.5 using NCBFE - 1, analyte deposition potential was -1.25V and deposition time was 300 sec. 89

Figure III.5.a Differential pulse anodic stripping voltammograms of Pb, Cd and Zn in sodium acetate solution of pH 6.5 using CNTMBFE, analyte deposition potential was -1.25V and deposition time was 300 sec. 89

Figure III.5.b Calibration plots of peak current vs. concentration for Pb, Cd and Zn using CNTMBFE. 89

Figure III.6.a SEM images of the Bi-film on bare carbon paste electrode (BFCPE) at two different magnifications (left is at low and right is at high resolution). 90

Figure III.6.b SEM images of the Bi-film on MWCNT-Nafion modified carbon paste electrode (CNTMBFE) at two different magnifications (left is at low and right is at high resolution). 90

Figure III.7.a Differential pulse anodic stripping voltammograms of Pb and Cd at different analyte deposition potentials (-0.55V to -1.25V) using BFCPE. 91

Figure III.7.b Differential pulse anodic stripping voltammograms of Pb and Cd at different analyte deposition potentials (-0.55V to -1.25V) using NCBFE – 1. 91

Figure III.7.c Differential pulse anodic stripping voltammograms of Pb and Cd at different analyte deposition potentials (-0.55V to -1.25V) using NCBFE – 2. 91

Figure III.7.d Differential pulse anodic stripping voltammograms of Pb and Cd at different analyte deposition potentials (-0.55V to -1.25V) using CNTMBFE. 91

Figure III.8 Comparison of stripping response of Pb (40μg $L^{-1}$) and Cd (30μg $L^{-1}$) for BFCPE, NCBFE – 1, NCBFE – 2 and CNTMBFE, analyte deposition potential: -0.9V, deposition time: 300 sec, from sodium acetate solution of pH 6.5. 94

Figure III.9 Effect of the addition of Cu on the Bi-stripping peak. Inset: corresponding calibration plot of 'peak A' (hollow circle), 'peak B' (solid circle). Each time 20 μg $L^{-1}$ Cu was added. 95

Figure III.10.a Effect of TX100 on the stripping peak of Zn, Cd and Pb with concentration of 300 μg $L^{-1}$, 90 μg $L^{-1}$ and 120 μg $L^{-1}$ respectively. Solid points are with nafion modification (NCBFE - 2) and the empty points are without nafion modifications. 97

Figure III.10.b Effect of SDS on the stripping peak of Zn, Cd and Pb with concentration of 400 μg $L^{-1}$, 120 μg $L^{-1}$ and 160 μg $L^{-1}$ respectively. Solid points are with nafion modification (NCBFE - 2) and the empty points are without nafion modifications. 98

Figure III.10.c Effect of CTAB on the stripping peak of Zn, Cd and Pb with concentration of 400 μg $L^{-1}$, 120 μg $L^{-1}$ and 160 μg $L^{-1}$vrespectively. Solid points are with nafion modification (NCBFE - 2) and the empty points are without nafion modifications. 99

Figure III.11.a SEM micrograph of the Sb film modified CPE. 107

Figure III.11.b SEM micrograph of the Sb–Au nano composite modified CPE used for Hg determination. 107

Figure III.12.a SEM image of point scan for the Sb-Au nano composite film pre-concentrated with Hg. 108

Figure III.12.b EDS spectra of point scan for the Sb–Au nano composite film pre-concentrated with Hg. 108

Figure III.13.a SEM image of area scan for the Sb-Au nano composite film pre-concentrated with Hg. 109

Figure III.13.b EDS spectra of area scan for the Sb–Au nano composite film pre-concentrated with Hg. 109

Figure III.14 Effect of deposition time of Sb deposition on the stripping peak of Cd (75μg $L^{-1}$), Sb deposition potential: -0.6V, from 10mM antimony trichloride solution (in 0.02 M HCl). 110

| | | |
|---|---|---|
| Figure III.15.a | Effect of pH on the Sb stripping characteristics in HCl solution, Sb deposition was carried out using 10 mM antimony trichloride solution (in 0.02 M HCl) at a deposition potential of -0.6 V for 100 sec. | 112 |
| Figure III.15.b | Effect of pH on the Sb stripping characteristics in sodium acetate solution, Sb deposition was carried out using 10 mM antimony trichloride solution (in 0.02 M HCl) at a deposition potential of -0.6 V for 100 sec. | 112 |
| Figure III.16 | Differential pulse anodic stripping voltammetric plots of Cd and Pb at varying concentrations on the SbMCPE, the Cd and Pb deposition was carried out at -1.0 V for 300 sec in 0.1 M sodium acetate solution at pH 6.0. Inset: corresponding linear calibration plot. | 114 |
| Figure III.17 | Comparison of peak potentials of anodic stripping peaks of Pb and Cd on BFCPE, HMDE and SbMCPE. | 116 |
| Figure III.18 | Differential pulse anodic stripping voltammetric plot of Cu at varying concentrations on the SbMCPE, Ex-situ Cu deposition at -1.0 V for 300 sec in 0.1 M sodium acetate solution at pH 6. Inset: corresponding linear calibration plot. | 117 |
| Figure III.19 | Differential pulse anodic stripping voltammetric plot of Hg using Sb–Au nano composite modified carbon paste electrode. Hg deposition at -0.6V for 300 sec and stripping was performed in 0.1 M sodium acetate solution. Inset: corresponding linear calibration plot. | 118 |
| Figure IV.1 | Chemical structure of melamine. | 124 |
| Figure IV.2 | Rosette crystal pattern of complex between melamine and cyanuric acid. | 126 |
| Figure IV.3 | Hydrogen bonding between melamine and uric acid. | 127 |
| Figure IV.4 | Cyclic voltammograms of melamine on SMDE in BR buffer of different pHs, Inset: plot of reduction peak potential of melamine with respect to pH of the solution. | 130 |
| Figure IV.5 | Cyclic voltammograms of melamine at pH 2 of BR buffer at different scan rate, Inset: Linear calibration plot of reduction peak current vs. Square root of scan rate. | 131 |
| Figure IV.6 | Differential pulse voltammograms of melamine reduction on SMDE with different concentration of melamine, Inset: Linear calibration plot of peak current vs. Concentration of melamine. | 132 |

Figure IV.7 Linear sweep anodic stripping voltammetry of 3.3 μM of $Cu^{2+}$ with different concentration of melamine. Deposition potential was −1.0 V for 10 sec. Inset: corresponding linear calibration plots of peak 1 and peak 2. 134

Figure IV.8 X-ray diffraction patterns of (a) graphene oxide and (b) reduced graphene oxide. 137

Figure IV.9 Scanning electron micrograph of the reduced graphene oxide–gold nanoparticles composite. 138

Figure IV.10 Atomic force micrograph and the corresponding line graph of reduced graphene oxide. 139

Figure IV.11.a Cyclic voltammogram of 1 mM $K_4[Fe(CN)_6]$ at the reduced graphene oxide–gold nanoparticles composite-modified electrode at scan rates of a. 10 mV $sec^{-1}$, b. 20 mV $sec^{-1}$, c. 30 mV $sec^{-1}$, d. 50 mV $sec^{-1}$, and e. 100 mV $sec^{-1}$. 140

Figure IV.11.b Twenty cyclic voltammograms of 1 mM $K_4[Fe(CN)_6]$ at the reduced grapheme oxide–gold nanoparticle composite-modified electrode at a scan rate of 50 mV $sec^{-1}$. 140

Figure IV.12 Square wave voltammograms of 0.01 mM $K_4[Fe(CN)_6]$ with the addition of melamine (top to bottom). 141

Figure IV.13 Probe approach plot of the platinum tip to the reduced graphene oxide–gold nanoparticle substrate: Experimental and fitted plot. 143

Figure IV.14 Scanning electrochemical micrograph of the reduced graphene oxide–gold nanoparticles substrate for 1 mM ferrocene in methanol. The tip electrode was 10-μm diameter platinum and scans were performed 1μm above the substrate. 143

Figure IV.15 Scanning electrochemical micrograph of the reduced graphene oxide–gold nanoparticles substrate for 1 mM ferrocene in methanol and 1μM melamine. The tip electrode was 10-μm diameter platinum and scans were performed above the substrate. 144

Figure IV.16 Interferences for the oxidation of $K_4[Fe(CN)_6]$ in (a) the absence of any interfering agents; (b) $K_4[Fe(CN)_6]$ with 100 ppb $Hg^{2+}$ and $Ag^{+}$ and 100 ppm of $Cu^{2+}$, $Bi^{3+}$, $Pb^{2+}$, $K^{+}$, $Na^{+}$, and $Cl^{-}$; (c) $K_4[Fe(CN)_6]$ with 1 g $L^{-1}$ casein; and (d) the stripping response of $Hg^{2+}$ (100 ppb), $Cu^{2+}$(100 ppb), and $Bi^{3+}$ (100 ppm) in the absence of $K_4[Fe(CN)_6]$. 145

Figure IV.17 Cyclic voltammogram of oxidation of melamine on MWCNT-nafion composite modified CPE. 148

Figure IV.18 SEM micrograph of gold nanoparticles electrochemically deposited on carbon paste electrode substrate. 149

Figure IV.19 Cyclic voltammograms of oxidation of melamine on AuNPs modified CPE at different scan rates, in PBS of pH 7. 150

Figure IV.20 Square wave voltammograms of melamine on AuNPs modified carbon paste electrode with successive addition of 0.5 μM melamine. Inset: Corresponding calibration plot. 151

Figure IV.21 Chemical structure of dopamine (DA), uric acid (UA) and L-ascorbic acid (AA). 154

Figure IV.22 Scheme of biosynthesis of DA. 154

Figure IV.23.a SEM image of CNSs. 158

Figure IV.23.b SEM image of FCNSs. 158

Figure IV.23.c Morphological image of FCNSs by AFM measurements. 158

Figure IV.23.d Phase contrast image of FCNSs by AFM measurements. 158

Figure IV.23.e The histogram depicting the distribution of size of the FCNSs. 158

Figure IV.24 FTIR spectra of FCNSs. 159

Figure IV.25 Raman spectra of FCNSs. 160

Figure IV.26 Effect of loading of FCNS in FCNSPE on the oxidation signal intensity of DA (concentration of DA in $5 \times 10^{-7}$M). 162

Figure IV.27.a Cyclic voltammograms of DA at different pH. 163

Figure IV.27.b Cyclic voltammograms of UA at different pH. 163

Figure IV.27.c Cyclic voltammograms of AA at different pH. 163

Figure IV.27.d Plot of peak potential vs. pH of the BR buffer for DA, UA and AA. 163

Figure IV.28.a Oxidation scheme of DA. 164

Figure IV.28.b Oxidation scheme of UA. 164

Figure IV.28.c Oxidation scheme of AA. 164

Figure IV.29.a Differential pulse anodic stripping voltammogram of DA oxidation at different accumulation potential. 166

Figure IV.29.b Dot-line representation of change in peak current of DA oxidation signal with accumulation potential. 166

Figure IV.29.c Differential pulse anodic stripping voltammogram of DA oxidation with variation of accumulation time at accumulation potential of 0V. 166

Figure IV.29.d Dot-line representation of the variation of oxidation peak current of DA with deposition time. Concentration of DA is $5x10^{-7}$M in PBS supporting electrolyte media of pH 7. 166

Figure IV.30.a Differential pulse anodic stripping voltammogram of DA oxidation at different concentrations, Inset: corresponding calibration plot of peak current vs. concentration. 167

Figure IV.30.b Differential pulse anodic stripping voltammogram of UA oxidation at different concentrations, Inset: corresponding calibration plot of peak current vs. concentration. 167

Figure IV.31 Differential pulse anodic stripping voltammogram of DA, UA and AA at varying concentration. AA was varied at 100 times higher and UA was varied at 10 times higher in concentration than DA. Experiments were carried out at pH 7 (PBS) accumulations at 0V for 600 sec. 168

Figure IV.32 Calibration plot of peak current vs. concentration of DA and UA when added simultaneously in PBS of pH7. 169

Figure IV.33.a Equation for ammonium carboxylate salt formation between carboxylate ions of FCNSs and primary amine of DA. 171

Figure IV.33.b Pictorial representation of interaction pattern and the entanglement of DA with the FCNSs modified paste electrode. 171

Figure IV.34 Nyquist plots using the FCNSs modified paste electrode in blank supporting electrolyte media and in presence of $0.5x10^{-6}$M DA. 173

Figure IV.35.a Equivalent electrical circuit for the electrochemical system having the FCNSs modified paste electrode in blank supporting electrolyte media (PBS of pH 7). 174

Figure IV.35.b Equivalent electrical circuit for the electrochemical system having the FCNSs modified paste electrode in presence of $0.5x10^{-6}$M DA in the supporting electrolyte media (PBS of pH 7). 174

Figure IV.36.a Differential pulse anodic stripping voltammetric plots during the spike recovery test of DA with $2.2x10^{-6}$M concentration in real blood sample. 176

Figure IV.36.b Differential pulse anodic stripping voltammetric plots during the spike recovery test of DA with $1x10^{-7}$M concentration in real blood sample. 176

Figure IV.37 HPLC plots during recovery test with successive addition of dopamine. 177

Figure IV.38 Differential pulse anodic stripping voltammograms of DA at $2\times10^{-7}$ M concentration with three sets of modified electrodes of same dimension. 178

Figure IV.39 Chemical structure of L-Cysteine (CySH). 181

Figure IV.40 Effect of switching potential of CV on oxidation of CySH and gold coating. 183

Figure IV.41 Cyclic voltammograms showing the effect of pH on CySH oxidation; Inset: Plot of oxidation peak potential against pH of the supporting electrolyte media. 183

Figure IV.42 Schematic diagram of oxidation of L-Cysteine to Cystine (CyS-SCy). 184

Figure IV.43 Cyclic voltammograms of CySH oxidation on repeated scans between 0V and 0.78V, Voltammetric response decreased substantially on successive scans. 185

Figure IV.44.a Cyclic voltammetry of CySH in phosphate buffer of pH 7.5 showing oxidation of CySH followed by desorption of oxidised species at negative potential. 186

Figure IV.44.b Effect of adsorption of the oxidised species upon oxidation of CySH when repeated scans were performed between 0V to 0.78V; voltammetric response due to oxidation decreased substantially due to adsorption of oxidised species of CySH; oxidation followed by desorption at negative potential (full scan) retains voltammetric response on successive scans. 187

Figure IV.45 Effect of scan rate variation on voltammetric signal of CySH oxidation; Inset: Linear calibration plot of peak current against scan rate. 188

Figure IV.46 Variation of peak potential of CySH oxidation with log of scan rate. 188

Figure IV.47 Nyquist plots of the electrochemical system when data were recorded by keeping the fresh AuNPs modified GCE, in the solution containing 10μM of CySH in phosphate buffer of pH 7.5, at 0V, 0.3V and 0.7V. 189

Figure IV.48 Nyquist plots of the electrochemical system when data were recorded by keeping the fresh AuNPs modified GCE electrode, in the solution containing 10μM of CYSH in PBS of pH 7.5, at -0.6V, and -0.6V after adsorption at 0.7V for 200 sec. 190

Figure IV.49 Probe approach plot by keeping the probe at 0.4 V and substrate at -0.2 V in 1 mM $K_4[Fe(CN)_6]$ solution. 191

Figure IV.50 CV plots of the Au tip probe electrode at the approach distance after treatment of the substrate electrode by different CV cycles in CySH solution. 192

Figure IV.51.a CV scans of the Au tip probe electrode at approach distance when a negative potential (-0.8V) was applied to the substrate after coated with cystine film. 193

Figure IV.51.b CV scans of the Au tip probe electrode at approach distance when a negative potential (-0.8V) was applied to the substrate without having any coating of cystine film. 193

Figure IV.52 AFM image of (a) freshly deposited AuNPs on bare GCE (b) Cystine coated AuNPs upon 50 Cyclic Voltammetry from 0V to 0.7V in CySH solution. 194

Figure IV.53.a Differential pulse anodic stripping voltammograms of different concentrations of the CySH in PBS of pH 7.5, using AuNPs modified GCE. 195

Figure IV.53.b Calibration plot of CySH oxidation peak Current vs. concentration of CySH in PBS of 7.5. 195

Figure IV.54 Chronoamperometry of CySH under stirring condition using the modified electrode. 196

Figure IV.55 Chemical structure of 2-(o-hydroxyphenyl)benzoxazole. 198

Figure IV.56.a Electrochemical responses for the redox behaviour of BNZ on bare GCE and GO coated GCE; concentration of the compound: 10μM; medium: 0.5M NaOH and scan rate: 100mV $sec^{-1}$. 200

Figure IV.56.b Cyclic voltammograms for the redox behaviour of BNZ in 0.5M NaOH medium, recorded at different scan rates (20 mV $sec^{-1}$, 50 mV $sec^{-1}$, 80 mv $sec^{-1}$, 100 mV $sec^{-1}$, 200 mV $sec^{-1}$, 300 mV $sec^{-1}$, 400 mV $sec^{-1}$ and 500 mV $sec^{-1}$). 200

Figure IV.57 Multiple scans dipping the composite electrode of FCNSs and 2-(-o-hydroxyphenyl)benzoxazole in 0.5M NaOH at a scan rate of 20mV $sec^{-1}$. 201

# LIST OF TABLES

| Table No. | Title | Page No. |
|---|---|---|
| Table III.1 | Detection limits/Limit of detections (LOD) obtained using BFCPE, NCBFE - 1 and NCBFE - 2 for Zn, Cd and Pb in aqueous solution. | 100 |
| Table III.2 | Limit of detection (LODs) for Zn, Cd and Pb reported in the literature using Bi-film electrode. | 100 |
| Table III.3 | Analysis result of the water samples collected from different places of India using NCBFE - 2 for water samples and BFCPE for solid samples, values under the parenthesis were obtained using HMDE. | 101 |
| Table III.4 | % RSD calculated from the analysis of real samples (collected from different places of India) for Zn, Cd, Pb, and Cu in real samples, using NCBFE – 2 and BFCPE | 102 |
| Table III.5 | Comparison of analytical parameters determined using SbMCPE and Sb-Au nano composite modified CPE with the results already published in the literature. | 119 |
| Table III.6 | Recovery test results of Hg, Cu, Pb and Cd using the SbMCPE and Sb-Au nano composite modified CPE. | 120 |
| Table III.7 | Analysis results of Cu, Pb, Cd and Hg in two samples collected from two regions of India using the modified electrode. Values in the parenthesis for Cu, Pb and Cd were calculated using ICPAES; while, for Hg, it was calculated using thermal decomposition atomic absorption technique. | 120 |
| Table IV.1 | Recovery of melamine in milk and water using the RGO–AuNPs composite-modified CPE and HPLC. | 146 |
| Table IV.2 | Comparison of the analytical figures of merit for determination of melamine by the method using the RGO-AuNPs composite modified CPE and other methods reported in the other literature. | 146 |
| Table IV.3 | Recovery test results of melamine in milk sample using AuNPs modified CPE. | 152 |

Table IV.4 Data for comparison of the analytical performance of the FCNSs modified paste electrode for determination of DA and UA with the previously reported literature 170

Table IV.5 Table showing the values of the fitting parameters of the equivalent electrical circuit represented in figure IV.35.a. 174

Table IV.6 Table showing the values of the fitting parameters of the equivalent electrical circuit represented in figure IV.35.b. 175

Table IV.7 Results of recovery study at two different concentration levels (2.2 µM and 0.1µM) of DA in blood serum using FCNSs modified paste electrode. 176

Table IV.8 Comparison of the results of the recovery test of DA in blood serum using the FCNSs modified paste electrode and HPLC technique. 177

# Chapter: I

## *Introduction*

## I. 1. Analytical Chemistry:

Analytical Chemistry is a powerful scientific discipline which deals with separation, qualitative and quantitative measurements useful in all fields of science [1]. It involves the application of a range of techniques to obtain and asses the qualitative, quantitative and structural information of the analyte. Analytical chemistry is art and science of determining what matter is and how much of it exists. Qualitative analysis enables us to identify the chemical species present in a sample, while quantitative analysis determines the absolute or relative amount of the species. Apart from the fundamental and applied research, gathering and interpretation of these results are required for quality control in manufacturing industries, clinical and biological studies, monitoring as well as controlling of pollutants, preparing geological assays and so on [2]. Analytical measurements are carried out by various analytical techniques. There are a wide variety of techniques used for analysis, from simple weighing (gravimetric analysis) to titrations (titrimetric) to very advanced techniques using highly specialized instrumentation. The most common techniques used for analytical measurements are gravimetry, titrimetry, atomic and molecular spectroscopy, mass spectroscopy, chromatography, thermal analysis, electrophoresis, electrochemical analysis, microscopy and radiochemical analysis [3]. The first two falls under classical analytical techniques (or wet Chemical methods) and the rest are instrumental techniques. Analytical Chemistry was practiced in its elementary form from ancient times but began to develop as an objective exercise during 17th century. During the 17th -19th centuries, analytical chemistry was largely empirical. The first instrumental analysis was flame emissive spectrometry developed by Robert Bunsen and Gustav Kirchhoff who discovered Rubidium (Rb) and Cesium (Cs) in 1860 [4]. Most of the major developments in analytical chemistry took place after 1900. During this period instrumental analysis became progressively dominant in this field. In particular many basic spectroscopic and spectrometric techniques were discovered during the early 20th century [5]. Thereafter, growth of analytical chemistry was tremendous and instrumental analysis revolutionized in the field of analytical chemistry. Now, the application of analytical chemistry is widespread over all disciplines of science.

## I. 2. Electroanalytical Chemistry:

Electrochemical methods form a new branch in analytical chemistry called Electroanalytical chemistry. Electroanalytical chemistry encompasses a group of quantitative analytical methods that are based upon the measurement of electrical parameters such as potential (E), current (I), resistance (R) / conductance (G) and total charge (Q) and relating these to the concentration of the analyte(s) (C) in the test solution when it is made part of an electrochemical cell [6] Electrochemical measurement for analytical purposes has been widely recognized in the field of medicine, environmental monitoring, nuclear industry, industrial quality control etc. apart from the research and development work [7-9].

### I. 2. 1. Electroanalytical Techniques:

Electroanalytical techniques are the tools to identify and quantify the analytes based on the electrical signals originated from either oxidation – reduction processes or adsorption – desorption or ingression-regression process at the interface of electrode and electrolyte. These techniques are capable of producing exceptionally low detection limits and wealth of characterization information describing electrochemical addressable system [3, 10]. The potential benefits of the powerful and versatile techniques are as follows:

1. High sensitivity, accuracy, precision and large linear dynamic range.
2. High selectivity resulting from the choice of the electrode material.

3. Possibility of furnishing results in the real time or close to real time.

4. Application as miniaturized sensor.

Apart from the above mentioned benefits, most importantly these techniques are fast, simple, cost effective, portable and highly efficient.

### I. 2. 2. Classification of Electroanalytical Techniques:

Electroanalytical techniques can be broadly classified in to two categories such as potentiostatic and potentiometric [11]. Potentiostatic (Controlled-potential) techniques deal with the study of charge transfer processes at the electrode–solution interface, and are based on dynamic (non-zero-current) situations. Here, the electrode potential is used to derive an electron transfer reaction and the resultant current is measured. On the other hand potentiometric techniques (zero current) involve measurement of potential without drawing any appreciable amount of current through the electrochemical cell [3].

Based on the above consideration mainly four types of electroanalytical techniques have been used for analysis such as Potentiometry, Coulometry, Voltammetry and Amperometry. These techniques are discussed briefly as follows:

#### I. 2. 2. 1. Potentiometry:

Potentiometric methods of analysis are based on direct measurement of potential of the electrochemical cell without drawing any appreciable current through the cell. In potentiometry the cell set up requires two electrodes: the measuring electrode, also known as indicator electrode and the reference electrode. The equilibrium potential developed across the indicator electrode is measured with respect to the reference electrode under a high impedance voltmeter. It is the only electroanalytical technique which measures the thermodynamic equilibrium potential given by the Nernst equation (eq. I.1).

$$E_{ind} = E'_{O/R} + \frac{RT}{nF} ln \frac{[O]}{[R]} \qquad \textbf{eq. I.1}$$

Where $E_{ind}$ is potential developed across the indicator electrode (V), $E'_{O/R}$ is the formal potential of the redox couple (V), T is the temperature (K), R is universal gas constant (8.313 J $K^{-1}mol^{-1}$), n is the number of electrons transferred during the redox process, F is Faraday constant (96487 Coulomb/mol), [O] is the concentration of oxidized species of the couple and [R] is the concentration of the reduced species. By judicious choice of the electrode material, the selectivity to a particular ion can be enhanced, in some cases very minimal interference in the measured potential from the other ions. Such electrodes are called ion selective electrodes [12]. Many ion selective electrodes for $H^+$, $Ca^{2+}$, $F^-$ etc. and gas sensing electrodes for $NH_3$, $CO_2$ etc. are used as potentiometric sensors. Direct potentiometry and potentiometric titrations are two major types of analytical techniques in potentiometry. In direct potentiometry the cell potential is measured and related to the concentration or activity of the individual chemical species. In the potentiometric titration variation of cell potential is monitored as a function of the volume of reagent added [13].

### I. 2. 2. 2. Coulometry:

Coulometry is an electroanalytical method which involves measurement of quantity of electricity (total charge in coulombs) needed to convert an analyte quantitatively to a different oxidation state. The principle of the technique is the manifestation of the Faraday's first law of electrolysis which tells the extent of chemical reaction at an electrode is directly proportional to the total charge/ quantity of electricity passes through it. Mass of the substance produced or consumed in an electrolysis involving Q coulombs of charge is given by the equation 1.2

$$m = \frac{MQ}{nF} \qquad \textbf{eq. I.2}$$

Where, m is the mass of the substance produced or consumed, M is molar mass of the substance, Q is total charge in coulomb. F is faraday constant and n is the number of electrons involved in the redox reaction. The fundamental criterion of the technique for the quantitative analysis is that the efficiency should be 100%, so that quantity of the substance reacted can be expressed by means of Faraday's law [14] or the efficiency should be calibrated to get the quantitative result. Mainly two techniques are used for the analysis purpose such as controlled current coulometry (Amperostatic) and controlled potential coulometry (Potentiostatic). These techniques are widely used for the determination of many inorganic species especially in the field of nuclear energy, for the determination of uranium (U) and Plutonium (Pu). This technique is used also in the popular Karl Fischer titration method [1].

### I. 2. 2. 3. Voltammetry:

Voltammetry is a group of electroanalytical techniques which are widely used in various fields of science and contemporary research, both applied and pure. Voltammetry involves measurement of current (I) with respect to the time dependent potential (E) applied to the electrode. The potential is varied in some systematic manner and the resulting current vs. potential plot is called voltammogram. This plot provides both qualitative and quantitative information about the analyte(s) involved in the redox reaction. Depending upon the different potential wave form (E vs t) different types of voltammetric techniques are evolved. Voltammetric studies are used to extract both qualitative and quantitative information about a redox system. The qualitative information covers the redox potential of the analyte, number of electrons transferred during a redox reaction, diffusion coefficient of the analyte in a particular medium [10]. The methods are also employed to extract the information about the kinetics of a reaction, reaction mechanism, reversibility of a redox reaction, adsorption processes at the surface of the electrode, determination of complexation and coordination values etc. Electrochemical sensors based on these techniques are employed for the precise quantification of various ionic species, biomolecules, pesticides and other hazardous chemical species in the environmental samples. These techniques have wide applicability in the field of energy related research such as fabrication of energy storage devices and electro-catalysts for generation of hydrogen and oxygen by splitting of water.

### I. 2. 2. 4. A brief historical review of Polarography and Voltammetric techniques:

On February 10, 1922, Professor Jaroslav Heyrovsky recorded the first dependence of the current flowing through the dropping mercury electrode (DME) on the applied potential and drew a corresponding graph in his laboratory notebook which can be considered as the first polarogram. The discovery of polarography by the Professor Heyrovsky leads to the development of voltammetry [15]. In polarography dropping mercury is used while in voltammetry hanging mercury drop electrode (HMDE) and solid electrodes are used. Development of polarographic techniques proceeded from classical Direct Current (DC) polarography [16], through oscillopolarography [17], Kalousek's switcher [18], AC polarography [19], tast polarography [20], normal pulse polarography [21] and differential pulse polarography [22]. Complexities in assembling and operation have made polarography a less ideal technique for routine analytical purposes. These disadvantages opened up the field of Voltammetry. The term 'Voltammetry' was introduced by I. M. Kolthoff and H. A. Laitinen in 1940s. In the 1950s and 1960s the HMDE and solid electrodes have replaced the use of DME. The advancement in theory, development in methodologies and instrumentation in the late 1960s made the voltammetric techniques more popular, versatile and relatively inexpensive for commercial purposes [23]. With this brief account of history of voltammetry different voltammetric techniques are discussed in the following section.

### I. 2. 3. Voltammetric Techniques:

The most common voltammetric techniques are as follows:

- DC Polarography (Historical importance).
- Linear Sweep Voltammetry.
- Cyclic Voltammetry
- Pulsed Voltammetry
    - Normal Pulsed Voltammetry.
    - Differential Pulsed Voltammetry.
    - Square Wave Voltammetry.
- Stripping Voltammetry.
- Staircase Voltammetry.

#### I. 2. 3. 1. DC Polarography:

Invention of DME by Professor Heyrovsky is of enormous importance to the history of electroanalytical chemistry. Using the DME he discovered a new form of voltammetry, which he named ‘polarography’. Very often this historic form is referred as ‘dc polarography or conventional polarography or classical polarography’. A capillary with an internal diameter of ~ $5 \times 10^{-3}$ cm is fed by a head of mercury 20 to 100 cm high. Mercury passes through the capillary to form a nearly spherical drop, which grows until its weight can no longer be supported by the surface tension. A mature drop typically has a diameter on the order of 1 mm. If electrolysis occurs during the drop’s growth, the current becomes time dependent which is the manifestation of both the expansion of spherical electrode and the depletion effects of electrodes. Upon falling the drop stirs the solution and largely erases the depletion effects, so that the new drops are formed into fresh solution environment. The current produced during the redox reaction is given by the Ilkovic equation (eq. I.3).

$$i_d = 708nD^{1/2}Cm^{2/3}t^{1/6} \qquad \textbf{eq. I.3}$$

The maximum current can be obtained when sampling is done just before the drop fall and therefore the maximum current is given by the following equation (eq. I.4)

$$(i_d)_{max} = 708nD^{1/2}Cm^{2/3}t_{max}^{1/6} \qquad \textbf{eq. I.4}$$

$t_{max}$ is the life time of the drop. $n$ is the number of the electron transfer that occur in the redox reaction, D is the diffusion coefficient of the analyte in a particular medium ($cm^2\ sec^{-1}$), C is concentration of the analyte ($mol\ cm^{-3}$), m is the mass flow ($mg\ sec^{-1}$), t is the time after the drop is formed (sec). The classical DME has two principal disadvantages. First, it has constantly changing area, which complicates the treatment of diffusion and creates a continuous background current due to the double layer charging. Second, its time scale is controlled by the lifetime of the drop, which cannot be varied conveniently outside the range of 05-10sec [3]. By 1980, Princeton Applied Research Corporation, later followed by the others, had commercialized a replacement of the classical DME that does not suffer these drawbacks.

### I. 2. 3. 2. Linear Sweep Voltammetry:

Linear sweep voltammetry (LSV) is a voltammetric method where the current at a working electrode is measured while the potential between the working electrode and a reference electrode is swept linearly with time, sweep rates ranging from 10mV $sec^{-1}$ to 1000 V $sec^{-1}$ with conventional electrodes and up to $10^6$ V $sec^{-1}$ with ultra-micro electrodes (UMEs) [10]. Oxidation or reduction of species is registered as a peak at the potential at which the species begins to be oxidized or reduced (Fig. I.1.a and Fig. I.1.b).

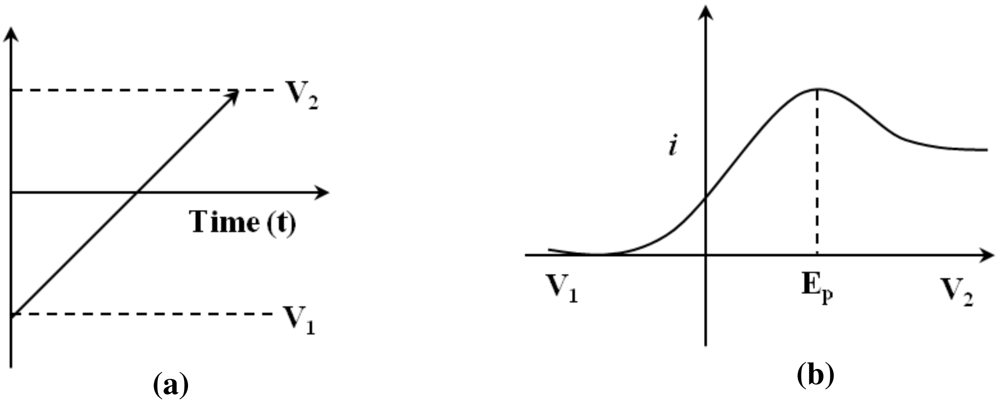

**Figure I.1:** **(a)** Potential excitation signal used for Linear Sweep Voltammetry (LSV); (b) Typical linear sweep voltammogram for a redox reaction.

The characteristics of the linear sweep voltammogram recorded depend on a number of factors including the rate of the electron transfer reaction(s), the chemical reactivity of the electroactive species and the voltage scan rate. Linear sweep voltammetry can identify unknown species and determine the concentration of solutions. Half wave potential ($E_{1/2}$) can be used to identify the unknown species while the height of the limiting current can determine the concentration. The sensitivity of current changes vs. voltage can be increased by increasing the scan rate.

### I. 2. 3. 3. Cyclic Voltammetry:

Cyclic voltammetry (CV) is a very important electroanalytical technique, which is widely used in many areas of chemistry. The popularity of the technique lies in its ability to provide thermodynamic and kinetic data of an electrochemical process [24, 25]. Usually CV is the first experiment to be carried out in an electrochemical investigation. This technique was first reported in 1938 and described by Randles and Sevsick [26, 27]. In a normal CV experiment, the working electrode potential is ramped linearly versus time. Unlike LSV, after the set potential is reached in a CV experiment, the working electrode's potential is ramped in the opposite direction to return to the initial potential i.e. a triangular E-t (Potential-time) wave form is used as an excitation signal (Fig. I.2.a) in which, the potential of the electrode is scanned from $E_i$ (starting potential) to $E_f$ (switching potential) and reversing back to $E_i$. These cycles of ramps in potential may be repeated as many times as needed. The current at the working electrode is plotted versus the applied voltage; the plot thus obtained is called cyclic voltammogram. Figure I.2.b shows a typical cyclic voltammogram of a reversible redox system (heterogeneous electron transfer is much faster than other processes such as diffusion, scan rate of potential ramp etc.). The parameters such as anodic peak current ($I_{pa}$), cathodic peak current ($I_{pc}$), anodic peak potential ($E_{pa}$), cathodic peak potential ($E_{pc}$) and half wave potential ($E_{p/2}$, potential corresponding to half of peak current) carry both thermodynamic and kinetic information of the electrochemical system.

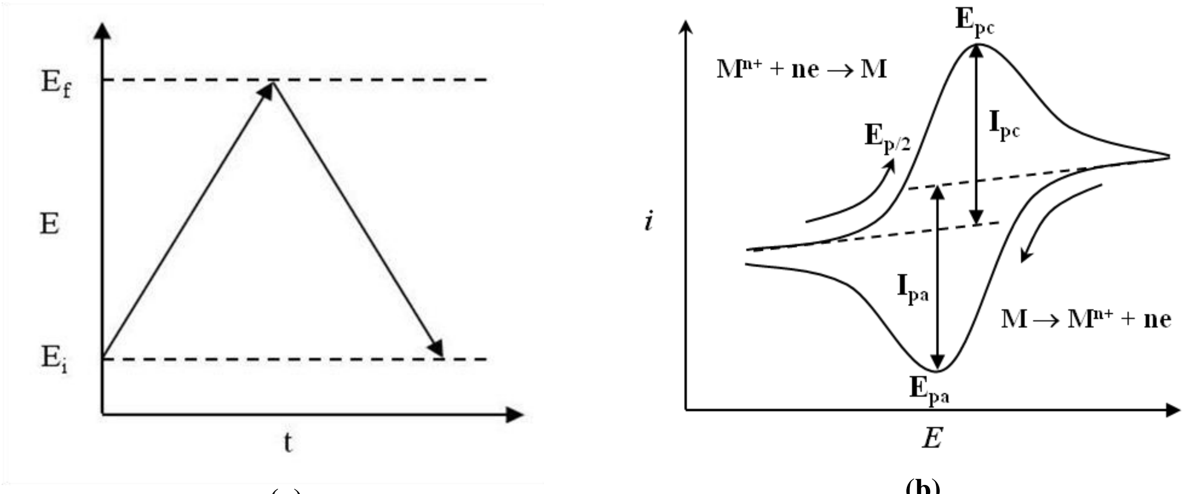

**(a)** **(b)**

**Figure I.2:** (a) Potential excitation signal used for Cyclic Voltammetry (CV); (b) Typical cyclic voltammogram for a reversible electrochemical system.

For an electrochemically reversible reaction the separation between the cathodic peak (reduction peak) and anodic peak (oxidation peak) is

$$\Delta E_p = \left|E_{pc} - E_{pa}\right| = 2.303RT/nF \qquad \textbf{eq. I.5}$$

in aqueous medium. Thus for a reversible process at 25$^{O}$C temperature $\Delta E_p$ should be 0.059/n V, where n is the number of electrons getting transferred. The formal reduction potential (E$^{O'}$) of a reversible couple is given by

$$\mathbf{E^{O'}} = \frac{(\mathbf{E_{pc}+E_{pa}})}{\mathbf{2}} \qquad \textbf{eq. I.6}$$

And the peak current can be obtained from Randles – Sevsick equation

$$\boldsymbol{I_p = 0.4463\, nFAC\left(\frac{nFvD}{RT}\right)^{1/2}} \qquad \textbf{eq. I.7}$$

At 25$^{O}$C temperature

$$\boldsymbol{I_p = (2.69\times 10^5)n^{3/2}AD^{1/2}Cv^{1/2}} \qquad \textbf{eq. I.8}$$

Where, $I_p$ is current maximum in amps, n is number of electrons transferred in the redox event, A is electrode area in cm$^2$, F is Faraday Constant in C mol$^{-1}$, D is the diffusion coefficient in cm$^2$ sec$^{-1}$, C is concentration in mol cm$^{-3}$, ν is scan rate in Vs$^{-1}$, R is Gas constant in J K$^{-1}$ mol$^{-1}$ and T is temperature in K. The importance of the equation lies in the determination of diffusion coefficient of an electro-active species in a particular medium, active surface area of an electrode and number of electrons getting transferred in a redox reaction. Extent of reversibility of an electrochemical reaction can also be judged by the following the equation (eq. I.9).

The peak current observed depend on the two components which are described below.

(a) Electron transfer rate constant [28]

$$\boldsymbol{K_f = K^O \exp\left(\frac{-\alpha nF}{KT}(E - E^{O'})\right)} \qquad \textbf{eq. I.9}$$

$K_f$ is the electron transfer rate constant of forward reaction, $K^O$ is the standard heterogeneous rate constant of electrochemical reaction and $\alpha$ is the charge transfer coefficient. The exponential dependence of $K_f$ on the applied potential accounts for the steep rise in the peak current.

(b) Mass transfer towards the electrode [29]

During electrolysis surface concentration of the analytes depletes resulting in the concentration gradient between the bulk electrolytic solution and the electrode. Therefore diffusion of the electrolyte occurs to the electrode. Current obtained is also dependent on the concentration gradient according to the following equation,

$$\boldsymbol{I = nFAD \left(\frac{\partial C}{\partial x}\right)_{x=0}} \qquad \textbf{eq. I.10}$$

The current is directly proportional to the concentration gradient, where $I$ is the current (A), $A$ is the area ($cm^2$), $D$ is diffusion coefficient ($cm^2\ sec^{-1}$), $\left(\frac{\partial C}{\partial x}\right)_{x=0}$ is the concentration gradient ($mol\ cm^{-1}$) at the electrode surface, $C$ is the concentration of the analyte ($mol\ cm^{-3}$) and $x$ is the distance from the electrode to the bulk (cm).

For a reduction to occur potential is shifted cathodically with time. When the potential approaches the vicinity of $E^{O'}$ of the analyte the reduction begins and the current starts to flow and the cathodic current ($I_r$) increases as potential grows more negative since the surface concentration of the oxidized form of the analyte decreases and flux to the surface (and the reduction current, $I_r$) increases. As the potential moves past $E^{O'}$ the surface concentration drops nearly to zero and the mass transfer to the surface reaches a maximum rate (Current achieves its maxima, $I_{pc}$) and then it declines as the depletion effects sets in [$\left(\frac{\partial C}{\partial x}\right)_{x=0}$ decreases]. The observation is therefore a peaked current potential curve. The current observed in LSV and normal CV is the combination of both faradaic and non faradaic processes that occur simultaneously.

### I. 2. 3. 4. Pulse Voltammetry:

Pulse voltammetric techniques, introduced by Berker and Jenkin in 1950s [30], are aimed at lowering the detection limits of voltammetric measurements. These techniques allow convenient measurements up to $10^{-9}$M concentration level. Because of their greatly improved performance, modern pulse voltammetric techniques have largely replaced classical polarography in electroanalytical experiments. The sensitivity of CV and polarography are restricted due to the continuous presence of double layer charging current ($I_C$). The basis of improved sensitivity of the pulse techniques is the development of large ratio of faradaic current ($I_f$) to the $I_C$ [31]. The various pulse techniques are based on a sample current/ potential step experiment. A sequence of such potential pulse (each pulse referring to one potential step), each with a duration of few msecs, is applied on the working electrode. Current is sampled after a time lag. On application of potential pulse there is a surge of $I_C$ which decays exponentially with time (eq. I.11) while $I_f$ decays slowly as described by the Cottrell equation (eq. I.12). Thus by sampling current late in the pulse life, an effective discrimination against charging current is achieved.

$$\boldsymbol{I_C = \frac{\Delta E}{R_u} \exp\left(\frac{-t}{R_u C_{dl}}\right)} \qquad \textbf{eq. I.11}$$

$$\boldsymbol{I_f = \frac{nFAD^{1/2}C}{(\pi t)^{1/2}}} \qquad \textbf{eq. I.12}$$

Where $\boldsymbol{\Delta E}$ is step potential, $\boldsymbol{R_u}$ is the solution resistance and $\boldsymbol{C_{dl}}$ is the double layer capacitance. Application of a pulse to an electrode maximises the flux by reducing the diffusion layer thickness [3]. This leads to the increase in the sensitivity.

Various pulse voltammetric techniques arose from the difference in the potential wave form and the current sample regime.

### I. 2. 3. 4. a. Normal Pulse Voltammetry (NPV):

This technique uses a series of potential pulse with increasing amplitude superimposed on a constant base potential (Fig. I.3.a) applied to the electrode [11]. The current measurement is done at the end of each pulse, thus allowing $I_C$ to decay. NPV is usually carried in unstirred solution at either DME (known as normal pulse polarography) or static electrode. The amplitude of the pulse increases linearly with time (in the order of mV sec$^{-1}$). The duration of the pulse, $t_p$, is usually 1 to 100 msec and the interval between the two pulses typically 0.1 to 5 sec. The sampled currents are plotted against the potential to which the pulse is stepped (Fig. I.3.b). NPV is 5 – 10 times sensitive than classical polarography with a LOD of $10^{-6}$ to $10^{-7}$M.

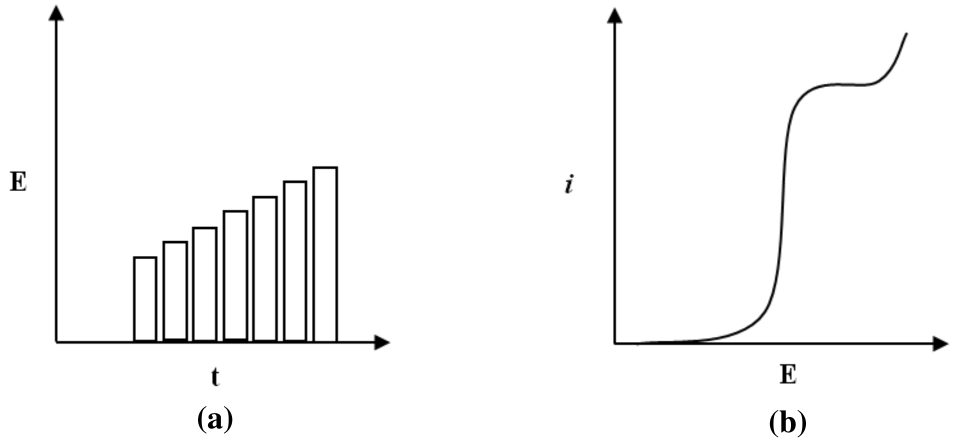

**Figure I.3:** (a) Potential excitation signal for a Normal Pulse Voltammetry (NPV); (b) Voltammogram for NPV.

### I. 2. 3. 4. b. Differential Pulse Voltammetry (DPV):

This technique is comparable to the NPV in that the potential is scanned with a series of pulses. However it differs from NPV because each potential pulse is fixed and of small amplitude (10 to 100 mV) and superimposed on a slowly changing potential base line or on a staircase potential applied on the electrode (Fig. I.4.a). The current is measured twice, just before the application of the pulse ($I_1$) and at the end of the pulse ($I_2$), when the charging current is decayed. The difference between the currents [ $\Delta I = (I_2 - I_1)$] is plotted against the base potential. The resulting peak shaped profile is called differential pulse voltammogram (Fig. 4.b). DPV is 10 – 100 times more sensitive than classical polarography with a LOD of $10^{-7}$M to $10^{-8}$M. The peak current is proportional to the concentration of the analyte as mentioned in the following equation (eq. I.13).

$$\boldsymbol{I_p = \frac{nFAD^{1/2}}{\sqrt{\pi t_p}}\left(\frac{1-\sigma}{1+\sigma}\right)C} \qquad \textbf{eq. I.13}$$

Where $\boldsymbol{\sigma = exp\left(\frac{nF\Delta E}{2RT}\right)}$, $\Delta E$ is pulse amplitude and $t_p$ is pulse duration and all other symbols have their usual notification. $\sigma$ describes the effect of $\Delta E$ on $I_p$. The reversible systems produce narrow and symmetric peak while the irreversible system produces broader peak with less current sensitivity. Peak shaped response (Fig. I.4.b) with very low background makes it a suitable technique for the analysis of mixture.

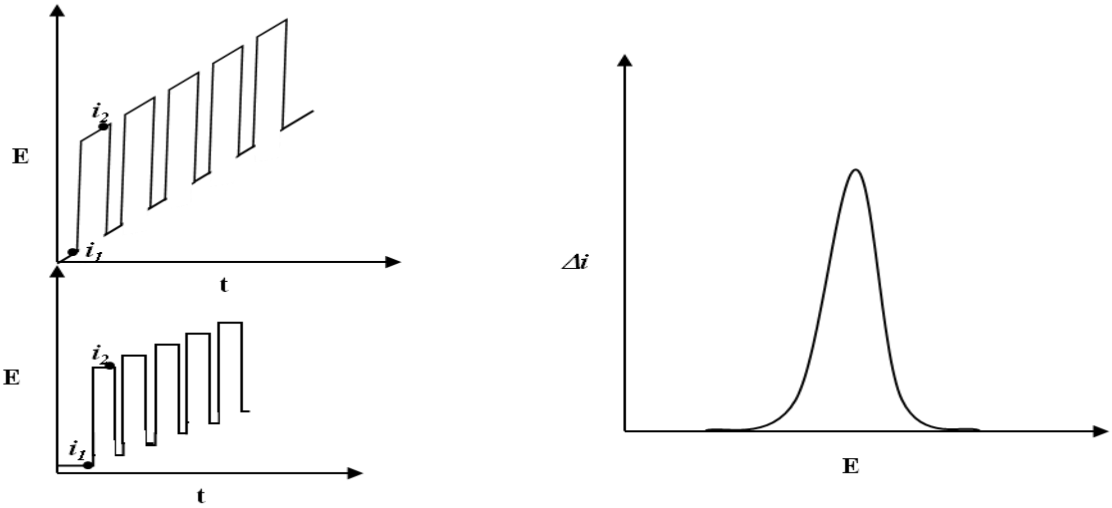

**(a)** **(b)**

**Figure I.4:** (a) Two types of potential excitation signal for Differential Pulse Voltammetry (DPV); (b) Peak shaped voltammogram for DPV.

### I. 2. 3. 4. c. Square Wave Voltammetry:

Square wave voltammetry (SWV) was invented by Ramaley and Krause [32], but has been developed extensively by Osteryoungs and their co-workers [33-35]. This technique can be viewed as combining the best aspects of several pulse voltammetric methods, including the back ground suppression and sensitivity of differential pulse voltammetry, the diagnostic value of normal pulse voltammetry and the ability to interrogate products directly in much the manner of reverse pulse voltammetry. It also offers access to a wider range of time scales than can be achieved by any of the pulse polarographic techniques [10]. SWV is generally carried out at a stationary electrode. As in other forms of pulse voltammetry the electrode is taken through a series of measurement cycles. The excitation wave form can be viewed as consisting of a stair case scan, each trade of which is superimposed by a symmetrical double pulse, one in forward direction and one in the reverse (Fig. I.5.a). Over many cycles, the waveform is a bipolar square wave superimposed on the staircase, and this view gives rise to the name of the method. The square wave is characterized by a pulse height, $\Delta E_p$ , measured with respect to the corresponding tread to the staircase, and a pulse width $t_p$. Alternatively, the pulse width can be expressed in terms of the square wave frequency $= {}^{1}\!/_{2t_p}$. The stair case shifts by $\Delta E_s$ at the beginning of each cycle; thus the scan rate $v = {}^{\Delta E_s}\!/_{2t_p} = f\Delta E_s$.

The scan begins at an initial potential, $E_i$, which can be applied initially for an arbitrary time to initialise the system as desired. Current samples are taken twice per cycle, at the end of each pulse. The forward current sample, $I_{forward}$ arises from the first pulse per cycle, which is in the direction of the staircase scan. The reverse current sample, $I_{reverse}$ is taken at the end of the second pulse, which is in the opposite direction. The net current ($\Delta I$) is obtained from the difference of $I_{forward}$ and $I_{reverse}$ ($\Delta I = I_{forward} - I_{reverse}$ ) and is plotted against the base staircase potential. The resulting peak shaped profile is called square wave voltammogram. The peak height is directly proportional to the concentration of the electrochemically active species and detection limit of $10^{-8}$M to $10^{-9}$M is achievable under optimized condition. SWV provides several advantages such as good accuracy, very high signal to noise ratio and the speed. The voltammogram can be recorded in a few seconds or even less than that. Application of SWV includes the study of kinetics, determination of some species in trace levels and its use in the electrochemical detection system in HPLC.

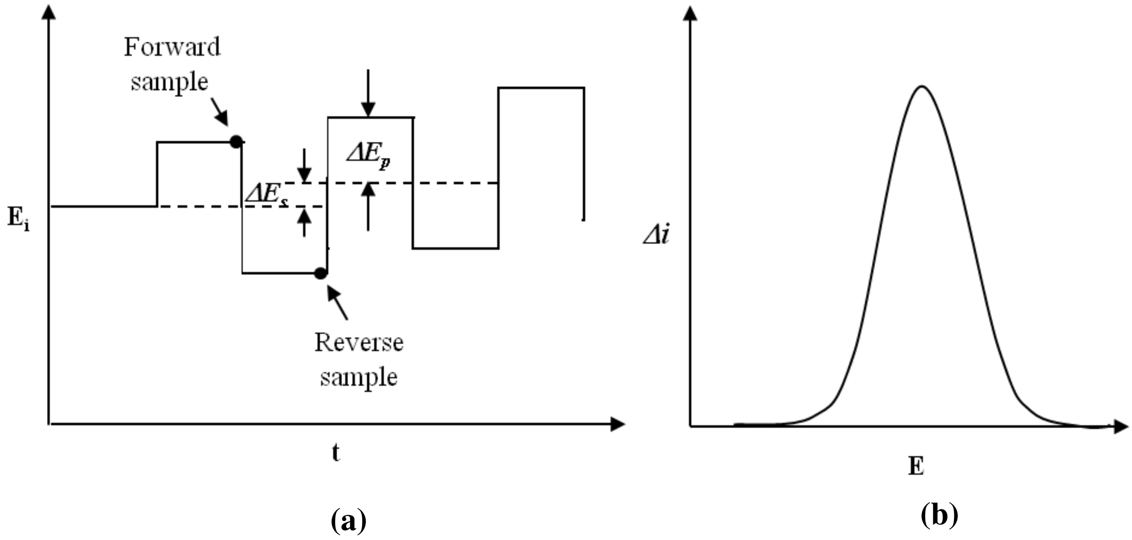

**Figure I.5:** (a) Potential excitation signal for a Square Wave Voltammetry (SWV); (b) Voltammogram of SWV.

### I. 2. 3. 5. Stripping Voltammetry:

Stripping voltammetry is one of the most sensitive electroanalytical methods for measuring trace amount of metal ions and organic molecules. The outstanding sensitivity of the technique is attributed to an effective pre-concentration step. The technique consists of three steps. The first step is the deposition or pre-concentration where the analytes in the solution are deposited or pre-concentrated either by application of potential or by adsorption process under the stirring condition (to maximise the deposition). Second step is the equilibrium step where the stirring is stopped to make the solution steady and third is the stripping which involves dissolution or stripping of the pre-concentrated/deposited analytes from the electrode under potential scan in a tranquil condition. The current produced due to the faradaic reaction that happens during the stripping is measured using any of the pulse techniques such as DPV or SWV. Stripping step may be done by cathodic potential scan or anodic potential scan creating either negative or positive current signal. Depending on the potential scan direction during stripping the stripping voltammetry is named as cathodic stripping voltammetry and anodic stripping voltammetry. Prior to cathodic stripping anodic deposition/preconcentration is performed while cathodic deposition/preconcentration is performed for anodic stripping voltammetry. There is another kind of stripping voltammetry which is called adsorptive stripping voltammetry. Here preconcentration is done by way of adsorption of the analyte from the solution at an adequate potential and then stripping is done either cathodically or anodically using DPV or SWV. Peak current obtained can be related linearly with the concentration of the analyte. Stripping voltammetry can produce detection limit of $10^{-9}$M to $10^{-12}$M.

### I. 2. 3. 6. Staircase Voltammetry:

Staircase voltammetry (SCV) is based on the excitation signal which is a staircase potential waveform; the wave form creates a potential ramp (Fig. I.6.a). The current is sampled at the end of each step. The current is plotted against the step potential and the voltammogram is called Staircase voltammogram. The sampling time and cycle duration can be varied over a wide range; the change in step potential ($\Delta E_{SCV}$) can also be varied freely, but this determines the resolution of the technique, therefore $\Delta E_{SCV} < 5$ mV is maintained for good resolution. The voltammogram obtained is peak shaped (Fig. I.6.b). A detection limit of $10^{-5}$M can be achieved by the technique. But, due to the limitation of scan rate and low signal to noise ratio this technique is not used very often for the analysis purpose.

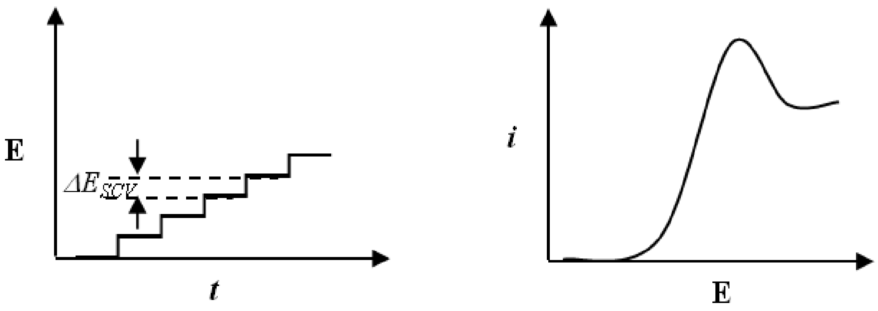

**(a)** **(b)**

**Figure I.6:** (a) Potential excitation signal for a Stair Case Voltammetry (SCV); (b) Voltammogram of SCV.

### I. 2. 4. Chronoamperometry:

Chronoamperometry (CA) is a technique which basically measures the current produced in the electrolytic cell with time when a fixed potential is applied to the working electrode. Potential is adjusted to a value at which redox reaction occurs. Current is monitored with respect to time and recorded as well; the resulting profile is called chronoamperogram. Actual experiment involves stepping of potential at working electrode from a value, say, $E_{start}$ at which no redox reaction occurs to a value $E_{final}$. The value of $E_{final}$ is so chosen that the concentration of electroactive species (say $X_{ox}$ of the couple $X_{ox} + ne \rightarrow X_{red}$) at the vicinity of the surface of the electrode falls to zero due to electrolysis as soon as it is applied on the working electrode. As a consequence a concentration gradient sets in for $X_{ox}$ and $X_{ox}$ must diffuse through the diffusion layer from the bulk to the electrode to react. The region within which the $X_{ox}$ is depleted is called diffusion layer, thickness of which is symbolized as δ (~$A^O$). On the application of $E_{final}$ initially concentration gradient ($\left(\frac{\partial C}{\partial x}\right)_{x=0}$) is very steep and the δ is very small. With time δ increases, concentration gradient decreases and the rate of diffusion falls resulting in the decrement in current (Fig. I.7.a, I.7.b and I.7.c).

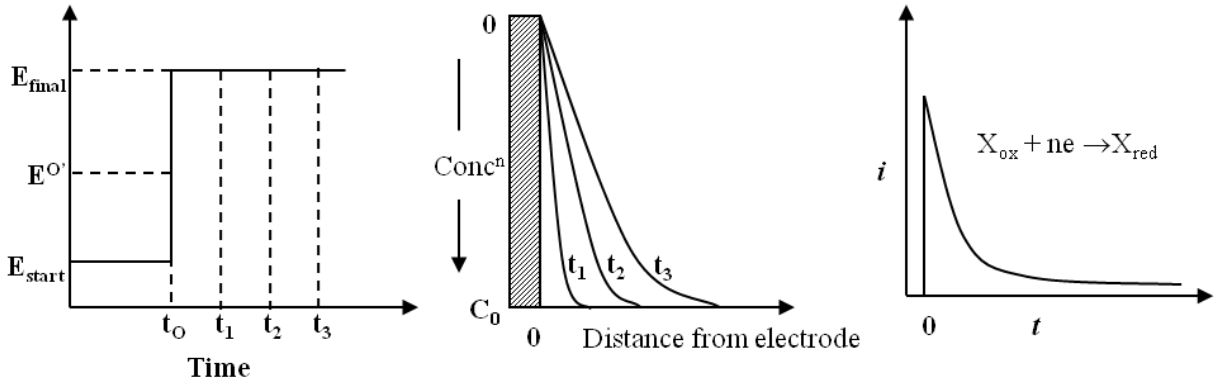

(a) (b) (c)

**Figure I.7:** (a) Potential excitation signal for a single potential step Chronoamperometry (CA); (b) Formation of concentration gradient with time during CA; (c) Chronoamperogram.

The most useful equation in chronoamperometry is the Cottrell equation, which describes the observed current (with planar electrode) at any time following a large forward potential step in a reversible redox reaction (or to large overpotential) as a function of $t^{-1/2}$ (eq. I.12). The current due to double layer charging, $I_{C,}$ described in a previous section (eq. I.11), also contributes to the total current following a potential step. By nature however, this capacitive current, $I_C$, decays exponentially and is only significant during the initial period (generally for a few msec) following the step. It can be easily recorded by performing the experiment in a cell containing only electrolyte, and digitally subtracted. Usually it can be avoided altogether by only considering i-t data taken during the last 90% of the step time. Chronoamperometry experiments are most commonly either single potential step, in which only the current resulting from the forward step as described above is recorded, or double potential step, in which the potential is returned to a initial value ($E_{start}$), the final potential in the reverse direction may be different from the $E_{start}$ if required, following a time period, usually designated as $\tau$, at the step potential ($E^{\prime}$) (Fig. I.8.a and I.8.b).

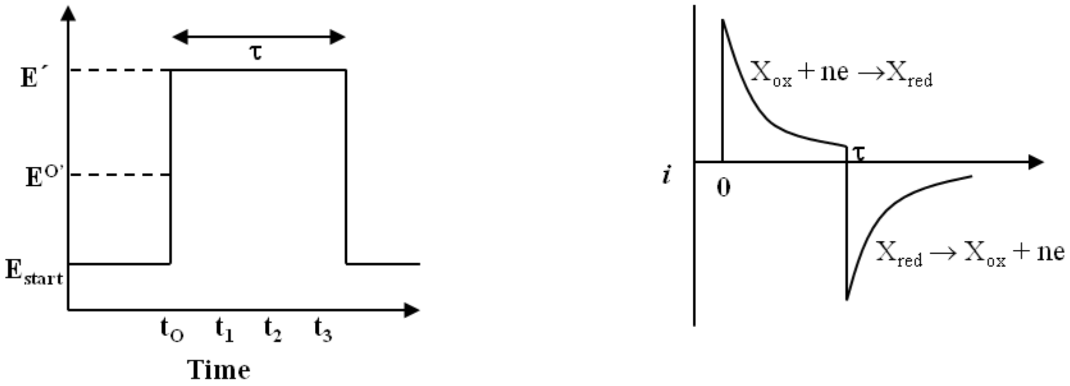

**(a)** **(b)**

**Figure I.8:** (a) Potential excitation signal for a double potential step Chronoamperometry where final potential input occurs in the reverse direction; (b) corresponding Chronoamperogram.

Chronoamperometry lends itself well to the accurate measurement of electrode area (A) by use of a well-defined redox couple (known n, C, and D). With a known electrode area, measurement of either n or D for an electroactive species is easily accomplished. The double potential step method is often applied in the measurement of rate constants for chemical reactions (including product adsorption) occurring following the forward potential step. Chronoamperometry is often carried out in hydrodynamic condition which includes convective mass transport of the electroactive species. Forced mass transport enhances the sensitivity of the technique. Steady state is achieved instantly under hydrodynamic condition. Due to the negligible contribution of $I_C$ this technique produces precise determination of the concentration of the electroactive species (current is proportional to the concentration of the electroactive species, eq. I.12).

### I. 3. Pathways of electrode process:

A typical electrode reaction $(O + ne \leftrightharpoons R)$ involves the electron transfer between an electrode and the species in the solution. The electrode reaction involves a series of steps as mentioned below:

1. Movement of the electroactive species (reactant) to the electrode, called mass transport.

2. Electron transfer between the electrode and the reactant.

3. Movement of the product away from the electrode to the bulk of the solution.

4. Different chemical reactions (e.g. protonation, dimerization, catalytic decomposition etc.) and other surface reactions (e.g. adsorption, desorption etc) may be associated preceding or following the electron transfer (Fig. I.9).

The simplest reaction involve only the mass transfer of a reactant to the electrode, the heterogeneous electron transfer or charge transfer and the mass transfer of the product to the bulk of the solution. Electron transportation occurs only when electroactive species is adjacent to the electrode surface. However, the initial step is the mass transport to the electrode from the bulk solution. This mass transport can occur by any of the following processes.

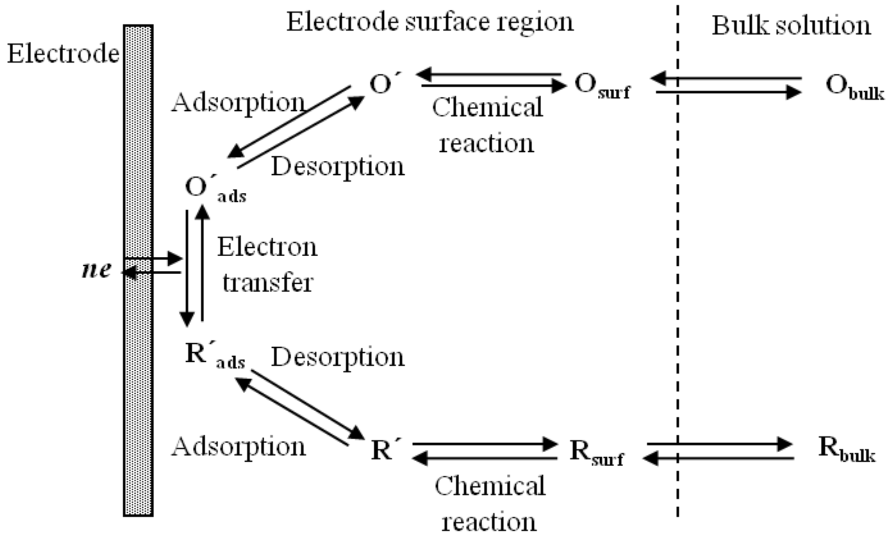

**Figure I.9:** Pathways of general electrode reaction.

### I. 3. 1. Diffusion:

It is the spontaneous movement of the species under a concentration gradient. During electrolysis of analyte at the working electrode, surface concentration of the analyte gets lowered compared to the bulk concentration resulting in a concentration gradient and the analyte transports from the higher concentration of bulk solution to the electrode surface. It is the most common mass transport process during any electrochemical reaction under tranquil condition.

### I. 3. 2. Migration:

It is the transport of charged species under potential gradient due to electrostatic force between the charged electrode and the ions /charged species. It can be minimized by addition of excess amount of supporting electrolyte which facilitates the migration of ions of supporting electrolyte restricting the migration of analyte of interest.

### I. 3. 3. Convection:

It is the transport of analyte due to the mechanical motion of the solution by stirring of the solution or by rotating electrode or by vibration of the solution or electrode. It is also observed due to formation of density gradient or temperature gradient in the solution. It is generally eliminated by keeping the experimental set up (electrode assembly, analyte solution etc) under quiet and stable condition.

In most of the electro-analytical technique the conditions are so created that mass transport due to migration and convection are eliminated and the mass transport is only controlled by diffusion process and the current thus obtained is called diffusion controlled current.

## I. 4. Types of electron transfer:

Depending upon the electron transfer rate between working electrode and the analyte electron transfer can be divided into three types such as reversible, irreversible and quasi-reversible electron transfer. These terms are relative to the rate of mass transport. These processes can be identified by CV experiments.

### I. 4. 1. Reversible electron transfer:

An electrochemical reaction is said to be electrochemically reversible if the electron transfer rate is much faster than the mass transfer rate; precisely $K^O$ (standard heterogeneous rate constant of electrochemical reaction) is much higher than mass transfer coefficient $m_T$ , where, $\boldsymbol{m_T} = \left(\frac{\boldsymbol{FDv}}{\boldsymbol{RT}}\right)^{1/2}$, $v$ is the scan rate in CV and all other terms bear their usual meaning. Matsuda and Ayabe [36] introduced the parameter, $\boldsymbol{\zeta}$, given by: $\boldsymbol{\zeta} = \boldsymbol{K^0}\left(\boldsymbol{RT}/_{\boldsymbol{FDv}}\right)^{1/2}$, where the following range is identified at a stationary electrode: $\boldsymbol{\zeta} \gg \mathbf{15}$ corresponds to the reversible limit. Both forward and reverse peaks in CV are observed for reversible electrochemical system. It follows nernstian behaviour assuming that both oxidized and reduced species are in equilibrium. The magnitude of the voltammetric current $I_p$ observed at an electrode is governed by the Randles–Ševcik equation (eq. I.7). The diagnostic criteria for the electrochemically reversible systems are as follows:

1. $\Delta \boldsymbol{E_p} = |\boldsymbol{E_{pc}} - \boldsymbol{E_{pa}}| = \mathbf{2.303}\boldsymbol{RT/nF}$ = 0.059/n V at 25 $^{O}$C temperature.
2. $\mathbf{E^{0/}} = \frac{(\mathbf{E_{pc}+E_{pa}})}{\mathbf{2}}$
3. $\boldsymbol{I_{pa}}/_{\boldsymbol{I_{pc}}} = \mathbf{1}$
4. $\boldsymbol{I_p} \propto \boldsymbol{v}^{1/2}$

5. $\boldsymbol{E_p}$ is independent of $\boldsymbol{v}$.

6. $\boldsymbol{E_p - Ep_{/2} = 0.0565/n}$ at 25°C.

### I. 4. 2. Irreversible electron transfer:

Here the electron transfer rate in an electrochemical reaction is slower compared to mass transfer rate where $\boldsymbol{\zeta}$ is identified as, $\boldsymbol{\zeta \ll 10^{-3}}$. This process does not follow nernstian behaviour. $\boldsymbol{E_p}$ gets shifted with variation of scan rate. For this type of reactions normally any one of the oxidation and reduction peak is observed, even if both the peaks are observed separation between the peaks is much more than 0.059/n V. Few diagnostic criteria are noted below:

1. $I_p^{irr} = \pm 0.496(\alpha n')^{1/2} nFAC\left({FDv}/_{RT}\right)^{1/2}$, where $\alpha$ is the charge transfer coefficient (usually assumed to be close to 0.5), $n$ is the total number of electrons transferred per molecule in the electrochemical process and $n'$ is the number of electrons transferred per mole before the rate determining step. $I_p^{irr}$ is the peak current in the irreversible reaction at a particular scan rate.
2. $\boldsymbol{E_p}$ shifts by **~30/ $\boldsymbol{\alpha n'}$** for each 10 fold increase in *v*.
3. $\boldsymbol{E_p - Ep_{/2} = 0.059/\alpha n'}$.

### I. 4. 3. Quasi reversible electron transfer:

Here the electron transfer rate and the mass transfer rate are comparable and $\boldsymbol{\zeta}$ is identified as $\boldsymbol{15 \gg \zeta \gg 10^{-3}}$. This is the intermediate case between reversible and irreversible electron transfer process. This process also does not follow nernstian behaviour. Diagnostic criteria for this type of process are given below:

1. $\Delta \boldsymbol{E_p} > 0.0591/n$ and increases with $\boldsymbol{v}$.

2. $\boldsymbol{E_p}$ shifts with increase in $\boldsymbol{\nu}$.

## I. 5. Sensors and applications:

A sensor is defined as a device which measures a physical quantity and transforms it into a signal which can be read by an observer or instrument. The world seems to have a natural division between chemical and physical sensors. Physical sensors are sensitive to the physical responses such as temperature, pressure, magnetic field etc. and do not have any chemical interface. However, there are those that do not classify easily, like relative humidity sensors, a chemical sensor traditionally lumped with physical sensors [37]. A useful definition for a chemical sensor is a small device that as the result of a chemical interaction or process between the analyte and the sensor device, transforms chemical or biochemical information of a quantitative or qualitative type into an analytically useful signal. The signal from a sensor is typically electronic in nature, being a current, voltage, or impedance/conductance change caused by changing analyte composition or quality or quantity. Chemical sensors contain a physical transducer and a chemically sensitive layer or recognition layer where selective chemistry takes place. Chemical sensors can be classified into following categories depending upon the transducer type

1. Mass sensitive,
2. Heat sensitive,
3. Optical and
4. Electrochemical sensors.

### I. 5. 1. Mass sensitive sensors:

Mass sensitive sensors use piezoelectric effect. Surface acoustic wave sensor which was particularly used for gas sensing is a type of such sensor. Acoustic gas sensing typically requires the crystal to be coated with an active layer, often a polymer or other non volatile coating, which performs a function similar to the stationary phase in a gas chromatograph. The change in the amount of the gas on the surface of the crystal is related to the shift in frequency of the oscillating crystal.

### I. 5. 2. Heat sensitive sensors:

Heat of a chemical reaction involving the analyte is monitored with transducers such as thermistor or a platinum thermometer; they are often called calorimetric sensors.

### I. 5. 3. Optical sensors:

Attenuation of light waves can be used to construct some of the most effective chemical sensors. The sensor design frequently uses a waveguide or optical fibre for convenient construction. If the analyte is placed at the interface of the fibre and a coating, it will have the opportunity to interact with the light. If the conditions are appropriate for either absorption or emission, the intensity and wavelength of the characteristic light provide the opportunity to obtain an analytical signal for quantitative and/or qualitative analysis. Optical techniques may often depend upon a coating and therefore derive many analytical properties, such as sensitivity, selectivity, and stability, from the choice of coating.

### I. 5. 4. Electrochemical sensors:

Compared to optical, mass and thermal sensors, electrochemical sensors are especially attractive because of their remarkable detect ability, experimental simplicity and low cost. They have a leading position among the presently available sensors that have reached the commercial stage and which have found a vast range of important applications in the fields of clinical, industrial, environmental and agricultural analyses [38]. There are three main types of electrochemical sensors: potentiometric (ion selective electrodes, ion selective field effect transistors), amperometric/voltammetric and conductometric. For potentiometric sensors, a local equilibrium is established at the sensor interface, where either the electrode or membrane potential is measured, and information about the composition of a sample is obtained from the potential difference between two electrodes. Voltammetric/Amperometric sensors exploit the use of a potential applied between a reference and a working electrode, to cause the oxidation or reduction of an electroactive species; the resultant current is measured. On the other hand, conductometric sensors are involved with the measurement of conductivity at a series of frequencies. Voltammetric/amperometric sensors are widely used for the various application in the field of biomedical [39], environmental [37], industrial [38] and agricultural analyses [40]. Electrochemical sensors provide several advantages over other sensors such as

- Inexpensive instrumentation
- Possibility of miniaturization
- Possibility of fabrication of potable sensors for onsite application
- Low detection limit and wide linear dynamic range
- High sensitivity and selectivity.

Here, in the thesis, reported works are based on voltammetric sensors which will be discussed in the later chapters, prior to that experimental set ups for the voltammetric sensors need to be discussed.

## I. 6. Experimental set up for the voltammetric sensors:

Any electrochemical experiment requires an electrochemical cell which is nothing but the physical boundary inside which electrochemical experiments are performed. The electrochemical cell for voltammetry comprises of the sample solution/experimental solution and the three electrode system. The three electrode system consists of a working electrode (WE), a reference electrode (RE) and a counter electrode (CE). These three electrodes are immersed into the experimental solution. RE serves to control potential over WE. The three electrode system is necessary to avoid passage of current through the reference electrode otherwise current flow would cause change in its potential via changes in activities of the chemicals within the RE. Moreover, the potential on WE cannot be controlled due to an unknown amount of IR drop owing to the solution resistance between WE and RE. Introduction of CE or auxiliary electrode as a current collector eliminates the issue. The voltammetric experiments are performed in a quiescent solution condition in presence of an excess of inert salt, called supporting electrolyte.

### I. 6. 1. Experimental solution:

Experimental solution for voltammetric sensor contains solvent and the supporting electrolyte other than the analytes. The solvent used for preparing the solution should have desirable properties such as (a) it should have high purity and wide liquid range, (b) it must solvate the analyte, (c) it must not react with the analyte, supporting electrolyte, the product of the redox reaction and the material of which the electrochemical cell is made, (d) It should offer a sufficient potential window for the study of the redox process of interest and (e) It should be stable on acid base treatment. Water is the most widely used solvent for the electrochemical experiment. For the organic analytes different non aqueous solvents are used. Acetonitrile, N,N-dimethylformamide (DMF), dimethylsulfoxide (DMSO), methanol, methylene chloride, propylene carbonate etc. are generally used as the non aqueous solvent.

Supporting electrolyte plays a vital role in the voltammetric experiment. It facilitates the charge transport in the solution and completes the circuit of the cell. Supporting electrolytes are nothing but the ionic salts or ionisable species which ionises either completely or partially in the solvent. These electrolytes must not react with the analyte of interest, must not corrode the electrodes and the materials of the cell vessel. They must not go into any chemical change (deposition of cations or liberation of anions) within the potential window where electrochemical reaction of the analyte occurs. They must be stable on acid base treatment (or pH variation). The supporting electrolytes have some rolls to play such as:

1. To increase the conductivity of the solution and minimise the uncompensated IR drop between the WE and the RE.

2. To eliminate the contribution of migration to the mass transfer of the analyte to the electrode.

3. To establish a uniform and high ionic strength throughout the solution and is not perturbed by the electrolysis of the analyte.

4. To restrict the potential drop across the interface within 10-20 Å which is necessary for the electron transfer that happens through quantum mechanical tunnelling [41].

The supporting electrolytes used are 100-1000times than the concentration of the analyte [12]. This is why the supporting electrolyte should be prepared very cautiously from ultrapure chemicals to maintain the high purity. The supporting electrolytes generally used are inorganic salts (KCl, $KNO_3$, $LiClO_4$, $NH_4Cl$, $Na_2SO_4$), Mineral Acids (HCl, $H_2SO_4$, $HClO_4$), base (KOH, NaOH), buffers (Phosphate, acetate, citrate and Britton-Robinson buffer) and tetraalkylammonium salts ($NR_4^+X^-$). $NR_4^+X^-$ salts are used as supporting electrolyte when organic media are used.

### I. 6. 2. Reference electrode:

A reference electrode has a stable and well defined electrochemical potential (at constant temperature) against which the applied or measured potentials in an electrochemical cell are referred. Therefore the roll of a reference electrode is to act as a reference in controlling and measuring the WE potentials in voltammetric experiments. The reference electrode should have the following properties:

1. RE should be ideally nonpolarizable electrode (INE) i.e. an electrode of constant potential irrespective of flow of current. In reality such an electrode is not available, commonly occurring REs show nonpolarizable behaviour when small amount of current is drawn [10].
2. Electrochemical reaction responsible for the development of the potential of the REs should be reversible and the potential should be calculated from the Nernst equation.
3. Electrode potential should be constant for a long period of time.

Commonly occurring REs are Normal hydrogen electrode/Standard hydrogen electrode (NHE/SHE: Pt/$H_2$[a=1]/$H^+$ [a=1,aqueous], $E^0$=0V), saturated calomel electrode (SCE: Hg/$Hg_2Cl_2$/KCl [saturated], $E^0$= 0.242V vs. NHE) and silver-silver chloride electrode (Ag/AgCl/KCl [saturated], $E^0$= 0.197V vs. NHE) [10]. These REs are aqueous based. For the non-aqueous media non-aqueous REs are used. In order to avoid contact between organic solvents and water from the reference electrode, in non-aqueous solutions usually a Ag wire in contact with $AgNO_3$ is used as a reference electrode. When using a 0.1 M $AgNO_3$ solution in acetonitrile, the electrode potential is around +0.36 V vs. SHE. As the electrode potentials of non-aqueous REs are less well defined, it is good practice to also use an internal reference when measuring in organic solvents. The ferrocene-ferricinium redox couple for example can be used for this purpose. The redox potential measured for this couple can then be used as an extra reference point.

### I. 6. 3. Counter Electrode:

Counter electrode (CE) or auxiliary electrode acts as the third electrode in an electrochemical cell for voltammetric analysis. As mentioned in the previous section it acts as the current collector. In voltammetric analysis the current flows between the WE and the CE. The name itself suggests that the reaction occurs at the CE is just the opposite to that of the WE, in other words if the WE acts as cathode then CE acts as anode. The main condition for an electrode to act as CE is that the electrode must not get dissolved in the experimental solution or react with the experimental solution and the reaction product during redox reaction at the CE must not react with WE. The working area of the CE should be much larger than that of the WE so as to confirm that the area of the CE does not control the limiting current.

### I. 6. 4. Working electrode:

Electrochemical reaction of the analyte of interest occurs on the working electrode (WE). Potential is applied on the WE with respect to the RE to carry out these electrochemical reactions. Depending upon the nature of the reaction WE acts as either cathode or anode. Every working electrode, immersed in a particular supporting electrolyte solution, has a potential window where it acts as the ideally polarizable electrode (IPE) i.e. within this potential window no charge transfer occurs across the electrode solution interface. The potential range also depends on the nature of the supporting electrolyte solution. The only faradaic current that can flow is due to the charge transfer occurring from the redox reaction of the trace amount of impurity or the analyte of interest. Other features, which are important for a good working electrode, are long term stability, easy renewability of the surface, ability to produce highly pure and reproducible surface etc. The most commonly used WEs can be categorized as (a) metal solid electrodes, (b) carbon based solid electrodes, (c) Liquid electrode and (d) conducting film electrodes. Platinum, gold, silver, lead electrodes comes under the first category; Glassy carbon/ vitreous carbon electrode, carbon paste electrode, diamond electrode etc. comes under the 2nd category; very well known mercury drop electrode is a liquid electrode which is widely used for voltammetric analysis. The forth categories of electrodes are mainly fabricated by casting a conducting film on a substrate (conducting or non conducting). The casting can be done by chemical vapour deposition technique (indium tin oxide, Fluorine doped tin oxide) [41], spray pyrolysis technique [42], polymerization (electrochemical or chemical, e.g. polyaniline, poly pyrrole etc) [43], electrochemical deposition on the conducting surface (Bi, Sb film) etc [44]. Sometimes these thin conducting films, casted on the metal solid electrodes or carbon based electrodes, are referred as electrode modifiers for enhancing the sensitivity of the electrodes towards the analyte of interests (will be discussed in the next chapter).

### I. 7. Objective of the present work:

Mercury electrodes are well known and widely used for the analysis of metal ions in trace level in the aqueous solutions. Due to large over potential for hydrogen evolution it provides a wide potential window (from 0 to -1v) for the determination of many metal ions in trace level, ability to form amalgams with the metals enables it to have very high sensitivity and low detection limit for these metal ions. In spite of all these advantages, toxicity of mercury and difficulty in handling mercury based electrodes has left the researchers to opt for alternative electrode materials for the analysis with similar sensitivity. On the other hand, development of methologies for many important biomolecules using electroanalytical techniques has gained a lot of importance in the last two/three decades. Investigation of electrochemical properties and sensitive determination of the concentration of these bio molecules require sensitive electrodes. The present thesis is aimed

- to minimise the use of mercury based electrodes,
- to fabricate alternate solid electrode materials,
- to improve the sensitivity towards different ions of interest by modifying the electrodes using thin films, nanoparticles etc.,
- to investigate the electrochemical properties of few important biomolecules and development of methologies for their detection using modified electrodes.

## I. 8. Scope of the present work:

Metal ions such as Cd, Pb, Zn, Cu and Hg in the environmental samples have been detected and analysed by using Bi and Sb thin film modified carbon paste electrode applying differential pulse anodic stripping voltammetry (DPASV). Carbon paste electrode (CPE) was fabricated by optimising several parameters to give a very low and smooth background current in the voltammetry experiment. CPE was also used for the electrochemical studies of melamine, an adulterant of milk product. It offers another advantage of easy renewability of its active surface. Bi and Sb thin film was electrochemically deposited. Functionalized carbon nano spheres were used for the fabrication of electrodes for the determination of dopamine (DA) and uric acid (UA) in the blood serum. Redox properties of another important biomolecule L-Cysteine were investigated. Several other methods such as atomic spectrometry, high performance liquid chromatography, electrophoresis, mass spectrometry, flow injection analysis etc. can be used for the analysis purpose, but, all these techniques are complex, expensive and require pre-treatment of the samples. These facts force the researchers to develop simple, fast, cost effective and highly sensitive electroanalytical techniques for the determination of aforementioned species. The main aspects taken care in this work are the use of thin metallic films, nanoparticles, reduced graphene oxide and composite materials to enhance the sensitivity of the electrodes; minimum loading of the modifiers; utilization of easy techniques for modification (electrochemical deposition, drop-casting etc.); improvement of sensitivity towards the analyte of interest (metal ions, bio molecules etc.); improvement of detection limits for the analyte; development of simple methodologies for the analysis; development of methodologies based on the modified electrodes which are free from the commonly occurring interfering agents; fabrication of electrodes which are mechanically and chemically stable and can be used for onsite application for the analysis; to study effects of surfactants and last but not the least investigation of electrochemical properties and adsorption-desorption behaviour of the biomolecules. For all the sensors developed, the various parameters studied include linear dynamic range, detection limit, effect of pH, effect of scan rate and interference from foreign species. The fabricated electrodes and the methodologies have been applied in real samples.

# Chapter II

## *Experimental*

## II. 1. Introduction

A brief sketch of the materials and methods used in the investigations is presented in this chapter. The instrumentation, devices and the electrode systems used are discussed. The general methods for the fabrication of the modified electrodes are presented in the chapter. Special emphasis is given on the practical aspects of preparation of carbon paste electrodes (CPE) from the graphitic carbon powder. Synthesis procedure of the graphene oxide from graphite powder is described and the procedure of modification of the CPE using reduced graphene oxide and carbon nanotubes are presented. A brief account on the electrochemical, microscopic and diffraction techniques used for the characterization of surface of the electrodes is discussed. Methods used to determine electrochemical surface area of the electrodes, diffusion coefficient, electron transfer rate constant and analytical treatment to the recorded data are detailed.

## II. 2. Reagents and Solutions:

The reagents and the solvents used were of analytical and/or spectroscopic grade. These were purchased from the local vendors. Bismuth nitrate ($Bi(NO_3)_3$), acetic acid ($CH_3COOH$), potassium hydroxide ($KOH$), potassium ferrocyanide ($K_4Fe(CN)_6$), boric acid ($H_3BO_3$), phosphoric acid ($H_3PO_4$), potassium nitrate ($KNO_3$), sodium acetate ($CH_3COONa$), zinc nitrate ($Zn(NO_3)_2$), potassium chloride ($KCl$), cadmium nitrate ($Cd(NO_3)_2$), lead nitrate ($Pb(NO_3)_2$), cupric nitrate ($Cu(NO_3)_2$), antimony trichloride ($SbCl_3$), mercuric nitrate ($Hg(NO_3)_2$), sodium di-hydrogen phosphate ($NaH_2PO_4$), di-sodium hydrogen phosphate ($Na_2HPO_4$) were of high purity BDH Aristar quality. Gold chloride salt (50% gold content) used for gold nano particles was of spectroscopic grade, Sigma and 2,4,6-Triamino-1,3,5-triazine (Melamine) used were of E. Merck G R grade. Multiwalled CNT (length 20nm and diameter ~15nm) were purchased from Nanostructured and Amorphous materials Inc., Texas, USA. Nafion (5% solution) was purchased from E. MERCK. Deionized water was used for preparation of all the aqueous solutions. Concentrated sulphuric acid ($H_2SO_4$), glacial phosphoric acid ($H_3PO_4$), potassium permanganate ($KMnO_4$), hydrochloric acid (HCl) and 30% hydrogen peroxide ($H_2O_2$) were of AR grade and purchased from S.D. fine chemicals for the preparation of graphene oxide. AR grade sodium borahydride ($NaBH_4$) used for preparation of reduced graphene oxide (RGO) was purchased from S.D. fine chemicals. Graphitic carbon nano spheres (CNSs) used for functionalization were of 'VULCAN XC 72 R', Suprapur HCl, $HNO_3$ & $H_2SO_4$ were of E. MERCK. Dopamine (DA), uric acid (UA) and L-Ascorbic acid (AA) were of spectroscopic grade from Sigma-Aldrich. L-Cysteine (CYSH) (98%) was purchased from AVRA Chemicals. Glassy Carbon electrode was purchased from CHI Instruments. TX 100, CTAB (95%) and SDS (99%) surfactants were of Sigma.

Acetate buffer solutions of pH 3.5 to 5.5 were prepared by mixing various proportions of 0.1 M $CH_3COOH$ and 0.1M $CH_3COONa$. Phosphate buffer solutions (PBS) of desired pH from 6 to 10 were prepared by mixing various proportions of 0.1M $NaH_2PO_4$ and 0.1M $Na_2HPO_4$. Britton-Robinson buffer solutions (BR buffer) were prepared by mixing of 0.1M $H_3PO_4$, 0.1M $H_3BO_3$ and 0.1M $CH_3COOH$. The desired pH (from pH 2 to 12) was achieved by addition of 1M KOH or HCl.

### II. 3. Instrumentation:

All the electrochemical measurements were carried out on Autolab PGSTAT 320N electrochemical system interfaced to a personal computer (PC). Data acquisition and analysis were performed by GPES 4.9 software. The apparatus used for the purpose was an electrolytic cell with conventional three electrode system. Modified carbon material based electrodes were used as WE, platinum rod as CE and saturated calomel electrode (SCE) or silver/silver chloride electrode (Ag/AgCl/KCl (satd)) was used as RE. The RE was kept very near to the WE to minimize the error due to potential drop. CE was kept away from the WE so as to avoid any chances of mixing of the reaction product from the CE. The potentiostat was calibrated periodically by using a dummy cell (a network of resistor and capacitor that gives a known result) as per the user manual supplied by the manufacturing company. Further verification of the software and the general performance of the instrument and electrodes was done using redox behavior of 50μM $K_4Fe(CN)_6$ solution in 0.1M KCl medium.

### II. 3. 1. Basic working principle of the potentiostat/galvanostat (PGSTAT):

In potentiostatic mode, a potentiostat/galvanostat (PGSTAT) accurately controls the potential of the counter electrode (CE) against the working electrode (WE) so that the potential difference between the working electrode (WE) and the reference electrode (RE) is well defined, and correspond to the value specified by the user. In galvanostatic mode, the current flow between the WE and the CE is controlled. The potential difference between the RE and WE and the current flowing between the CE and WE are continuously monitored. By using a PGSTAT, the value specified by the user (i.e. applied potential or current) is accurately controlled, anytime during the measurement by using a negative feedback mechanism. As can be seen from the diagram, the CE is connected to the output of an electronic block which is called Control Amplifier (CA). The control amplifier forces current to flow through the cell. The value of the current is measured using a Current Follower (Low CF) or a Shunt (High CR), for low and high currents, respectively. The potential difference is measured always between the RE and WE with a Differential Amplifier (Diff amp). Depending on the mode the instrument is used (potentiostatic or galvanostatic) the PSTAT/GSTAT switch is set accordingly. The signal is then fed into the summation point (Σ), which together with the waveform set by the digital-to-analog converter (DAC) are used as an input ($E_{in}$) for the CA (Fig. II.1).

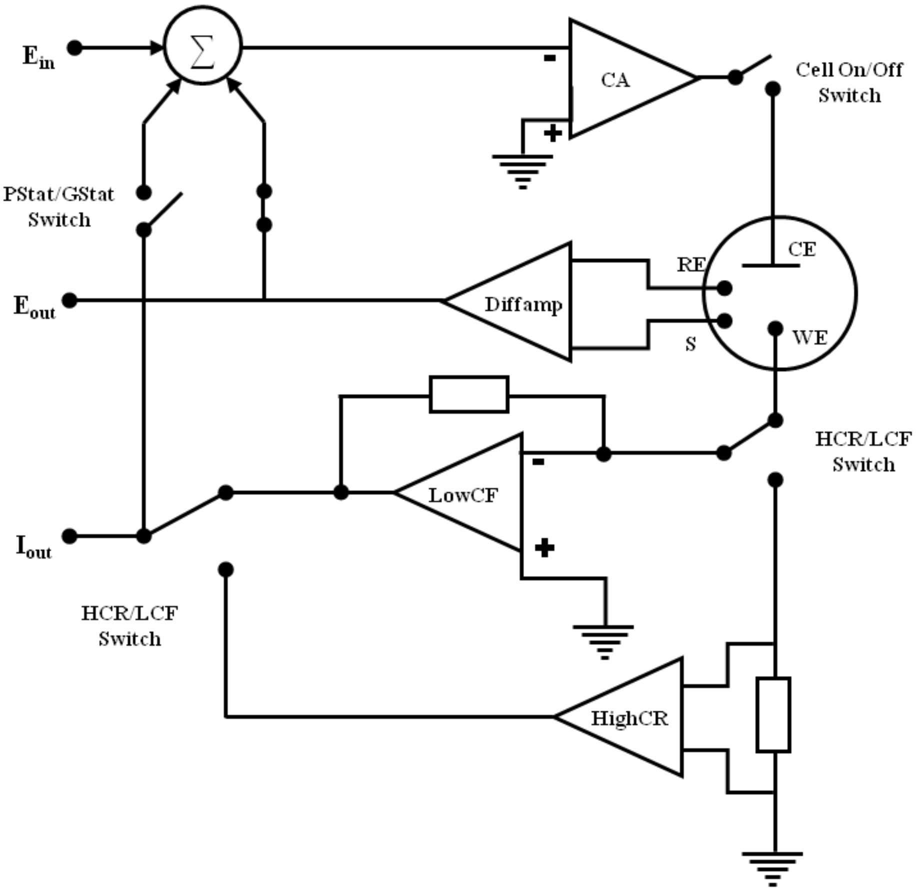

**Figure II.1:** Block diagram of potentiostat/galvanostat

### II. 3. 2. Working principles of the reference electrodes used:

- **Saturated Calomel Electrode:**

Saturated calomel electrode (SCE) was used for most of the studies presented in the thesis. It is a half cell composed of mercurous chloride ($Hg_2Cl_2$, calomel) in contact with mercury and KCl in a paste form. The paste was dipped under a saturated solution of potassium chloride (KCl). A platinum wire is generally used to allow contact to the external circuit. The half cell reaction is described as

$$Hg_2Cl_2(s) + 2e^- \leftrightharpoons 2Hg(l) + 2Cl^-(saturated)$$

with an $E^O$ value of +0.244V. Contact to the experimental solution was made by using a porous glass frit which allows the ions to pass but not the bulk solution. The potential of the

SCE was regularly checked by comparing its potential with that of the SCE commercially available. If the potential difference is more than 5mV, the prepared SCE was considered to be faulty.

- **Silver/Silver Chloride Electrode:**

Silver/silver chloride electrode (Ag/AgCl/KCl) was fabricated by dipping a silver chloride (AgCl) coated silver wire into a solution saturated with KCl. Contact to the experimental solution was made similarly by using a porous glass frit which allows the ions to pass but not the bulk solution. The pertinent half cell reaction is

$$\boldsymbol{AgCl(s) + e^{-} \leftrightharpoons Ag + Cl^{-}(saturated)}$$

The theoretical $E^{O}$ value is 0.224V, but, the actual potential of the half cell prepared in this way is 0.197V, because in addition to the KCl, AgCl also contributes to the chloride activity which is not exactly unity.

Both the SCE and the Ag/AgCl/KCl reference electrodes offered stable half-cell potentials that did not change over time. In addition, the loss of electrolyte due to evaporation did not change the saturated nature of the solution, nor the potential.

### II. 3. 3. Counter Electrode:

CE (Pt rod, 99.99% purity) was purchased from Metrohm. After each experiment the CE was cleaned with 0.5M $HNO_3$ and de-ionized water under sonication (20KHz) to get a clean and identical surface every time.

## II. 4. Carbon Paste Electrode (CPE) as working electrode:

In the present work carbon paste electrode (CPE) has been extensively used as the WE. Carbon paste is a homogeneous mixture of carbon (graphite) powder and a binder (pasting liquid) [45-47]. It is compacted into a suitably designed holder which constitutes CPE. CPEs are widely applicable in electrochemical studies due to their low background current (compared to solid graphite or noble metal electrodes), low cost, feasibility to incorporate different substances during the paste preparation (in the case of modified CPEs), easy preparation, simple renewal of their surface and possibilities of miniaturization [48].

### II. 4. 1. A brief background of the Carbon Paste Electrode:

The carbon paste electrode (CPE) was invented by Ralph Norman Adams, University of Kansas in Lawrence, at the end of the 1950s [49, 50]. Adams had the original concept to develop a dropping carbon electrode (DCE), which would have simulated the function of the DME for anodic oxidations of organic compounds, where the mercury-based electrode could not be employed [49, 51]. The experiments with the DCE, performed mainly by Adams's student Kuwana [52], had finally led to the invention of a new electrode material, carbon paste, whose properties were already close to those expected for the original concept, the dropping carbon dispersion. Carbon paste has been widely applied in electrochemistry mainly as a substitute for noble metals because, depending on the supporting electrolyte, it can be used at both positive and negative potentials ranging from -1.4V to +1.7V against the SCE [53]. The early studies of Adam's group dealt with the various constituents of the carbon paste and their application in anodic and cathodic stripping voltammetry [50, 54]. Their work on carbon paste electrode got the world wide popularity and over the last five decades carbon paste electrodes became one of the most popular electrode materials used for the laboratory preparation of various electrodes, sensors, and detectors [55].

### II. 4. 2. Constituents of the Carbon Paste:

Powdered carbon (graphite) is the main carbon paste component, which ensures the proper function of an electrode or a sensor in electrochemical measurements. Other than graphite powder, other carbonaceous materials are used for preparation of the carbon paste. Suitable carbonaceous materials should have the following criteria:

i) Particle size in micrometers or sub micrometers, ii) uniform distribution of the particles, iii) high chemical purity, and iv) low adsorption capabilities. Naturally, the type and quality of graphite used, as well as its overall amount in the carbon paste mixture, are reflected in all typical properties of the respective mixture.

From the introduction of CPEs in electrochemical science up until now, the most often selected carbon powder is spectroscopic graphite with particles in the low micrometric scale (typically, 5 – 20 mm). It can be estimated that 80 – 90% of carbon pastes reported had been made from such graphites [56, 57]. So far, the carbon paste mixtures were prepared from: i) soot and charcoal [51, 58], ii) acetylene black [59], iii) glassy carbon powders with globular particles [60, 61], iv) pulverized diamond of both natural and synthetic origin [62], v) template carbon, vi) porous carbon foam, vii) carbon microspheres [63], viii) fullerenes (C-60) [64], ix) carbon nanofibres [65] and x) various types of carbon nanotubes [66-70].

Traditional carbon pastes contain organic liquids which link mechanically the individual carbonaceous particles. These liquids are often called pasting liquids or binder. However, beside this main function of holding the particles together inside the paste, the binder as the second main moiety of carbon paste also co-determines the properties of the carbon paste. Typical parameters required for pasting liquids are:

i) Chemical inertness and electro-inactivity, ii) high viscosity and low volatility, iii) minimal solubility in aqueous solutions, and iv) immiscibility with aqueous and organic solvents.

Bromophenol was used as the binder for the fabrication of the first CPE [49]. The most popular binding agents used for preparation of carbon pastes are mineral (paraffin) oils;

namely, i) Nujol and ii) Uvasol. 70% carbon paste mixtures have been made of these mineral oils. Other potentially applicable liquids are i) aliphatic and aromatic hydrocarbons, including their iv) halogenated derivatives, as well as v) silicone oils and greases [49, 51, 58], or nearly solid silicone rubbers [71], vi) organic esters of the organophosphate and dialkyl phthalate type [72]. Apart from these binders some electrolytes e.g. $H_2SO_4$ [73] and ionic liquids [74] are now being used as the binders.

### II. 4. 3. Classification of Carbon Paste Electrode:

CPEs can be classified into two categories, i) Unmodified CPE and ii) Modified CPE.

#### II. 4. 3. 1. Unmodified Carbon Paste Electrode:

Mixtures containing merely two main components, carbon powder and the liquid binder, are now commonly classified as unmodified carbon pastes. Carbon is usually represented by spectroscopic graphite powders or related materials and acts as the electro active sensing site of the paste. In the classical conception, the binder (pasting liquid) is a lipophilic organic liquid. One can name aliphatic hydrocarbons and their mixtures [53, 75] as typical representatives of such substances. Such types of CPEs are often known as bare CPEs or virgin CPEs. In order to lower adsorption capabilities of graphite, adsorbed oxygen can be removed by heating in vacuum with subsequent stabilization by impregnating with a ceresin wax [76]. This is done prior to the addition of binder. The nature and behaviour of the carbon paste electrodes can be portrayed by its physicochemical properties such as microstructure of the carbon paste, specific ohmic resistance, stability of the paste in aqueous and non aqueous media, ease of renewability and ageing of the paste. The heterogeneous mixture of carbon paste can be classified as solid dispersion. Investigation of microstructure of carbon paste revealed that the graphite particles are coated with the thin film of the binder liquid. The graphite particles are connected physically to each other by the thin layer of the binder. The consistency of the carbon paste also plays an important role to determine its physicochemical properties. Consistency can be correlated with the compactness of the paste. Consistency of the paste depends upon the components used to fabricate the paste, their size distribution, graphite powder to binder liquid ratio and extent of homogenization. Although the consistency as such is not directly associated with the resultant electrochemical behaviour of carbon pastes, this physical parameter may indicate some important consequences. For example, too "dry" as well as too "liquid" paste mixtures are very difficult to be packed to make an electrode, and moreover, the surface of such pastes is usually not renewable in reproducible way [75, 77]. Despite the presence of typically insulating binders common carbon paste mixtures exhibit a very low ohmic resistance. The carbon pastes made of paraffin oil had the average resistances of 20 ‐ 50 Ω, whereas some silicon oil-based CPEs were reported to have the resultant values even below 10 Ω. Exact reason for such a high conductivity is not known, although, there were several different hypotheses; for example, i) percolation theory, concerning the movement of fluids through porous materials, ii) tunnelling effect etc. None of them were unambiguously experimentally proven. It also seems that minimal resistance of carbon pastes can be explained via the tightest systematic arrangement of spherical particles. High ohmic resistance produces high background current while doing voltammetry; on the other hand the stable electrochemical signal is not observed in potentiometry. High resistance may arise due to unsuitable combination of the graphite powder and the binder, lack of compactness of the electrode fabricated (presence of air gap/adsorbed gases), inconsistency and insufficient homogenization of the graphite particles in the mixture. Ageing of the carbon paste has significant role to its physicochemical behaviour. Ageing may lead to the inconsistency of the paste and the unstable and non reproducible electrochemical behaviour. Volatility of the binder causes ageing of the paste. Less volatile binder (e.g. silicone oil) provides longer life against ageing of the paste [78].

Proper storage of the electrode also proved to be effective. Due to lipophilic behaviour of binder composition of the carbon paste electrode has high significance on its electrochemical response. Carbon pastes containing Nujol or silicone oil exhibit background currents of about 10-500 nA [51] whereas the background of tricresyl phosphate-based CPE may exceed the current level of tens of μA [79] per square cm.

### II. 4. 3. 2. Modified Carbon Paste Electrode:

When a foreign constituent is added into the binary mixture of carbon paste modified carbon paste electrodes (MCPE) are obtained. The modifying agent is generally one substrate, but, in some special cases more than one modifier is also used, e.g. carbon paste based biosensors containing enzyme together with appropriate modifier [80] or MCPEs with two modifiers [81]. Modified electrodes are of two types i) chemically modified CPE (CMCPE) and ii) biologically modified CPE or carbon paste biosensors. The modification of carbon paste electrodes began in 1964 with the fundamental studies of Kuwana and co-workers [82, 83]. Adams et al introduced surfactant into the carbon paste as a stabilizer against the disintegration of the paste in the organic solvents [84]. It was Cheek and Nelson [85] who prepared CPE made of chemically pre-treated graphite (with functional groups immobilized on its particles). This is in reality the first representation of CMCPE with an accomplishment of specific interaction with the analyte of interest. In the stripping voltammetric mode, their innovative concept enabled a highly effective accumulation of target ions down to the sub-nM level. In 1981, Ravichandran and Baldwin suggested a simpler method of direct mixing of the modifier into the plain carbon paste [86]. The idea was to mix an insoluble particulate component into the carbon powder. This simple method of bulk modification attracted a lot of electrochemists in the successive years. The first carbon paste based biosensor (oldest configuration) was prepared by Yao and Musha by modifying the carbon paste electrode with nicotinamide adenine dinucleotide [87]. Incorporation of enzyme for the bulk modification of carbon paste electrode to prepare carbon paste based biosensor was first reported by polish scientists in 1988 [88]. Later on different methods for the preparation of CMCPEs and carbon paste based biosensors with different chemical and biological modifiers have been evolved and successfully used for the sensor applications in the last three decades.

The primary purpose behind modifying an electrode is to improve its analytical performance either by increasing its sensitivity and selectivity or by protecting the surface from unwanted reactions. According to Kalcher [53] there are four main reasons for modifying CPEs involving typical modifier-substrate interactions which enhance the analytical performances of the electrodes:

- Preferential entrapment of the desired species.
- Mediation of electrochemical reactions via immobilised molecules or their fragments.
- Exploitation of catalytic electrochemical responses/ acting in catalytic reactions.
- Alteration of the surface characteristics of a CPE.

### II. 4. 3. 2. a. Different substances for modification of Carbon Paste Electrode:

Carbon paste offers a wide spectrum of possible modification by a diversity of substances. These modifiers are listed below:

- **Metal and metal oxides and fluorides:** Here carbon paste electrode acts as a conducting substrate and the surface of the electrode is modified with metallic films or metal oxide films. These types of modified electrodes are mainly used for stripping voltammetry analysis of metal ions. Hg [88], Bi [89, 90], Sb [91, 92], have been used for surface modification of the carbon paste. On the other hand HgO was mixed with the paste to form Hg thin film on carbon paste electrode [93]; $Sb_2O_3$ and $Bi_2O_3$ [94] were used for bulk modification of the electrode. AuF-CPE, SbF-CPE, BiF-CPE, $RuO_2$-CPE, $TiO_2$-

CPE, $PbO_2$-CPE, $ZrO_2$-CPE, $Al_2O_3$-CPE are few modified CPEs to name under this group.

- **Commonly used analytical reagents:** Classical analytical reagents like dimethylglyoxime [95], 8-hydroxyquinoline [81, 96, 97], dithizon [98, 99], diphenyl carbazide [100, 101] oxine [102-104], PAN [105, 106], Pyrogallol red [107] or derivatives of 2-naphthol [108] have been used as selective modifiers for adsorptive accumulation of selected ions. Some compounds of this type contained in the paste may be slightly soluble in water and, hence, have to be stabilised against "bleeding" (dissolution) by fixing with an additional adhesion agent [81].

- **Clay Minerals (Zeolites and Familiar Materials):** These substances are capable of acting as both ion-exchangers and "ion-traps" excluding ion species of inappropriate size. Moreover, zeolites [109, 110] and related materials (e.g., montmorrilonite [111, 112] or vermiculite [113]) also exhibit adsorption and catalytic capabilities. Due to these synergistic effects, zeolites have become apparently the most frequently used modifiers. Carbon pastes with dispersed zeolites (up to 50% w/w) can be employed to study the behaviour of numerous inorganic ions in their natural environment when zeolite-modified CPEs are applicable to their speciation in real samples.

- **Ion exchangers and surfactants:** Ion exchangers having ion exchange and ion pairing ability proved to have very significant role in modifying carbon paste electrodes. Amberlite LA-2 [114], Dowex 50W [115], tricresyl phosphate [116] have been used for this purpose. Ionic surfactants having ion pairing capability (e.g. CTAB [117] and SDS [118]) are also used to modify the electrode. On the other hand non ionic surfactant (Triton X 100) [119] are also used as modifier to enhance lipophilicity.

- **Macro cyclic ligands and macromolecules:** Different macro cyclic ligands such as crown ethers [120], cyclodextrines [121], calixarines [122] are used as modifiers for their suitable host-guest chemistry. Humic acids [123] also play the role of electrode modifiers.
- **Conducting polymers:** Different conducting polymers e.g. polyaniline [124], poly pyrrole [125], PEDOT [126] are used as modifiers; these polymers can be prepared both electrochemically and by chemical reactions.
- **Organometallic substances:** Ferrocene and ferrocene derivatives [127, 128], complexes of pthalocyanine [129] and porphyrine derivatives [130] are used as modifiers.
- **Biological modifiers:** Usually enzymes or enzyme containing tissues are most common modifiers such as glucose oxidase (GOD) [131], tyrosinase [132], polyphenol oxidase [1333], horse radish peroxidise (HRP) [134], alcohol dehydrogenase [135], lactate oxidase etc. DNA (deoxyribonucleic acid) [136] is very useful substrate for carbon paste biosensors.
- **New generation modifiers:** Application of materials prepared from newer technologies has become a trend in fabrication of modified electrodes. Development of easier technology and attractive physical and electrochemical properties of newer carbon materials such as carbon nanotubes, carbon dots, graphene oxide, carbon nanofibres etc. have drawn the attention of the scientists to use those materials as modifiers or as constituent for CPEs [137-140]. Apart from those carbonaceous materials metallic and bimetallic nanoparticles [141-143] have been used extensively for the modification of the CPEs. Metallic oxide nanoparticles are also being tested as the modifiers [144, 145]. Polymer composites with the metallic nanoparticles, carbon nanotubes are also being used as modifiers [146, 147]. Ultrathin multilayer films of Mo(VI)-polyoxometalate type [148] and supramolecular helical chains [149] have been used as well.

### II. 4. 3. 2. b. Possible ways to modify Carbon Paste Electrode:

Different methods have been adopted to modify the CPEs [55]. These methods are discussed in brief in the following sections.

- **In situ modification:** Here modifiers are added to the solution and the bare carbon paste surface is exposed to the modifier. Hydrophobic carbon paste may entrap the lipophilic modifiers [150].
- **Bulk modification:** Modifier is directly mixed into the paste bulk mechanically. The bulk modification leads to the high extent of homogeneity and the uniformity of the modifiers in the mixture. Usually, the content of modifiers in carbon pastes varies between 1 – 5% (w/w) [77]; however, there are MCPEs with 30 – 50% of the respective modifier [151] and if some chemically active binders are considered as special modifiers, the resultant content can be yet higher, up to 70% [72].
- **Dissolution:** here the modifiers get dissolved into the pasting liquid and then mixed with the graphite powder/ carbonaceous powder to form paste. CPEs modified with ion exchangers such as Dowex 50W, Amberlite LA-2 etc. are few examples of such modification [114, 115]. Modification by lipophilic substances can also be done by the method [119].
- **Impregnation:** Graphite particles are soaked with a solution containing dissolved modifier. After evaporation of solvent, pre-treated carbon powder is mixed and homogenized with the liquid binder [152].
- **Chemical pre-treatment:** Here the graphite powder is chemically treated so as to form chemical bonds between modifiers and graphite particles. In this way of modification some functional groups or some molecules get anchored into the graphite particles. The

biggest advantage is that the modifiers do not leach out of the paste due to the formation of the chemical bond [153].

- **Electrolytic activation (anodization/cathodization):** It involves forced electrode oxidation or reduction to make hydrophilic sites on the carbon paste surface those are able to repel hydrophobic molecules of the binder from the outer layer [154].
- **Casting:** This is only restricted to the modification of surface. These can be of two types e.g. i) manual casting and ii) casting by electrochemical deposition. The first case involves dispersion of the modifier into a suitable solvent and layering of the dispersion on the electrode surface mechanically. Evaporation of the solvent produces thin layer of the modifier on the electrode surface. In the later case the modifier is electrochemically deposited directly on the electrode surface from its precursor solution. Metallic thin film modified CPEs [88, 92] are some examples of this kind. Modification by electro-polymerization [124] can also be included under the second category of casting.
- **Multiple modifications:** This is a step by step modification of carbon paste electrode using the methods mentioned early. The main aim for these types of modification is to get higher sensitivity, selectivity and specificity towards the analytes of interest [115, 117, 155]. Both CMCPE and carbon paste biosensors can be made by multiple modification.

### II. 4. 4. Practical aspects of preparation of a bare CPE:

Fabrication of a practically usable good CPE depends upon few parameters [78]:

- Choice of graphite powder,
- Choice of binder liquid,
- Choice of graphite to binder ratio,
- Extent of homogenization during preparation of the paste and
- Fabrication of compact electrode by filling the holder with the paste.

Importance of all these parameters is discussed in the earlier sections.

### II. 4. 5. Typical properties and specifics of CPEs in electrochemical measurements:

Physicochemical properties of carbon pastes are always mirrored in the overall electrochemical behaviour of CPEs, resulting in some special features and benefits as mentioned below [55].

- **Background signal (residual current):** Common type of bare CPEs and CMCPEs provide very low background, typically below 1μA. Better signal to noise ratio is obtained for faradaic measurement. But, it may vary with the pH and concentration of the solution.
- **Individual polarizability:** Polarizability of the CPEs greatly depends on the composition of the paste (quality of the graphite powder, nature of binder, graphite to binder ratio). Therefore, variable potential windows can be obtained for the CPE depending on its composition and supporting electrolyte.
- **Specific reaction kinetics:** carbon pastes have typically hydrophobic surface which, in aqueous solutions, repel hydrophilic species involved in the electrode reaction of numerous redox systems of both inorganic and organic origin. Thus the specific reaction kinetics depends upon the carbon paste composition and the quality of the both main components.
- Various alternative procedures for pre-treating, conditioning and regenerating the electrode surface and carbon paste itself.
- Variability in utilising various interactions and their synergistic effects at both CPEs and MCPEs such as electrolysis, catalysis, adsorption, extraction, ion-pairing, and their combination.

### II. 4. 6. Preparation of the bare Carbon Paste Electrode:

The spectroscopic grade 0.5 g graphite powder taken in a quartz boat was heated at $400^{O}C$ for 4 hrs in an inert atmosphere ($N_2$ atmosphere). After heating, the powder was transferred to a beaker containing high purity paraffin dissolved in n-hexane. The mixture was kept in a fume hood maintained at negative pressure and the n-hexane was allowed to evaporate. After that the mixture was kept under a hot air blower for complete removal of n-hexane. Heating removed the adsorbed gases from the surface of the carbon paste and upon paraffin impregnation the re-adsorption of gases is minimized. An optimized amount of ~1.5% (wt %) of paraffin wax was added to the carbon powder. After paraffin impregnation, the required quantity of silicone oil was added as the binder (25% of the total mass of the binder and carbon powder) and ground well to get a homogeneous paste. The carbon paste was filled into a glass tube with 1.5/2 mm diameter from the bottom end. A platinum wire was used to connect the carbon paste electrode to the instrument. The proportion of silicone oil to the mass of the graphite powder plays an important role in determining the electrochemical properties of the fabricated electrode. The proportion of the silicone oil to the total mass of the paste (mass of binder and carbon powder) was varied from 10% (wt %) to 40% (wt %). The performance of the electrode fabricated from the paste was checked monitoring the redox behaviour of the 50µM $K_4[Fe(CN)_6]$ in 0.1M KCl solution. $[Fe(CN)_6]^{3+}/[Fe(CN)_6]^{4+}$ is well known electrochemically reversible couple. The electrode with the 25% (wt %) silicone oil content in the carbon paste matrix showed the reversible nature of the couple (Fig. II.2). The anodic and the cathodic peak potentials remained unaltered upon the variation of the scan rate from 10mV $sec^{-1}$ to 500mV $sec^{-1}$, $\Delta E_p$, the difference between the anodic and the cathodic peak potential, was 66 mV, which was very close to the expected value of 59.1mV and $I_{pa}/I_{pc}$ (the ratio of peak currents) was 1.012. With higher content of the oil $\Delta E_p$ increases and $I_{pa}/I_{pc}$ deviates more from unity. Although the lower content of the binder oil showed expected reversibility of the redox couple, frequent drying of the paste and lack in compactness and consistency of the paste made the electrode unsuitable for renewability of the surface and longer usage purpose. In view of these facts the oil content was optimized at 25% (wt %) of the total mass of the paste. The plot of peak current against the square root of the scan rate (Vsec$^{-1}$) followed a linear regression equation as $I_{pc} = 3.67\times10^{-4}\upsilon^{1/2} + 9.68\times10^{-6}$ with $R^2 = 0.998$.

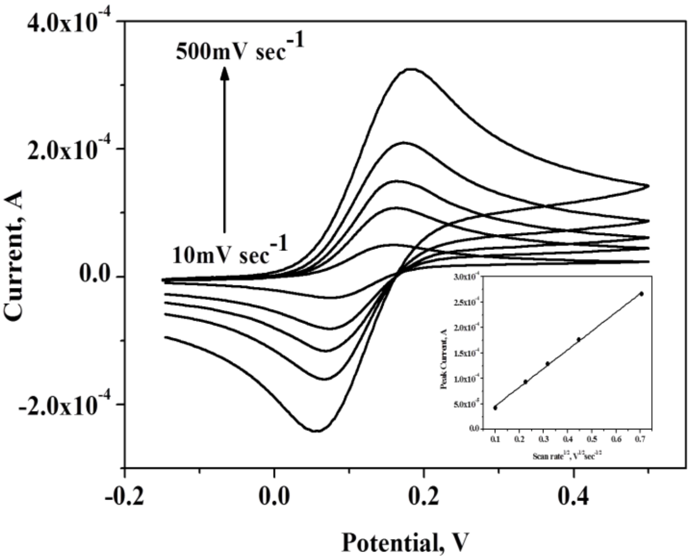

**Figure II.2:** Voltammogram of $K_4[Fe(CN)_4]/K_3[Fe(CN)_3]$ couple on CPE, inset: plot of oxidation peak current vs. square root of scan rate

- **Regeneration of carbon paste surface:** Electrode surface was regenerated by peeling the paste from the surface and pressing new carbon paste on the top of the carbon paste pool of the electrode. Reproducibility of the surface was checked each time from the redox behaviour of the $[Fe(CN)_6]^{3+}/[Fe(CN)_6]^{4+}$ couple.
- **Ageing:** Carbon paste was prepared using less volatile, highly viscous silicone oil as binder liquid. The paste was kept inside an air tight container to avoid evaporation of the binder oil. The same carbon paste was used for more than 6 months.

- **Storage of the electrode:** After the fabrication of CPEs, the electrodes were stored into air tight containers with the electrode surface dipped into nano pure water.

In the present work modifications of the CPEs were carried out by different species based on the requirements. The individual modification and characterization of the modified surface is discussed in the respective chapters.

### II. 5. Graphene Oxide (GO) and Reduced Graphene Oxide (RGO):

Graphene is a one atom layer thick carbon sheet, two-dimensional crystal. Graphene has been considered as basic building block for all $sp^2$ graphitic materials including fullerenes, carbon nanotubes and graphite [156]. Ever since its discovery in 2004 graphene has been making a profound impact in many areas of science and technology due to its remarkable physicochemical properties These include a high specific surface area (theoretically 2630 $m^2/g$ for single-layer graphene) [157-159], extraordinary electronic properties and electron transport capabilities, unprecedented pliability and impermeability, strong mechanical strength and excellent thermal and electrical conductivities [160-166]. These unique physicochemical properties suggest that it has great potential for providing new approaches and critical improvements in the field of electrochemistry. The high surface area of electrically conductive graphene sheets can give rise to high densities of attached analyte molecules. This in turn can facilitate high sensitivity and device miniaturization. Facile electron transfer between graphene and redox species opens up opportunities for sensing strategies based on direct electron transfer rather than mediation.

Currently, many methods had been explored to prepare graphene. Novoselov and Geim [167] firstly observed a single layer of graphene from highly oriented pyrolytic graphite using micromechanical exfoliation method. It is a simple way to prepare graphene, but the yield of graphene was very low, and cannot achieve high-quality industrial production. Srivastava et al. [168] prepared “petal” graphite sheet with ~ 20nm thickness by chemical vapor deposition (CVD). Even though thickness of graphite sheet prepared by CVD method significantly decreased than ever, impurities of Ni element in graphite sheet was another new problem. Solvent stripping method [169] is a new approach that emerged in recent years. Its principle is destroying Van der Waals Force between the graphite layers in a solvent to obtain graphene sheets. Method of solvent stripping does not destroy the structure of the graphene and presents no surface defects in the graphene sheet. However, the low yield of graphene is still a drawback. Chemical oxidation method [159, 170-175] is the most popular method to prepare graphene. In this method graphene oxide (GO) is produced which can be considered as a precursor for graphene synthesis by either chemical or thermal reduction processes. GO consists of a single-layer of graphite oxide and is usually produced by the chemical treatment of graphite by strong oxidising chemicals, followed by subsequent dispersion and exfoliation in water or suitable organic solvents [176, 177]. Chemical oxidation introduces functional groups such as carbonyl, hydroxyl, epoxy and peroxyl in between the carbon layers of graphite. These functional groups weaken the Van der Waals bond between the carbon layers which causes the graphene layers to peel off layer by layer from graphite [178]. The precise atomic structure of GO is still uncertain due to uncertainty pertaining to both the nature and distribution of the oxygen-containing functional groups [179], its non stoichiometric atomic composition (depends on the synthesis protocol and extent of reaction) and the lack of sufficiently sensitive analytical techniques for characterizing the GO structure. Compared to pristine graphene, oxygenated functional groups in GO can indeed give rise to remarkable structure defects which is associated with loss in electrical conductivity in GO, which possibly limits the direct application of GO in electrically active materials and devices. Presence of oxygenated groups in GO is also responsible to alter electronic and mechanical properties of pristine graphene. However, presence of the oxygenated functional groups provides potential advantages when fabrication of modified electrodes is concerned. Polar oxygenated functional groups make GO highly hydrophilic; this gives GO very high dispersibility to many polar solvents, mainly to water. The resulting GO dispersion can be subsequently deposited on various substrates in order to prepare thin films by means of common methods such as drop-casting, spraying, or spin-coating. Thus it can be used as a very good electrode modifier. In addition, using well-known strategies, these functional groups can be modified or functionalized which can be employed to immobilize various electroactive species through covalent or non-covalent bonds for the design of sensitive electrochemical sensors. Although the GO provides such advantages, due to the presence of a high degree of disorders in pristine graphene structure arising from the incorporation of $sp^3$ carbon they exhibits high sheet resistance ($R_S$) (1012 $\Omega$ $sq^{-1}$ or more) [180]. This in turn represents transport barriers leading to the absence or disruption of percolating pathways among the $sp^2$ carbon clusters, which allows classical carrier transport to occur [181]. The reduction of GO (i.e. removal of oxygen) using a variety of chemical and thermal treatments, which facilitates the carrier transport to occur, can result in a decrease in ($R_S$) by several orders of magnitude and hence transform the material into a semiconductor and ultimately into a graphene-like semimetal [182-185]. The conductivity of the reduced GO (RGO) samples can reach ~1000 S/m [185, 186]. Due to the very high conductivity RGO has been used for fabrication of highly sensitive modified electrode.

### II. 5. 1. Introduction on the preparation of GO by Chemical oxidation method:

As discussed in the earlier paragraph, synthesis of graphene oxide involves the separation of graphite layers, by way of rupturing Van der Waals force of attraction between the layers, by oxidising the layers of graphite. The origin of graphite oxidation came into view, when Brodie [187] in 1859 first reported oxidation of graphite by addition of $KClO_3$ into slurry of graphite in fuming $HNO_3$. The C/H/O ratio of the oxidation product was determined to be

2.19/1.00/0.80, which is the typical composition of graphite oxide [188]. About 40 years later, Staudenmaier [189] modified the Brodie method by using concentrated $H_2SO_4$ and fuming $HNO_3$ as the oxidizing agents. This modified Brodie method required slow addition of the (potassium chlorate) $KClO_3$ over a period of one week. In the following decades, many other similar methods have been reported [190, 191]. The method most commonly used today was reported by Hummers in 1958 [172]. In the Hummers method, preparation of graphite oxide was accomplished by treating graphite with essentially a water-free mixture of concentrated $H_2SO_4$, $NaNO_3$ and $KMnO_4$. Compared to the Brodie-Staudenmaier methods, the Hummers method requires less than 2 hrs for completion at temperatures below 45° and can be carried out safely. These three methods are the primary routes to prepare graphite oxide from graphite. However, all three reactions involve the liberation of toxic gas $NO_x$ and/or $ClO_2$. Some modifications based on the Hummers method have been proposed. Kovtyukhova [192] added a pre-oxidized procedure using $H_2SO_4$, $K_2S_2O_8$ (potassium persulphate), and $P_2O_5$. The C/O ratio of the oxidation product was 4.0/3.1, illustrating that this was richer in oxygen than the graphite oxide prepared by the Hummers method. The method proposed by Kovtyukhova is defined as a typical modified Hummers method and has been cited by many researchers in recent years [193-195]. In 2010, Marcano [196] found another method by adding $H_3PO_4$ to the formation of graphene oxide nanoribbons (GONRs) from multiwalled carbon nanotubes; it shows that more GONRs were produced with more intact graphitic basal planes [197]. This modified Hummers method (sometimes called improved Hummers method), using $KMnO_4$, $H_2SO_4$, and $H_3PO_4$ as the oxidizing agents, avoids the release of $NO_x$ and yields a greater amount of hydrophilic oxidized graphite material compared to the original Hummers method. Due to its simpler protocol and equivalent conductivity upon reduction, this newly modified Hummers method is attractive for preparation of GO on a large scale [198].

### II. 5. 2. Methods for reduction of GO:

Reduction of graphene oxide is a process to convert sp$^3$ carbon of the graphene oxide to sp$^2$ carbon. The process involves elimination of oxygen from the oxygenated functional groups. The reduced product cannot be pure graphene rather it is graphene like as it contains structural defects. Therefore the reduced product is called reduced graphene oxide (RGO) although mechanical, electronic, thermal properties and morphology are similar to that of pristine graphene [199, 200].

RGO can be produced from the GO using a variety of reduction methods. The most popular is a chemical reduction procedure. In this procedure Graphene oxide is treated with reducing agents such as i) hydrazine hydrate ($N_2H_4 \cdot H_2O$) [201], ii) dimethylhydrazine [199], hydroquinone [202], oxalic acid [203], sodium hydrosulfite [200] and Sodium borohydride ($NaBH_4$) [185, 204, 205]. However, both hydrazine and sodium borohydride are highly toxic to human beings as well as the environment. In addition, the hydrophobic nature of obtained RGO sheet would lead to irreversible agglomerate of RGO in solutions under Van der Waals interactions [186]. In recent years, much attention has been paid to exploring environmentally friendly reductants for production of graphene from graphite oxide with good dispersibility in solvents. L-ascorbic acid (L-AA) [206], D-glucose (D-GLC) [174], L-Cysteine [207] and tea polyphenol (TP) [208] are water-soluble and mild reductants. But these reductants require optimized conditions for effective reduction of the GO. Another commonly used method is thermal reduction by heating GO to above 1000 °C [194, 209, 210]. Besides, some other novel reduction methods, such as the photo-catalytic method [211-214], supercritical fluid method [215], hydrothermal method [216, 217] and electrochemical method [218], were proposed for the reduction of GO.

### II. 5. 3. Synthesis of RGO:

GO was prepared here following modified Hummers method. 2g of graphite powder and 12g of $KMnO_4$ were taken. 360ml of Concentrated $H_2SO_4$ and 40ml of Concentrated $H_3PO_4$ were mixed. In a 1 litre flat bottom flask graphite powder was taken. 400ml acid mixture was poured into the flask which was initially kept in ice bath (to minimise any possible heat generation). After addition of acid mixture the flask was kept under stirring condition for 1.5hrs for a good mixing of graphite into the acid mixture. Finely ground $KMnO_4$ solid was then added into the acid mixture at ice cold condition to suppress any possible accidents due vigorous reaction. The mixture was then kept under stirring condition for 4 days at room temperature. After 4 days of stirring, the mixture was kept on oil bath at 45$^{o}$C for 5hrs under stirring condition in order to confirm the completion of the reaction. 0.5ml solution was taken from the mixture and to it few drops 30% $H_2O_2$ was added. Yellow colour formation hints at the graphene oxide formation. The acid mixture of the flask was poured into ice blocks of deionized water under stirring condition and 25-30 ml of $H_2O_2$ was added to neutralize excess $KMnO_4$ leading to the formation of yellow colour of the mixture. The mixture was allowed to settle down; the yellow mass was washed with 0.1M HCl and deionised water repeatedly using centrifugation. Solid gel type mass was filtered out and dried inside a vacuum oven at 50$^{o}$C temperature for 2 days. The yellowish brown solid was crushed into powder. GO was reduced using 0.1 M sodium borohydride, washed with water and dried in a vacuum oven at 35$^{o}$C. Characterization of the GO and RGO was carried out by Fourier transform infrared spectroscopy (FTIR), scanning electron microscopy (SEM), atomic force microscopy (AFM), powder X-ray diffraction technique (XRD) and Raman spectroscopy. The characterizations are discussed in detail in the subsequent chapter (Chapter IV. 1). The RGO was used for the modification of CPE (Chapter IV. 1).

## II. 6. Different characterization techniques used in the work:

Fourier transform infrared spectroscopy (FTIR) was used to get the information about the presence/elimination of different functional groups in the modifiers or modified electrode materials used for the electrode preparation; the high-resolution, three-dimensional images produced by scanning electron microscopy provided with the topographical and morphological information of the micro/sub micro structure of the electrode surface, modifiers and the modified electrode materials; in addition to that, coupling of energy dispersive spectroscopy (EDS) with SEM produced compositional information of the materials. Atomic force microscopy (AFM) was also used to get the topographical information of the materials prepared, in addition to that it was used to get the average thickness of the GO and RGO films. Structural information was obtained from the powder X-ray diffraction technique (powder XRD) and analysis of the data from 'Joint Committee on Powder Diffraction Standards' (JCPDS) database. Raman spectroscopy was used as well to get structural information of the graphene based materials.

FTIR was performed using FTIR instrument, made of 'Bruker', model Tensor II, with Deuterated Lanthanum α Alanine doped TriGlycine Sulphate (DLaTGS) detectors. SEM images were taken from Field Emission Gun-Scanning Electron Microscopes (FEG-SEM), made of JEOL, model JSM-7600F, coupled with EDS facility. AFM studies were carried out using 'Nanosurf easyscan 2 flex AFM' with both high resolution and low resolution scanner head. Powder XRD experiments were carried out using Cu Kα X-ray in Rikagu miniflex XRD, Japan instrument. Scanning electrochemical microscopy was performed using a CHI 920 D instrument.

HPLC measurements were performed on a JASCO PU 2080 Plus dual pump HPLC system, Japan, with a JASCO 2075 Plus tunable absorption detector (placed in our institute), using a

C18 reversed phase HiQ Sil column (5 µm, 4 x 250 mm). The eluting solvents (1 mL/min) used in HPLC were; $H_2O$ (solvent A) and acetonitrile (solvent B) with 0.1% trifluoroacetic acid.

### II. 7. Electrochemical Techniques used in the present investigation:

Cyclic voltammetry, linear sweep voltammetry, differential pulse anodic stripping voltammetry (DPASV), adsorptive stripping voltammetry, square wave voltammetry, hydrodynamic amperometry and scanning electrochemical microscopy were used in the present investigation.

### II. 8. Determination of electrochemical surface area of the electrodes:

The electrochemical surface area of the bare carbon paste electrode and the modified electrodes were determined using randles sevcik equation (eq. I.7) written in the chapter 1. For Bi and Sb modified CPE, $Cd^{2+}/Cd$ redox couple was taken as the reference system; based on the CVs at different scan rates electrochemical surface areas of the electrodes were calculated. For bare carbon paste electrode $[Fe(CN)_6]^{3-}/[Fe(CN)_6]^{4-}$ redox couple has been taken as the reference system. The diffusion coefficients of these redox couples were obtained from the literature.

### II. 9. Analytical Treatment of the recorded data:

The electrochemical experiments were carried out 6 times to ensure repeatability and to calculate the uncertainty involved in the measurements (assuming systematic errors to be absent). Practically it is very difficult to calculate the true value of population mean (µ), as it requires a huge number of measurements. The arithmetic mean calculated from of the small number of measured values from the equation $\bar{x} = {\sum_i^n x_i}/{n}$ is not the true value of the population mean. By evaluating the confidence interval for such a small size sample it can be asserted that the true value of the population falls within the interval with a certain degree of confidence/ with certain probability [219]. So confidence interval is nothing but a range within which true value of population mean can be obtained with certain probability. The extreme points of the range are called confidence limits of the mean; for small samples confidence limits are given by $\overline{\boldsymbol{x}} \pm {}^{\boldsymbol{t}}{}_{\boldsymbol{n-1}}\boldsymbol{s}/\sqrt{\boldsymbol{n}}$ ; where t is a statistical parameter called 'Student's t' whose value depends on the degrees of freedom $(\boldsymbol{n}-\mathbf{1})$ and the degree of confidence required. The term 'degrees of freedom' refers to the number of *independent* deviations which are used in calculating sample standard deviation '$\boldsymbol{s}$'. In this case the number is **(*n* - 1)**, because when **(*n* - 1)** deviations are known the last can be deduced, since $\sum_i(\boldsymbol{x}_i-\overline{\boldsymbol{x}})=0$. The value of '**t**' for a particular degrees of freedom for a required degree of confidence/probability can be obtained from literature. '$\boldsymbol{s}$' is calculated from the following equation,

$$\boldsymbol{s}=\sqrt{\sum_i(\boldsymbol{x}_i-\overline{\boldsymbol{x}})^2/(\boldsymbol{n}-\mathbf{1})} \qquad \textbf{eq. II.1}$$

$\boldsymbol{x}_i$ is the individual measured value, $\overline{\boldsymbol{x}}$ is the arithmetic mean of the sample, $\boldsymbol{n}$ is the total number of measurements in the sample.

Relative standard variation (RSD) of coefficient of variation (CV) is another parameter to measure the uncertainty. RSD or CV is often expressed in percentage (%) and is mathematically calculated by the following equation,

$$\boldsymbol{RSD}=\frac{\boldsymbol{s}}{\overline{\boldsymbol{x}}}\times\mathbf{100}\% \qquad \textbf{eq. II.2}$$

RSD is the measure of relative error and often used to compare the precision of results which have different units or magnitudes.

The calibration plots are constructed by plotting the analytical response (Peak current, $I_p$) at different modified electrodes against the analyte concentration. Standard addition methods were employed for the construction of the calibration plot and for the real sample analysis. For each analyte separate linear dynamic range (LDR) is obtained. By using origin-8 software the linear regression line and the linear regression equation were constructed for the LDR. The coefficient of determination ($R^2$) was determined for each LDR. $R^2$ indicates the variation from linearity.

Limit of detection (DL) is the smallest quantity of analyte which can be detected with a certain degree of confidence. In general terms, the limit of detection of an analyte may be described as that concentration which gives an instrument signal (*y*) *significantly different* from the 'blank' or 'background' signal. Though the use of 'significantly different' phrase is debatable, most of the cases limit of detection is expressed as the analyte concentration giving an analytical signal which is equal to summation of mean blank value ($\boldsymbol{Y_b}$) and three standard deviation of the blank ($\boldsymbol{s_b}$) i.e.

$$\boldsymbol{DL} = {}^{(\boldsymbol{Y_b} + \boldsymbol{3s_b})}\!/_{\boldsymbol{m}} \qquad \textbf{eq. II.3}$$

Where, $\mathbf{m}$ is the slope of the calibration curve; $\boldsymbol{s_b}$ is multiplied by 3, which ensures that there is 99.7% probability that analytical signal due to the blank falls within the range $\boldsymbol{Y_b} \pm \boldsymbol{3s_b}$.

In order to check the efficiency and performance of the modified electrodes spike recovery tests have been carried out. Here the test solution is spiked with the analyte solutions of known concentration and the corresponding analytical signals were recorded. The quantitative recoveries were calculated using the following equation,

$$\boldsymbol{Recovery} = \frac{\boldsymbol{concentration\ of\ analyte\ determined}}{\boldsymbol{concentration\ of\ analyte\ spiked}} \times \mathbf{100\%} \qquad \textbf{eq. II.4}$$

This test provides the validity of the proposed method of analysis as well.

## II. 10. Electrochemical Impedance study for the electrochemical characterization of modified electrode:

An electrochemical reaction at the electrode - electrolyte interface cannot be fully understood by using traditional electrochemical measurements. Those methods provide only currents made of faradaic and non faradaic components. A complete description requires impedance measurements made over a broad frequency range at various potentials and determination of all the electrical characteristics of the interface, the technique called electrochemical impedance spectroscopy (EIS). The technique is based upon complex mathematical transforms. The term impedance (***Z***) was first invented by Oliver Heaviside in the late 19th century [220] to extend the concept of electrical resistance to the alternating current (ac) circuit. As a respected mathematician, Heaviside is also credited with the invention of terminologies such as admittance and conductance. Impedance is simply the opposition force to electrical current in a circuit made of resistors, capacitors, or inductors, or any combination of these and is measured in the same units as resistance, ohm (Ω). Heaviside defined the 'operational impedance' as the complex ratio of the voltage and current in an ac circuit [221] which is expressed as

$$\boldsymbol{Z(j\omega) = \frac{E(j\omega)}{I(j\omega)}} \qquad \textbf{eq. II.5}$$

Where, $\boldsymbol{Z}$ is the impedance, $\boldsymbol{E}$ is the potential, $\boldsymbol{I}$ is the current, $\boldsymbol{j}$ is the imaginary component and $\boldsymbol{\omega}$ is the frequency of alternating potential. Impedance of an electrode is measured at its equilibrium potential/open circuit potential or at a potential when the electrode is polarized. The impedance $\boldsymbol{Z}$ of a system is generally determined by applying a sinusoidal potential perturbation of small amplitude (5 – 10mV) with variable frequency (0.01 Hz to 100 KHz) and measuring the current response [222]. The sinusoidal potential ($\boldsymbol{E_t}$) can be represented by the following equation

$$\boldsymbol{E_t = E_0 \sin \omega t} \qquad \textbf{eq. II.6}$$

where $\boldsymbol{E_0}$ is the amplitude of the potential signal and $\boldsymbol{\omega}$ is the radial frequency in rads$^{-1}$ ($\boldsymbol{\omega = 2\pi f, f}$ *is the frequency in Hz*). The measured current will also be sinusoidal of same frequency but with different phase and amplitude (Fig. II.3.a) as represented by the following equation

$$\boldsymbol{I_t = I_0 \sin(\omega t + \varphi)} \qquad \textbf{eq. II.7}$$

Here, $\boldsymbol{I_0}$ is the amplitude of the sinusoidal current and $\boldsymbol{\varphi}$ is the phase angle which separates the phases of $\boldsymbol{E_t}$ and $\boldsymbol{I_t}$**.** From the definition of the impedance ($\boldsymbol{Z}$) it can be expressed as

$$\boldsymbol{Z = \frac{E_0 \sin \omega t}{I_0 \sin(\omega t + \varphi)} = Z_0 \frac{\sin \omega t}{\sin(\omega t + \varphi)}} \qquad \textbf{eq. II.8}$$

The impedance is therefore expressed in terms of a magnitude, $\boldsymbol{Z_0}$, and a phase shift, $\boldsymbol{\varphi}$. With Eulers relationship, $\boldsymbol{e^{j\theta} = \cos\theta + j \sin\theta}$, $\boldsymbol{Z}$ can be expressed in complex function as following

$$\boldsymbol{Z(\omega) = Z_0(\cos\varphi - j\sin\varphi)} \qquad \textbf{eq. II.9}$$

$$\boldsymbol{Z(\omega) = Z_{real} - jZ_{im}} \qquad \textbf{eq. II.10}$$

Where, $\boldsymbol{Z_{real}}$ and $\boldsymbol{Z_{im}}$ are the real and imaginary components of the impedance. The magnitude of $\boldsymbol{Z}$, written $|\boldsymbol{Z}|$ is given by $|\boldsymbol{Z}|^2 = \boldsymbol{Z_{real}}^2 + \boldsymbol{Z_{im}}^2$ and the phase angle, $\boldsymbol{\varphi}$ is given by $\boldsymbol{\tan\varphi = \frac{Z_{im}}{Z_{real}}}$ (Fig. II.3.b).

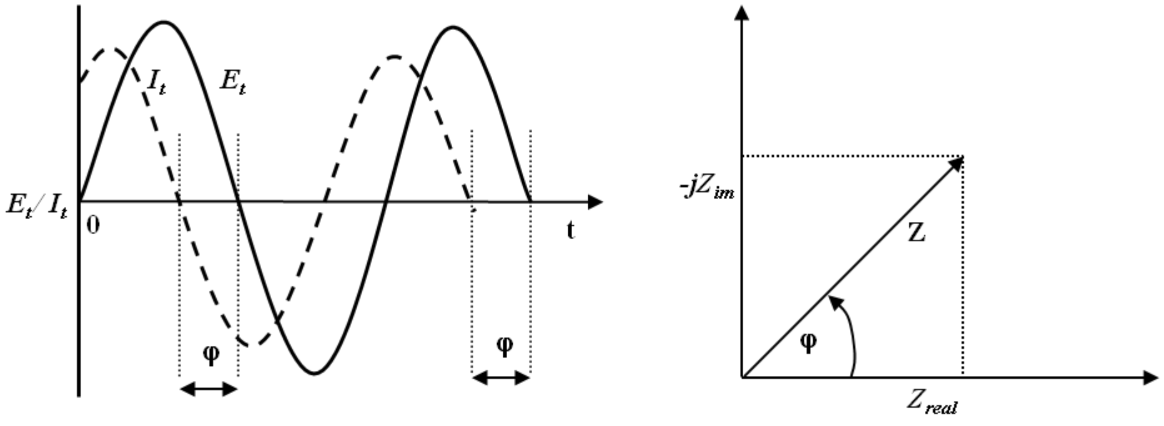

**(a)** **(b)**

**Figure II.3:** (a) Diagram showing relationship between alternating current and excitation potential signal at frequency *ω*; (b) Vector diagram of impedance, Z and its real and imaginary component.

The variation of impedance with frequency is displayed in different ways. In Bode plot, ***log|Z|*** or ***φ*** is plotted against ***logω***, while in Nyquist plot $Z_{im}$ is plotted against $Z_{real}$ for different values of ***ω***. Each point of Nyquist plot is the impedance at a particular frequency. The frequency dependence of **Z** can reveal the processes at the interface of electrode and the solution. The impedance spectrum obtained is commonly analysed by fitting it to an equivalent electric circuit model. An electrode surface/solution interface in an electrochemical cell can be considered to produce impedance to a small sinusoidal excitation. The performance of the electrode can be represented by an equivalent circuit, comprising of combination of capacitor, resistor and/or inductor, which allows passage of an alternating current of same frequency and phase angle that the real cell does under the given excitation. In a simple case, the interface can be modelled by an equivalent circuit (Fig. II.4.a), also called a Randles circuit (223), made of a double-layer capacitor ($C_{dl}$) in parallel with a charge transfer resistor ($R_{ct}$) (also taken as a polarization resistor ($R_p$)) and a Warburg impedance ($Z_W$) which represents a kind of resistance to mass transfer, connected in series with a resistor that measures the resistance of the electrolyte solution ($R_S$). The corresponding Nyquist plot is shown at figure II.4.b. Depending on the types of electrochemical reactions involved at the interface, the equivalent circuit can be much more complicated. Bode plot can be helpful to find capacitive or inductive effects of electrochemical systems.

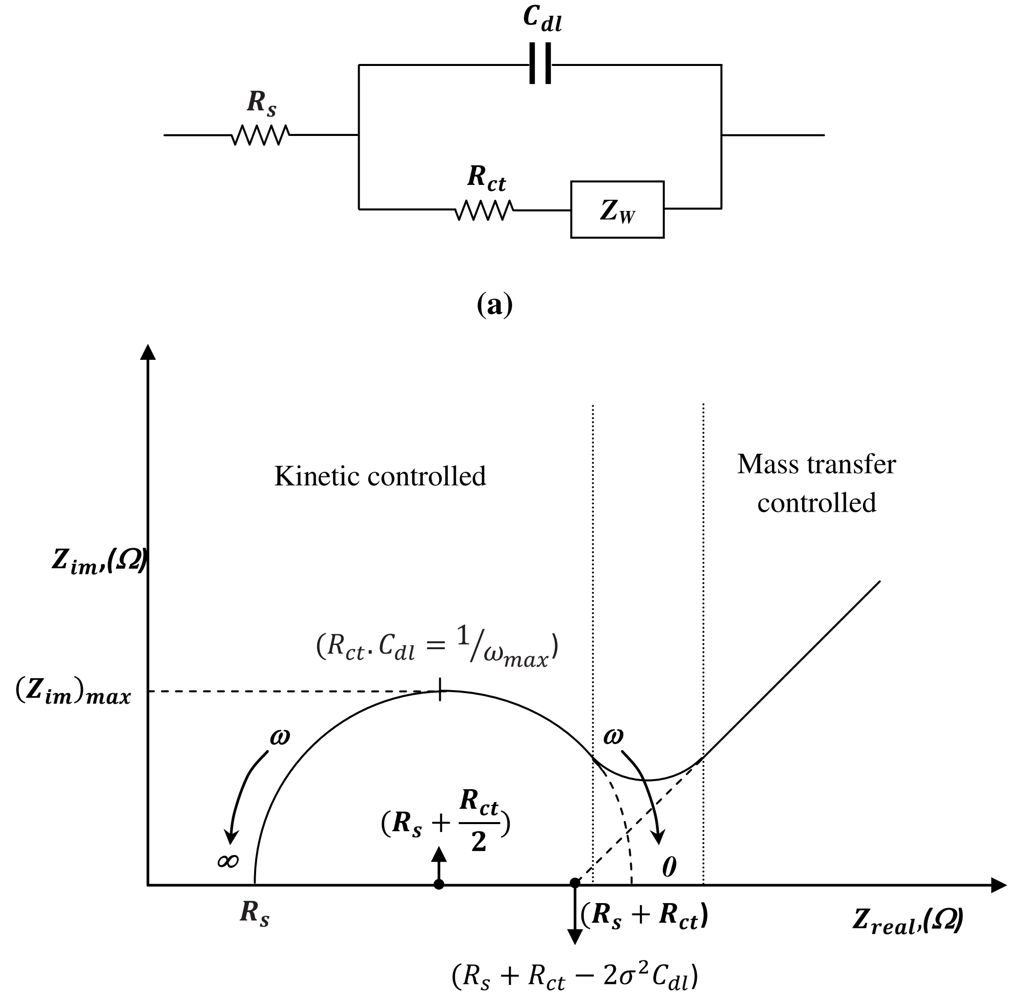

**(a)**

**(b)**

**Figure II.4:** (a) Equivalent electrical circuit of an electrochemical cell; (b) Nyquist plot for the corresponding electrochemical system.

Two fundamental equations which describe the real and imaginary components of the impedances neglecting the contribution from Warburg impedance from the Nyquist plot are

$$Z_{real} = R_s + \frac{R_{ct}}{1+\omega^2 R_{ct}{}^2 C_{dl}{}^2} \qquad \textbf{eq. II.11}$$

$$Z_{im} = \frac{R_{ct}{}^2 C_{dl}\omega}{1+\omega^2 R_{ct}{}^2 C_{dl}{}^2} \qquad \textbf{eq. II.12}$$

$$Z(\omega) = R_s + \frac{R_{ct}}{1+\omega^2 R_{ct}{}^2 C_{dl}{}^2} - j\frac{R_{ct}{}^2 C_{dl}\omega}{1+\omega^2 R_{ct}{}^2 C_{dl}{}^2} \qquad \textbf{eq. II.13}$$

At high frequencies, Warburg impedance is not observed as diffusion occurs over much longer time periods than the operational frequency and thus the relatively slow movement of molecules in solution renders impedance contributions to be obsolete. Hence, Warburg contributions are generally seen in the low frequency region. Elimination ω from the pair of equations yields

$$\left(Z_{real} - R_s - \frac{R_{ct}}{2}\right)^2 + Z_{im}{}^2 = \left(\frac{R_{ct}}{2}\right)^2 \qquad \textbf{eq. II.14}$$

$Z_{im}$ vs. $Z_{real}$ gives a circular plot centered at $Z_{real} = R_s + \frac{R_{ct}}{2}$ and $Z_{im} = 0$ and having a radious of $\frac{R_{ct}}{2}$ (Fig. II.4.b). The semicircular feature of the Nyquist plot ignoring the contribution from the $Z_W$ can be described as at very high perturbation frequency the capacitive reactance ($X_C$) of the double layer capacitor is very low that it does not offer any impedance and therefore the total current is charging current; the only impedance the current sees is the ohmic resistance. As the frequency drops the finite impedance of the double layer capacitor manifests itself as significant $Z_{im}$. At very low frequency the double layer capacitor offers very high impedance leading to the most of the current passage through the pure resistor components of the circuit, thus $Z_{im}$ falls off again. In actual case $Z_{im}$ does not fall to zero at very high frequency, instead, it increases linearly due to the contribution from $Z_W$.

At low frequency region contribution of $Z_W$ is appreciable. $Z_W$ can be mathematically expressed as $Z_w = \sigma\omega^{-1/2}(1 - j)$ provided $\sigma = \frac{RT}{n^2F^2A\sqrt{2}}\left(\frac{1}{D_O^{1/2}C_O} + \frac{1}{D_R^{1/2}C_R}\right)$, where $D_O$ and $D_R$ are the diffusion coefficients of the oxidised and reduced species respectively, $A$ is the area of the electrode, $F$ is the faraday constant, $R$ is the universal gas constant, $T$ is temperature in Kelvin and $C_O$ and $C_R$ are the bulk concentration of the oxidised and reduced species respectively. The magnitude of $\boldsymbol{Z_W}$ can be expressed as $|\boldsymbol{Z_W}| = \boldsymbol{\sigma}\left(\frac{2}{\omega}\right)^{1/2}$. As $\boldsymbol{\omega \rightarrow 0}$, the relation between $\boldsymbol{Z_{im}}$ and $\boldsymbol{Z_{real}}$ takes the form $\boldsymbol{Z_{im} = Z_{real} - R_s - R_{ct} + 2\sigma^2 C_{dl}}$. Thus the plot of $\boldsymbol{Z_{im}}$ vs. $\boldsymbol{Z_{real}}$ is linear with unit slope. The extrapolated line intersects the real axis at $\boldsymbol{R_s + R_{ct} - 2\sigma^2 C_{dl}}$. Extraction of the system characteristics requires interpreting the Nyquist plot. At high frequencies, the frequency dependent term of **equation II.13** vanishes, resulting in $\boldsymbol{Z(\omega) = Z_{real} = R_s}$ which is an intercept on the $\boldsymbol{Z_{real}}$ axis on the high-frequency side ($\boldsymbol{\varphi = 0}$ **or** $\boldsymbol{Z_{im} = 0}$). For $\boldsymbol{\omega \rightarrow 0}$, **equation II.13** becomes $\boldsymbol{Z(\omega) = Z_{real} = R_s + R_{ct}}$, which is an intercept on the $\boldsymbol{Z_{real}}$ axis on the low frequency side. At the frequency where a maximum $\boldsymbol{Z_{im}}$ is observed, the straightforward relationship $\boldsymbol{R_{ct}.C_{dl} = 1/\omega_{max} = 1/2\pi f_{max}}$, which is the time constant ($\tau$) of the electrochemical reaction, can be shown and indicates how fast the reaction takes place. $\boldsymbol{R_{ct}.C_{dl}}$ is known from the $\boldsymbol{f_{max}}$, $\boldsymbol{C_{dl}}$ can be obtained because $\boldsymbol{R_{ct}}$ is already known from the low-frequency intercept on the $\boldsymbol{Z_{real}}$ axis. The Nyquist plot gives all the necessary information about the electrode - electrolyte interface and the reaction. The higher frequency regions are kinetically controlled while the very low frequency region is mass transfer controlled as shown in the Nyquist plot (Fig. II.4.b). If an electrochemical reaction is very sluggish, it will show a large $\boldsymbol{R_{ct}}$, and may display only a very limited frequency region where mass transfer is a significant factor. On the other hand if the reaction is kinetically very facile $\boldsymbol{R_{ct}}$ will be so small in comparison to the ohmic resistance ($\boldsymbol{R_s}$) and the Warburg impedance that mass transfer control region will play a significant role in the plot and the semicircular feature may not be well defined. From the value of $\boldsymbol{R_{ct}}$ exchange current ($\boldsymbol{i_0}$) and the standard heterogeneous electron transfer rate constant ($\boldsymbol{k^0}$) can be evaluated using the following equations,

$$\boldsymbol{R_{ct} = \frac{RT}{nFi_0}} \qquad \textbf{eq. II.15}$$

$$\boldsymbol{i_0 = nFAk^0C} \qquad \textbf{eq. II.16}$$

From the intercept of the Warburg limited region on $\boldsymbol{Z_{real}}$ axis, $\boldsymbol{R_s + R_{ct} - 2\sigma^2 C_{dl}}$, σ and subsequently diffusion coefficients can be calculated [222].

Randles equivalent circuit gives the simplest way of representing the electrochemical process at the electrode solution interface. However, the real case may also include contribution from polarization, adsorption and induction leading to a very complex picture of the electrochemical process. Careful and proper fitting of the circuit components is needed to interpret the Nyquist plot obtained by the EIS.

EIS has been intensively used, for example, for the elucidation of corrosion mechanisms [224-226], the characterization of charge transport across membranes and membrane/solution interfaces [227, 228], characterization of modified electrodes [229-231] and it serves a very important role in the field of fabrication of energy storage devices [232, 233] and field of biosensors.

### II. 11. Scanning Electrochemical Microscopy:

Scanning electrochemical microscopy (SECM) is an Electroanalytical scanning probe technique capable of imaging substrate (conductive, semiconductive or insulating substrate) topography and local reactivity with high spatial and temporal resolution. Scanning electrochemical microscopy (SECM) employs an ultramicroelectrode with a tip diameter of 10 μm or less (UME), also known as a tip, to scan in close proximity to a surface of interest. The electrochemical response of the tip (or of the substrate in response to the tip) provides quantitative and qualitative information about the interfacial region. The technique was first reported in 1989 concurrently by Allen J. Bard [234] and Engstrom [235]. The instrumentation, theory, modes, and initial applications were developed in the Bard laboratories during the 1980’s. Since its inception in 1989, it has expanded into a wide variety of research areas including biology, corrosion, energy, kinetics, instrumental development, and surface modification.

### II. 11. 1. Instrumentation:

A typical scanning electrochemical microscope consists of four essential components (Fig. II.5). First, a low current bipotentiostat (≤pA) is used to precisely measure and control the current and potential at both a probe and a substrate. A high resolution three-dimensional (3D) positioning system allows for accurate movement of a probe and a substrate using an x, y, z stage with stepper and piezoelectric motors for coarse and finer movements, respectively. The third component is a small scale probe with dimensions in the low micrometre (μm) to nanometre (nm) range, also referred to as a SECM tip. This critical component defines the resolution of an SECM measurement. Finally, a data acquisition system (i.e., computer) is required to synchronize and coordinate each component to perform a successful measurement. Depending on the application, additional components can be added to a SECM instrument, including an inverted optical microscope for biological measurements involving live cells, a fluorescence detection system, or a constant distance unit.

Designing a SECM experiments requires the careful consideration of several important factors including the following:

Redox mediator and/or substrate being investigated, solvent in which the electrochemical reaction(s) will occur and probe that should be used.

The success of an experiment relies on the identification of the right combination of these three parameters.

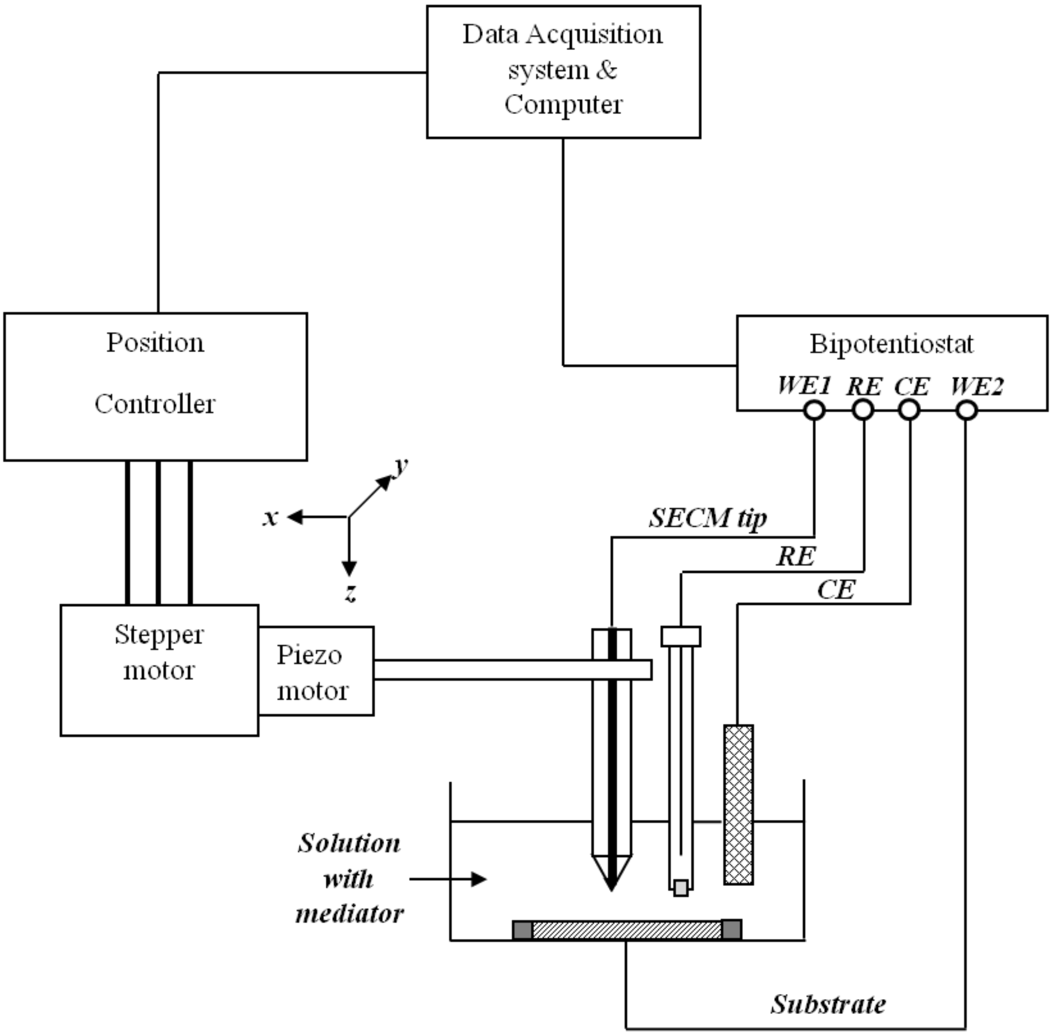

**Figure II.5:** Block diagram for the instrumentation of a Scanning Electrochemical Microscopy (SECM).

### II. 11. 2. Different modes of operation:

There are several modes of operation of SECM that continue to be used in developing new applications. Historically, feedback and generation/collection modes were the first to be introduced. Redox competition mode, direct mode, potentiostatic mode, transient mode etc. constitutes the other modes of operation.

**Feedback mode**: The most frequent mode of operation is the feedback mode where only the tip current of a potentially biased tip is monitored. Tip current is generated due to the oxidation of the redox mediator, ‘R’ according to the following equation

$$\boldsymbol{R - ne^{-} \rightarrow O} \qquad \textbf{eq. II.17}$$

The faradaic current resulting from the electrochemical reaction of the mediator is recorded at the probe and depends on the topography and the electrochemical activity of the substrate. When a probe is positioned at a tip-to-substrate distance ($\boldsymbol{d}$) greater than 10 times the radius ($r$) of the tip i.e. $\boldsymbol{d} > 10\boldsymbol{r}$ (Fig. II.6.a), the measured current,$\boldsymbol{i_T}$**,** equals the diffusion limited current, $\boldsymbol{i_{T,\infty}}$ (i.e., steady state current). For a probe with disk geometry, the steady state current is defined as $\boldsymbol{i_{T,\infty} = 4nFDCa\beta}$**,** where **C** is the concentration of the redox mediator, $\boldsymbol{a}$ is the tip area and $\boldsymbol{\beta}$ is the geometric co-efficient [236]. When the tip approaches the substrate the tip current is perturbed by the presence of the substrate either by blockage of the diffusion of redox mediator 'R' to the tip (negative feedback, $\boldsymbol{i_T} < \boldsymbol{i_{T,\infty}}$) or by regeneration of 'R' at the substrate (positive feedback, $\boldsymbol{i_T} > \boldsymbol{i_{T,\infty}}$) as shown in figure II.6.b and II.6.c. Positive and negative feedback effects enable the investigation of both electrically conducting and insulating surfaces; it also makes possible the imaging of surfaces and the reactions that occur there. The tip current-distance curves shown in figure II.7.a and II.7.b are known as negative (a) and positive (b) feedback approach curves, where $\boldsymbol{I_T}$ is the ratio of the tip current ($\boldsymbol{i_T}$) at normalized distance $\boldsymbol{L}$ ($\boldsymbol{d/r}$) and that at an infinite distance ($\boldsymbol{i_{T,\infty}}$) from the underlying substrate. Thus using feedback mode, approach curve can be constructed and tip to substrate distance can be evaluated. This mode of operation is useful to determine the heterogeneous rate constant for the charge transfer at an interface [237-240]. The topographical information of the substrate can be obtained as well from the current measurement in this mode, since the current response in feedback mode is highly dependent on tip-to-substrate distance, it is preferable to use as small a distance as possible (without crashing) to increase sensitivity.

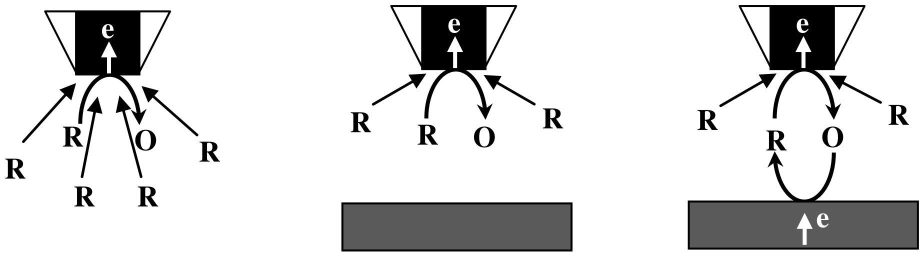

**(a)** Steady-state behaviour (diffusion limited) in bulk solution

**(b)** Negative feedback

**(c)** Positive feedback

**Figure II.6:** Pictorial representation of interaction of redox active species with ultramicroelectrode (a) during steady state (diffusion limited) behaviour; (b) in the negative feedback mode and (c) in the positive feedback mode of SECM experiment.

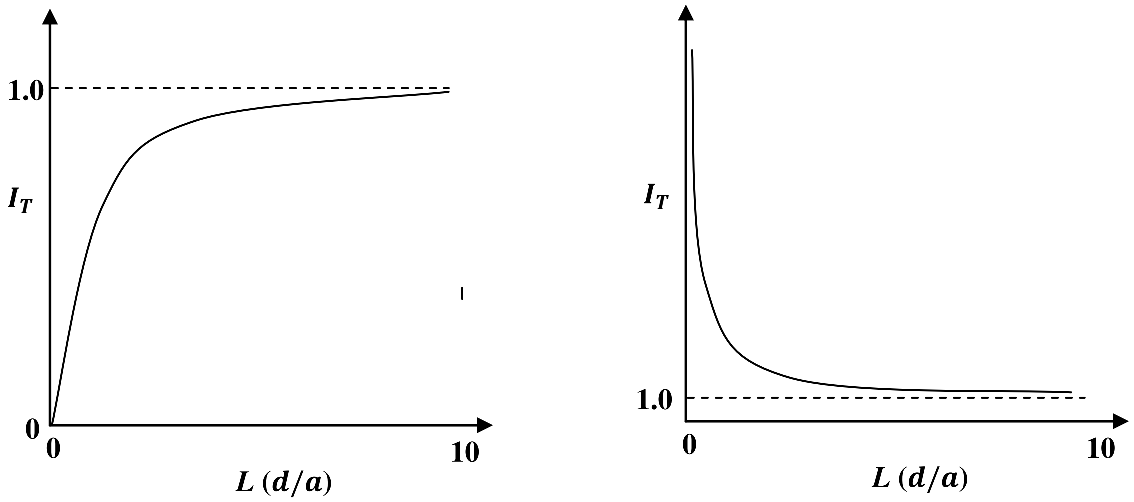

**(a)** **(b)**

**Figure II.7:** Tip current-distance curve for (a) negative feedback and (b) positive feedback mode of SECM experiment.

**Generation/Collection mode:** In the generation/collection (G/C) modes of SECM, the tip is generally located at distance on the order of ten tip radii or less from the substrate and both tip current ($i_T$) and substrate current ($i_s$) are monitored. There are two types of SECM G/C modes: the tip generation/substrate collection (TG/SC) mode and the substrate generation/tip collection (SG/TC) mode [241, 224]. In the tip generation/substrate collection (TG/SC) mode, the tip is used to generate a reactant that is detected at a substrate electrode (Fig.

II.8.a). For example, the tip is held at a potential where the reaction $\boldsymbol{O} + \boldsymbol{ne^-} \rightarrow \boldsymbol{R}$ occurs and the substrate is held at a different potential where the product R of the tip reaction will react and be collected according to the $\boldsymbol{R} - \boldsymbol{ne^-} \rightarrow \boldsymbol{O}$ reaction. Usually the substrate is considerably larger than the tip, so that the collection efficiency, given by $(\boldsymbol{i_S}/\boldsymbol{i_T})$, is essentially 1 or 100% for a stable tip-generated species, R, and if the tip is close to the substrate (i.e, on the order of two tip radii). If R reacts on transit from tip to substrate, $(\boldsymbol{i_S}/\boldsymbol{i_T})$ becomes smaller and its change with separation distance, $\boldsymbol{d}$, can be used to determine the rate constant of the homogeneous reaction [243]. TG/SC mode is predominantly used for the measurement of reaction kinetics and to perform modifications to the substrate. In the alternative substrate generation/tip collection (SG/TC) mode (Fig. II.8.b) the substrate is the generator and the tip is the collector. Thus, in SG/TC, the tip detects the species formed at the substrate.

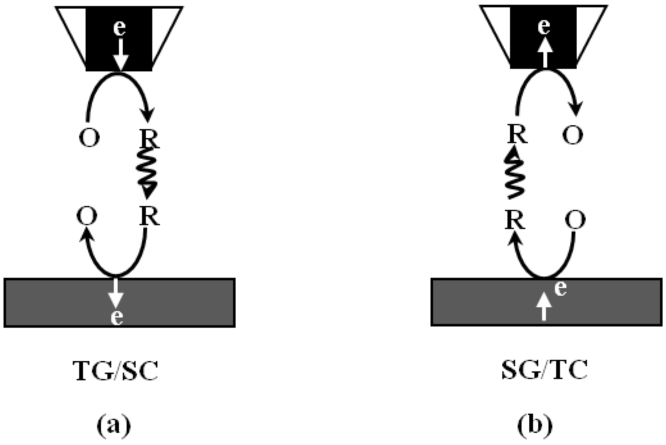

**Figure II.8:** Pictorial representation of interaction of redox active species with ultramicroelectrode in the (a) tip generation/substrate collection mode and (b) substrate generation/tip collection mode of SECM experiment.

Typically, SG/TC mode is used for the measurements of concentration profiles or chemical flux from a substrate. A tip scanned perpendicular to the substrate surface can probe a concentration profile, whereas a tip scanned over the substrate surface can identify active spots where reactions occur at a higher rate. However, SG/TC suffers from several disadvantages, including low collection efficiency, interference between substrate and tip reactions, and a lack of steady state at large substrate. Nevertheless, this mode has proven quite useful in both corrosion and enzymatic measurements.

**Redox Competition mode:** The use of redox competition (RC) mode is less prominent than feedback and GC, but since its development by Schuhmann and co-workers [244] it has found a place in the measurement of surface catalytic activity and corrosion [244, 245]. In this mode, the SECM tip and the substrate, which are in close proximity to each other, compete for the same redox species, as shown in figure II.9. In such experiments potentials are applied to both the substrate and the SECM tip (say for the reaction, $\boldsymbol{O} + \boldsymbol{ne^{-}} \rightarrow \boldsymbol{R}$, to occur). However, the current is measured at the SECM tip and not at the substrate. To avoid complete depletion of the redox mediator within the tip-to-substrate gap, the substrate is biased at a reduction potential, while a reductive potential pulse is applied to the SECM tip. When scanning over an inactive region of the substrate, the reductive current measured at the SECM tip remains constant. Over an active region of the substrate where the reduction process occurs, i.e. the catalytic spot, the redox species is consumed at both the SECM tip and the substrate, leading to a decrease in measured current at the SECM tip. This decrease in current can then be correlated with substrate activity.

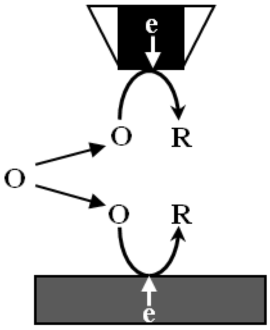

**Figure II.9:** Pictorial representation of interaction of redox active species with ultramicroelectrode in the redox competition mode of SECM experiment.

**Direct mode:** Direct mode is a specific subset of SECM in which the electrochemical cell configuration is reversed such that the microelectrode tip is used as the counter electrode and the substrate is used as the working electrode, as illustrated in Figure 3G. When a potential is applied, the electric field is localized between the tip and the substrate (shown by the shaded area in figure II.10. Direct mode has been mainly used for the surface modification, particularly for semiconductor etching, enzyme deposition, and micro-patterning [246-248].

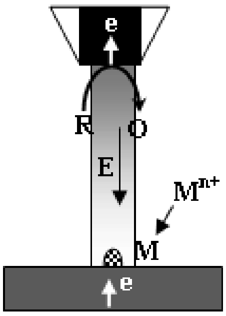

**Figure II.10:** Pictorial representation of interaction of redox active species with ultramicroelectrode in the direct mode of SECM experiment.

In transient mode tip current is measured with respect to time. The transient mode is useful in the measurement of homogeneous kinetics, for systems that are changing with time, and for determining the diffusion coefficient of a species without needing to know the solution concentration or number of electrons transferred in the electrode reaction [249, 250]. In potentiometric mode potential is measured instead of current. Use of this mode provides several advantages including high selectivity and measurement of non electroactive species or electroactive species with standard reduction potentials outside the solvent window. Furthermore, since no faradaic reaction is occurring or required, the concentration and oxidation state of the analyte species is unchanged during the measurement. Ultramicroelectrodes are used as potentiometric probe mainly for the selective recognition of local concentration of particular ions/species [251]. Different mediators are used for the different modes of operation depending upon the solvent used for the experiment and nature of study. Some common mediators used in aqueous medium are ferrocenemethanol, ascorbic acid/dehydroascorbic acid, hydroquinone, dopamine/dopamine-o-quinone, ferrocenecarboxylic acid, hexacyanoferrate (III), hydrogen peroxide, dihydrogen orthophosphate etc.

Here we have used SECM for the investigation of adsorption behaviour of melamine and L-Cysteine on the modified electrode (Chapter IV.1 & IV.3). The details of the investigations are discussed in the respective chapters.

## II. 12. Modified electrodes used in the study:

Following is the list of modified electrodes used in the study.

- Bi film modified CPE, Bi-nafion film modified CPE, Bi-nafion-MWCNT composite modified CPE,
- Sb film modified CPE, Sb-AuNPs composite modified CPE,
- AuNPs modified CPE,
- AuNPs-RGO modified CPE,
- Functionalized carbon nano spheres paste electrode and
- AuNPs modified glassy carbon electrode.

Preparation, characterization and application of these electrodes are discussed in detail in the following chapters.

# Chapter III

## *Modified carbon paste electrode as electrochemical sensor for heavy metal ions*

## Introduction:

Heavy metals are naturally occurring elements that have a high atomic weight and a density at least 5 times greater than that of water [252]. Although heavy metals are naturally occurring elements that are found throughout the earth's crust, anthropogenic activities such as mining and smelting operations, industrial production and use, and domestic and agricultural use of metals and metal-containing compounds causes most environmental contamination and human exposure [253-256]. Metals such as cobalt (Co), copper (Cu), chromium (Cr), iron (Fe), magnesium (Mg), manganese (Mn), molybdenum (Mo), nickel (Ni), selenium (Se) and zinc (Zn) are essential nutrients as these are required for various biochemical and physiological functions. Inadequate supply of these micro-nutrients results in a variety of deficiency diseases or syndromes [257]. Again, excessive levels can be damaging to the organism. Other metals such as aluminium (Al), antinomy (Sb), arsenic (As), barium (Ba), beryllium (Be), bismuth (Bi), cadmium (Cd), gallium (Ga), germanium (Ge), gold (Au), indium (In), lead (Pb), lithium (Li), mercury (Hg), nickel (Ni), platinum (Pt), silver (Ag), strontium (Sr), tellurium (Te), thallium (Tl), tin (Sn), titanium (Ti), vanadium (V) and uranium (U) have no established biological functions and are considered as non-essential metals [258]. Any metal (or metalloid) species may be considered a contaminant/toxic if it occurs where it is unwanted, or in a form or concentration that causes a detrimental human or environmental effect. Prolonged exposure to very commonly occurring heavy metals such as cadmium, copper, lead, nickel, and zinc can cause deleterious health effects in humans [259]. Several studies have demonstrated that reactive oxygen species (ROS) production and oxidative stress play a key role in the toxicity and carcinogenicity of metals such as arsenic [260-262], cadmium [263], chromium [264, 265], lead [266, 267], and mercury [268, 269]. Because of their high degree of toxicity, these five elements rank among the priority metals that are of great public health significance. They are all systemic toxicants that are known to induce multiple organ damage, even at lower levels of exposure. According to the United States Environmental Protection Agency (U.S. EPA), and the International Agency for Research on Cancer (IARC), these metals are also classified as either "known" or "probable" human carcinogens based on epidemiological and experimental studies showing an association between exposure and cancer incidence in humans and animals. Therefore determination of the concentration of these heavy metal ions in the environmental samples, industrials effluents, potable water, food samples, medicines (ayurvedic samples) etc. is necessary and plays an important role in the quality control of the drinking water and the food products. For heavy metal detection in the trace level, spectroscopic techniques such as atomic absorption spectroscopy [270] inductively coupled plasma mass spectroscopy (ICP-MS) [271] X-ray fluorescence and neutron activation analysis are the most commonly used. These techniques have the advantages of their versatility since they are suitable for a large panel of elements, sensitivity and low limit of detection (LOD) (ppb/ sub ppb level). However they suffer from several major drawbacks: expensive and large volume equipments and qualified operators are needed to perform the multi-step sample preparation and complex analytical procedures, which are unsuitable for on-site and on time measurements necessary to prevent transient phenomena monitoring. Using these techniques only total metal concentration can be determined, and speciation data can be reached only by associating supplementary extraction and separation techniques such as chromatography to the spectroscopic detection [272]. These additional steps significantly increase the risk of contamination of the sample and some modifications of the speciation may occur during sample storage or handling. On the contrary electrochemistry represents an interesting alternative due to its numerous advantages. Electrochemical devices are mostly user-friendly since they require simple procedures. They are of low cost, and well-suited for miniaturization and automatic in situ measurements with minimal sample changes. Thus, contamination by reagents or losses by adsorption on containers are drastically decreased. Electrochemical systems also allow quite fast analyses with experimental data obtained mostly in real time or in a few minutes. Hence, on-line monitoring of water samples becomes possible, providing dynamic data of relevance for biogeochemical survey. The technique provides high selectivity for the analysis of heavy metal ions with very low detection limit (ppb/ sub ppb level). Electrochemical methods based on the anodic stripping voltammetry using either mercury drop or the mercury film as the working electrode provides excellent method of the determination of heavy metal ions. However, use of mercury as the working electrode material is a debatable issue considering the toxicity of mercury. Besides that, difficulty in handling the mercury based electrode and the need of selective and the sensitive detection of the analytes in the complex matrix requires fabrication of modified solid electrodes (Chemically modified, boron-doped diamond, and screen printed electrodes as well as noble metals). Soft metallic thin films capable of pre-concentrating the heavy metal ions are in demand as an alternate to the mercury drop electrode. Bismuth and antimony were chosen for this purpose. Modification of carbon paste electrodes by electrochemically deposited bismuth and antimony films and their composites are discussed in this chapter in detail.

# Chapter III.1

## *Bismuth film on carbon paste electrode modified with nafion film embedded multiwalled carbon nanotubes for the determination of heavy metals.*

### III. 1. 1. Abstract:

This chapter discusses modification of carbon paste electrode with Bi film and Bi film composites with nafion and multiwalled carbon nanotubes (MWCNT) and their potential use as a voltammetric sensor for the determination of Pb, Cd and Zn. The effects of these modifications on the sensitivity for these elements are presented. Effects of three types of surfactants on the sensitivity of the modified electrodes are discussed. A probable method for determination of Cu is approximated.

### III. 1. 2. Brief account on Bi film and its composites with nafion and MWCNT as electrode modifier:

Bi, known to be an environmentally friendly material is used in a wide variety of cosmetics and also in medicines [273-279]. The bismuth-film electrode (BFE), consisting of a thin bismuth film electroplated on an inert substrate, has been introduced since it has been shown to possess performance comparable to mercury film electrode's (MFE's) in ASV [273, 274, 280, 281]. The advantageous properties of bismuth are attributed to its ability to form ''fused'' or ''low-temperature'' alloys with heavy metals [282, 283] facilitating the nucleation process during accumulation of heavy metal ions and leading to sensitivity similar to MFE's. Although BFE can be prepared on different metal substrate by electro-deposition, but, in the recent years most frequently used substrates are carbon based materials. In most of the related work on the BFEs, Bi-films were deposited on glassy carbon electrodes [284, 281, 286-288]. Bi film was also deposited on the carbon paste electrodes and used in stripping voltammetry [280, 289, 290]. CPE reduces the possibility of the memory effect due to its easy renewability. One of the most serious interferences in anodic stripping voltammetry (ASV), arise from various surface-active compounds that adsorb on the electrode causing fouling of its surface [291]. There were some efforts to reduce the surfactant effect on the stripping peaks based on physically separating these bulky surfactant molecules from the electrode surface by hindering their diffusion through the permselective membrane [292-300]; On the other hand, the smaller metal cations can easily diffuse through the membrane and ultimately reach the electrode surface. Nafion film, a cation exchanger, is an ideal permselective membrane which has been tested in stripping voltammetry, introduced by Hoyer et al [301]. Nafion films have also been used for application on BFE to improve the detection of heavy metal ions [302-305]. Carbon nanotubes (CNT) modified electrodes have been used in stripping voltammetry due to the enhanced charge transfer and adsorption property of the nanotubes [306-309]. In the present investigation Bi-films were produced by ex-situ electro-deposition on CPE under optimized parameters of deposition time, deposition potential, pH and concentration of the precursor solution. Bi films were modified by nafion film both before and after the deposition of Bi film on the CPE surface. A composite of MWCNT and nafion were used as well, as the modifier for enhancing the sensitivity in the stripping analysis. The activity of the working electrode with nafion modification and also by the MWCNT modification was investigated by depositing the analytes at different deposition potentials. Determination of Cu using Bi-film electrode is also an important issue as the stripping peak due to Bi appears before the Cu stripping peak. This issue has been successfully attempted in the similar line as reported by Wang and co-workers [274]. The anomalies in the findings on the determination of Cu using Bi film electrode have been discussed in the present chapter. Bi film electrode was used for the analysis of heavy metal ions in water samples.

### III. 1. 3. Modification of CPE:

Preparation of carbon paste is already discussed in chapter II (section II. 4. 6). The carbon paste was filled inside a glass tube with 2 mm diameter at the bottom end; the connection from the carbon paste to the electrode connector of the instrument was made using a platinum wire. Performance of the electrode was checked by the method described in that section. In the present investigation CPE was modified with Bismuth film (BFCPE), nafion coated Bi films (NCBFE - 1 & 2) and carbon nanotubes modified nafion film coated Bi-films (CNTMBFE).

### III. 1. 3. 1. Deposition of Bi film on CPE:

Conditions of the deposition of Bi films on carbon paste electrode were optimized. For the electrodeposition of Bi films, 0.3 mM $Bi(NO_3)_3$ solution was used. Deposition solution was buffered using 0.1 M acetate buffer at pH 4.5. At pH lower than 4.5 enhanced hydrogen evolution reactions damaged the quality of the Bi films. At higher pH Bi was hydrolyzed, thus, a pH of 4.5 was found to be suitable for the deposition of Bi films. Deposition potential was varied from -0.4 V to -1.3 V. A deposition potential of -0.8 V was found to be suitable for the present purpose. Optimization of the deposition time was very important in the present study as the stripping current changed considerably on the variation of the deposition time of the Bi films. Deposition time decides the Bi film to be thick or thin in nature. The stripping property of the analytes varied significantly with respect to the change in the thickness of the Bi films on the carbon paste electrode surface. The results of the effect of the deposition time are shown in figure III.1. The deposition time was varied from 50 sec to 600 sec at a deposition potential of -0.8 V. It was observed that with increase in the deposition time from 50 sec, stripping current of Cd increased and a sudden surge in the increment was observed at a change in deposition time from 200 sec to 300 sec. After 300 sec of deposition time the stripping current was found to decrease drastically. This might be due to the fact that at 300 sec deposition time, a thin complete film of Bi was formed on the electrode surface. Below this deposition time the film might not have been complete, resulting in a lesser stripping peak current. At a higher deposition time than 300 sec the Bi-film might be getting thicker. On a thicker film the stripping current might be reduced compared to the stripping on a thinner film.

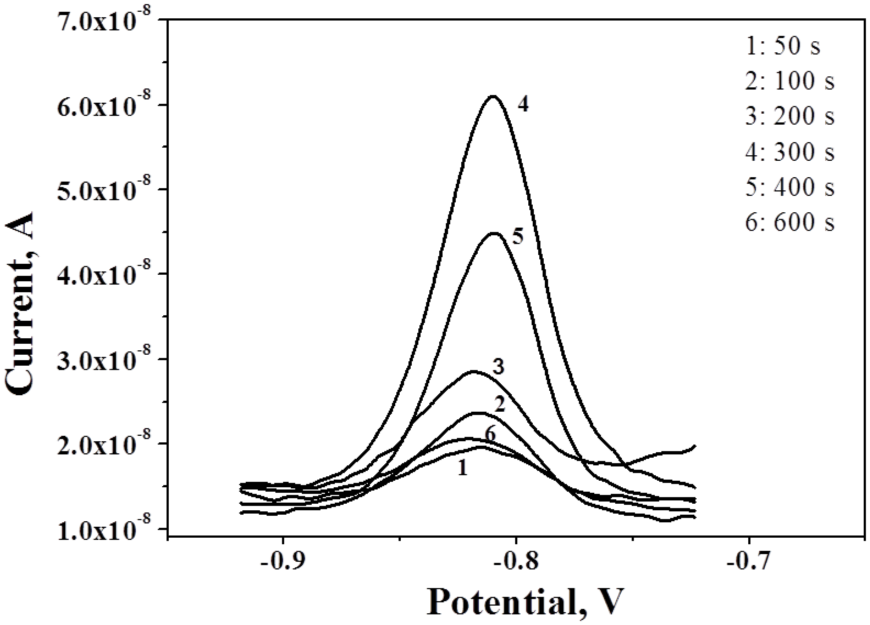

**Figure III.1:** Effect of deposition time of Bi deposition on the stripping peak of Cd, deposition potential was fixed at -0.8 V (SCE). Concentration of $Cd^{2+}$was 30 µg $L^{-1}$.

Thickness of the Bi film was determined from the stripping peak area of the Bi-peak [287, 302] The average thickness of the Bi film on bare carbon paste electrode surface using 0.3 mM $Bi(NO_3)_3$ solution for 300 sec deposition time was 0.15 nm. The average thickness of the Bi-film on nafion coated surface was 0.11 nm. The thickness was calculated considering complete removal of the Bi by stripping from the carbon paste surface. Thickness can be controlled by using different concentrations of $Bi^{3+}$ solution and also by varying the deposition time.

### III. 1. 3. 2. Modification of CPE by Nafion and Bi film composite:

In this fabrication, 5% nafion solution was diluted to 0.2% using HPLC grade methanol. The dilute nafion solution was used to modify the electrode in two ways. Initially BFE was coated with the dilute nafion solution to prepare an electrode NCBFE - 1. Again bare CPE was coated with nafion by drop casting and Bi film was electrochemically deposited on it preparing NCBFE - 2 (Fig. III.2). Concentration of the nafion solution was varied from 1% to 0.001%. A 0.2% nafion concentration was found to be suitable in terms of stability of the electrode and higher sensitivity of the measurements.

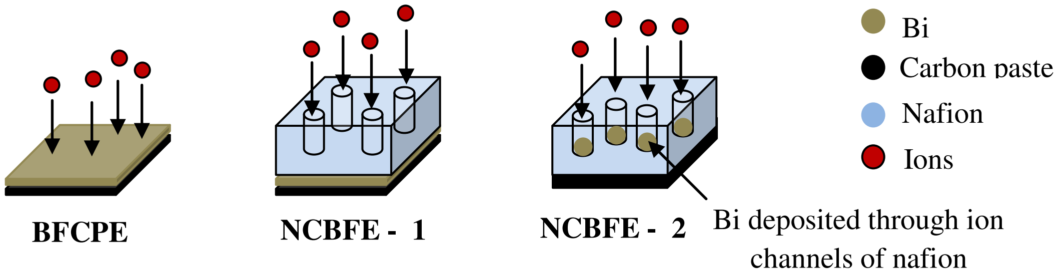

**Figure III.2:** Pictorial representation of BFCPE, NCBFE-1 and NCBFE-2.

### III. 1. 3. 3. Modification of CPE by nafion-MWCNT- bismuth film composite:

Carbon nanotubes were sonicated in the dispersion solution (0.2% nafion) for 10 min and then drop casted on the bare CPE surface. After drying, this electrode was put inside the $Bi(NO_3)_3$ solution and Bi-film was deposited. This CNTMBFE was then washed using nano pure water and then used for the analysis.

### III. 1. 4. Results and Discussions:

Simultaneous detections of the heavy metal ions ($Zn^{2+}$, $Cd^{2+}$ and $Pb^{2+}$) were carried out by differential pulse anodic stripping voltammetry (DPASV), where these ions were deposited on the surface of modified electrode by constant potential deposition in the first step (deposition potential of the analytes was -1.25V, deposition time 300 sec) under hydrodynamic condition (stirring at 2500 rpm) and anodic oxidation in the second step (stripping). Since Bi film is insensitive towards the reduction of oxygen, purging with inert gas was not performed prior to the experiment. Bi film has been deposited ex-situ on the CPE. In situ deposition of Bi films was not suitable in the present case as the Bi film was deposited on the carbon paste electrode instead of the glassy carbon electrode normally used [274, 284-288]. CPE comprises of carbon particles which offers faster kinetics for hydrogen evolution resulting in hydrogen evolution at less negative potential than on glassy carbon electrode. Thus, deposition and determination of Zn was difficult in the case of in situ deposition procedure, as it was required to apply a deposition potential of around -1.25 V. At this potential hydrogen evolution was a problem at pH 4.5 on the carbon paste electrode. A higher pH than 4.5 was not recommended due to the possibility of hydrolysis of $Bi^{3+}$. Thus, an ex-situ procedure was proposed considering the hydrolysis of $Bi^{3+}$ and the hydrogen evolution on CPE. After preparation of a modified electrode, it was dipped into the solution containing these ions and analytical responses for these metal ions were obtained by DPASV technique. The analyte solutions were prepared using sodium acetate (NaOAc) and the pH of the solution was optimised to 6.5 in order to minimise the hydrogen evolution and to get good sensitivity for the metal ions. Calibration plots were prepared from the analytical responses obtained for each electrode. Figure III.3.a and III.3.b show the analytical response of the metal ions on the BFCPE and the corresponding calibration plot. The same electrode was used for every scan, prior to each scan the electrode was cleaned by applying a conditioning potential of -0.4V for 300 sec and the analyte ions were further deposited at the optimized potential. Conditioning was performed to regenerate the fresh electrode surface and to minimise the memory effect. Inset of figure III.3.a shows the irresponsive nature of bare CPE for Zn, Cd and Pb at concentrations of 150, 90 and 120 μg $L^{-1}$respectively.

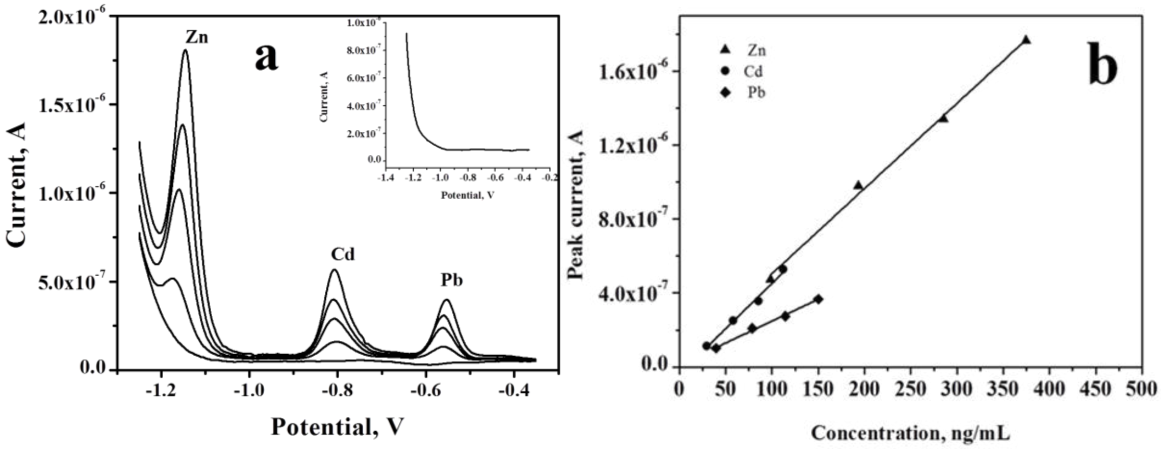

**Figure III.3:** (a) Differential pulse anodic stripping voltammograms of Pb, Cd and Zn in sodium acetate solution of pH 6.5 using BFCPE, analyte deposition potential was -1.25V and deposition time was 300 sec (Inset: Response of bare CPE for Zn, Cd and Pb of concentration 150, 90 and 120 μg $L^{-1}$ respectively); (b) Calibration plots of peak current vs. concentration

Well distinguished stripping peaks were obtained at -0.55V, -0.8V and -1.15V for Pb, Cd and Zn respectively. Peak currents of all these elements followed linear relationship with the increase in concentration of the analytes. Electrochemical response on NCBFE-1 of the three metal ions with varying concentrations is shown in figure III.4. When compared with the stripping on bare BFCPE, NCBFE - 1 had stable background current and the possibility of hydrogen evolution was reduced. The absolute value of the stripping current remained similar to that of BFCPE.

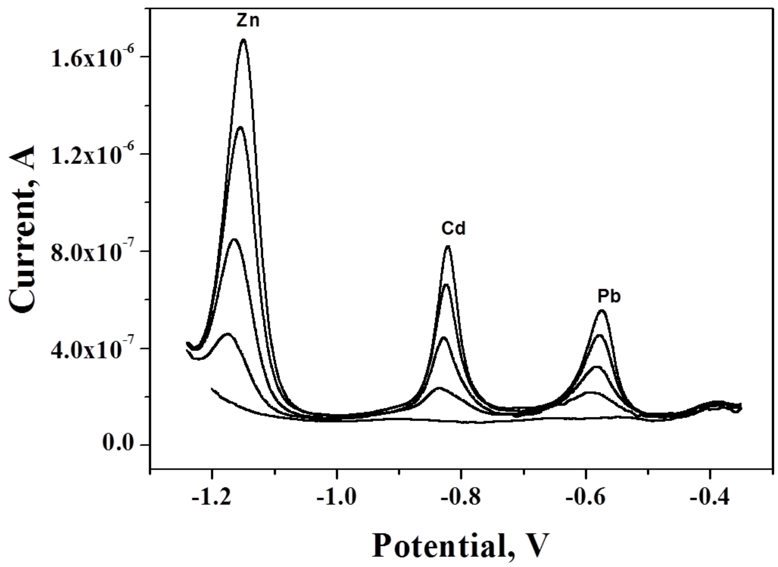

**Figure III.4**: Differential pulse anodic stripping voltammograms of Pb, Cd and Zn in sodium acetate solution of pH 6.5 using NCBFE - 1, analyte deposition potential was -1.25V and deposition time was 300 sec.

In order to improve the sensitivity of the determination CNTMBFE was prepared. Voltammetric response and calibration using this electrode is shown in figure III.5.a and III.5.b. Sensitivity of the CNTMBFE was substantially higher than BFCPE and NCBFE-1.

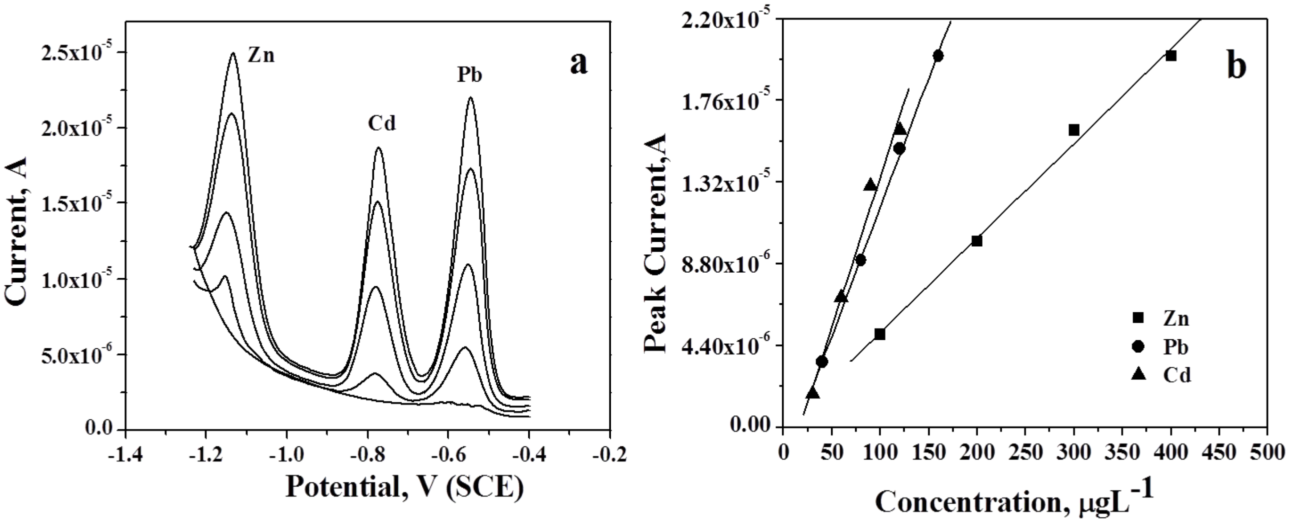

**Figure III.5: (a)** Differential pulse anodic stripping voltammograms of Pb, Cd and Zn in sodium acetate solution of pH 6.5 using CNTMBFE, analyte deposition potential was -1.25V and deposition time was 300 sec; (b) Calibration plots of peak current vs. concentration for Pb, Cd and Zn using CNTMBFE.

### III. 1. 4. 1. Scanning electron microscopy (SEM) on the surface of BFCPE and CNTMBFE:

Scanning electron microscopy (SEM) of the Bi films deposited on bare carbon paste and on the MWCNT-nafion modified surface was obtained and shown in figure III.6.a and III.6.b. In the low resolution image as shown in figure III.6.a the Bi films were seen as the discrete flakes like deposits on the bare CPE surface. In case of CNTMBFE the deposits were continuous and more uniform (Fig. III.6.b). At higher resolution the Bi films on MWCNT-nafion modified surface appeared to be more continuous and uniform compared to that on a bare carbon paste surface.

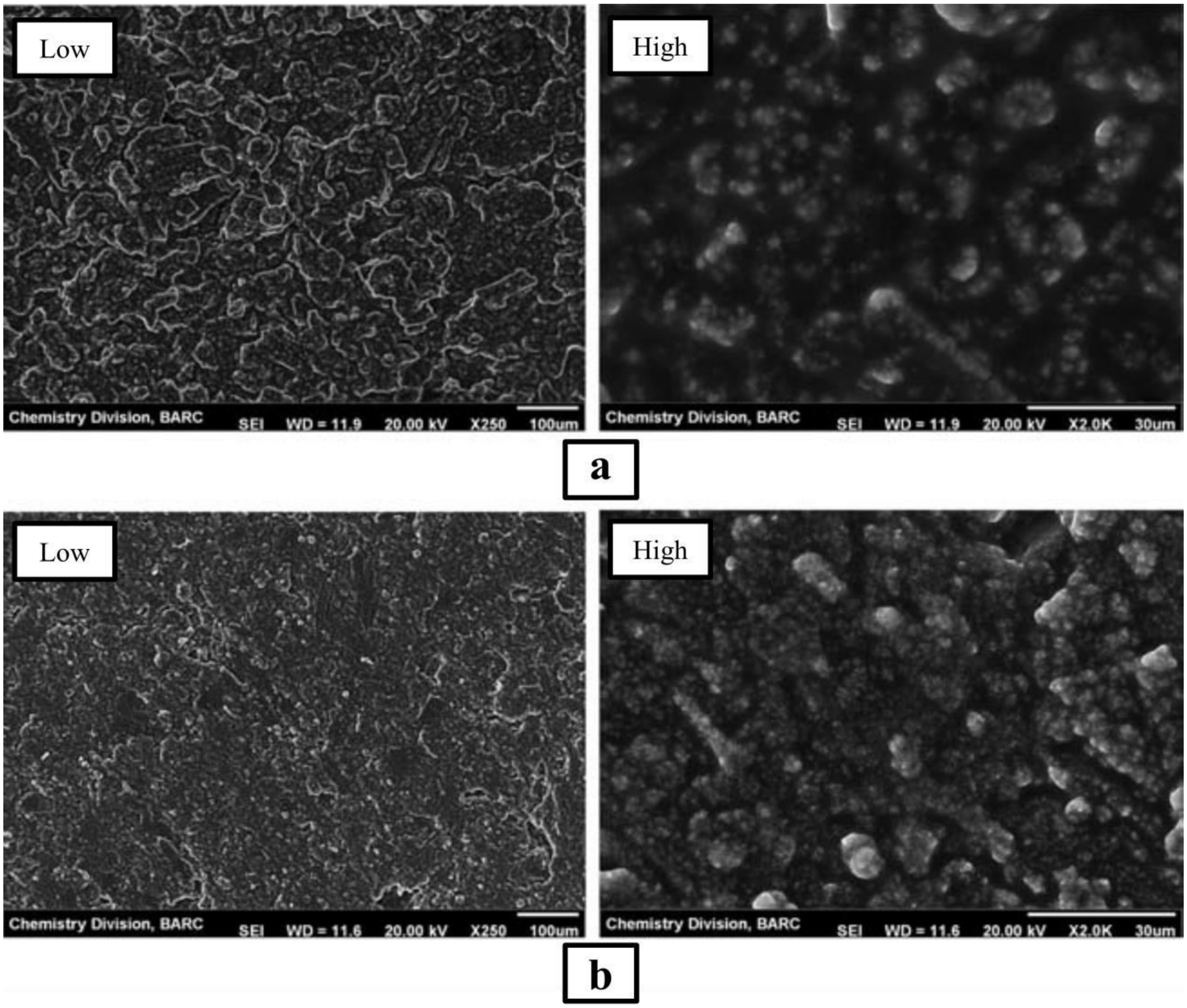

**Figure III.6:** SEM images of the (a) Bi film on bare carbon paste electrode (BFCPE) and (b) Bi film on MWCNT-nafion modified carbon paste electrode (CNTMBFE) at two different magnifications (left is at low and right is at high resolution).

### III. 1. 4. 2. Effect of the deposition potential on analyte deposition:

Addition of nafion on the BFCPE, i.e., in the case of NCBFE - 1, sensitivity of the measurements did not increase considerably over the bare BFCPE. The mass accumulation effect due to the use of nafion film might not be pronounced. Application of a highly negative deposition potential of -1.25 V might be the reason for not observing the enhancement of sensitivity in the case of NCBFE - 1 over BFCPE. Application of higher deposition potential might have compensated the mass accumulation effect of nafion.

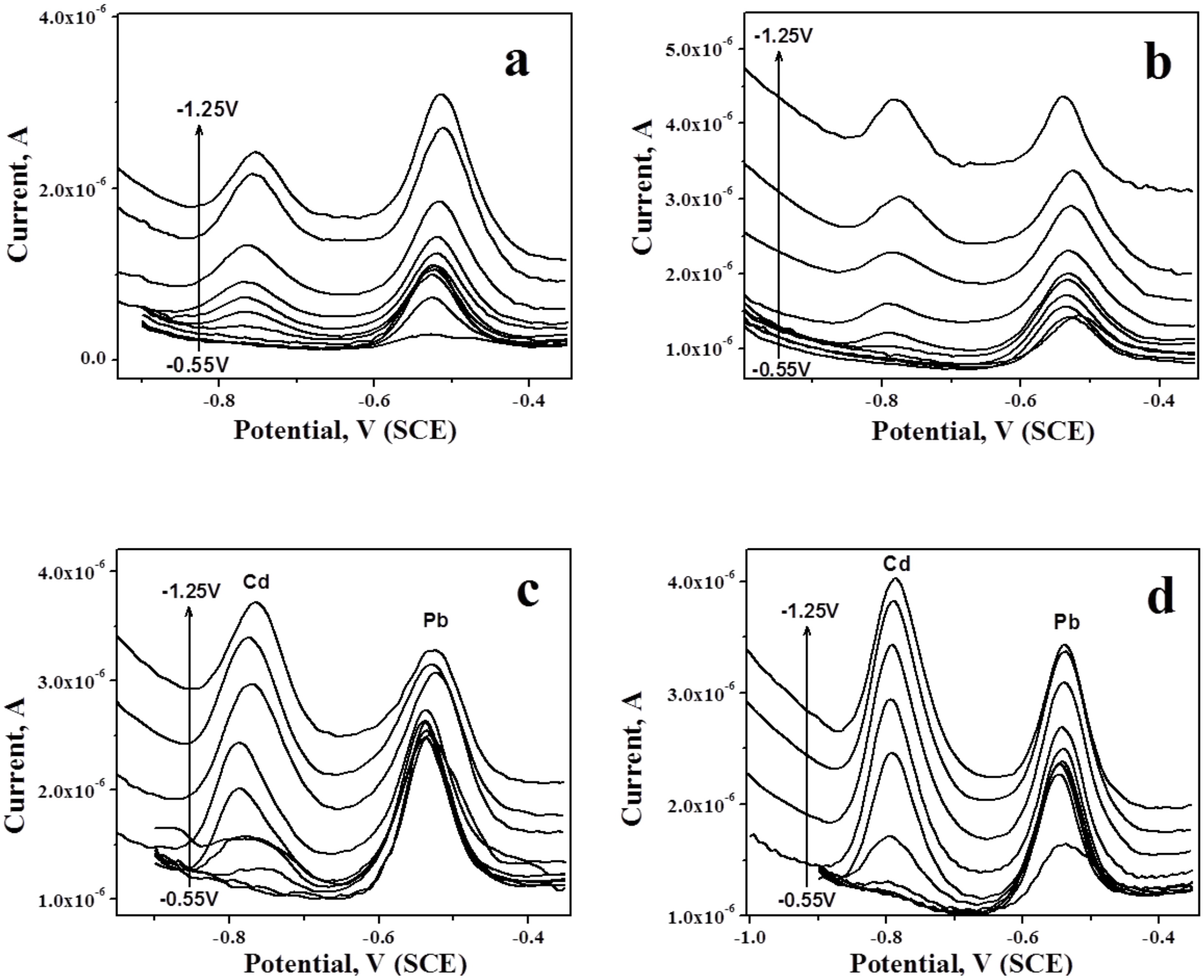

**Figure III.7:** Differential pulse anodic stripping voltammograms of Pb and Cd at different analyte deposition potentials (-0.55V to -1.25V) using (a) BFCPE, (b) NCBFE – 1, (c) NCBFE – 2 and (d) CNTMBFE.

In order to validate the assumptions, deposition potentials were varied from less negative to more negative values for Cd and Pb using the BFCPE, NCBFE – 1, NCBFE - 2 and CNTMBFE electrodes. The corresponding voltammograms are shown in figure III.7.a, III.7.b, III.7.c and III.7.d respectively. It was observed that in all cases with increase in the deposition potential stripping peaks of both Pb and Cd increased up to a certain potential. In the case of BFE, the peak height increased almost up to the deposition potential of -1.25 V.

In the case of NCBFE - 1, the improvement over the BFCPE was not significant; rather the increased baseline could be detrimental in the measurements. Enhancement of the sensitivity with increase in analyte deposition potential (in the negative direction) on NCBFE - 1 at a lower range of potential thus agreed with our assumptions that when a higher deposition potential (more negative, at -1.25V) was applied, like that applied in constructing the calibration plot (Fig. III.4), enhancement of the mass transport effect due to the cation exchange behaviour of nafion film was less pronounced. It was observed however that, nafion film on the top of the Bi-films, NCBFE - 1, provided better physical stability to the modified electrode on prolonged use and also on storing. In NCBFE - 2 the response was much superior compared to the bare BFCPE.

### III. 1. 4. 3. Comparison of sensitivity of the electrodes:

Excellent sensitivity was observed when the carbon paste electrode was modified with carbon nanotubes, i.e., in the case of CNTMBFE. The stripping response of Pb and Cd is shown in figure III.8 for all the four cases at a deposition potential of -0.9 V. It was observed that peak position of both the peaks remained unchanged in all the four cases. The enhancement of the sensitivity due to nafion modification was observed in NCBFE - 2. This enhancement in the stripping current on nafion modification confirmed the increased mass transport through the nafion, i.e., due to the non faradaic type of preconcentration process. NCBFE - 1 could not produce higher sensitivity compared to the BFCPE as observed earlier when the analyte deposition potential was -1.25V. Lower sensitivity of the NCBFE - 1 compared to NCBFE - 2 can be speculated in the following manner. For NCBFE - 1, Bi film is covered with the nafion film. Although the nafion film can allow non faradaic preconcentration of ions through its ion channels due to its cation exchange behaviour resulting in the enhancement of sensitivity; this phenomena is compensated by the blocking of the large fraction of active Bi sites by the large non-conducting polymer residue of the nafion film. On the other hand, when nafion film is coated prior to the deposition of Bi, Bi gets deposited only through the ion channels of the nafion, thus almost all the active Bi sites are available for the deposition of the analytes; non faradaic preconcentration of the ions by nafion adds to the higher sensitivity (Fig. III.8). In the case of CNTMBFE the much higher sensitivity was due to the enhanced surface area of the modified electrode. Increase in active surface area can be explained clearly from the SEM images (Fig. III.6), deposition of Bi on MWCNT modified surface was more uniform than the Bi deposition on bare carbon paste; thus more active sites are available to the analytes on CNTMBFE compared to BFCPE. However the effect of nafion modification or the MWCNT modifications on the kinetics of the electron transfer rates were not pronounced as the peak position of the stripping peak remained unaltered in different ways of modifications. The fact that in all the cases the deposition and the stripping phase was Bi film, thus a marginal change in the kinetics of the electron transfer processes was expected during the stripping process. In the case of the MWCNT modifications no considerable peak shifting was observed.

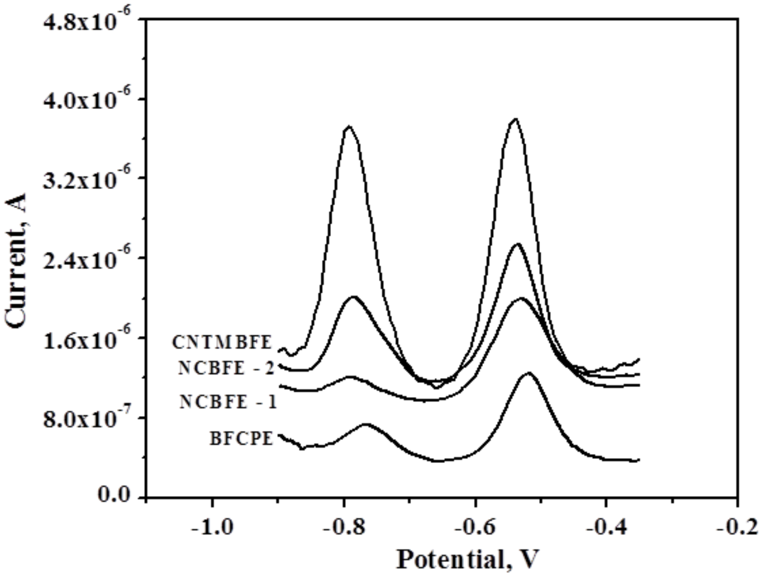

**Figure III.8:** Comparison of stripping response of Pb (40µg L$^{-1}$) and Cd (30µg L$^{-1}$) for BFCPE, NCBFE – 1, NCBFE – 2 and CNTMBFE, analyte deposition potential: -0.9V, deposition time: 300 sec, from sodium acetate solution of pH 6.5.

The base line of the stripping peaks on use of NCBFE and CNTMBFE has increased compared to the bare BFE. This might be due to the enhanced capacitance on modifications with nafion films and by MWCNTs. The capacitance values were measured from the impedance measurements which suggested a 20% and 30% increase in the capacitance value on NCBFE and CNTMBFE respectively as compared to that of BFE.

### III. 1. 4. 4. Determination of Cu:

Determination of copper using Bi-film electrode was an issue as the Bi film oxidizes before the appearance of the Cu stripping peak. This was successfully discussed in the earlier work by Wang and co-workers [274]. In the present study we also investigated this issue. Present findings correlated with the reported literature with some additional features, shown in figure III.9. Anodic stripping of pure Bi film on CPE produced two peaks (peak A and peak B) instead of one peak reported by Wang et al. [274]. They used glassy carbon electrode for Bi-deposition where the entire Bi film might have behaved like one phase. In the present case, Bi film was deposited on carbon paste electrode which is expected to have surface inhomogeneity. The Bi deposits on the top of the carbon particle would be more active compared to the deposits at the valley of the carbon particles. Thus the Bi film at the active site produced the first oxidation 'peak A' and the Bi film at the valley produced the 'peak B'.

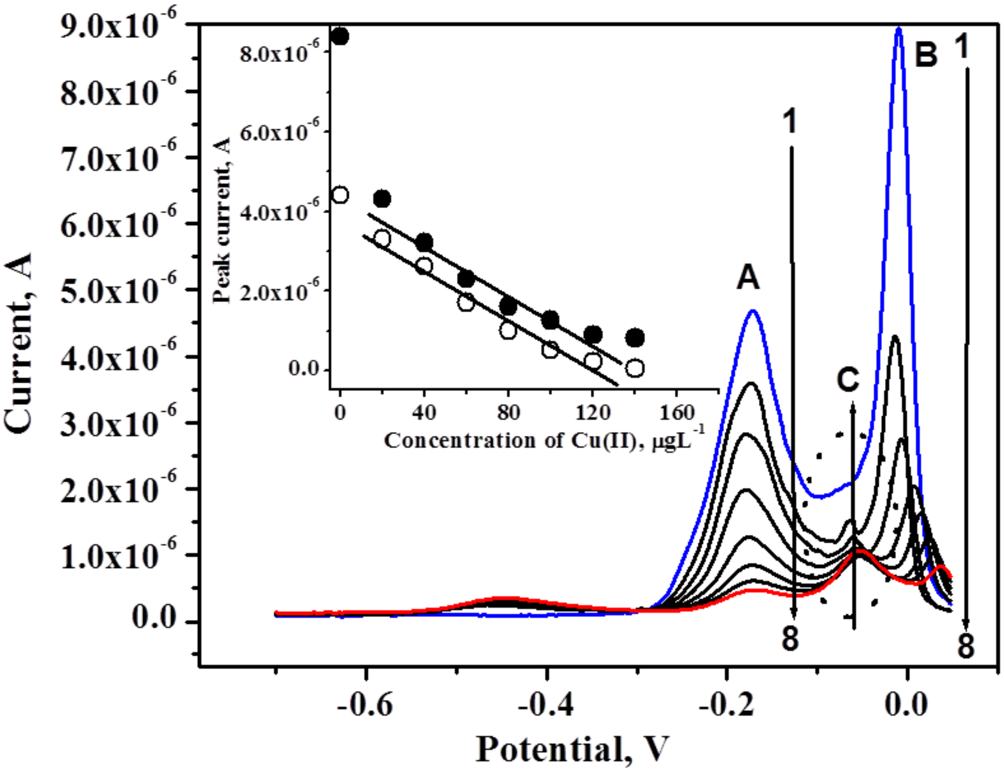

**Figure III.9:** Effect of the addition of Cu on the Bi stripping peak. Inset: corresponding calibration plot of 'peak A' (hollow circle), 'peak B' (solid circle). Each time 20 μg L$^{-1}$ Cu was added

In the present study Bi deposition was carried out in situ with Cu. The deposition potential was optimized at -0.8 V for simultaneous deposition of Cu and the Bi films. Three peaks were observed, which were designated as A, B and C in figure III.9. On successive addition of Cu in the solution, peak height of 'peak A' was reduced proportionately till the addition of 150 μg L$^{-1}$

of Cu. Corresponding calibration of the decrease in the peak current is shown in the inset (hollow circles) of figure III.9. Peak current corresponding to the 'peak B' was also reduced upon addition of standard Cu in the solution. However, the decrease of the peak current corresponding to 'peak B' (solid circles in the inset) was not proportional enough for the quantitative determination of Cu. At a higher Cu concentration (more than 150 μg $L^{-1}$) linearity in the decrease in the peak height of 'peak A' was not maintained. The third peak 'peak C' was more pronounced only at a concentration more than 50 μg $L^{-1}$. Thus, for the determination of Cu, the calibration plot for the decrease in the current of 'peak A' can be used at lower concentration, and the calibration plot for the increase in peak current of the 'peak C' can be used at higher concentration.

### III. 1. 4. 5. Effect of surfactants on the measurements:

Effect of surfactants was a major concern in the determination of heavy metal ions using voltammetry [302-305] Wang and co-workers have developed a method of addition of fumed silica into the sample in order to resolve the problem due to surfactants [310]. In the case of stripping voltammetry using solid electrodes or film electrodes, permselective membranes are very much popular to reduce the surfactant effect. Permselective membranes restrict the bulky surfactants whereas the metal ions diffuse through the membranes to the electrode surface. In the present investigation nafion was used as the permselective membrane to reduce the effect of surfactants on the measurements. Neutral, cationic and anionic surfactants were used for the study. The results of the effects of three different surfactants on BFCPE and on NCBFE - 2 are shown in figure III.10.a, III.10.b and III.10.c (Concentrations of Zn, Cd and Pb were 400 μg $L^{-1}$, 120 μg $L^{-1}$ and 160 μg $L^{-1}$). In the presence of neutral surfactant TX100, the stripping peaks of all the heavy metals Zn, Cd and Pb were reduced sharply (Fig. III.10.a). Beyond around 10 μM of the TX100 concentration the peak currents were found to be stabilized and remained stable up to 30 µM concentration, beyond that the voltammograms became noisy. Both the BFCPE and NCBFE - 2 have shown similar behaviour on the use of surfactants in the stripping solution. No improvement was observed on nafion modifications over the BFCPE.

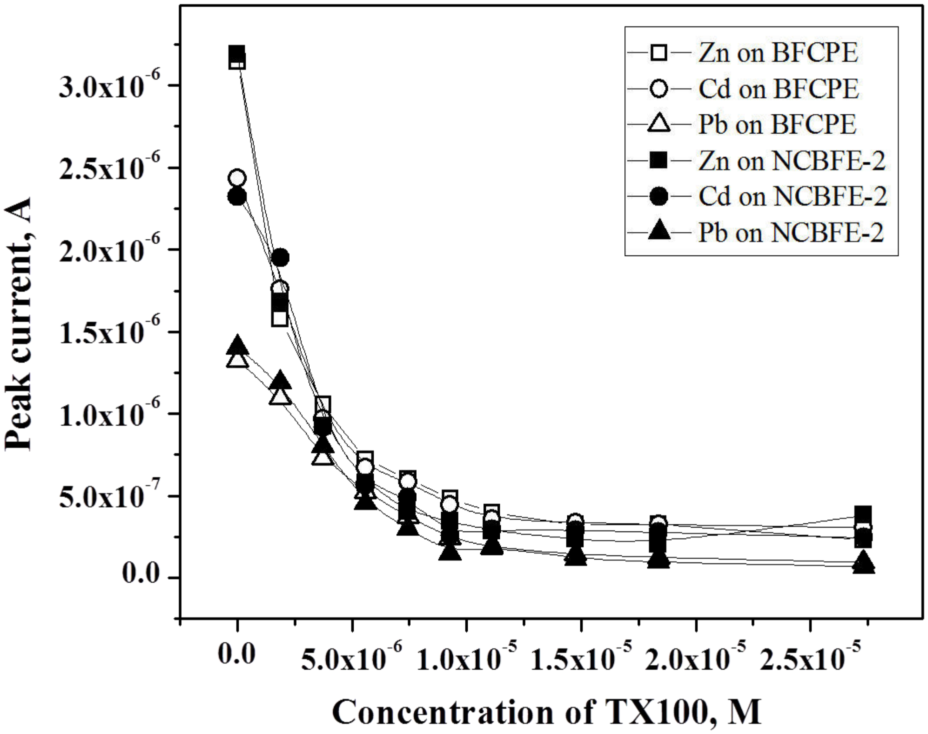

**Figure III.10.a:** Effect of TX100 on the stripping peak of Zn, Cd and Pb with concentration of 300 µg L$^{-1}$, 90 µg L$^{-1}$ and 120 µg L$^{-1}$ respectively. Solid points are with nafion modification (NCBFE - 2) and the empty points are without nafion modifications.

On addition of anionic surfactant, SDS in the stripping solution, the peak current was observed to get reduced slowly (Fig. III.10.b) as compared to the TX100. In this case a marginal increase or a shallow decrease in the stripping peak for all the metal ions was observed with both BFCPE and NCBFE - 2 in the surfactant concentration up to around 15 µM. Such effect of increase in the peak current was more pronounced for Zn. This might be due to the entanglement of the cationic analytes with the anionic surfactant head groups. Though initially the observed rate of decrease in the stripping peak on addition of surfactants on BFCPE and NCBFE - 2 were similar, beyond 20 µM of surfactant concentration the stripping peaks on BFCPE were diminished.

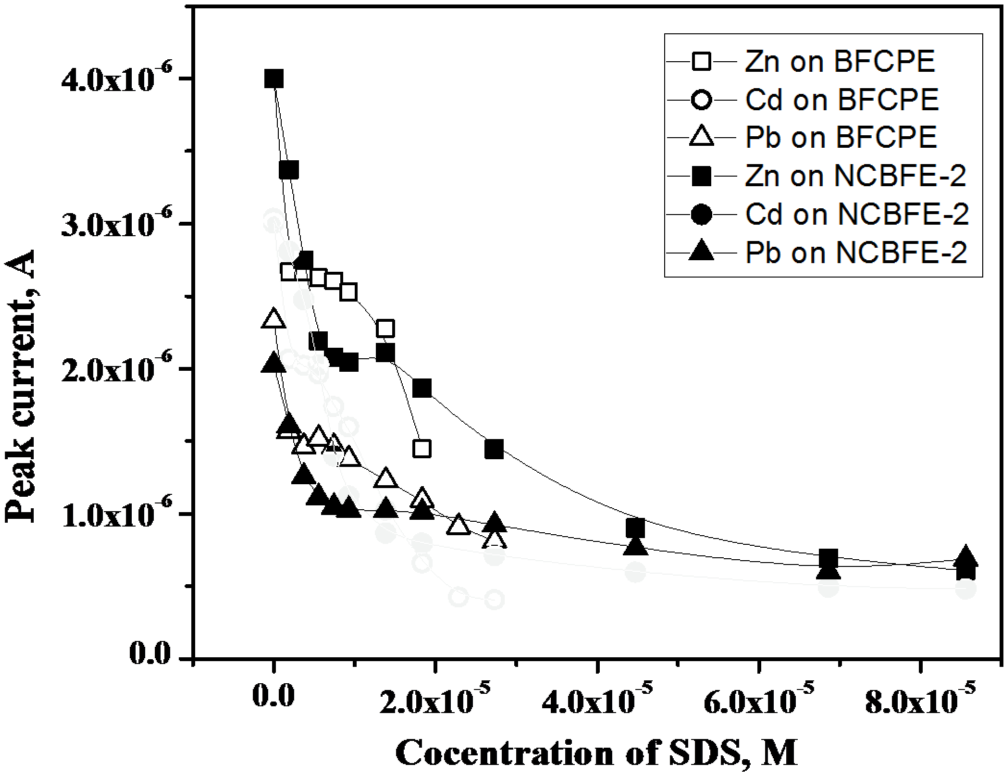

**Figure III.10.b:** Effect of SDS on the stripping peak of Zn, Cd and Pb with concentration of 400 µg L$^{-1}$, 120 µg L$^{-1}$ and 160 µg L$^{-1}$ respectively. Solid points are with nafion modification (NCBFE - 2) and the empty points are without nafion modifications.

However with NCBFE - 2, though the stripping peak reduced considerably beyond 20 µM of surfactant concentration but remained observable even up to around 90µM concentration.

In the case of a cationic surfactant CTAB, as shown in figure III.10.c, the stripping peaks were reduced on addition of the surfactant. The stripping peaks of Cd and Pb have shown a shallow change over addition of CTAB in the initial CTAB concentration, similar to what was observed in the case of SDS. The Zn peak however has reduced sharply even from a very low addition of CTAB and no shallow behaviour was observed. Interestingly it was observed that on BFE the stripping was diminished even on the addition of around 15µM of CTAB. Whereas the stripping peak on NCBFE- 2 remained stable and observable up to the addition of around 50 µM of CTAB concentration. Thus on nafion modifications of the Bi-film electrodes the stripping peaks of the heavy metal ions sustained with much higher surfactant concentrations with ionic surfactants. Neutral surfactants affected the stripping peaks at a higher extent and the peaks became unstable beyond 30 µM of TX100.

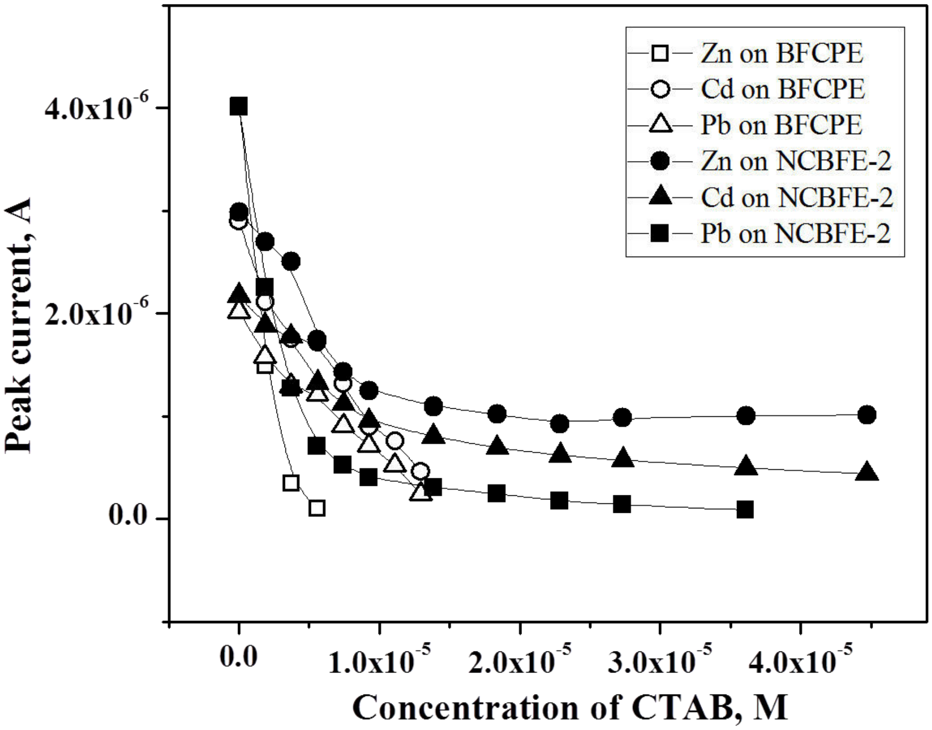

**Figure III.10.c:** Effect of CTAB on the stripping peak of Zn, Cd and Pb with concentration of 400 µg L$^{-1}$, 120 µg L$^{-1}$ and 160 µg L$^{-1}$vrespectively. Solid points are with nafion modification (NCBFE - 2) and the empty points are without nafion modifications.

### III. 1. 4. 6. Study of interferences:

Effect of commonly occurring metal ions on the stripping voltammetric determination of Zn, Cd, Pb and Cu was investigated. It was observed that the stripping peak remained unaltered on addition of Fe, Mn, Ni, Cr, V, U, Hg in the stripping solution at 1000 times higher concentration than the analyzing metal ions of Zn, Cd, Pb and Cu. However Cd and Pb peaks were affected by Mo and Nb at 10 times higher concentration than the analytes.

### III. 1. 4. 7. Analytical treatment of the recorded data:

Analytical responses obtained from all these modified electrodes were reproducible. The three sigma limit of detections (LOD) for Zn, Cd and Pb against each modified electrodes were calculated following the method described in chapter II (section II. 9). Calculated LODs were tabulated in table III.1. Though the sensitivity was enhanced with CNTMBFE, LOD of the measurements did not improve due to the higher blank value in the measurements. As a comparison to the present method, LODs obtained by other methods reported in earlier literature [287, 311, 312] are reported in table III.2. The three sigma LOD of Cu was obtained as 4.6 µg $L^{-1}$ using BFCPE.

| Element | BFCPE (µg $L^{-1}$) | NCBFE-2 (µg $L^{-1}$) | CNTMBFE (µg $L^{-1}$) |
|---|---|---|---|
| Zn | 17.3 | 37.1 | 17.7 |
| Cd | 16.9 | 16.2 | 16.5 |
| Pb | 11.9 | 10.9 | 17.6 |

**Table III.1:** Detection limits/Limit of detections (LOD) obtained using BFCPE, NCBFE - 1 and NCBFE - 2 for Zn, Cd and Pb in aqueous solution.

| Reference | Zn (µg $L^{-1}$) | Cd (µg $L^{-1}$) | Pb (µg $L^{-1}$) |
|---|---|---|---|
| 311 | 600 | 2.2 | 23.1 |
| 312 | ----- | 1.48 | 1.03 |
| 287 | 0.4 | 0.1 | 0.1 |

**Table III.2:** Limit of detection (LODs) for Zn, Cd and Pb reported in the literature using Bi film electrode.

### III. 1. 4. 8. Sample Analysis:

NCBFE - 2 was used for the analysis of lake water and potable water samples and BFCPE was used for the analysis of two types of triphala samples coded as M7205 and M7206. Triphala is an ancient ayurvedic medicine and its preparation is noted in the Ayurvedic Formulation of India (AFI). Triphala is basically the combination of three medicinal plants: amalaki, bibhitaki and haritaki. There are many manufacturers of triphala in India; we have analyzed the Zn, Cd, Pb and Cu content of triphala from two different manufacturers. Digestion of the solid samples (M7205 and M7206) was carried out using Anton Paar Microwave Digester, Multiwave-3000. An aliquot of 1 g of the solid sample was taken with 5 ml of concentrated nitric acid and digested at 150 $^{O}$C for 20 min. After complete digestion, the solutions were diluted with nano pure water and made up to the volume of 50 ml. Aliquot of this sample solution was taken in the voltammetric cell and voltammetric scans were recorded. Analysis results are tabulated in table III.3. Samples were also analysed using hanging mercury drop electrode (HMDE) and the values were tabulated in the Table inside the bracket.

| Sample | Zn (μg L$^{-1}$) | Pb (μg L$^{-1}$) | Cd (μg L$^{-1}$) | Cu (μg L$^{-1}$) |
|---|---|---|---|---|
| Powai lake | 160 (155) | 12 (13) | ND (1.4) | 26 (30) |
| Tap water | 121 (150) | 16 (15) | ND (1.0) | 10 (11) |
| M7205 | 42(44) | 36(33) | ND (0.02) | 8.5(8.8) |
| M7206 | 30(32) | 8.1(7.6) | ND (0.31) | 15(16) |

**Table III.3:** Analysis result of the water samples collected from different places of India using NCBFE - 2 for water samples and BFCPE for solid samples, values under the parenthesis were obtained using HMDE.

% RSD (sample number, n = 6) calculated for the metal ions for the above real samples were tabulated below (Table III.4).

| Sample | Electrode used | Zn (%RSD) | Pb (%RSD) | Cu (%RSD) |
|---|---|---|---|---|
| Powai lake | NCBFE - 2 | 4.1 | 3.7 | 3.2 |
| Tap water | NCBFE - 2 | 4.1 | 3.7 | 3.4 |
| M7205 | BFCPE | 5.2 | 3.8 | 6.7 |
| M7206 | BFCPE | 5.2 | 3.8 | 6.6 |

**Table III.4:** % RSD calculated from the analysis of real samples (collected from different places of India) for Zn, Cd, Pb, and Cu in real samples, using NCBFE – 2 and BFCPE.

### III. 1. 5. Conclusion:

CPE was modified using Bi films for the determination of heavy metal ions. Bi-film was modified with nafion coating for the stability of the film and also to enhance sensitivity of the material. Nafion coating before the deposition of Bi films was found to have enhanced the sensitivity. Almost an order of magnitude enhancement in the sensitivity was observed when carbon paste was modified with MWCNT and nafion. Effect of the deposition potential for the determination of Cd and Pb was studied in detail in order to evaluate the effect of different modifications on the voltammetric response. Effects of three different surfactants were investigated on nafion coated Bi film electrodes. Nafion modifications improved the tolerance of ionic surfactants in the stripping solutions. No improvement was observed for neutral surfactant on nafion modifications. Generally, the method was found to be tolerant in presence of surfactants in the real water samples and could be applied for the determination of targeted heavy metal ions directly on judicial application of deposition and conditioning potentials.

# Chapter III.2

## *Antimony and antimony-gold nano composite modified carbon paste electrodes for the determination of heavy metal ions*

### III. 2. 1. Abstract:

This chapter presents the important aspects of modification of carbon paste electrode (CPE) by antimony (Sb) film for the determination of the heavy metal ions such as Cd, Pb and Cu. An ex situ analytical method based on this Sb film modified CPE (SbMCPE) for the determination of Cu is discussed. Modification of CPE by Sb-Au nano composite for sensitive determination of Hg in sub µg $L^{-1}$ level concentration is explored here. Finally, application of these modified electrodes for the analysis of the real sample is presented.

### III. 2. 2. A brief account of antimony film and its composite with gold as sensing platforms for heavy metal ions:

In the search of electrode materials alternative to mercury for stripping voltammetric analysis thin metal-film electrodes gained widespread popularity in electrochemical stripping analysis due to their relatively simple fabrication and surface regeneration. Wang et al. developed a Bi film as an electrode material for the determination of heavy metal ions [273]. The electrode was quite successful in stripping voltammetry when plated over a glassy carbon electrode (GCE) [274, 281, 284-288] or on a CPE. [89, 280, 289, 290]. The use of antimony as an electrode material for potentiometric pH measurement was first reported in 1923 by Uhl and Kestranek [313] followed by other contributions, e.g., application of an antimony based electrode for measuring pH in whole blood [314]. As an electrode material, antimony/antimony oxide has been successfully used for decades for pH measurements, as a solid metal/ metal oxide ion-selective electrode in laboratory and biomedical (e.g., dental) applications [315-318] exploiting a well-known $Sb/Sb_2O_3$ surface equilibrium. It was 2007 when Hocevar et al. first reported the use of Sb film as sensitive electrode material for the stripping analysis of heavy metal ions [319]. Sb film was deposited on GCE in situ for analysis of Cd, Pb, Bi ang Hg. In the majority of initial reports, the Sb film was generated by plating over the surface of a GCE [319-326]. Later, Sb film was also deposited over the surface of a CPE for analytical applications [94, 327-335]. To improve the sensitivity and application for a specific purpose, Sb films were deposited over many substrates including boron doped diamond electrodes [340], silicon wafers [337] and carbon nanotubes [336, 338]. An antimony microelectrode was fabricated by plating Sb film on a single carbon fibre microelectrode [339]. Due to the easy fabrication and cost effectiveness, the CPE is the ultimate choice [340]. For the determination of Cd and Pb, the Sb film was applied successfully [319-322, 328]. However, there are only a few reports on the determination of Cu and Hg [326, 333, 335]. Interestingly, in most previous reports, the Sb film modified electrode was used in a highly acidic medium and electrodes were mostly fabricated in situ. Since their introduction, Sb film electrodes were applauded for their excellent characteristics in highly acidic solutions with $pH < 2$. Only one report [339] is available for the application of Sb film electrodes in neutral solutions. Here this work presents ex situ fabrication of Sb film modified CPE for the analysis of heavy metal ions in near neutral pH. SbMCPE was not suitable for the sensitive and reproducible determination of Hg in the $\mu g\ L^{-1}$ level of concentration. Gold is known to be superior substrate for working electrode [341] owing to its high affinity for mercury, which enhances the preconcentration effect. Several kinds of gold electrodes were used for the voltammetric determination of mercury such as solid gold electrodes [342, 343], gold films [344, 345], gold micro wire [346-348], gold fibre [349] and gold ultramicroband array [350]. Gao et al. [351] electrodeposited gold nanoparticles (AuNPs) onto a gold electrode, followed by a modification with a mercaptoethanesulfonate monolayer for the same purpose. It was Ornella Abollino and his group who used AuNPs modified glassy carbon electrode for the determination of Hg [352] by anodic stripping voltammetry, the work was followed by Barnalte et al. to modify screen printed electrode (SPE) for the same purpose [353]. Sahoo et al. applied gold nano particle modified CPE for the same purpose [354]. Here, the present work explored the incorporation of gold in the antimony film to prepare a nano composite which worked quite sensitively for the determination of Hg in the μg $L^{-1}$ level of concentration.

### III. 2. 3. Fabrication of modified electrodes:

CPE was prepared by the method already described in chapter II (section II. 4. 6). Sb film was electrochemically deposited from the 10mM $SbCl_3$ solution in 0.02M HCl using constant potential deposition technique to prepare SbMCPE. Highly acidic condition was maintained to avoid hydrolysis of $Sb^{3+}$, which occurs at higher pH of the solution. The deposition potential was varied from -0.2V to -1.0V and a value of -0.6V was optimized for the faster deposition of the Sb on the CPE. At a more negative deposition potential than -0.6 V, hydrogen evolution from the surface of the electrode was observed, which made the films unstable. The deposition time was optimised at 100 sec. Thickness of the film depends on the time of deposition and the performance of the electrode in the stripping voltammetry strongly depended upon the thickness of the film which will be discussed in the subsequent section of this chapter. On the other hand, SbMCPE was not suitable for sensitive and reproducible detection of Hg, Au was incorporated in the form of Sb-Au nano composite as a surface modifier. The modification of CPE by Sb-Au nano composite was carried out by simultaneous electrochemical deposition of the Au and Sb at a constant potential of -0.6V for 100 sec from mixed solution containing 10mM of $SbCl_3$ and 1mM of $AuCl_3$ in 0.02M HCl. After deposition of the modifier films the electrode surfaces were rinsed with deionized water prior to use to make the electrode surface free from any residual precursor ions.

### III. 2. 4. Results and Discussions:

#### III. 2. 4. 1. Morphological study using SEM and EDS:

Morphological information about the films was obtained from scanning electron microscopy (SEM) imaging. SEM image of SbMCPE showed well dispersed globular Sb nanodeposits of 50 to 100 nm in diameter over the surface of the carbon paste electrode (Fig. III.11.a). Formation of Sb nanoparticles deposit was also supported by an article published by Asrafi et al. [355]; the article reported formation of separate Sb agglomerate and crystalline Bi deposits when Sb and Bi were co-deposited. This substrate was used for the analysis of Cd, Pb and Cu. In contrast, SEM images of Sb-Au nano composite exhibited dendrimeric structures (Fig. III.11.b). The SEM with energy dispersive spectra (EDS) of a point scan and an area scan for the Sb–Au nano composite film pre-concentrated with Hg are shown in figure III.12.a, III.12.b and III.13.a, III.13.b respectively. The presence of Sb on the Sb-deposited carbon paste electrode was clearly observed in both the point and area scans. The signature due to the Au and Hg was also observed in the EDS measurements of the Sb –Au modified nano composite.

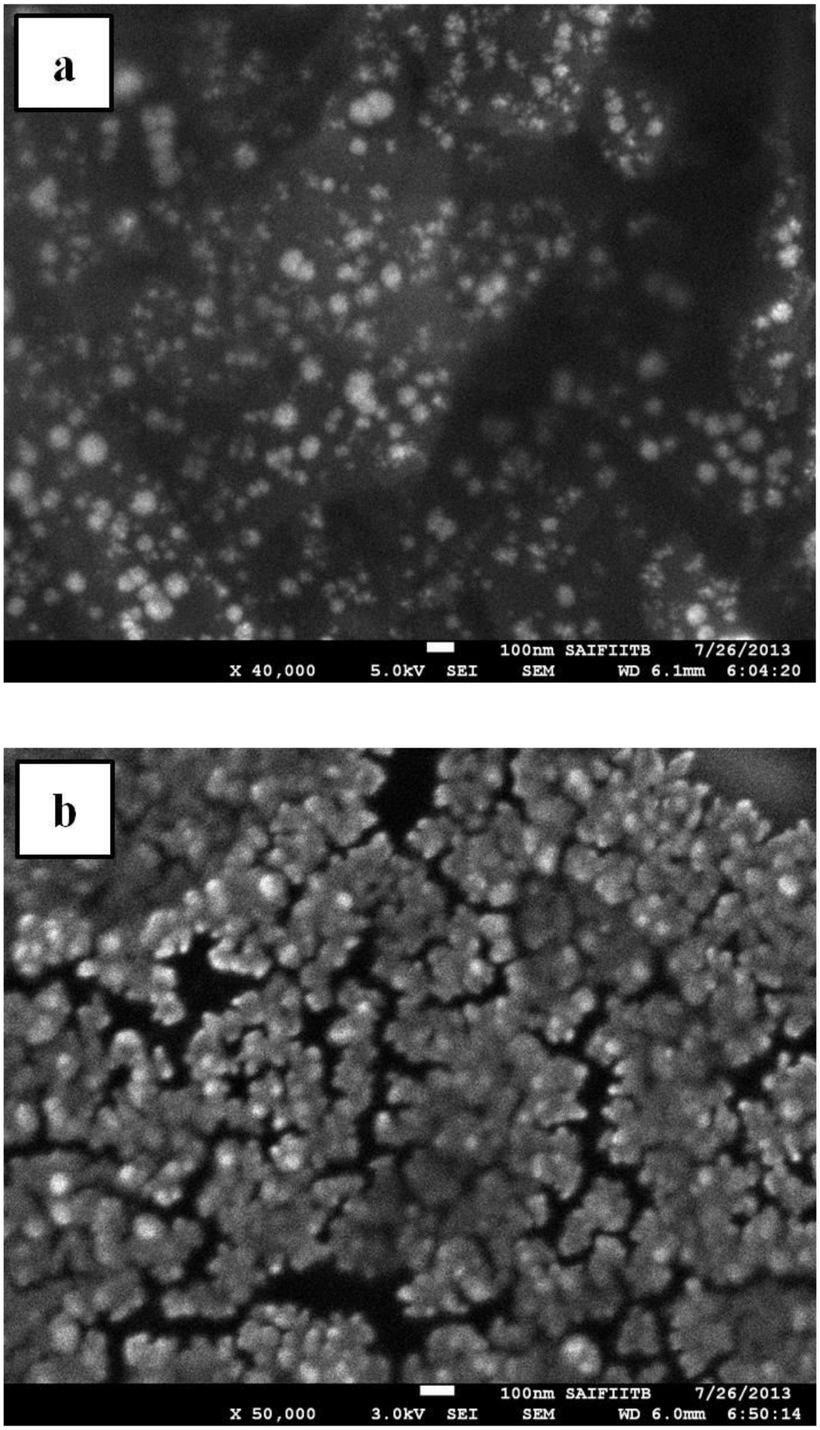

**Figure III.11:** SEM micrograph of (a) the Sb film modified CPE and (b) the Sb–Au nano composite modified CPE used for Hg determination.

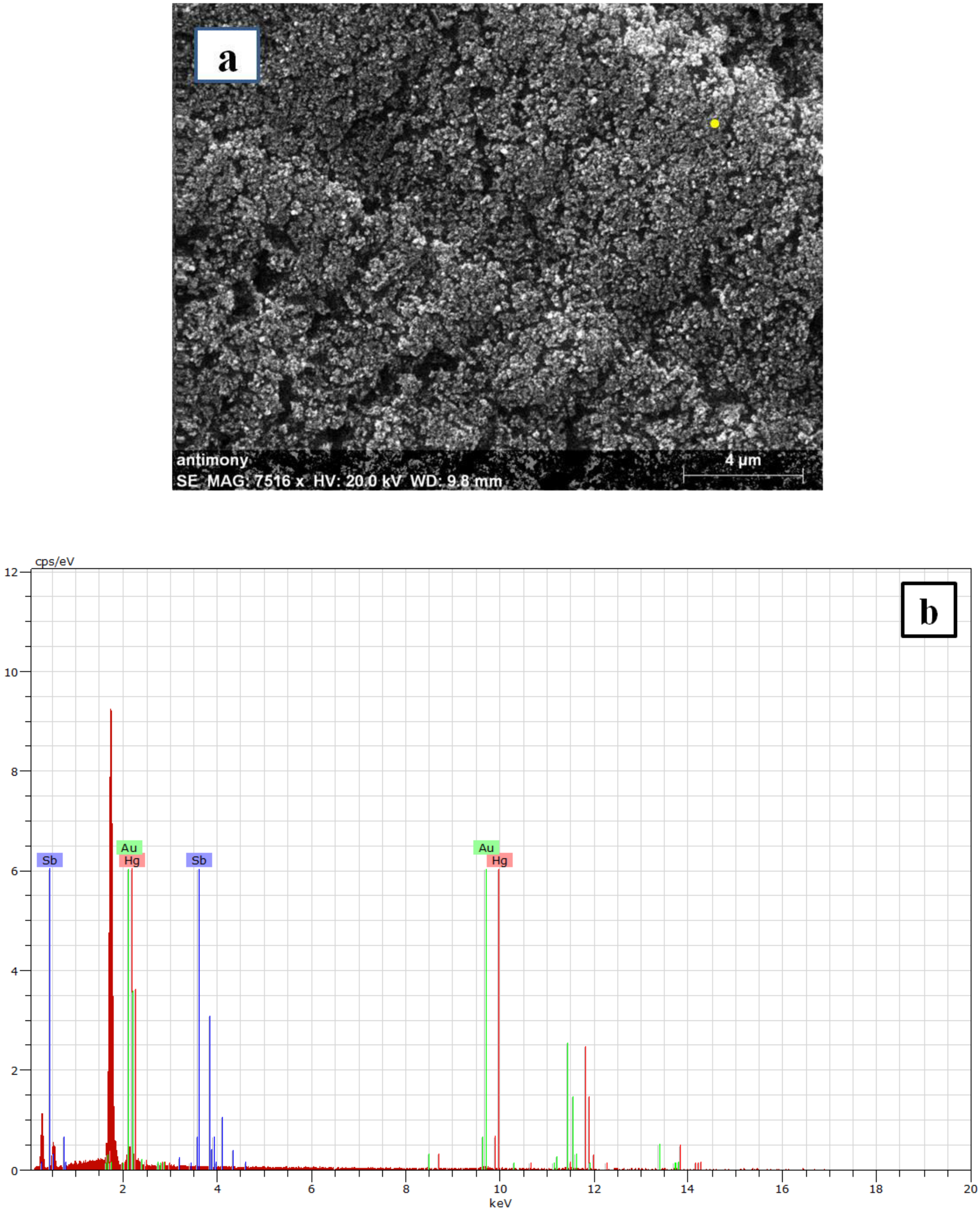

**Figure III.12:** (a) SEM image and (b) EDS spectra of point scan of point scan for the Sb-Au nano composite film pre-concentrated with Hg.

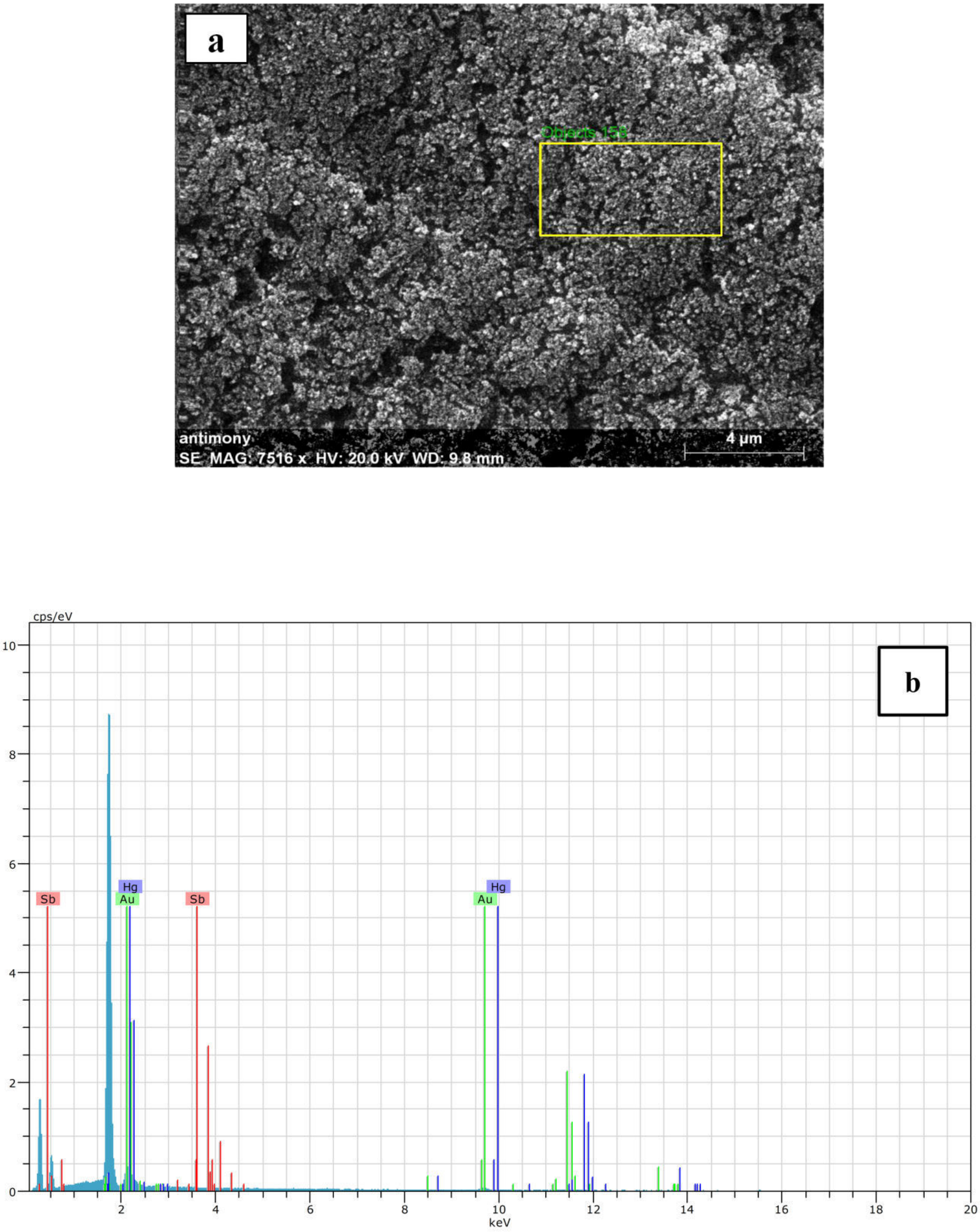

**Figure III.13:** (a) SEM image and (b) EDS spectra of area scan of point scan for the Sb-Au nano composite film pre-concentrated with Hg.

### III. 2. 4. 2. Effect of the thickness of the Sb film on the analytical response of the modified electrode:

The Sb film deposited over the surface of the carbon paste electrode was applied for the determination of heavy metal ions. Thickness of the Sb film was optimized by measuring the stripping response of Cd while varying the deposition time of the Sb film; corresponding results are shown in the figure III.14. A thin film generated using deposition times of 50 sec and 100 sec exhibited a better stripping response in the presence of Cd. At higher deposition times of 150 sec and 200 sec, the stripping response of Cd was reduced. These results reflect the fact that a thin Sb film is important for the stripping voltammetry. In this case, the preconcentrated Cd would remain predominantly at the surface of the film because the surface to volume ratio of a thin film is higher than that of a thick film. The formation of intermetallic compounds also played an important role in the stripping response.

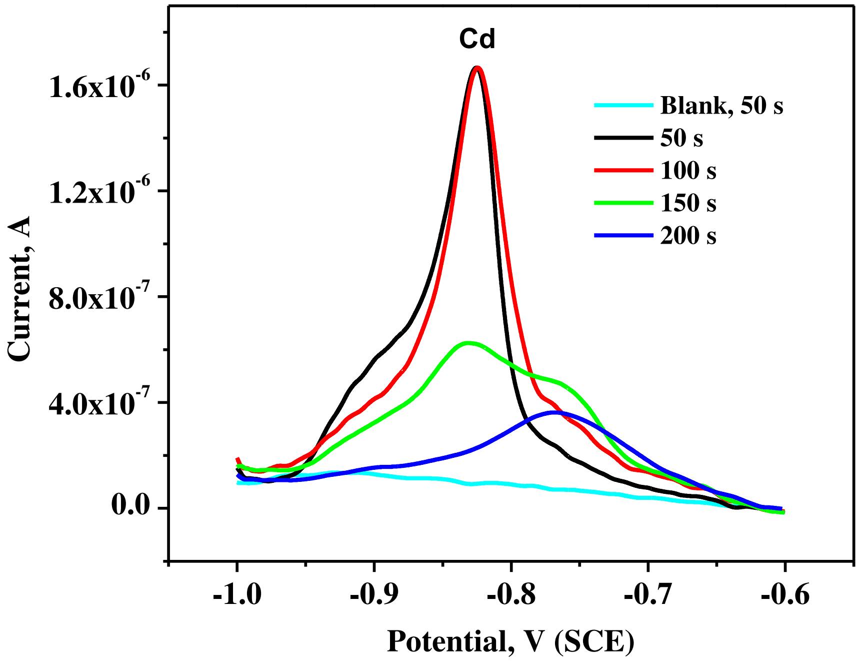

**Figure III.14:** Effect of deposition time of Sb deposition on the stripping peak of Cd (75µg L$^{-1}$), Sb deposition potential: -0.6V, from 10mM antimony trichloride solution (in 0.02 M HCl).

From these observations, a deposition time of 100 sec for Sb film deposition was found to be optimum. The Sb content for the ultimate stripping signal was also investigated previously for the determination of Pb and Cd [339] and for Cu [334, 339]. Similar observation was also reported in a previous investigation, which showed that beyond a certain amount of Sb relative to the amount of analytes, the stripping response to heavy metal ions was reduced. In this investigation, the film thickness was optimized using the Cd stripping signal. This was due to the fact that the presence of Cd in natural water is much lower than the concentrations of Pb and Cu; thus, it is advisable to optimize the sensor response with respect to Cd. Moreover, it was observed that the sensitivity of the measurements for Pb and Cu was very good when using the Sb film thickness optimized by measuring the Cd stripping response.

### III. 2. 4. 3. Effect of pH on the stripping peak of Sb films deposited over the surface of carbon paste electrode:

In stripping voltammetric measurements, the Cu stripping peak appears after the Sb stripping peak. Thus, it was necessary to separate these two stripping peaks to observe the stripping response of Cu on the Sb film modified CPE. The dissolution behaviour of antimony after deposition was investigated in two supporting electrolyte media: HCl and sodium acetate (NaOAc) at different pH values. This set of experiments was performed to confirm the dissolution characteristics of the Sb film and also to optimize the supporting electrolyte media to obtain a clear separation between the Sb and Cu stripping peaks. The stripping response of the deposited Sb films at different pH values in an HCl solution is depicted in figure III.15.a. Two stripping peaks were observed during the anodic dissolution of the Sb film [356]. The potential region where the peaks were observed is the active dissolution range of antimony. At highly acidic pH values in the range of 1 to 2, two stripping peaks of Sb were observed: one at -0.07 V and the other at 0.06 V. When the pH of the stripping solution was increased, the stripping peak shifted towards a more negative direction and the stripping peak height was reduced.

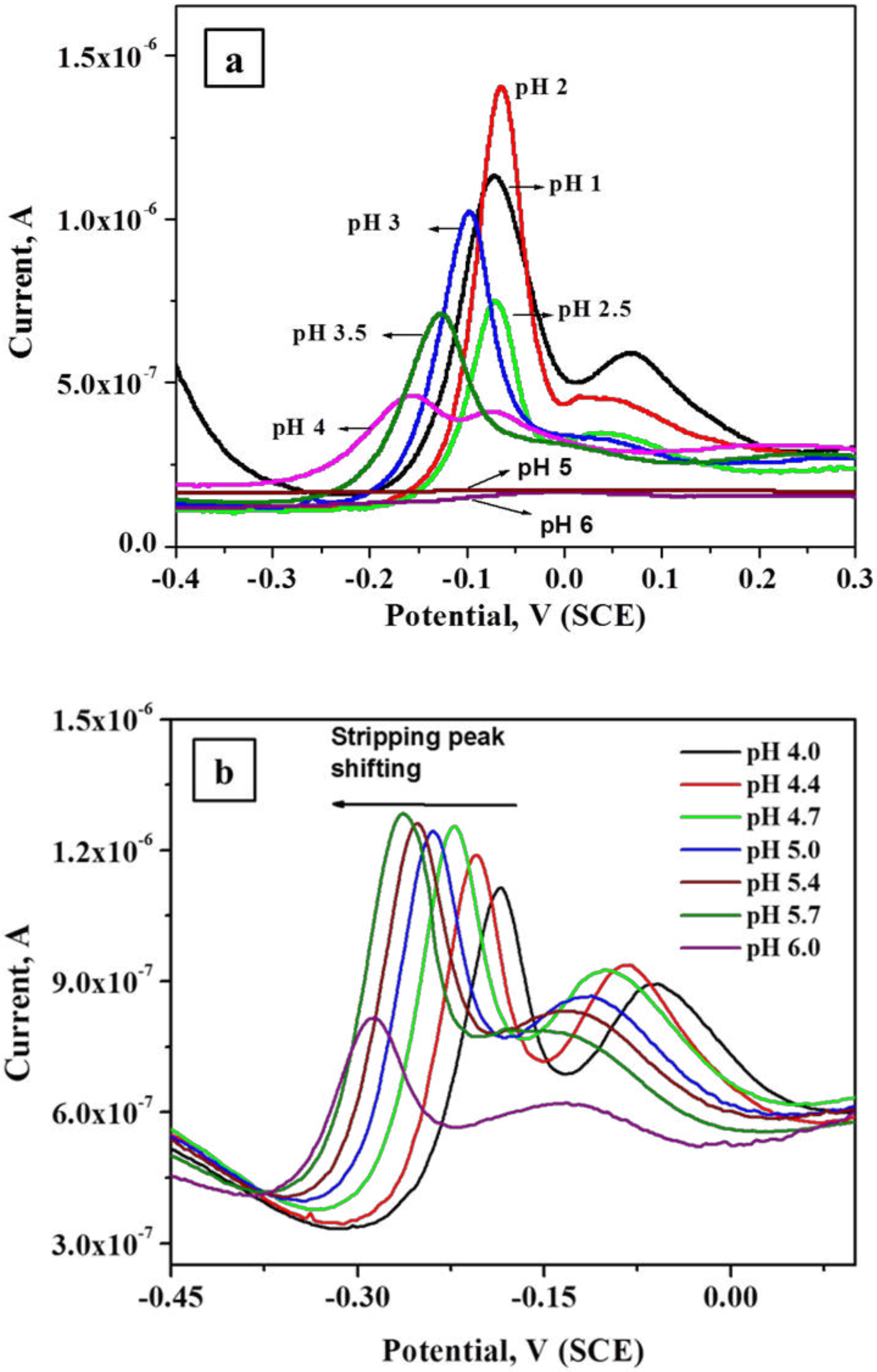

**Figure III.15:** Effect of pH on the Sb stripping characteristics in (a) HCl solution and (b) sodium acetate solution; Sb deposition was carried out using 10 mM antimony trichloride solution (in 0.02 M HCl) at a deposition potential of -0.6 V for 100 sec.

At pH 4, the stripping peak of Sb was observed approximately at -0.16 V. Above the pH 4, the stripping peak was reduced further and nearly vanished at pH 5. The Sb film was not as stable after the repeated use of the modified electrode during the standard addition method in the hydrochloric acid solution. Sodium acetate at a concentration of 0.1 M was chosen as an alternate stripping solution as it is a good supporting electrolyte medium in stripping analysis. The effect of the pH on the stripping peak of Sb film was investigated in the sodium acetate solution and the results are shown in figure III.15.b. Similar to that of the HCl solution, two stripping peaks were observed. When the pH of the solution was increased, the stripping peaks shifted negatively in the acetate medium. At pH 6, the Sb stripping peak was reduced, but unlike in the HCl solution, it did not vanish completely. The second stripping peak was reduced significantly, which made it possible to observe the stripping peak of Cu separated from the Sb stripping peak. Thus, by adjusting the pH of the solution, it was possible to shift the Sb stripping peak towards a negative direction such that the Cu stripping peak could be separated from the Sb peak. At higher pH values, the Sb film was oxidised to form a passive Sb oxide film at the surface of the electrode, which reduced the Sb stripping current. Furthermore, at a lower pH value of approximately 1, the corrosion potential of Sb remained in the active region. At a highly acidic pH, the Sb dissolved according to the following two steps [356]:

$$Sb + H_2O \rightarrow SbO(ads) + 2H^+ + 2e^-$$

$$SbO(ads) \rightarrow Sb(O)^+ + \ e^-$$

When the pH increased, a passive film was formed with an inner layer of porous antimony oxide ($Sb_2O_3$) and an outer layer of antimony pentoxide ($Sb_2O_5$) [356]. At a higher pH, the passive oxide film was predominantly formed, which shifted the peak potential towards a negative potential. The stripping peak current was reduced due to the passivation of the surface of the electrode. This interesting property of the Sb film has made it attractive for use in stripping voltammetry predominantly for the determination of metal ions with peak potentials close to the Sb stripping peak [319, 326, 335]. In this study, 0.1 M sodium acetate with a pH of 6 was optimized as the supporting electrolyte medium for all metal ions investigated.

### III. 2. 4. 4. Analytical responses for Cd and Pb:

After optimising the deposition time of Sb and the pH of suitable supporting electrolyte, SbMCPE was used for the determination of Cd and Pb. 0.1M NaOAc of adjusted pH 6 was taken as supporting electrolyte medium for the anodic stripping voltammetry of Pb and Cd.

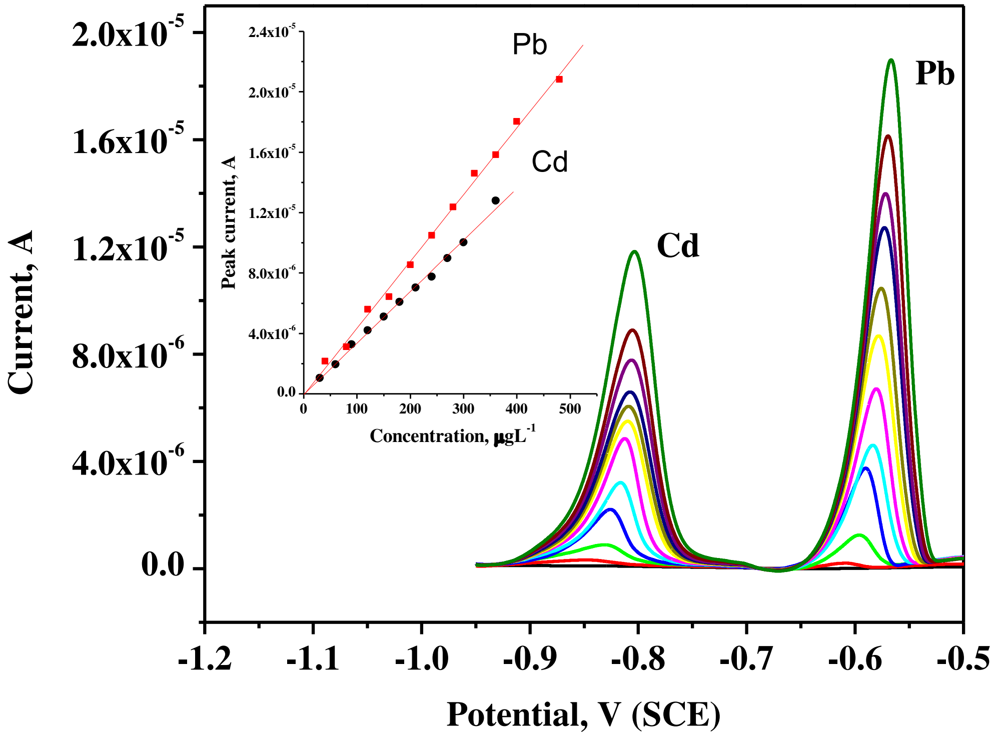

**Figure III.16:** Differential pulse anodic stripping voltammetric plots of Cd and Pb at varying concentrations on the SbMCPE, the Cd and Pb deposition was carried out at -1.0 V for 300 sec in 0.1 M sodium acetate solution at pH 6.0. Inset: corresponding linear calibration plot.

This preferred condition of the supporting electrolyte solution was chosen to maintain a uniform stripping solution condition for detection and quantitative estimation of all the metal ions (Cd, Pb and Cu), as higher pH was required for the determination of Cu. Analyte deposition potential was optimized at -1V for simultaneous deposition of Cd and Pb for 300 sec. Pb and Cd was found to produce stripping signals at -0.56V and -0.8V respectively with respect to SCE (Fig. III.16).

The peak potentials were negatively shifted relative to those found on HMDE, but, almost superimposed on the peak positions obtained from BFCPE (Fig. III.17). This behaviour implies there are similar processes associated with the formation of metal alloys with bismuth and can apparently be predicted also for antimony. While comparing the results with published articles related to Sb film modified electrodes, the results of the present work were found to be in good agreement with the previously reported data [319]. Calibration plot was constructed by recording the stripping signals of Cd and Pb with subsequent increase of their concentration. The same electrode was used for every scan, prior to each scan the analyte solution was purged for 300sec to remove dissolved oxygen from the solution so as to minimize the nuisance caused during scanning in the anodic direction, the electrode was cleaned by applying a conditioning potential of -0.45V for 300 sec and the analyte ions were further deposited at the optimized potential. Conditioning stripped the deposited metals back to the solution in the form of ions due to oxidation and regenerate the fresh electrode surface. The corresponding linear calibration plots are shown in the inset of figure III.16. The Pb calibration curve exhibited a linear relationship with a slope of 4.42 A $\mu g^{-1}$ L and a correlation coefficient of 0.998. The Cd calibration plot also exhibited a linear relationship with a slope of 3.42 A $\mu g^{-1}$ L and a correlation coefficient of 0.997. The modified electrode worked well for Pb and Cd at pH 6 and also in acidic solution.

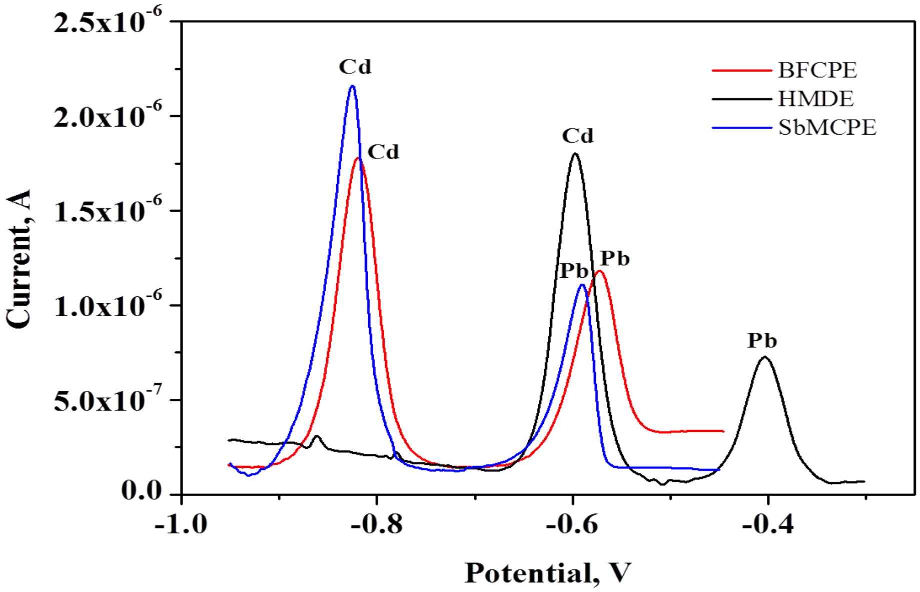

**Figure III.17:** Comparison of peak potentials of anodic stripping peaks of Pb and Cd on BFCPE, HMDE and SbMCPE.

### III. 2. 4. 5. Analytical response for Cu:

Very weak stripping signal of Sb film in 0.1M NaOAc solution of pH 6 improved its application for determination of Cu. $Cu^{2+}$ was deposited at -1.0V for 300 sec. Fresh Sb film was deposited ex situ every time prior to the deposition of Cu and its stripping. The stripping voltammogram plot is shown in figure III.18. Cu stripping peak is well separated from that of Sb. Sb stripping peak was so weak that Cu stripping peak was well observable at -0.07V (vs. SCE). The voltammetric response increased with the increase in concentration of the $Cu^{2+}$. A linear calibration plot was constructed (inset of Fig. III.18) with a slope of 4.42 A $\mu g^{-1}$ L and a correlation coefficient of 0.998.

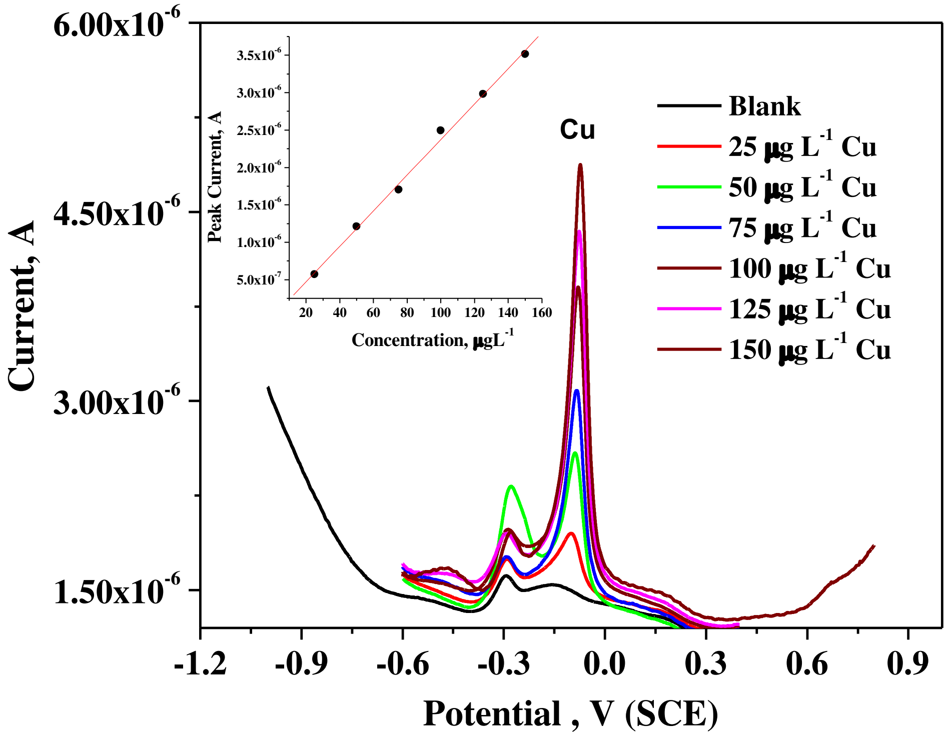

**Figure III.18:** Differential pulse anodic stripping voltammetric plot of Cu at varying concentrations on the SbMCPE, Ex-situ Cu deposition at -1.0 V for 300 sec in 0.1 M sodium acetate solution at pH 6. Inset: corresponding linear calibration plot.

### III. 2. 4. 6. Determination of Hg:

In a recent report, determination of Hg was reported using an Sb film electrode [335]. In our study, the stripping response of Hg could not be detected at 1 µg L$^{-1}$ and a low concentration range on a bare SbMCPE electrode. To improve the sensitivity, Sb–Au nano composite material was casted on CPE using the electrodeposition route, described in the earlier section (section III. 2. 3). The dendrimeric deposits of Sb–Au nano composite material exhibited good sensitivity towards Hg. The conditions for Hg deposition on the composite modified electrode were optimized at -0.6V and 300sec. Deposition of Hg at a potential more negative to -0.6V yields non reproducible and low analytical response for Hg, this might be because of facilitated hydrogen evolution from gold nano deposites of the composite material. Under these optimized conditions the modified electrode produced appreciable stripping signal for Hg of 0.5 μg $L^{-1}$ concentration (Fig. III.19) at 0.15V. The stripping peak current increased linearly with the concentration (inset of Fig. III.19) constructing a linear calibration plot with a slope of 4.12 A $\mu g^{-1}$ L and a correlation coefficient of 0.998.

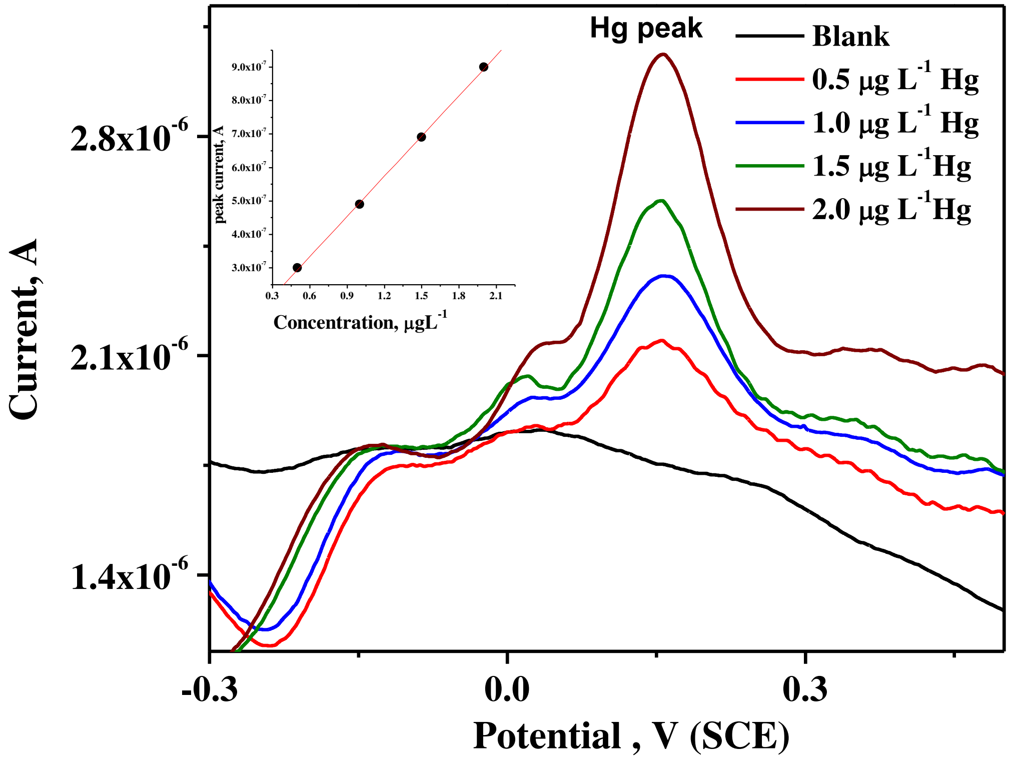

**Figure III.19:** Differential pulse anodic stripping voltammetric plot of Hg using Sb–Au nano composite modified carbon paste electrode. Hg deposition at -0.6V for 300 sec and stripping was performed in 0.1 M sodium acetate solution. Inset: corresponding linear calibration plot.

### III. 2. 4.7. Analytical treatment of the recorded data:

Analytical signals for the analyte ions were reproducible for both types of modified electrodes. LODs of all the metal ions were calculated based on the procedure described in chapter II. Six No. of samples were taken for the measurement of LOD of each metal. LODs of Pb, Cd and Cu were determined to be 2.65 µg L$^{-1}$, 2.32 µg L$^{-1}$ and 9.73 µg L$^{-1}$using SbMCPE. On the other hand LOD of 0.052 µg L$^{-1}$for Hg was obtained using Sb-Au nano composite modified CPE in the aqueous solution. Our group reported AuNPs modified CPE for determination of Hg [354] with a LOD of 0.24 µg L$^{-1}$ in aqueous solution. In the present study the AuNPs were embedded in the Sb film matrix, this improved the overall and the inter particle conductivity of the composite material. This results in the improvement of the detection limit. The LODs obtained in the present work was compared with some literature reports as shown in table III.5.

| **Reference** | **Element(s)** | **Modified electrode** | **Solution condition** | **Detection Limit(µg L$^{-1}$)** |
|---|---|---|---|---|
| 333 | Cu | Sb modified CPE | pH 2 | 1.45 and 1.10 |
| 335 | Hg | Sb modified CPE | 1M HCl | 1.3 |
| 326 | Hg | Sb modified CPE | 1M HCl | 0.39 |
| 356 | Pb and Cd | Sb and Bi co-deposited film modified CPE | pH 2 | 1.4 and 1.1 respectively |
| This work | Hg, Cu, Pb and Cd | Sb-AuNPs modified CPEs for Hg and Sb film modified CPE for Cu, Pb and Cd. | pH 6 | 0.052, 9.73, 2.65 and 2.32 respectively |

**Table III.5:** Comparison of analytical parameters determined using SbMCPE and Sb-Au nano composite modified CPE with the results already published in the literature.

The LOD of Hg in the present work was superior compared to that reported in the other literature, while LODs of Cd, Pb and Cu were found to be either higher or comparable to those reported in the other literature.

### III. 2. 4. 8. Recovery Test and Sample analysis:

A recovery test was performed using tap water samples by spiking known concentrations of Hg, Cu, Pb and Cd and determination was carried out using the fabricated electrodes. The test results are shown in table III.6. All elements were recovered within 10% deviation from the added concentration.

| Element | Spiked concentration ($\mu g\ L^{-1}$) | Recovery concentration ($\mu g\ L^{-1}$) | % of Recovery |
|---|---|---|---|
| Hg | 5 | 5.03±0.24 | 100.6% |
| Cu | 20 | 21.5±1.14 | 107.5% |
| Pb | 10 | 9.6±0.59 | 96% |
| Cd | 5 | 5.3±0.24 | 106% |

**Table III.6:** Recovery test results of Hg, Cu, Pb and Cd using the SbMCPE and Sb-Au nano composite modified CPE.

The modified electrodes were applied for the determination of heavy metal ions in real water samples. Two water samples collected: one from the Powai Lake in the Mumbai suburban area and another ground water sample from the OSCOM (Odissa Sands Company) mining area. The analysis results are shown in table III.7.

| Sample | Cu ($\mu g\ L^{-1}$) | Pb ($\mu g\ L^{-1}$) | Cd ($\mu g\ L^{-1}$) | Hg ($\mu g\ L^{-1}$) |
|---|---|---|---|---|
| Powai lake | 26±1.38 (30) | 12±0.74(10) | Not detected | 0.25±0.012 (0.55) |
| OSCOM | 49±2.59 (63) | 50±3.1 (56) | 10±0.46 (11) | 145±6.96 (134) |

**Table III.7:** Analysis results of Cu, Pb, Cd and Hg in two samples collected from two regions of India using the modified electrodes. Values in the parenthesis for Cu, Pb and Cd were calculated using ICPAES; while, for Hg, it was calculated using thermal decomposition atomic absorption technique.

The analytical results were cross verified using the results from inductively coupled plasma atomic emission spectrometry (ICPAES) technique for Cu, Cd and Pb and the total mercury analyser based on the thermal decomposition atomic absorption technique for Hg (in the parenthesis). The analytical results for most of the measurements were in good agreement between two methods. The Hg content in the Powai Lake water sample determined using the modified electrode was not in agreement with the measured values from the total mercury analyser. In the Powai Lake water sample, Pb was pre-concentrated by the evaporation pre-concentration method. The water sample from OSCOM was collected from a mining area where the heavy metal ion content was higher due to mining activities. The Hg content in that sample was significantly higher than the limit prescribed by the World Health Organization (WHO) for potable water.

### III. 2. 5. Conclusion:

CPE was modified with Sb film and Sb-Au nano composite by simple electro deposition technique and the procedure of modification was optimized considering sensitivity and selectivity of the modified electrode for the determination of the targeted analytes. The SbMCPE was used for the determination of Cd, Pb and Cu while the Au-Sb nano composite modified CPE could be used for Hg. LODs for these metal ions were found to be superior to those obtained for the Bi film/composite modified CPEs discussed in the previous chapter. The feasibility of the direct determination of Cu and Hg by the Sb film/composite modified CPE was the real advantage over the Bi film/composite modified CPEs, the only disadvantage compared to Bi modified CPEs as discussed in the first part of this chapter as the need of deoxygenation of the dissolved oxygen from the experimental solution prior to scanning. Most importantly, the modified electrodes could be applied in a near neutral solution with pH 6. Water samples were not required to be digested before analysis. Real samples were analysed using the modified electrode. This development opened up the possibility of fabricating sensors based on these modified electrodes for field application.

# Chapter IV

## *Engineered Nanomaterial Based Electrochemical Sensors for Biomolecules*

## Introduction:

Quantification of biological or biochemical processes is of utmost importance for medical, biological and biotechnological applications. However, converting the biological information to an easily processed electronic signal is challenging due to the complexity of connecting an electronic device directly to a biological environment [357]. Electrochemical biosensors provide an attractive means to analyze the content of a biological sample due to the direct conversion of a biological event to an electronic signal. The sensing of biomolecules including glucose, dopamine, proteins, enzymes, uric acid, DNA, RNA, and $H_2O_2$ traditionally employs enzymes, nucleic acids, antibodies, whole cells, and receptors as recognition element. These recognition elements are immobilized on the electrode surface. Of these, enzymes are the most commonly used recognition elements (or transducers which translate the interaction of the analyte with the biological element into electrochemical signal) [358]. However, these enzymes denature easily, therefore the enzymeless methods are highly desired. In order to increase sensitivities and to lower detection limits down to even individual molecules, nanomaterials are promising candidates due to the possibility to immobilize an enhanced quantity of bioreceptor units at reduced volumes, in addition to that they can itself act as transducer element as well. Among such nanomaterials, gold nanoparticles [359], semiconductor quantum dots [360-362], polymer nanoparticles [363, 364], carbon nanotubes [365-368], nanodiamonds [369], and graphenes [370-375] are intensively studied. One rapidly growing area of biosensor design involves incorporation of carbon based nanomaterials in working electrodes [376, 377]. This chapter deals with the inspection of redox properties of few important biomolecules such as melamine, dopamine, uric acid and L-cysteine using nanomaterials based enzymeless electrodes and further, development of electrochemical methods for the determination of the concentration of these molecules in different media. The chapter comprises of three parts where part 1 deals with the electrochemical property of melamine, in part 2 the electrochemical property of important neurotransmitter, dopamine is explored and in part 3 the electrochemistry of cysteine is discussed. Apart from these biomolecules the electrochemical property of another important organic molecule 2-(o-hydroxyphenyl)benzoxazole is discussed in another part. In addition to the bio-chemical application it has importance as energy storage materials when a composite of it with different form of carbon is fabricated.

# Chapter IV.1

## *Investigation of electrochemical properties of melamine and development of methods for its determination in milk samples*

### IV. 1. 1. Abstract:

The present work is entitled to extract the electrochemical properties of melamine (2,4,6-Triamino-1,3,5-triazine) on different electrodes and development of electroanalytical methods for its determination in milk products. Static mercury drop electrode (SMDE) and AuNPs modified CPE were used to investigate the redox properties of the species. Effect of melamine on the electrochemical response of ferrrocyanide/ferricyanide redox couple on RGO-AuNPs composite modified CPE electrode is discussed in this chapter. Optimization of different experimental parameters, solution conditions for development of methods for its determination using electrochemical techniques are accounted here.

### IV. 1. 2. Introduction to melamine:

Melamine is an organic base and a trimer of cyanamide, with a 1,3,5-triazine skeleton. Its IUPAC name is 1,3,5-triazine-2,4,6-Triamine, it contains 67% nitrogen by mass (Fig. IV.1). Due to the presence of high content of nitrogen it acts as fire retardant, when mixed with resins it releases nitrogen gas upon burning.

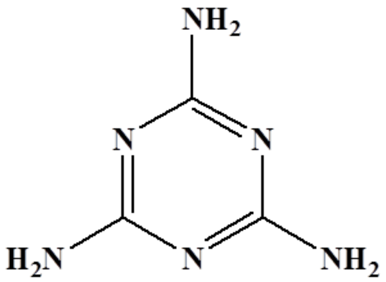

**Figure IV.1:** Chemical structure of melamine.

It has several other industrial applications. It forms a very durable thermosetting plastic when it combines with formaldehyde. Melamine can be used as a pesticide; it forms a major component in pigment yellow 150, which is a colorant in plastics and inks. Melamine is also used as a super plasticizer to make high resistant concrete. Sulfonated melamine formaldehyde is used as a cement admixture to increase the fluidity and workability of the mixture while reducing the water content in the mixture during its handling and pouring. It results in a concrete with higher mechanical strength and a lower porosity, exhibiting a longer lifetime and an improved resistance to corrosive environments. Being a nitrogen rich compound it attracted its use as an adulterant in food products, mainly in milk and milk products to increase the apparent protein content. Standard tests, such as the Kjeldahl and Dumas tests, estimate protein levels by measuring the nitrogen content, so they can be misled by adding melamine.

### IV. 1. 3. Toxicity of melamine:

Melamine is described as harmful if swallowed, inhaled or absorbed through the skin. Chronic exposure may cause cancer or reproductive damage. It is eye, skin and respiratory irritant. In 2004 and 2007, outbreak of crystalluria and death in animals in china were caused by contamination of animal feeds with a combination of the stone forming synergists melamine and cyanuric acid [378-380]. Studies suggested little toxicity of melamine or cyanuric acid when ingested individually, but showed that co-ingestion, even at far lower doses than either alone, led to crystal formation [381, 382]. Infants in China fell ill in 2008 when infant formula containing large amounts of melamine [383-386] without evident co-ingestion of cyanuric acid or other melamine related compounds (MRCs). This illness was characterized by urinary tract crystals and kidney stones and, less frequently, by renal impairment from tubular injury and obstructive uropathy. This fact revealed that melamine alone could cause its own toxicity when ingested at larger dose; the formation of urinary tract crystals and kidney stones may be caused due to the combination of melamine with endogenous urate [385, 386]. Melamine and cyanuric acid or other MRCs may complex when combined. Reimschuessel et. al. and Ranganathan et. al. [381, 387] reported a rosette crystal pattern while examining melamine and cyanuric acid together on a slide, which might result from hydrogen bonding between melamine and cyanuric acid (Fig. IV.2). It is possible that a similar reaction with urate (Fig. IV.3) was the cause of the Chinese formula illnesses to the infants in 2008. These patterns are also most likely related to the increased crystal formation at sufficient concentrations in the kidney [387-391].

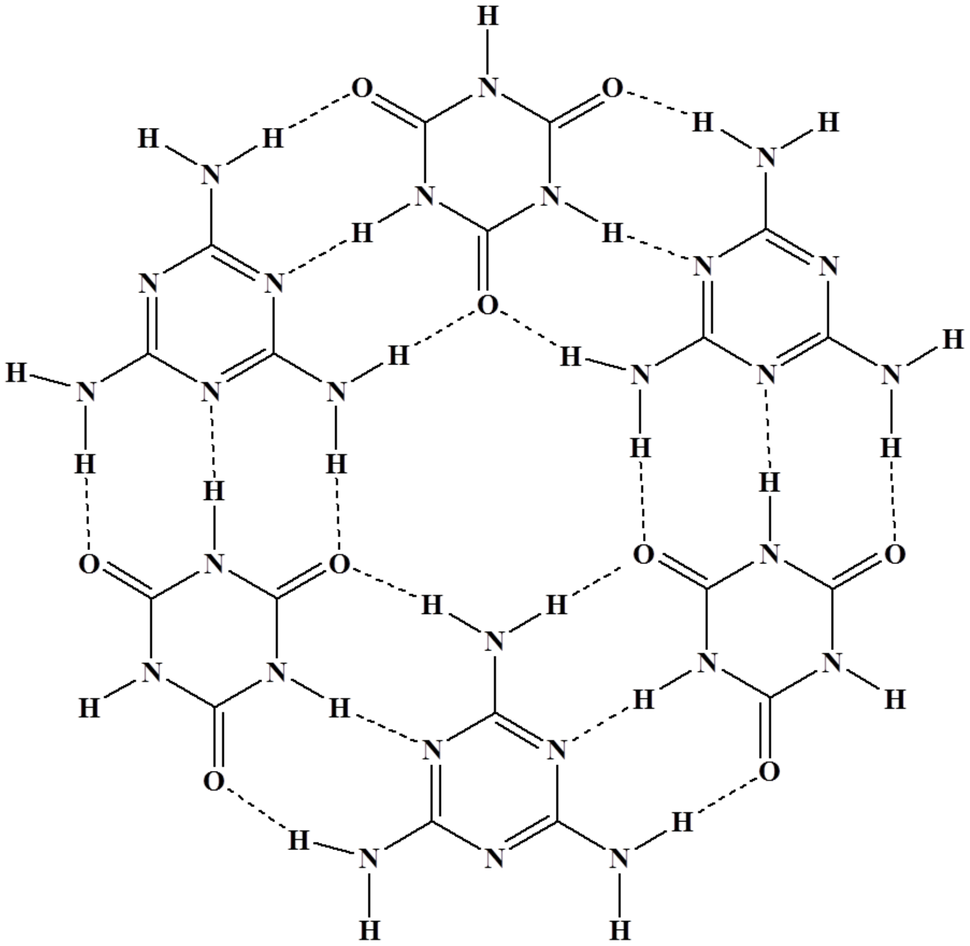

**Figure IV.2:** Rosette crystal pattern of complex between melamine and cyanuric acid.

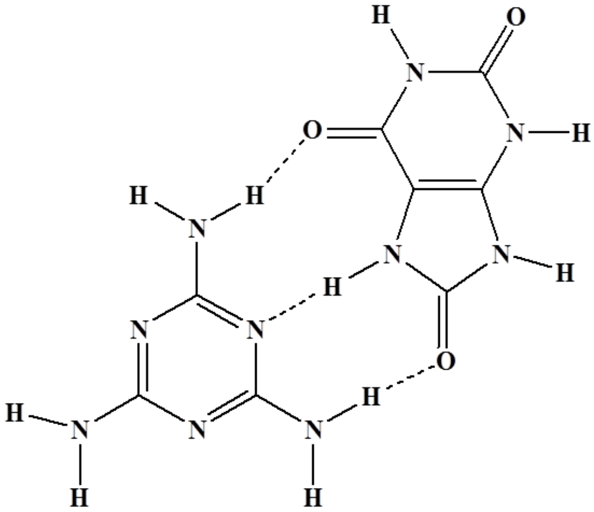

**Figure IV.3:** Hydrogen bonding between melamine and uric acid.

Human exposure data on melamine are limited, from the available toxicology and toxicokinetic data from animal studies, melamine and cyanuric acid are considered not acutely toxic because of their large lethal doses ($LD_{50}$). For melamine, these $LD_{50}$ range from 3.1 g/kg to more than 6.4 g/kg in rats and from 3.2 g/kg to 7.0 g/kg in mice [392, 393]. Several early studies on rats suggested that melamine could be carcinogenic in high doses when added to their feed. Cancer formed exclusively in the bladder of animals that developed stones, suggesting that the tumors grew as a result of bladder epithelial irritation and hyperplasia, not because of a genotoxic effect of the chemical itself [392, 394-398]. When stones were analyzed in one of the studies, melamine and urate were demonstrated in equal molar amounts [395]. Considering such toxicity of melamine Food Safety and Standards Authority of India (FSSAI) has proposed permissible limits of 1 mg/kg in powdered infant formula, 0.15 mg/kg in liquid infant formula and 2.5 mg/kg in other foods.

### IV. 1. 4. A brief account on the analysis of melamine:

Considering the toxic effects of melamine it is very important to determine melamine in milk products along with other food materials. There are some reports of determination of melamine based on chromatography [399-401] colorimetry [402, 403] and electrochemistry [404-406]. Besides the advantages of low cost measurement and simplicity in operation, electrochemical determination offers the advantage of providing an understanding of the chemical processes involved in the molecule in addition to the determination. Response from the direct electron transfer process in melamine is quite poor [407]. Cao *et al.* [404] have reported the decrease in the ferricyanide signals due to the presence of melamine on oligoneucleotide modified gold electrode for the determinations of melamine. Liao *et al.* [405] have reported the oxidation of uric acid as the recognition signal on screen printed electrode for the determination. In another report, electrochemical signal of ascorbic acid was used as the recognition signal in carbon nano tube (CNT) modified electrode for the determination [406]. Recently an article reported the determination of melamine from the decrease in the electrochemical signal from potassium ferrocyanide on gold nano particle modified indium tin oxide (ITO) electrode [408]. Determination of melamine using electrochemical techniques is becoming popular [409, 410]. Melamine was determined from the reduction signal of bismuthyl chloride by pre-concentrating it on a carbon composite electrode by solid phase micro-extraction [409, 411]. It was also determined in quail egg and milk samples by capillary zone electrophoresis [410, 412]. In a recent publication, an ordered mesoporous carbon and Nafion-modified glassy carbon electrode was used for the determination of melamine based on the melamine dimer oxidation [413]. As direct electrochemical determination of melamine is difficult, most electrochemical procedures involve indirect determination by measuring the change in the electrochemical signal of any electrochemically active compound in the presence of melamine. The determination of melamine using electrochemical methods still requires attention and investigation to resolve important issues. Present report explores the electrochemical properties of melamine using static mercury drop electrode (SMDE) and AuNPs modified CPE and presents methods for its determination in milk sample using AuNPs modified CPE and RGO-AuNPs modified CPE, which will be explored in three parts.

## IV. 1. A. Investigation of redox properties of melamine with static mercury drop electrode.

### IV. 1. A. 1. Reduction behavior of melamine:

With an aim to explore the electrochemical behavior of melamine, which is electrochemically not so active over conventional electrode and highly adsorptive in nature, cyclic voltammetry was performed using SMDE in BR buffer solution (see chapter II). While, carrying out the CV a peak due to reduction of the melamine was observed at -0.93V at pH 2 of the buffer solution and it was found that the peak position shifted in the cathodic direction when pH of the buffer was gradually increased from pH 2 to pH 9, when pH was increased above 5 the electrochemical response merged with current produced due to the hydrogen evolution (Fig. IV.4). Shifting of reduction peak potentials is linear with pH of the buffer (inset of Fig. IV.4) with a slope of -0.116 V/pH, the result reflected involvement of double number of proton to that of electron in the reduction process, if the shift in peak potential is approximated only due to the proton concentration.

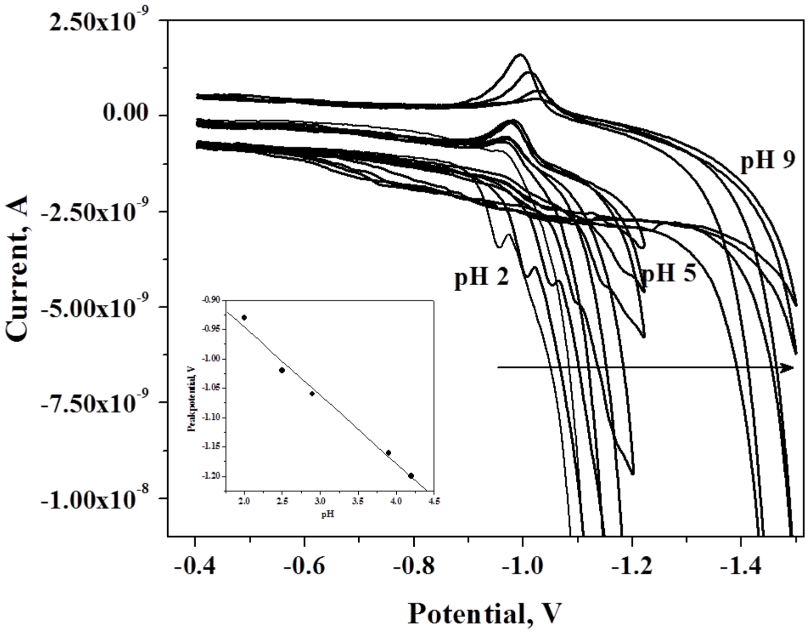

**Figure IV.4:** Cyclic voltammograms of melamine on SMDE in BR buffer of different pHs, Inset: plot of reduction peak potential of melamine with respect to pH of the solution.

Thus the electrochemical process could be summarized as the one electron and two proton transfer process; the positive charge at that carbon centre possibly takes up one more electron to get neutralized. Scan rate variation in CV (Fig. IV.5) produced linear relationship ,with a slope of $1.176\times10^{-8}$ A $V^{-1/2}$ $sec^{1/2}$ , between the observed peak current against square root of scan rate (in volt) reflecting that the electrochemical process was diffusion controlled in the BR Buffer medium (pH 2), although the peak potential got shifted towards more negative potential at higher scan rate.

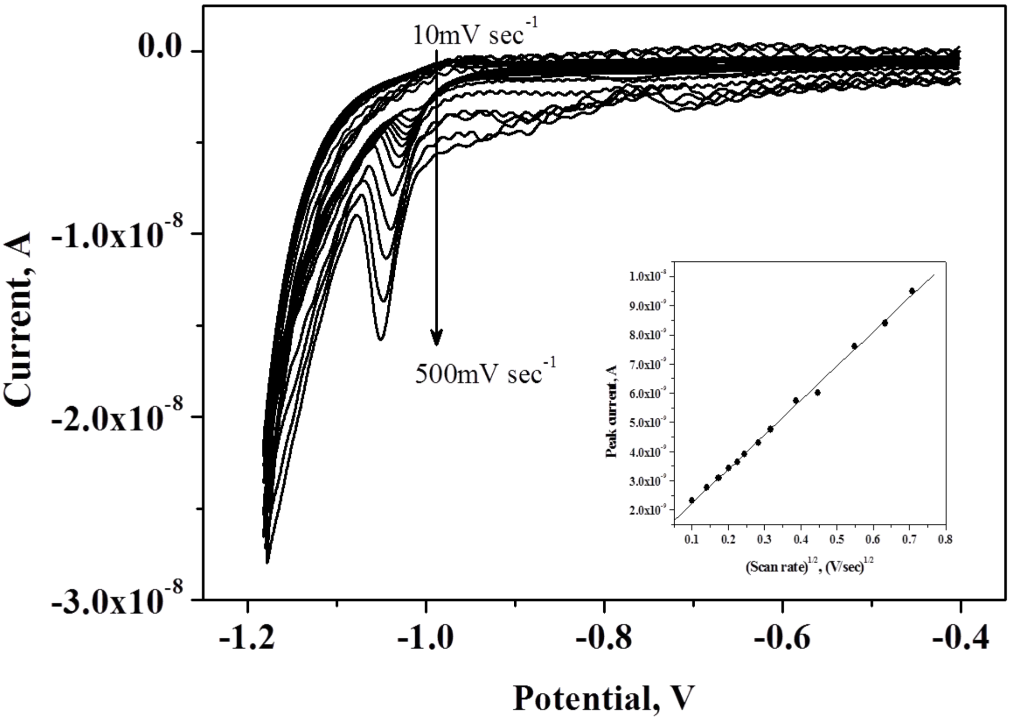

**Figure IV.5:** Cyclic voltammograms of melamine at pH 2 of BR buffer at different scan rate, Inset: Linear calibration plot of reduction peak current vs. Square root of scan rate.

### IV. 1. A. 1. 1. Evaluation of important analytical parameters:

During scanning in the reverse direction another peak was found around -0.95V, which did not increase with increase in the scan rate signifying that this peak was not due to oxidation of the reduced product of melamine. Identity of the peak could not be retrieved. However, a calibration plot was constructed by measuring the reduction peak current using differential pulse cathodic stripping voltammetry technique with successive addition of the melamine from 1μM to 100μM at pH 2 in BR buffer; the peak current increased proportionately with the concentration of melamine (Fig. IV.6) following a linear equation $i_p = 2.2527\times10^{-12}+1.1998\times10^{-5}C$, with linear regression co-efficient ($R^2$) of 0.99968 and slope of $1.1998\times10^{-5}$A $M^{-1}$. Concentrations are expressed here in M. LOD was calculated to be 0.2μM (sample No. 3). Prior to each scan solution was purged for 300 sec with nitrogen gas for de-oxygenation of the solution.

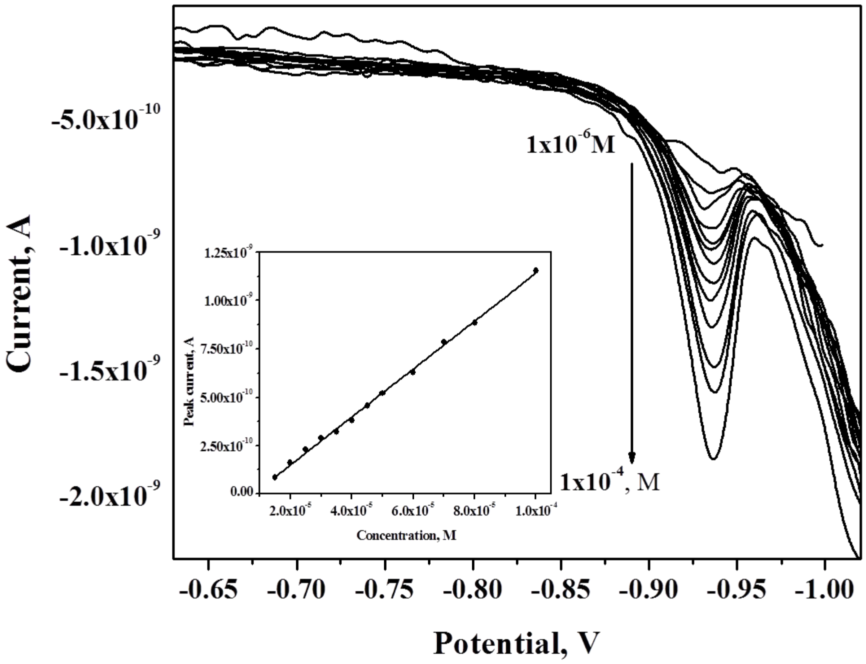

**Figure IV.6:** Differential pulse voltammograms of melamine reduction on SMDE with different concentration of melamine, Inset: Linear calibration plot of peak current vs. Concentration of melamine.

### IV. 1. A. 1. 2. Interferences:

Although the method provides simplicity in determination of melamine at μM concentration level, it suffered from the interference of commonly occurring Zn even in sub μM concentration and Ca in the mM concentration level.

### IV. 1. A. 1. 3. Sample preparation and recovery test

This method was used for the spike recovery test in the real milk sample. Recovery test was carried out by adding known amount of melamine in milk powder sample. For milk, sample treatment and measurement procedures were adopted from a previous report [414]. Milk sample was treated by taking 1 g of milk powder and mixing with 5 mL 0.1 M $CaCl_2$, then 5 mL of 0.5 M trichloroacetic acid and 35 mL of 5 M methanol was added. After 10 min of ultra-sonication, this mixture was centrifuged and the solution was filtrated, through a 0.45 μm membrane to obtain the samples for detection of melamine. Electrochemical measurements were carried out using this filtrate. The test results in only 48% recovery from the added concentration of melamine (50μM in the sample solution). This could be due to the presence of high content of Ca in the milk sample. Thus this method could not be accepted for real sample analysis.

## IV. 1. A. 2. Interaction of melamine with $Cu^{2+}$ as a tool to determine its concentration using SMDE:

### IV. 1. A. 2. 1. Study of analytical response and evaluation of analytical parameters:

Melamine has strong interaction with $Cu^{2+}$, which generates electrochemical signals. These electrochemical signals could be a measure of melamine concentration [407]. However a clear electrochemical signal for quantitative detection of melamine was not attempted previously. We have explored for the quantitative determination of melamine by monitoring the stripping signal of copper in linear sweep stripping voltammetry using SMDE. Anodic stripping voltammetry of copper was carried out with deposition of $Cu^{2+}$ at a potential of −1.0 V for 10 s and then the potential was scanned from −1.0 V to 0.2 V. The stripping peak due to the oxidation of Cu was observed at around 0 V as shown in figure IV.7.

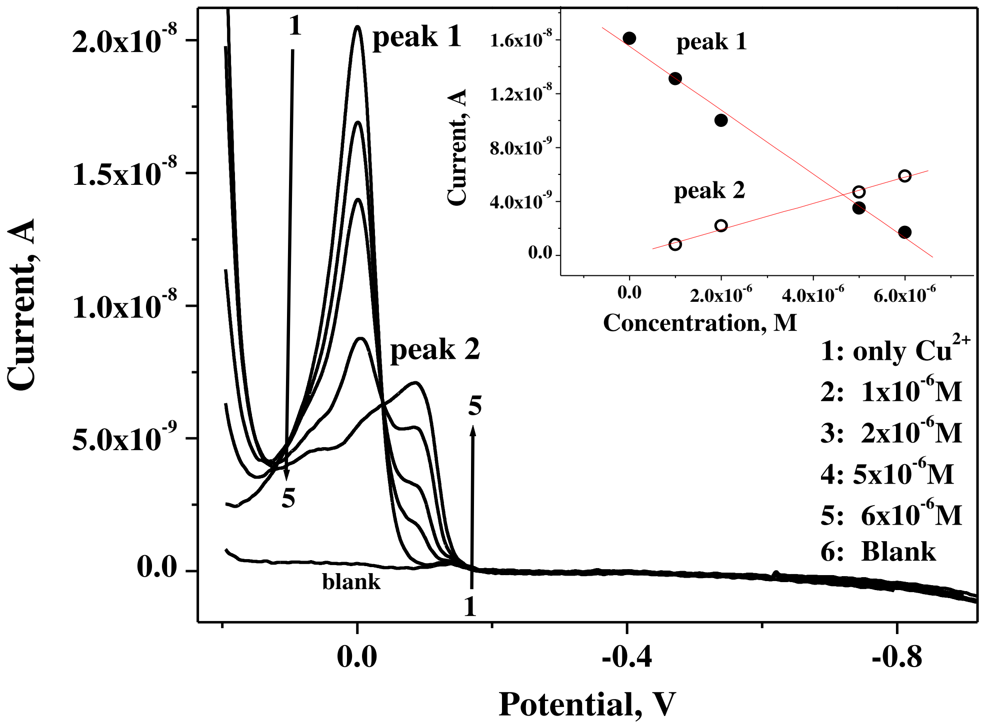

**Figure IV.7:** Linear sweep anodic stripping voltammetry of 3.3 μM of $Cu^{2+}$ with different concentration of melamine. Deposition potential was -1.0 V for 10 sec. Inset: corresponding linear calibration plots of peak 1 and peak 2.

Melamine was gradually added in the test solution containing 3.3 μM of $Cu^{2+}$. During the electrochemical scan Cu was stripped into the solution as $Cu^{2+}$ ion. The original Cu stripping peak current was gradually decreased with the addition of melamine and a new pre-peak at more negative potential to that of the Cu stripping peak was appeared. A calibration plot was constructed from the decrease in the stripping peak of copper which was shown in the inset of figure IV.7 (peak 1). The calibration plot followed the linear regression equation $i_p = 1.55 \times 10^{-8} - 2.37 \times 10^{-3}$ C with correlation coefficient of 0.998 and standard deviation of $6.15 \times 10^{-10}$, C in molar (M) concentration. The three sigma LOD from the linear calibration plot was obtained as 0.778 μM. For indirect determination of melamine this measurement was most workable procedure to determine melamine as it is very easy to obtain reproducible mercury drop for regular analysis. The new peak which was appeared at −0.09 V was found to be increased proportionately with the melamine concentration, corresponding linear calibration plot was shown in the inset of figure IV.7 (peak 2) The calibration plot followed the linear regression equation as $i_p = -7.05 \times 10^{-12} + 9.71 \times 10^{-4}$ C with correlation coefficient of 0.996 and standard deviation of $2.503 \times 10^{-10}$, C in molar concentration. The three sigma LOD from the linear calibration plot was obtained as 0.773 μM. It was observed that both the decrease in the stripping peak and the increase in the pre-peak generated similar proportionality and the detection limits obtained from both the ways were similar. This indicated that the type of interaction responsible for the decrease in the stripping current of Cu and generation of a new pre-peak was the same.

### IV. 1. A. 2. 2. Interference and recovery study:

This method was affected by the interference due to the presence of $Ag^+$, $Pb^{2+}$ and $Bi^{3+}$ at 10 times higher concentrations as the method involved pre-concentration step prior scanning. However, the sprike recovery test could not provide us with satisfactory result showing ~ 35% deviations from the added concentration of melamine. This might be due to the interaction of the organic molecules, present in the milk sample even after pre treatment, with $Cu^{2+}$; possible interference due to deposition of other major metal ions such as $Ca^{2+}$ and $Zn^{2+}$ during preconcentration step on Hg surface cannot be withdrawn. Therefore effort was extended to another indirect way to determine melamine by monitoring oxidation signal of $K_4[Fe(CN)_6]$ on RGO-AuNPs composite modified CPE, which is discussed in the following part (IV. 1. B).

## IV. 1. B. Determination of melamine by a RGO-AuNPs composite modified CPE:

### IV. 1. B. 1. Why RGO-AuNPs composite?

Usage of metallic nanoparticles in the sensing devices has been increased worldwide in the last decades due to their favourable physicochemical and electronic behaviour for sensor application. Gold nanoparticles-modified surfaces are excellent substrates for electrochemical devices due to their enhanced surface-to-volume ratio, localized surface plasmonics, quantized charging/discharging, high conductivity, catalytic and photocatalytic activity and good physical properties [415]. Gold nanoparticles-modified substrates as sensing platforms received much interest in the field of analytical chemistry [416-420]. Graphene and GO based materials are good choice due to the excellent electronic and surface property (Section II. 5) required sensor [421, 422]. Due to the easy functionalization and favourable electrochemical properties of graphene sheets, there is a rush to use graphene and metallic nanoparticle composites for sensor application. Composites of metallic nanoparticles and graphene especially improved the electrochemical property of graphene, useful for electrochemical sensors. As described in the section II. 5, preparation of pristine graphene sheet is very difficult, therefore RGO are prepared to obtain electronic and other physicochemical properties, required for electrochemical sensor, nearly approaching to those of pristine graphene. Due to the excellent properties of the composite, it was used as the platform for electrochemical sensors [423-426].

### IV. 1. B. 2. Preparation of RGO-AuNPs composite modified CPE:

RGO was prepared by modified hummer’s method as described in section II. 5. RGO thus formed was washed with water and dried under vacuum oven. RGO powder was ultra-sonicated for 5 min in 1:1 methanol water mixture to make good suspension. The suspended

RGO solution was drop casted on to the CPE surface to fabricate the RGO modified CPE. AuNps were electrochemically deposited from 0.1mM Au(III) solution on the RGO modified CPE at a constant potential of -0.3V (vs. SCE) for 100s. The RGO-AuNPs composite modified CPE thus formed was washed with ultrapure water and used as the sensing application.

### IV. 1. B. 3. Characterization of the composite:

The X-ray diffraction patterns of GO and RGO showed (Fig. IV.8) the characteristic diffraction peak of graphite at 2θ angle of 26.5° corresponding to the (0 0 2) plane was almost eliminated upon oxidation and formation of GO. The peak at 10.5° corresponded to the stacked graphene sheets due to the functionalization with carboxylic acid and hydroxyl group. This functionalization is responsible for the separation of graphene sheets in graphite. This peak was eliminated upon the borohydride reduction and the broad diffraction pattern from 20° to 30° was more prominent. The absence of the peak at 10.5° signifies the reduction of the GO sheets.

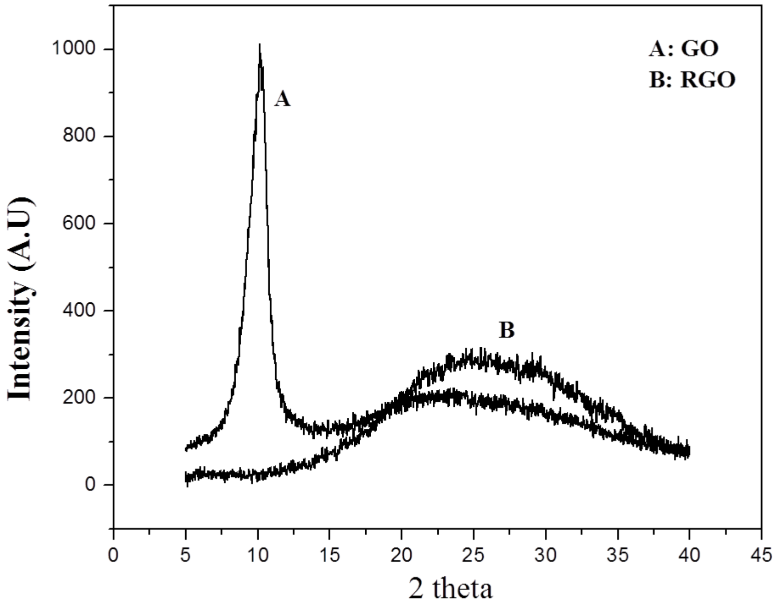

**Figure IV.8:** X-ray diffraction patterns of (a) graphene oxide and (b) reduced graphene oxide.

The broad diffraction pattern from 20° to 30° is due to the diffraction from the short range order of (0 0 2) plane due to the agglomeration of RGO sheets.

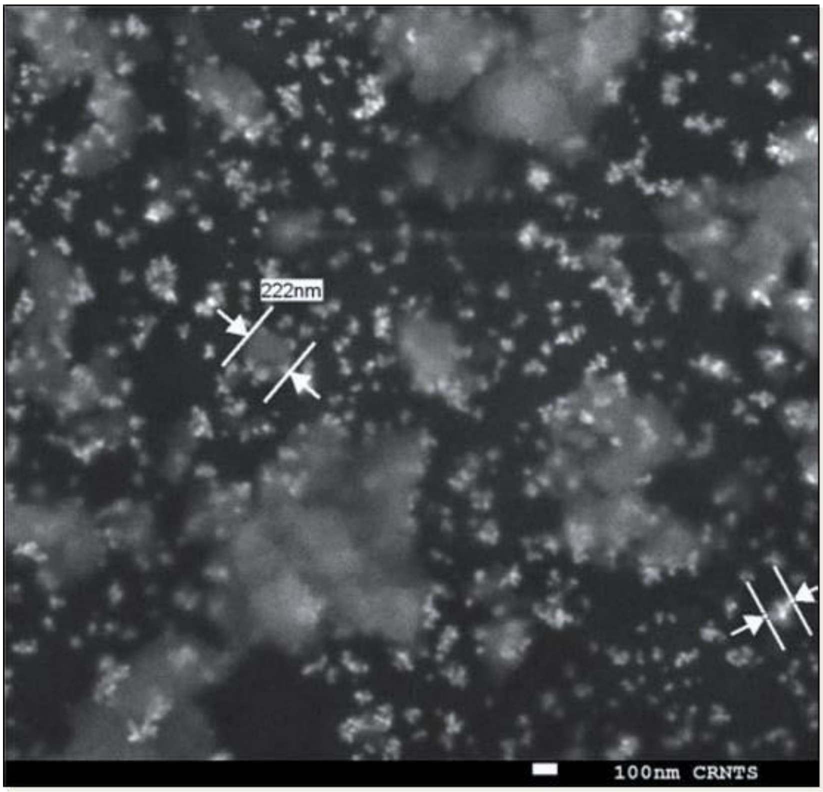

**Figure IV.9:** Scanning electron micrograph of the reduced graphene oxide–gold nanoparticles composite.

A scanning electron micrograph (Fig. IV.9) of the RGO-AuNPs composite modified carbon paste revealed that clusters of AuNPs were embedded across the graphene sheets. AuNPs were preferentially deposited at the edges of the graphene sheets. The individual AuNPs had diameters from 20 to 30 nm and their aggregate size varied from 50 to 200 nm. To record the atomic force micrograph, the suspended RGO was drop casted on freshly peeled mica. The corresponding micrograph and the line graph are shown in figure IV.10. The width of the graphene sheet was 1 nm. This thickness of the graphene sheets correlates well with previously reported work [184]. The pristine graphene sheet was approximately 0.5 nm in width. Hence, a thickness of 1 nm was due to two graphene sheets or one hydrated graphene sheet.

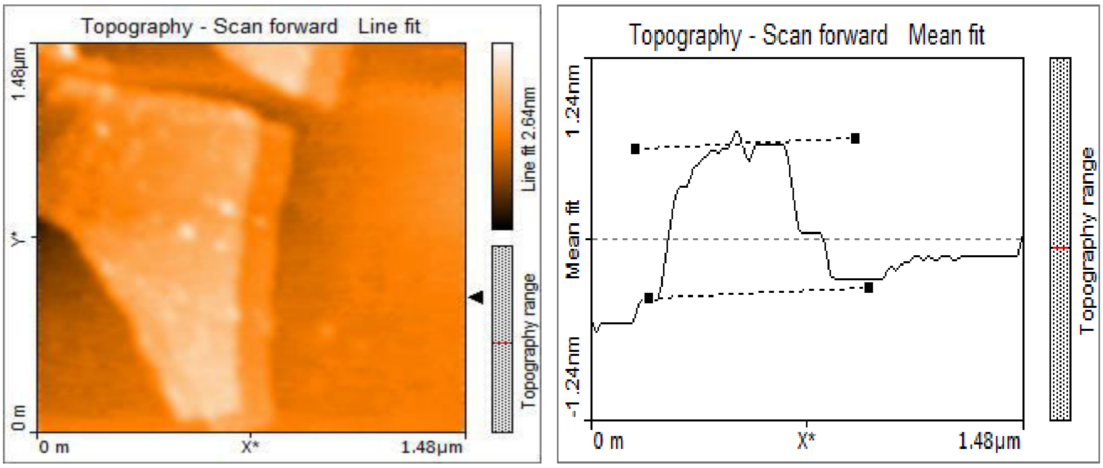

**Figure IV.10:** Atomic force micrograph and the corresponding line graph (right) of reduced graphene oxide.

### IV. 1. B. 4. Electrochemical performance of the modified electrode:

Cyclic voltammetry was performed in 1 mM $K_4[Fe(CN)_6]$ in 0.1 M KCl solution using the modified electrode. Cyclic voltammograms at different scan rates demonstrated the reversible oxidation of ferrocyanide (Fig. IV.11.a). Repetitive cyclic voltammetry scans, recorded at 50 mV $sec^{-1}$, showed reproducible behaviour (Fig. IV.11.b). No specific adsorption was observed. Square wave voltammetry was performed using $10^{-5}$ M ferrocyanide and the oxidation of ferrocyanide was measured using the modified electrode (Fig. IV.12). The potential was scanned from 0 to 0.4 V. The oxidation peak due to the oxidation of ferrocyanide to ferricyanide was observed at 0.22 V.

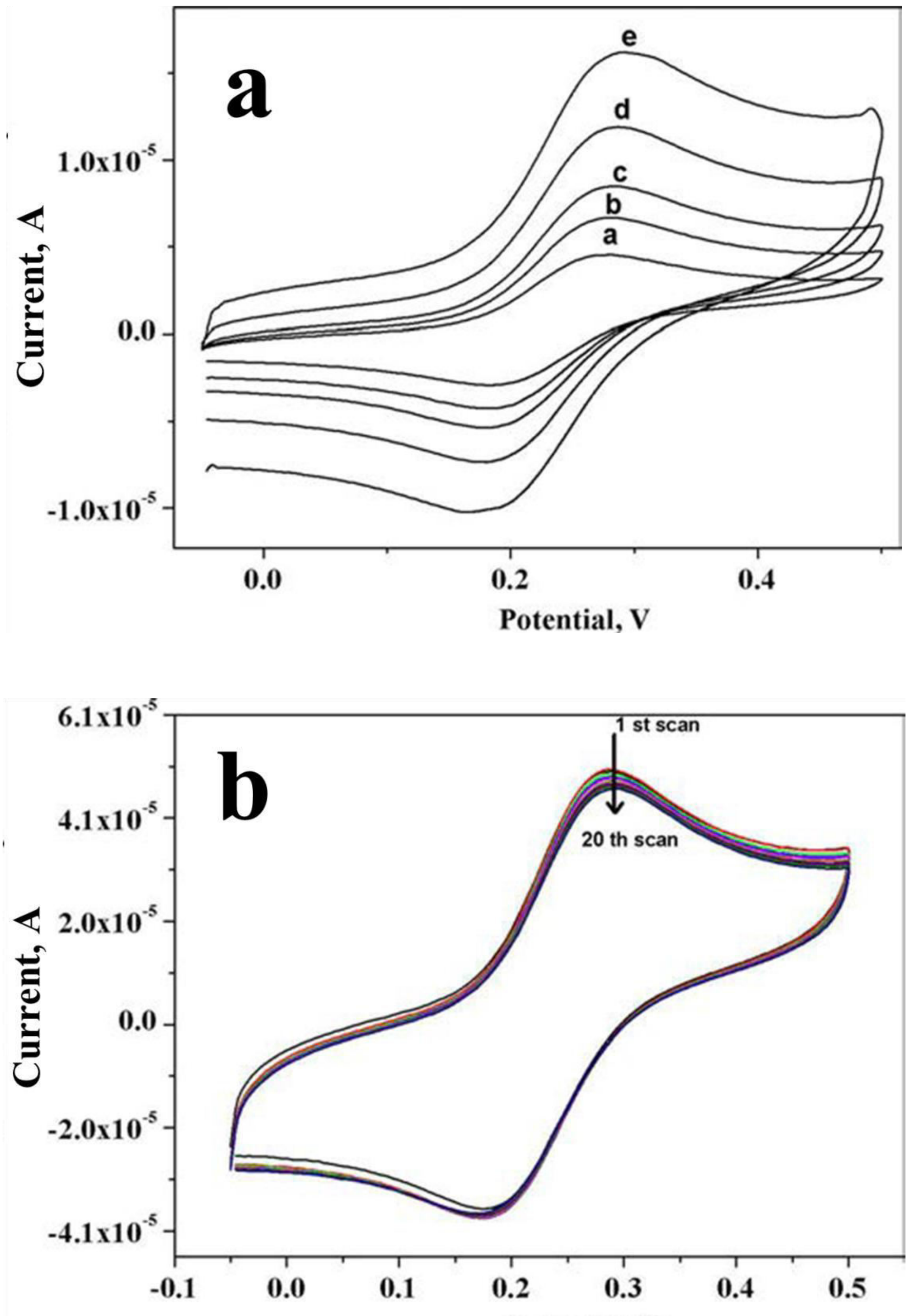

**Figure IV.11:** (a) Cyclic voltammogram of 1 mM $K_4[Fe(CN)_6]$ at the reduced graphene oxide–gold nanoparticles composite-modified electrode at scan rates of a. 10 mV sec$^{-1}$, b. 20 mV sec$^{-1}$, c. 30 mV sec$^{-1}$, .d. 50 mV sec$^{-1}$, and e. 100 mV sec$^{-1}$; (b) Twenty cyclic voltammograms of 1 mM $K_4[Fe(CN)_6]$ at the reduced graphene oxide–gold nanoparticles composite-modified electrode at a scan rate of 50 mV sec$^{-1}$.

### IV. 1. B. 5. Effect of melamine on the voltammetric response of oxidation of ferrocyanide:

The current density due to the ferrocyanide oxidation without the addition of melamine was approximately $6.5\times10^{-5}$ A cm$^{-2}$. Melamine was added and the oxidation peak of ferrocyanide decreased (Fig. IV.12). The current decreased by 40% due to the addition of 160 μM of melamine. This decrease in the ferrocyanide oxidation current was proportional to the melamine concentration. A calibration plot was constructed by plotting the peak current vs. the concentration of melamine. The calibration plot of melamine was a straight line with a slope of 0.0025 AM$^{-1}$ and a correlation coefficient of 0.997. The LOD was calculated to be 2.23 μM.

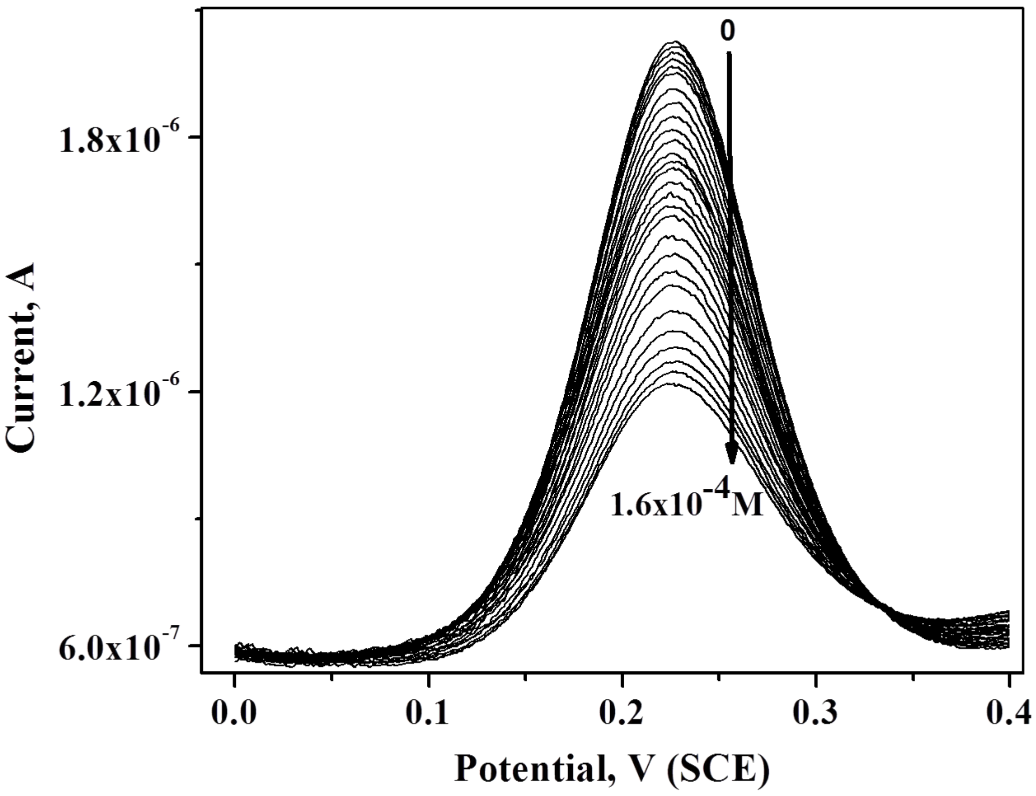

**Figure IV.12:** Square wave voltammograms of 0.01 mM $K_4[Fe(CN)_6]$ with the addition of melamine (top to bottom).

Melamine strongly interacts with AuNPs [411, 412, 427, 428] and the interaction is enhanced in the presence of modifying agents [412]. Hence, AuNPs have been commonly used for the determination of melamine [429, 430]. The RGO used here to hold the AuNPs and also improved the transport of charge to the electrode surface. Computational investigations showed that aminotraizines interact strongly with graphene sheets and form two-dimensional molecular assemblies. Melamine has strong interaction with graphene with the adsorption affinity reported to be 22.6 kCal $M^{-1}$ [427]. Therefore, the RGO-AuNPs composite strongly interacted with melamine which improved the analytical determination. Since melamine is electrochemically inactive, this interaction with the composite electrode substrate decreased the electrochemically active surface area for the oxidation of ferrocyanide. Therefore, the oxidation peak current decreased with the increase in the concentration of melamine. In order to check the adsorption phenomenon of melamine SECM experiment was conducted.

### IV. 1. B. 6. SECM study to characterize adsorption of Melamine on the electrode:

Electrochemical measurements were performed to characterize the adsorption of melamine on the RGO-AuNPs composite. Electrochemical imaging of the substrate provided information about the adsorption of melamine on the composite. SECM was performed using a platinum electrode with a 10-µm diameter tip [234, 431]. 1 mM solution of ferrocene in methanol was used as the redox probe. The corresponding probe approach plot is shown in figure IV.13. The y-axis shows the normalized current during the approach. The x-axis is the ratio of the distance of tip from the substrate to the radius of the electrode.

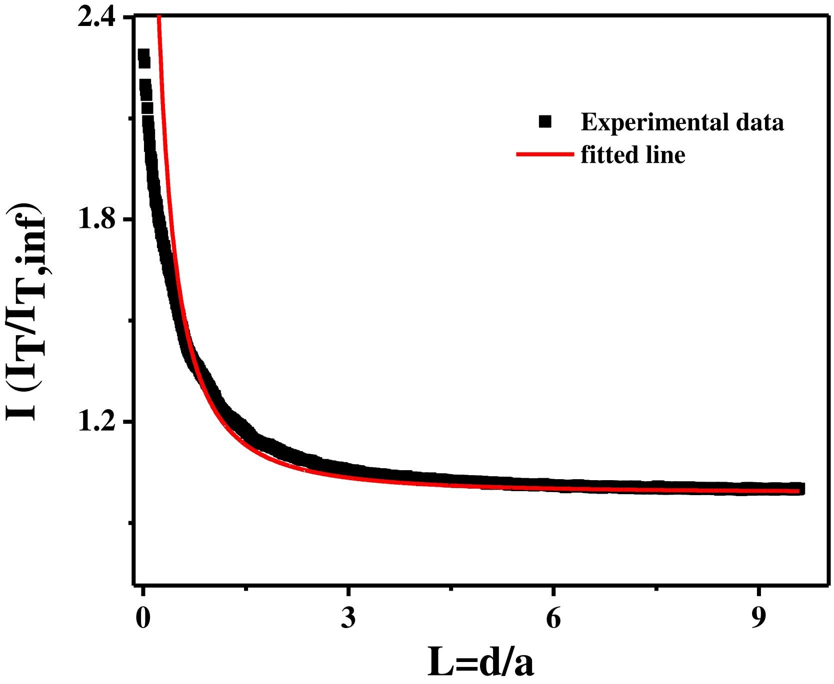

**Figure IV.13:** Probe approach plot of the platinum tip to the reduced graphene oxide–gold nanoparticles substrate: Experimental and fitted plot.

Positive feedback was observed during the approach to the substrate and the distance between the tip and the substrate was 1 µm. At this distance, the substrate was scanned and the corresponding image is shown in figure IV.14. The measured current across the substrate was approximately 2.5 $\times 10^{-9}$ A, with occasional spikes in current.

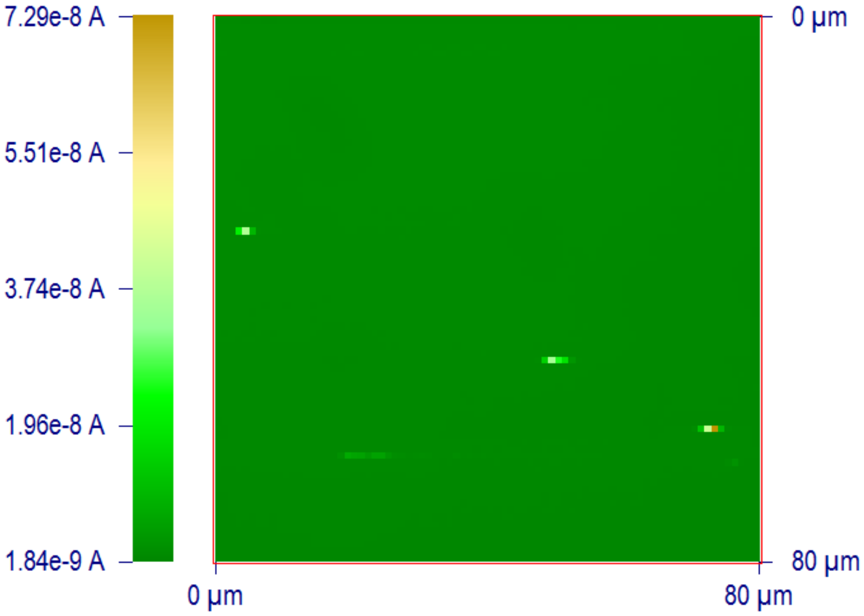

**Figure IV.14:** Scanning electrochemical micrograph of the reduced graphene oxide–gold nanoparticles substrate for 1 mM ferrocene in methanol. The tip electrode was 10 µm diameter platinum and scans were performed 1µm above the substrate.

The spikes may be due to the agglomerated deposition of RGO and AuNPs on the substrate. After this scan, melamine was added at a concentration of $1\times10^{-6}$ M. An additional scan was recorded and is shown in figure IV.15.

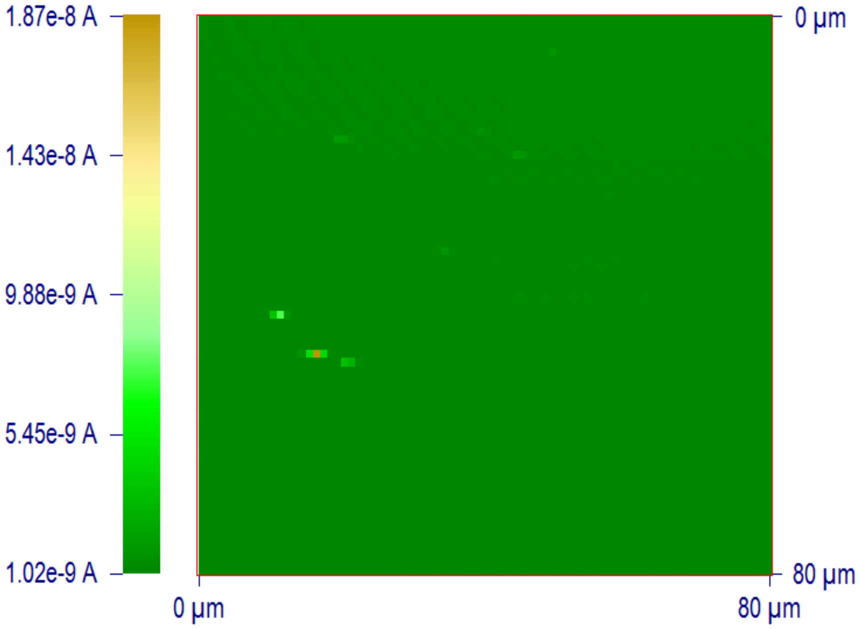

**Figure IV.15:** Scanning electrochemical micrograph of the reduced graphene oxide–gold nanoparticles substrate for 1 mM ferrocene in methanol and 1µM melamine. The tip electrode was 10-µm diameter platinum and scans were performed above the

The feedback from the substrate to the tip was reduced and the overall substrate current was approximately $1.1\times10^{-9}$ A. The current from the spikes were also reduced upon the addition of melamine. This decrease in the feedback response for the substrate was due to the adsorption of melamine on the active substrate. Therefore, the scanning electrochemical measurements confirmed the efficient adsorption of melamine on the RGO-AuNPs substrate. Furthermore, the feedback from the substrate was reduced due to adsorption.

### IV. 1. B. 7. Interferences:

Interferences from common metal ions including $Hg^{2+}$, $Ag^{+}$, $Cu^{2+}$, $Bi^{3+}$, $Pb^{2+}$, $K^{+}$, $Na^{+}$, and $Cl^{-}$ were investigated. Square wave voltammograms were obtained for potassium ferrocyanide without any interferences at $10^{-5}$ M, followed by measurement of the response following the addition of 100 ppb $Hg^{2+}$, $Cu^{2+}$, and $Ag^{+}$ and 100 ppm of $Bi^{3+}$, $Pb^{2+}$, $K^{+}$, $Na^{+}$, and $Cl^{-}$. The peak height and the shape were unchanged following the addition of the ions (Fig. IV.16).

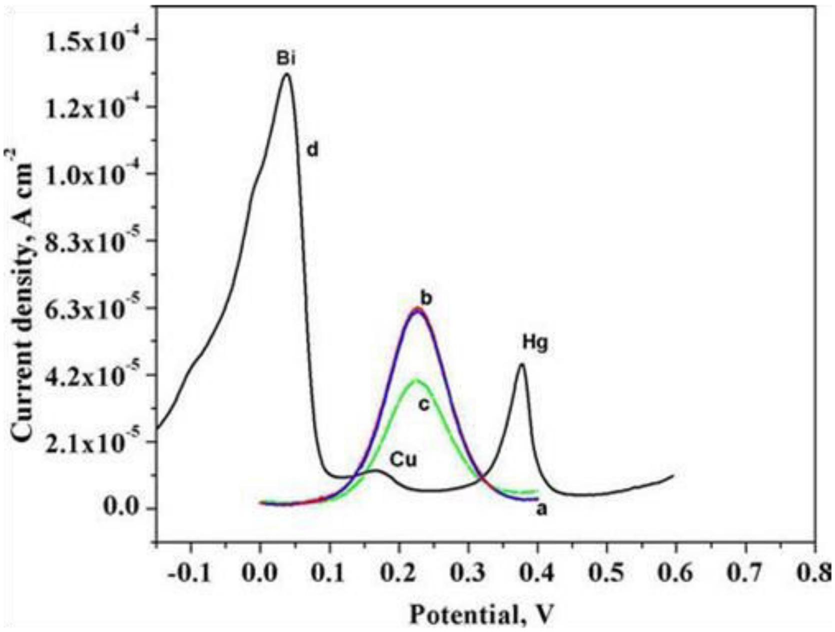

**Figure IV.16:** Interferences for the oxidation of $K_4[Fe(CN)_6]$ in (a) the absence of any interfering agents; (b) $K_4[Fe(CN)_6]$ with 100 ppb $Hg^{2+}$ and $Ag^{+}$ and 100 ppm of $Cu^{2+}$, $Bi^{3+}$, $Pb^{2+}$, $K^{+}$, $Na^{+}$, and $Cl^{-}$; (c) $K_4[Fe(CN)_6]$ with 1 g $L^{-1}$ casein; and (d) the stripping response of $Hg^{2+}$ (100 ppb), $Cu^{2+}$(100 ppb), and $Bi^{3+}$ (100 ppm) in the absence of $K_4[Fe(CN)_6]$.

However, the peak current was reduced by the addition of 1 g $L^{-1}$ casein. Therefore, milk proteins interfere with the analysis, requiring additional sample preparation. $Hg^{2+}$, $Cu^{2+}$, and $Bi^{3+}$ might interfere as their stripping peaks are near the ferrocyanide oxidation peak; the response of $Hg^{2+}$, $Cu^{2+}$, $Bi^{3+}$ following deposition for 300 sec at -0.5 V was recorded using the modified electrode. The stripping peaks due to the metal ions were close to the oxidation of potassium ferrocyanide. Since the present measurement does not involve a deposition step, these interferences are not expected to be present.

### IV. 1. B. 8. Recovery test and validation:

The recovery efficiency of the method was characterized by the addition of melamine to milk powder and water. For milk, sample preparation was discussed in section IV. 1. A. 1. 3. Electrochemical measurements were performed using the treated sample solution. Results are shown in table 8. The recovery was validated by the measurement of melamine by high-performance liquid chromatography (HPLC) [432] as shown table IV.1. The results from the HPLC and electrochemical methods were comparable.

| Sample | Spiked concentration | Recovered concentration using the present method | Recovery using present method | recovered by HPLC | Recovery by HPLC (%) |
|---|---|---|---|---|---|
| Milk Powder | 5μM | 5.6±0.2μM | 112% | 4.9±0.08 | 98% |
| Tap water | 2μM | 2.2±0.1μM | 110% | 2.3±0.03 | 115% |

**Table IV.1:** Recovery of melamine in milk and water using the RGO–AuNPs composite-modified CPE and HPLC.

The analytical figures of merit obtained in the present work were compared with some literature reports as shown in table IV.2.

| References | Limit of Detection | Linear Dynamic Range |
|---|---|---|
| 401 | $25.37 \times 10^{-9}$ mol/kg | $79.3 \times 10^{-9}$ to $15.86 \times 10^{-9}$ mol/kg |
| 402 | $0.317 \times 10^{-6}$ M | Not specified |
| 403 | $39.64 \times 10^{-9}$ M | Not specified |
| 404 | $9.6 \times 10^{-9}$ M | $3.9 \times 10^{-8}$ to $3.3 \times 10^{-6}$ M |
| 405 | $12.68 \times 10^{-9}$ M | 0 to $1 \times 10^{-6}$ M |
| Present Method | $2.23 \times 10^{-6}$ M | 5 to 160 $\times 10^{-6}$ M |

**Table IV.2:** Comparison of the analytical figures of merit for determination of melamine by the method using the RGO-AuNPs composite modified CPE and other methods reported in the other literature.

The present modified electrode is easy to fabricate and operates at higher concentration ranges compared to the literature reports. Thus, the RGO-AuNPs modified CPE was successfully used for the determination of melamine in milk sample.

With an aim to detect the direct oxidation signal of melamine the work was further extended to measure the oxidation signal directly generated from the oxidation in the melamine centre. Corresponding results are discussed in the following Part.

## IV. 1. C. Determination of Melamine from Its Direct Oxidation:

As the electrochemical oxidation behavior of melamine is quite poor it is difficult to obtain the direct electrochemical oxidation peak due to melamine. With bare CPE no response due to oxidation of melamine (in phosphate buffer of pH 9) was observed as shown in figure IV.17. In order to improve the electro-oxidation property of melamine, CPE was modified with MWCNT and nafion composite. Interestingly the electrochemical injection from the melamine molecules was improved on the MWCNT modified surface. This interaction of melamine with MWCNT was explored for the direct determination of melamine in contaminated samples. Use of nafion films has the advantage of suppression of interference besides holding the CNTs on the electrode surface.

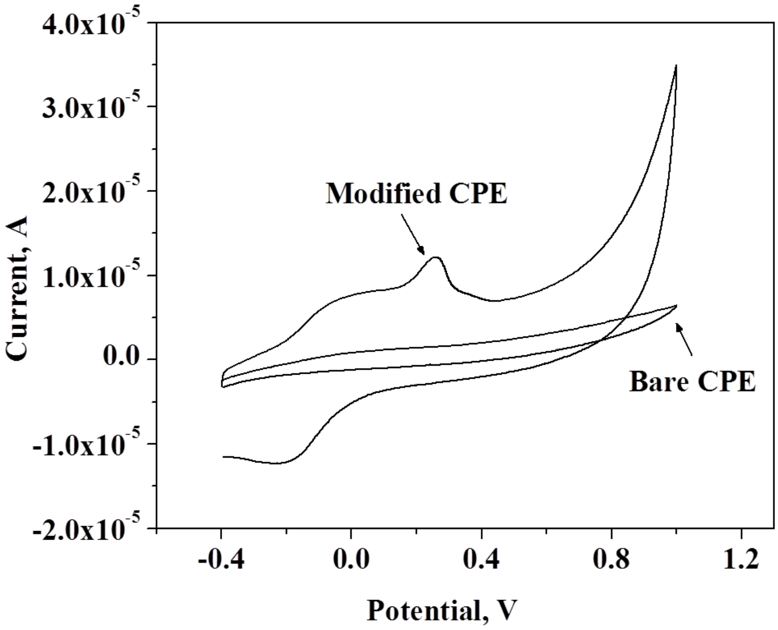

**Figure IV.17:** Cyclic voltammogram of oxidation of melamine on MWCNT-nafion composite modified CPE.

However, due to strong interaction of MWCNT with melamine, the electrode regeneration was an issue to use the sensor for actual application. To solve this problem another approach of modifying the electrode with AuNPs was proposed as AuNPs has strong interaction with melamine [411, 412, 427, 428], although, the oxidation peak due to melamine was not experimentally observed on bulk gold electrode. The following sections describe the important findings of melamine oxidation on AuNPs modified CPE.

### IV. 1. C. 1. Preparation and characterization of AuNPs modified CPE:

Carbon paste electrode was prepared following the method which was already discussed in chapter II (section II. 4. 6). Carbon paste electrode was modified with AuNPs by electrochemical deposition method. Electro-deposition of AuNPs over carbon paste electrode surface was carried out from auric chloride solution of 1mM concentration. Deposition was carried out at -0.3 V for 300 sec. Deposits were characterized using SEM; corresponding micrograph is shown in figure IV.18.

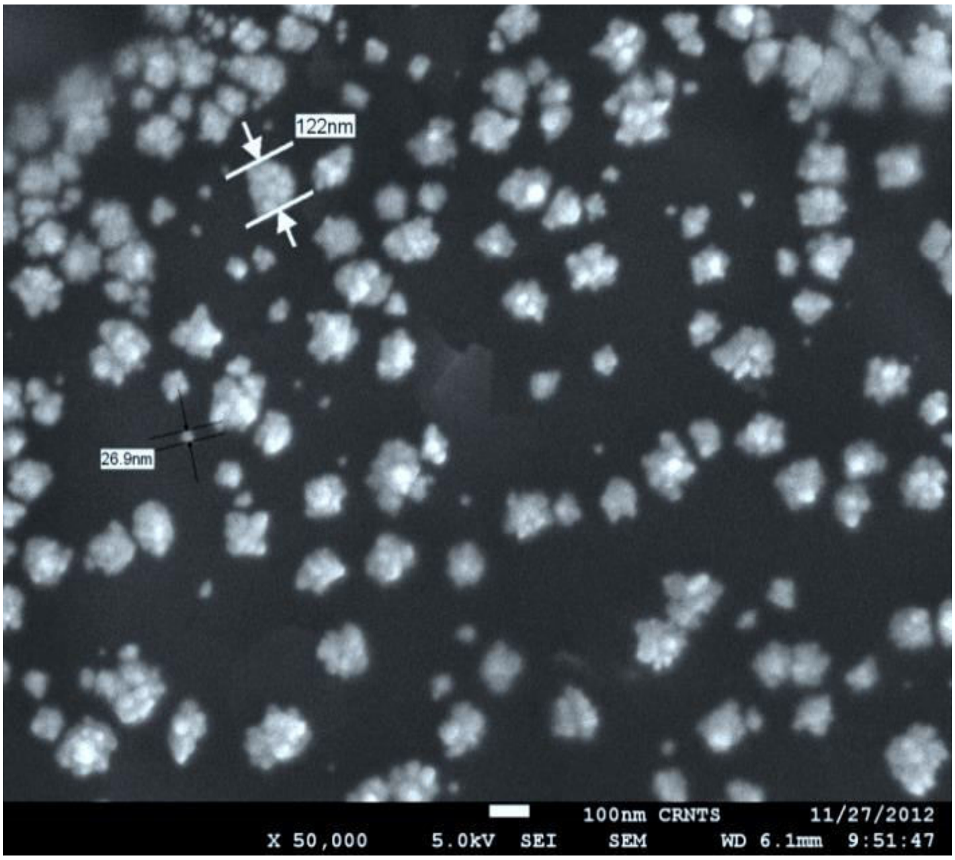

**Figure IV.18:** SEM micrograph of gold nanoparticles electrochemically deposited on carbon paste electrode substrate.

Sizes of most of the deposits were in the range of 100 to 120 nm with some occasional smaller deposits of around 30 nm. The bigger deposits actually comprise of smaller particles.

### IV. 1. C. 2. Analytical response for the oxidation of melamine:

An oxidation signal at ~0.15V was obtained when CV was carried out at a scan rate of 20mV $sec^{-1}$ in PBS of pH 7. The peak potential shifted toward more positive direction and landed at 0.23V at a scan rate of 200mV $sec^{-1}$(Fig. IV.19). The CV profile clearly indicates the non-reversibility of the redox process. Measurement of peak current with respect to the square root of the scan rate was found to be non linear reflecting the fact that the electrochemical process was not fully diffusion controlled; the result was associated with the effect of adsorption of melamine on the AuNPs as discussed in previous part (section IV. 1. B. 6). In order to get the quantifiable analytical response due to the oxidation of

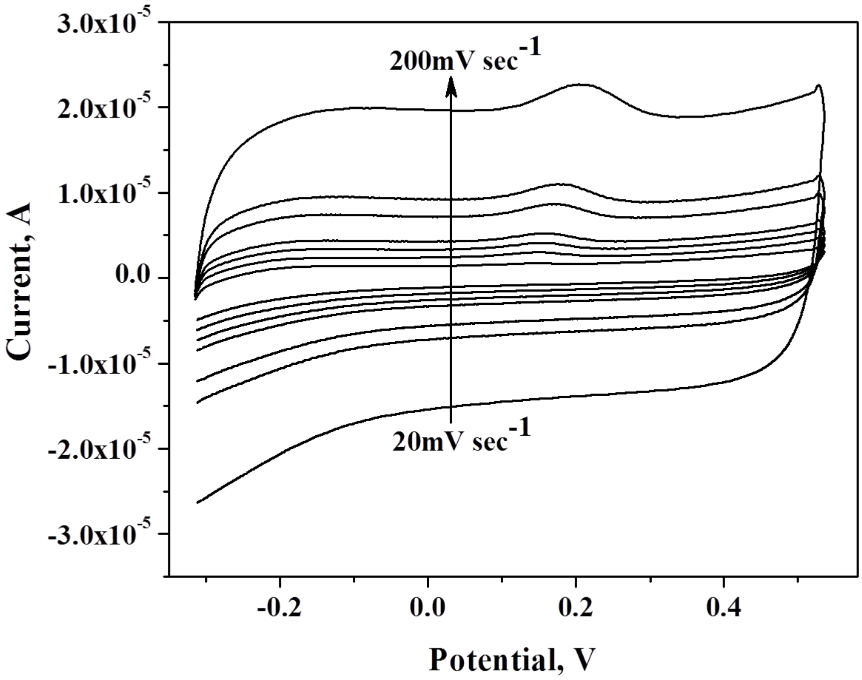

**Figure IV.19:** Cyclic voltammograms of oxidation of melamine on AuNPs modified CPE at different scan rates, in PBS of pH 7.

melamine square wave voltammetry (SQWV) was carried out (Fig. IV.20). Although, the oxidation process on the modified electrode was not reversible in nature, to minimise the effect of adsorption on the response a faster technique, SQWV, was adopted. The voltammetric signal was increased with the increase in concentration of melamine. Two calibration regions were observed one at low and the other at high concentrations (inset of Fig. IV.20). Three sigma LOD using this procedure was obtained as 0.43 μM.

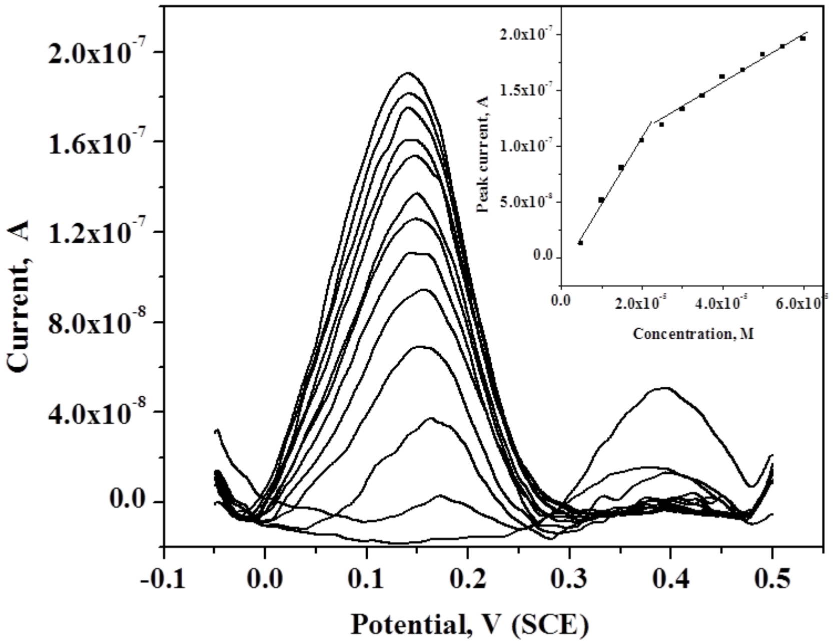

**Figure IV.20:** Square wave voltammograms of melamine on AuNPs modified carbon paste electrode with successive addition of 0.5 μM melamine. Inset: Corresponding calibration plot.

### IV. 1. C. 3. Effect of interfering species:

Present method was free from interferences form the metal ions like, $Cu^{2+}$ $Ag^{+}$, $Pb^{2+}$, $Bi^{3+}$, $U^{6+}$ and $Hg^{2+}$ at 100 fold higher concentration than melamine since the method does not include any preconcentration step. This is the biggest advantage of detection of melamine using its direct oxidation signal.

### IV. 1. C. 4. Sample recovery test:

Sample preparation for milk was discussed in section IV. 1. A. 1. 3. Recovery test results were shown in table IV.3. Recovery test has shown good recovery of melamine in milk sample, recovery within 10%.

| Melamine added | Melamine recovered | % Recovery |
|---|---|---|
| 2μM | 2.2±0.08μM | 110% |
| 5μM | 5.4±0.1μM | 108% |

**Table IV.3:** Recovery test results of melamine in milk sample using AuNPs modified CPE.

### IV. 1. D. Conclusion:

Electrochemical investigation of melamine revealed both reduction and oxidation behaviour. The reduction process of melamine was investigated using static mercury drop electrode and the direct oxidation process was explored using AuNPs modified CPE. The reduction behaviour of melamine is highly pH sensitive and the reduction signal is highly delicate for reliable determination of melamine. Indirect method of determination was proposed based on the electrochemical signal of $Cu^{2+}$ or from the decrease in the electrochemical signal from ferrocyanide. Determination based on the direct oxidation signal of melamine was also proposed with the detection limit of 0.43 μM. These methods were applied for the recovery of the spiked melamine concentration in the milk sample.

# Chapter IV.2

## *Electrochemical determination of dopamine and uric acid using functionalized carbon nano spheres modified electrode*

### IV. 2. 1. Brief introduction of Dopamine and Uric acid:

Dopamine (DA) is one of the most important neurotransmitters in central and peripheral nervous system of mammals. It has significant role in modulating the brain function [433]. Some of its notable functions are movement, memory, pleasurable reward, behaviour and cognition, attention, inhibition of prolactin production, sleep, mood and learning. It belongs to the catecholamine family, with IUPAC name of 4-(2-Aminoethyl) benzene-1, 2-diol. The chemical structure is shown in figure IV.21. It is biosynthesized mainly in dopaminergic neurons and cells of the medulla of the adrenal glands [434]. The primary biosynthesis pathway is shown in figure IV.22. Dopaminergic neurons are located mainly at few discrete regions in the brain such as substantia nigra, ventral tegmental area and dorsal striatum [435]. DA was chemically synthesized from catechol by George Berger and James Ewens in the year of 1910, later in late 1950s it was discovered to be a neurotransmitter by Arvid Carlsson and N. A. Hillarp [436]. This discovery encourages further investigations related to its role in the central nervous system and in neurological disorders. In presence of lower concentration of DA in human leads to various neurological disorders, Parkinson's disease and hyperactivity. Higher level of DA leads to the mental disorder due to abnormal brain function. Uric acid (UA) is another important metabolic product in biological system. In human body system UA is the catabolic product of purin. It is a heterocyclic compound of carbon, nitrogen, oxygen, and hydrogen with IUPAC name of 7,9-Dihydro-1H-purine-2,6,8(3H)-trione. The chemical structure is shown in figure IV.21.

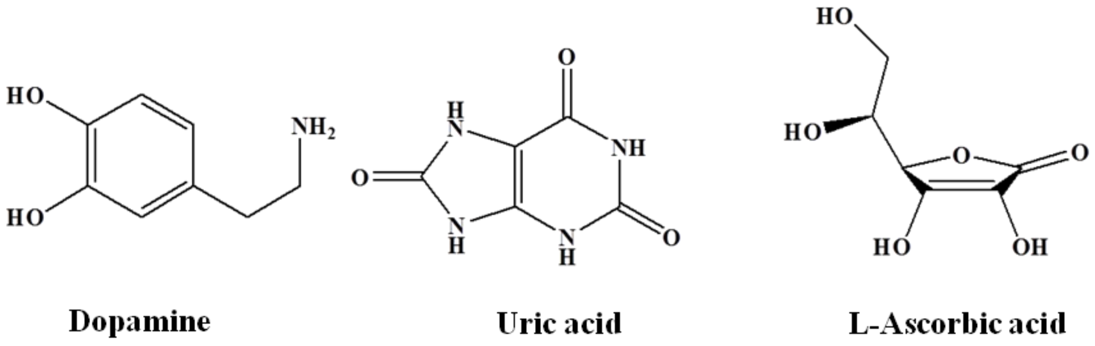

**Figure IV.21:** Chemical structure of dopamine (DA), uric acid (UA) and L-ascorbic acid (AA).

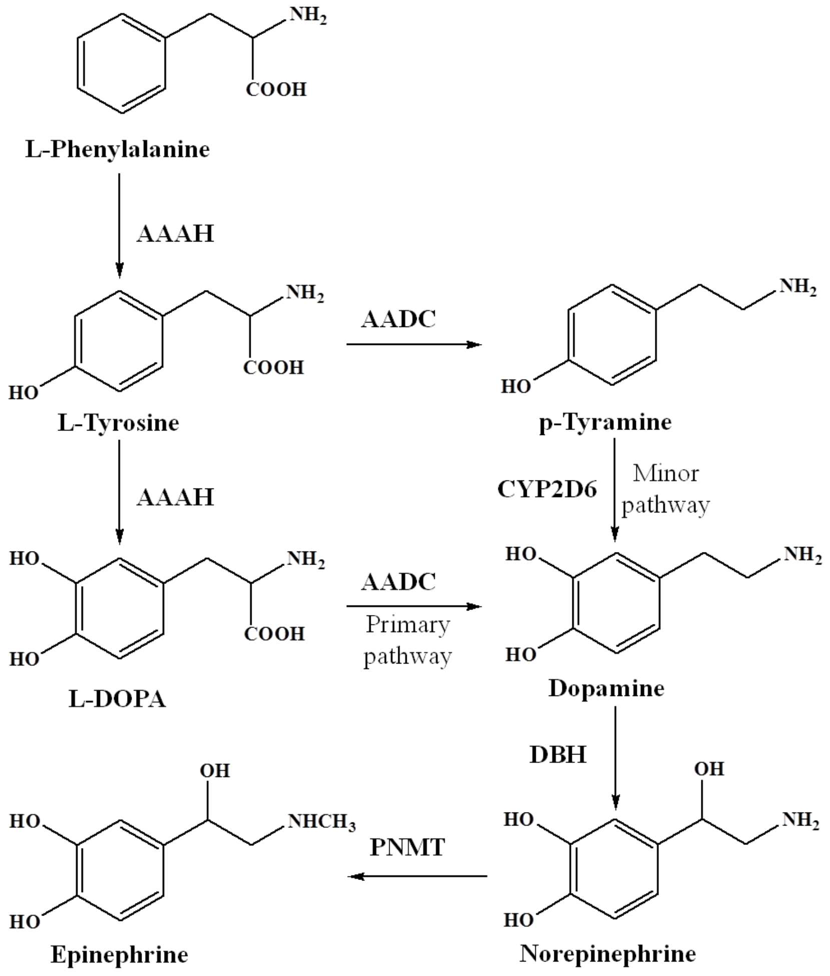

**Figure IV.22:** Scheme of biosynthesis of DA.

An elevated UA concentration in body system may cause renal failure and gout. It may even cause leukaemia and lymphoma at adverse conditions [437]. Therefore determination of DA and UA in blood, urine and any biological fluids is important to evaluate the metabolic functioning of the body system.

### IV. 2. 2. A brief account on sensing Dopamine and Uric acid:

Electrochemical method is one of the important techniques for the determination of DA and UA in biological samples and has important advantages over other available techniques, as the electrochemical methods offer direct measurement. Other techniques based on spectroscopy and chromatography, have disadvantages like, sample pre-treatment and removal of sample from the sample chamber for the analysis [438]. Electrochemical methods are highly sensitive, selective and offer better understanding of the chemical process in addition to the detection. L- Ascorbic acid (AA) (chemical structure, Fig. IV.21) is also one more constituent present in biological system along with DA and UA. The major challenge is to separate the electrochemical peak due to DA, UA and AA, since the electrochemical potential of these three biological molecules are close and it is important to generate the separate electrochemical response from three molecules [439]. Electrochemical methods based on modified electrode have been discussed for the determination of DA [372, 440-472] and these methods are better suited for the determination of biological compounds due to the easy fabrication of the modified electrode, disposability and the possibility of onsite/online determination. Among different modifications, carbon-based nanomaterials such as activated carbon, graphene and carbon nanotubes (CNTs) are important materials of modifications, due to their good electrochemical activity and the large active surface area and these materials are either used in the form of carbon paste or modifier over glassy carbon electrode surface by casting through physical or chemical means [372, 440-461]. Graphene doped with nitrogen has been used for this purpose and it has shown good activity for the determination of DA [473]. In the recent time carbon in the form of nano spheres (CNSs) has been used in various electrochemical applications. CNSs, are the spherical carbon materials, are attractive in various functional nano devices due to their excellent physical and chemical properties. In addition to that CNSs have good structural stability, thermal insulation and excellent conductivity [474]. These materials are applied widely in lithium ion batteries [475-478], adsorption [479], catalyst supports [480, 481] and so on. Therefore it is likely that carbon nano spheres would be good candidate for electrode modification for electroanalytical application by improving the redox response of analytes. Different nanoparticles in polymeric matrices also have shown good detection sensitivity of the DA and UA [482-485]. Some of the recent papers have reported the simultaneous methods of determination of DA and UA using modified electrode based on different form of carbon [486-489].

### IV. 2. 3. Abstract of the present work:

This chapter presents the fabrication and characterization of functionalized carbon nano spheres (FCNSs) and its application as electrode material for the selective determination of DA and UA simultaneously in presence of AA in aqueous medium and human blood serum. Several aspects of development of a method of determination of DA and UA are detailed revealing the advantages of using the newly fabricated electrode over other electrodes. Important analytical parameters regarding the analysis of DA and UA are presented. Except some limited studies [469, 485], where carbon nanoparticles was applied for the determination of DA, no such investigation was reported about the simultaneous determination of DA and UA in a simple way of modification as presented in this work.

### IV. 2. 4. Preparation of functionalized carbon nano spheres and its paste electrode:

The method adopted for the functionalization of graphitic carbon nano spheres (CNSs) was based upon the earlier report published in literature [490, 491]. The CNSs were washed thoroughly by dilute $HNO_3$, HCl and deionized water to eliminate the possible metal impurities in the carbon powder prior to the functionalization. 500 mg of the washed CNSs was soaked in 50mL of an acid mixture (1:1) of 50% $HNO_3$ and 50% $H_2SO_4$ for 1 h. Then the whole mixture was refluxed at 90$^o$C for 6 h under vigorous stirring condition. Subsequently, the solution was centrifuged and the black residue was collected and washed thoroughly with deionized water and kept inside a vacuum furnace for 12 h at 50$^o$C for drying. The dried FCNSs were characterized using spectroscopic and microscopic techniques. These FCNSs were mixed with CNSs at different proportions. A paste was made with this mixture adding adequate amount of silicone oil (around 20%), the paste was used to make the modified electrode. The modified electrode was fabricated by filling a glass tube with the paste and a Pt wire was used to connect the paste to the potentiostat, this modified electrode was abbreviated as FCNSPE. This FCNSPE was used for the investigation of electrochemical properties of DA, UA and AA in PBS of pH 7.

### IV. 2. 5. Characterization of functionalized carbon nano spheres:

#### IV. 2. 5. 1. SEM and AFM imaging:

After functionalization, the carbon powders were well suspended in water which is an evidence of the functionalization of the nano spheres. SEM and FTIR measurements were carried out for further investigation on the material's characteristics. SEM image (Fig. IV.23.a and IV.23.b) shows that the particles are spherical in shape. The size and shape of the CNSs did not change on functionalization. The FCNSs were also characterized using AFM measurements and the morphological and phase contrast images are shown in figure IV.23.c and IV.23.d respectively. No significant differences between the topography and phase contrast images were observed, indicating the similar interactions between the AFM tip and all the functionalized carbon nano spheres spread across the substrate. The histogram depicting the distribution of size of the nano spheres is shown in figure IV.23.e, the average size of the nano spheres were obtained as 35.5 nm.

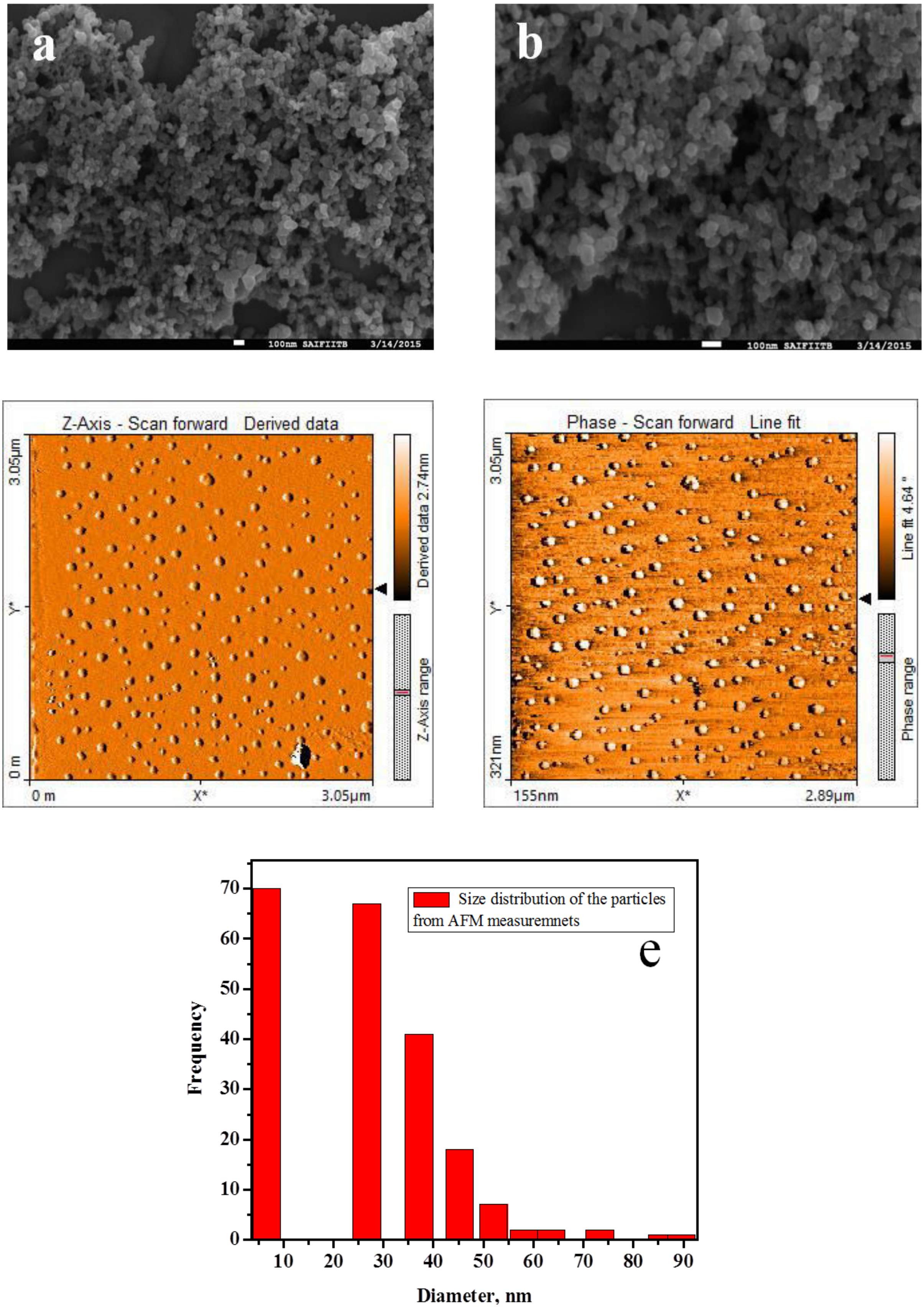

**Figure IV.23:** SEM image of (a) CNSs and (b) FCNSs; (c) Morphological and (d) Phase contrast image of FCNSs by AFM measurements; (e) The histogram depicting the distribution of size of the FCNSs.

### IV. 2. 5. 2. FTIR measurement:

The FTIR measurements were recorded on the FCNSs and the spectra are shown in figure. IV.24. The broad peak at 3400 cm$^{-1}$ is related to the O-H stretching from carboxylic acid. The band at 1725 cm$^{-1}$ is related to the stretching vibration of the C=O group present in carboxylic acid. The sharp band at 1591cm$^{-1}$ is related to the vibration of the adsorbed water molecules or skeletal vibrations of un-oxidized C-C bonding. Additionally, the peak at 1425 cm$^{-1}$ is due to the O-H bending vibration and the peak at 1385 cm$^{-1}$ is related to the O-H deformation vibration of the tertiary C-O-H group. The band at 1260 cm$^{-1}$ is due to the C-O stretching vibration and the band at 1107 cm$^{-1}$ is related to the C-O-C stretching of the oxo functional group incorporation in the surface of the CNSs. Therefore the FTIR measurements indicated the incorporation of plenty of functional groups like OH, COOH and epoxy on the surface of the carbon nano spheres.

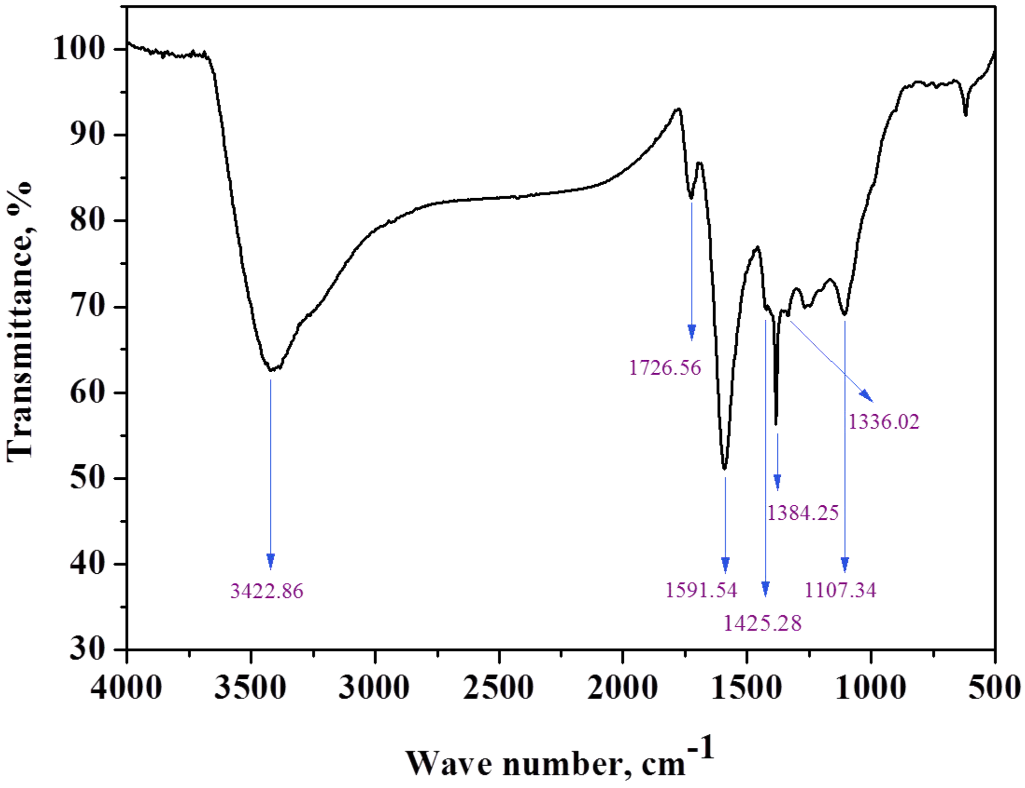

**Figure IV.24:** FTIR spectra of FCNSs.

### IV. 2. 5. 3. Characterization by Raman spectroscopy:

Raman spectroscopy is an excellent tool for characterization of carbon materials. Excitation was carried out at 514.5 nm. In Raman spectroscopic measurements three peaks were observed at 1336 $cm^{-1}$, 1606 $cm^{-1}$ and at 2740 $cm^{-1}$ as shown in figure IV.25. The Raman peak due to the ideal lattice vibration of graphite normally appears at 1580 $cm^{-1}$. In a real case many defect bands or D-bands appear in the Raman spectra. These D bands are due to the disorder in the graphitic structure. Such D-bands are of very high intensity. Presently the peak at 1336 $cm^{-1}$ is designated as the D1 band. The peak due to the pure lattice vibration of graphite lattice was not observed. The peak at 1606 $cm^{-1}$ is due to shifted G band; sometime this band was assigned as the second defective band or D2 band [492-498]. The ratio of the D/G intensities was obtained as 1.36. This D/G band intensity ratio is a measure of the presence of structural defects in the system. This may arise due to the disruption of $sp^2$ bond in the graphite structure. Sometime this disruption of the $sp^2$ spectra is correlated to the formation of $sp^3$carbon which introduces the deformation in the lattice.

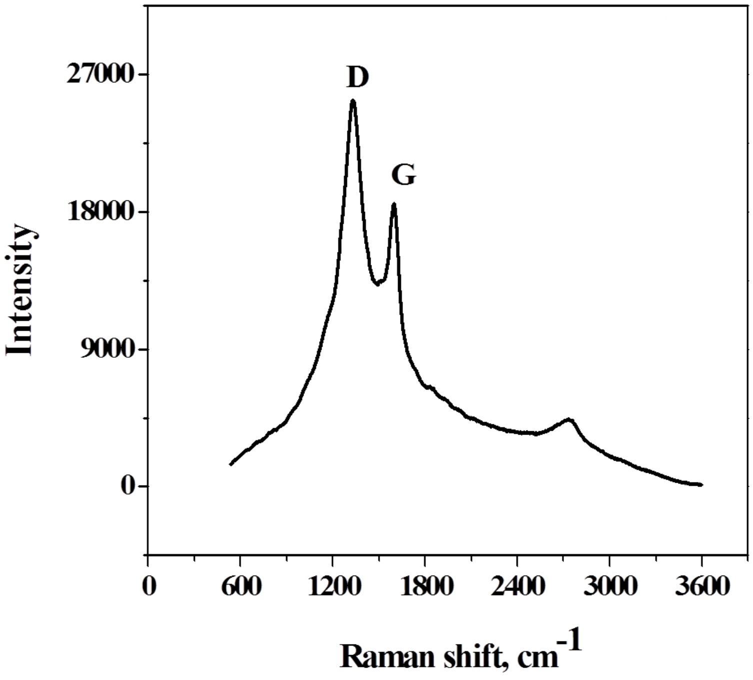

**Figure IV.25:** Raman spectra of FCNSs.

Presently upon functionalization in oxidising acids the CNSs undergo oxidation at the surface. Obtaining the higher D/G band intensity ratio is the evidence of oxidation of the CNSs upon functionalization. The Raman spectra also consisted of the second order bands, the peak at 2740 $cm^{-1}$ is related to the overtone of the D1 peak [492-498].

## IV. 2. 6. Results and Discussions:

### IV. 2. 6. 1. Basic experimental conditions:

All the experiments were performed using a two step process which includes accumulation or preconcentration as the first step and electrochemical oxidation by differential pulse anodic stripping voltammetry (DPASV) as the second step. During accumulation, hydrodynamic condition was maintained by stirring the solution at 2500 rpm using magnetic needle, while stripping was carried out under tranquil condition. After each scan the electrode was regenerated for further use by dipping it into 0.01M $HNO_3$, 0.01M $NH_4OH$ and deionized water in the stated order for one minute each. All the experimental solutions were prepared in phosphate buffer of pH 7 except the effect of variation of pH which was conducted in BR buffer. Although the modified electrode was successfully applied for the determination of DA and UA, all electrochemical parameters were optimized using the DA signal since DA, present in human body system at lowest concentration compared to UA and AA, is the most challenging one to be determined among the three molecules.

### IV. 2. 6. 2. Optimization of loading of FCNSs in the electrode:

The percentage of loading of FCNSs in the carbon paste was optimized by varying its content in the modified material and recording the oxidation peak current of DA. As shown in figure IV.26, the stripping peak current of DA was increased with increase in the loading of the FCNSs into the paste. The oxidation peak current of DA attends maxima at around 40% to 50

% loading. The peak current was increased due to the incorporation of more functionalized materials into the paste. Beyond that the peak current was decreasing. With increase in the loading of functionalized material the resistance of the electrode was increased. Furthermore at higher loading of the FCNSs, the electrode is transformed in to a highly hydrophilic substrate. It was difficult to stabilise the electrode with the functionalized materials loading beyond 60-70% as it was coming out from the surface on repetitive scans. Therefore 50% loading of FCNS was optimized in the present case for all the experiments.

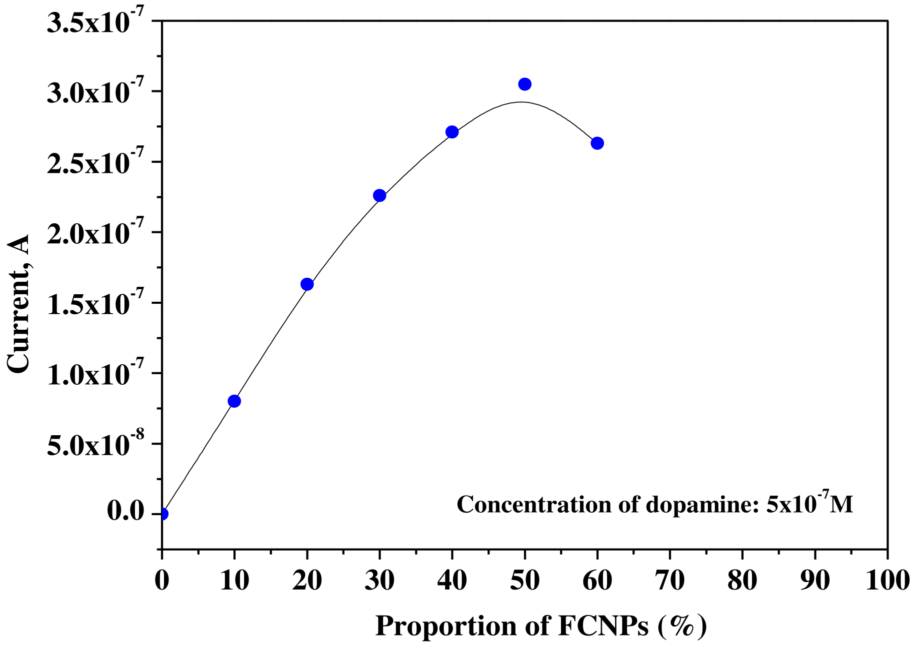

**Figure IV.26:** Effect of loading of FCNS in FCNSPE on the oxidation signal intensity of DA (concentration of DA in $5x10^{-7}$M).

### IV. 2. 6. 3. pH dependent cyclic voltammetric response of DA, UA and AA on FCNSPE:

FCNSPE was able to produce good oxidation response for DA and UA, although oxidation signals of AA were broad and the peaks of the waves were not very prominent. Effect of pH on the oxidation peak potential of DA, UA and AA was investigated by recording the cyclic voltammetry scans in BR buffer solution by varying the pH from 2.3 to 9.1. Corresponding CV plots for DA, UA and AA are shown in figure IV.27.a, IV.27.b and IV.27.c. Peak potentials of all the three compounds were shifted towards the negative potentials with increase in pH of the media. The slope of the linear plot in the case of DA, UA and AA were obtained as 58, 63 and 46 mV/pH respectively (Fig. IV.27.d).

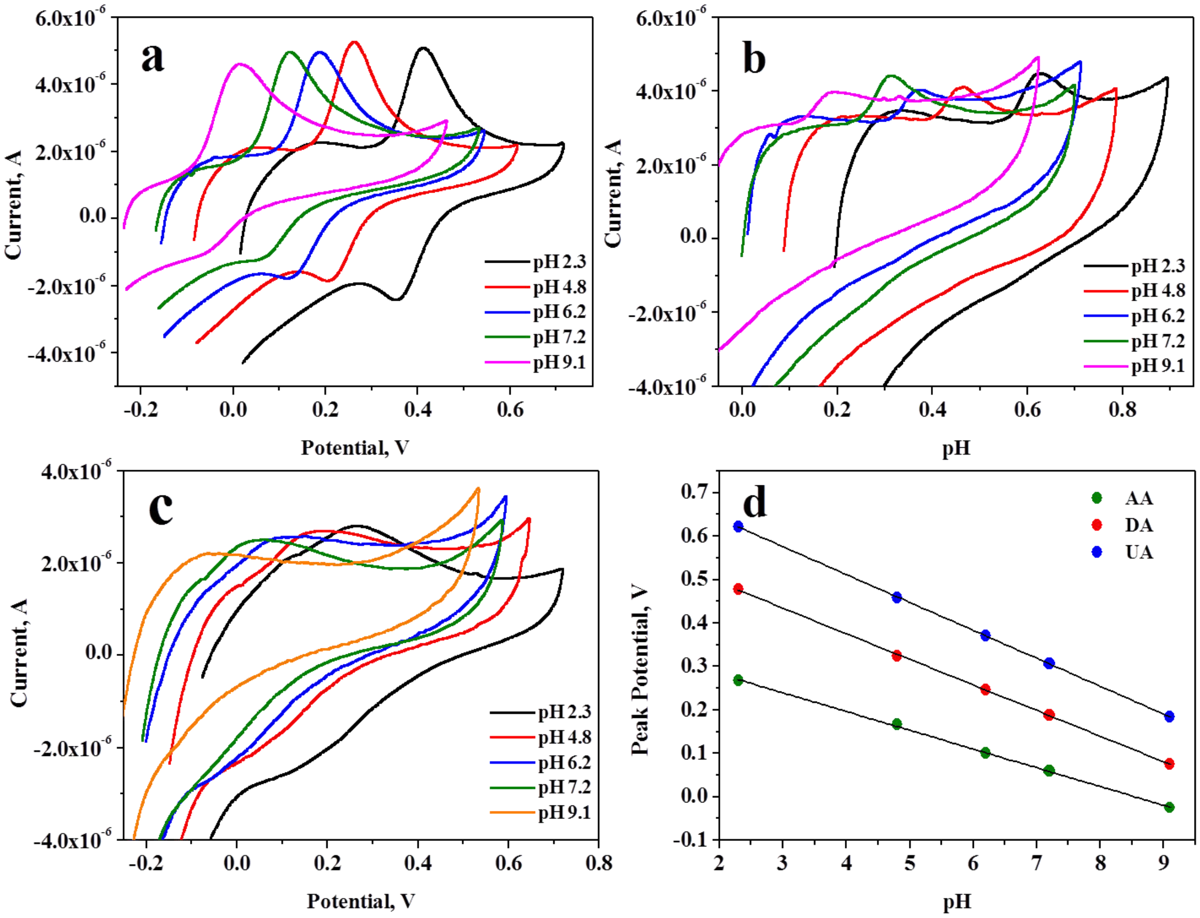

**Figure IV.27:** Cyclic voltammograms of (a) DA, (b) UA and (c) AA at different pH; (d) Plot of peak potential vs. pH of the BR buffer for DA, UA and AA.

The slope of around 60mV/pH in the cases of DA and UA was observed, indicated the liberation of equal numbers of protons and electrons during the oxidation process. Oxidation of DA is 2 electron transfer process, therefore the oxidation mechanism of DA followed the 2 electron and 2 proton transfer process, which agreed well with the previously reported literature [499-503]. Where, most of the reports have reported the 2 electron and 2 proton transfer process to form the dopamine ortho-quinone as the oxidation product. The paper by Avendano et al. have investigated the mechanism of the electrochemical oxidation of DA in detail and the 1 electron 1 proton intermediate oxidation step was also identified [501]. The mechanism of the electrochemical of DA is shown in the figure IV.28.a, where DA undergoes 2 electron 2 proton oxidation processes from DA to dopamine ortho-quinone. The mechanism of the oxidation of UA and AA is shown in the figure IV.28.b and IV.28.c respectively [504].

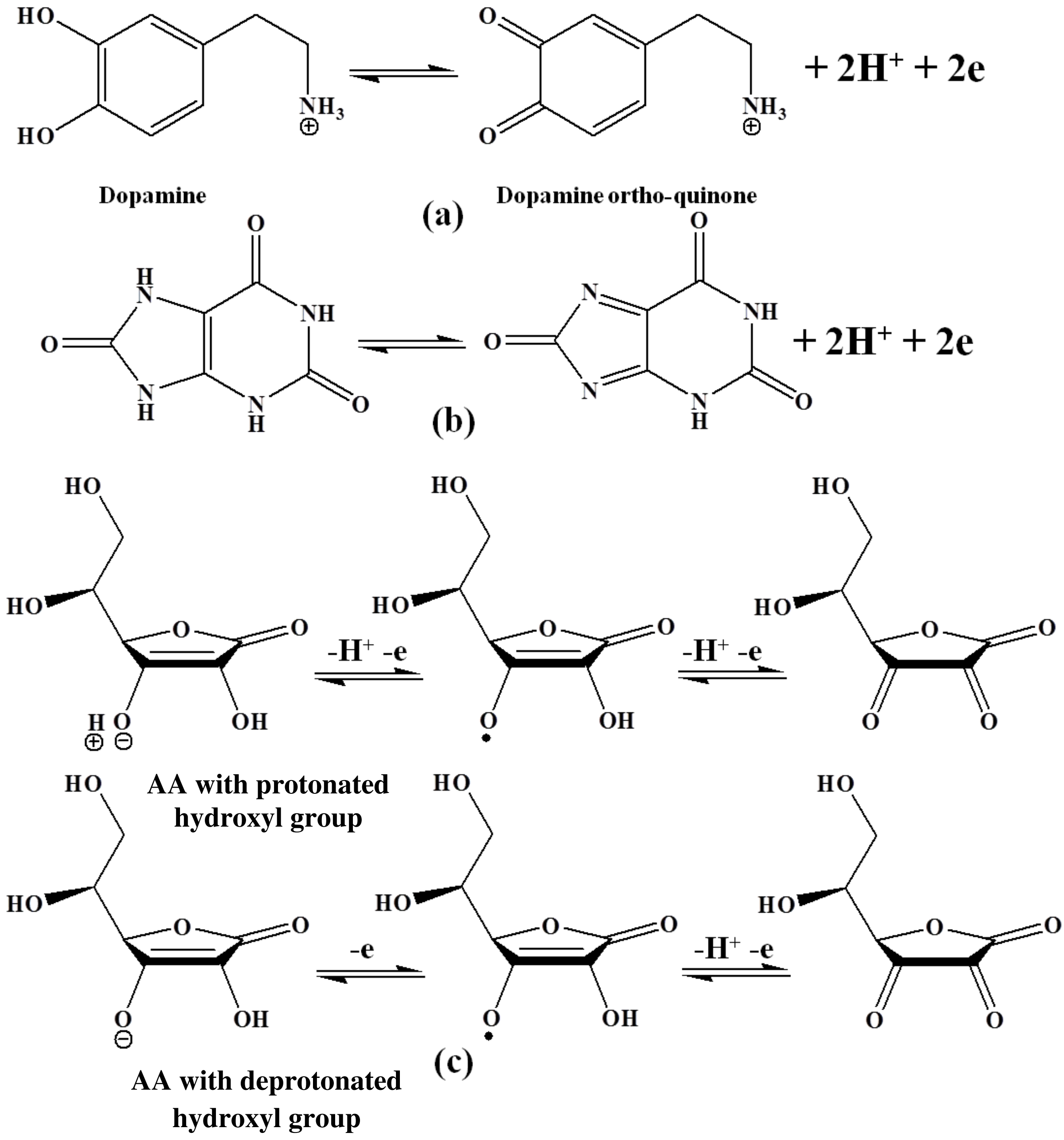

**Figure IV.28:** Oxidation scheme of (a) DA, (b) UA and (c) AA

The slope in the case of AA was obtained as 46 mV/pH and the value is midway between the 2 electrons and 2 protons and 2 electrons and one proton transfer process. The reduction at the protonated hydroxyl group present in the equilibrium will undergo the 2 electrons and 2 protons transfer process and the deprotonated hydroxyl group will undergo 2 electrons and 1 proton transfer process. Such partial protonation of the hydroxyl group would result in the positioning the slope of the potential vs. pH plot at the midway between the 2 electrons 2 protons and 2 electrons 1 proton transfer process.

### IV. 2. 6. 4. Optimization of accumulation potential and accumulation time:

Accumulation/pre-concentration plays a vital role in order to obtain high sensitivity for the analytical determination. Therefore, both accumulation potential and accumulation time were varied and the voltammetric scans were recorded to optimise their values. Measurements were carried out at a DA concentration of 0.5μM. The voltammograms recorded at different accumulation potentials are shown in figure IV.29.a. The stripping peak current due to the oxidation of DA was found to be highest for accumulation potential of -0.3V (vs. Ag/AgCl/KCl(satd)) (Fig. IV.29.b). The accumulation potential of -0.3 V, though produced good oxidation peak of DA with high sensitivity, the voltammetric response was not linear on successive addition of DA (plots are not shown). Therefore the accumulation potential of -0.3 V was avoided. Similar non linear response was found in other negative accumulation potentials. Accumulation potential of 0.1V was avoided as it is very close to the peak potential of DA oxidation and 0V was taken as optimized accumulation potential. Effect of accumulation time was optimized with respect to DA by keeping the accumulation potential at 0 V. Corresponding results are shown in figure IV.29.c and IV.29.d. It was observed that with increase in the accumulation time the voltammetric peak current was increased very fast till 600 sec. After that the increase in the peak current became less prominent. In order to keep the time of making a measurement less and also to have the good sensitivity in the measurements the accumulation time of 600 sec was optimized.

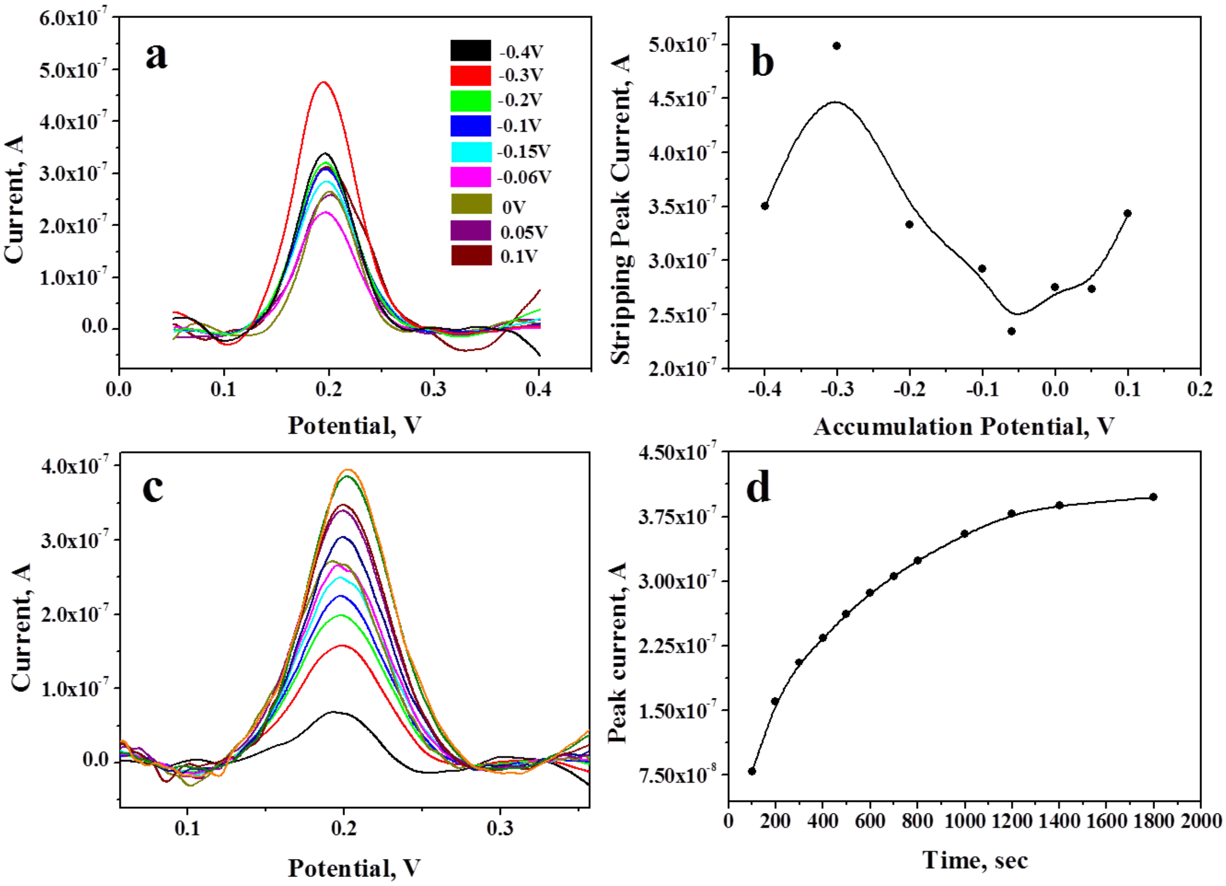

**Figure IV.29: (a)** Differential pulse anodic stripping voltammogram of DA oxidation at different accumulation potential; (b) Dot-line representation of change in peak current of DA oxidation signal with accumulation potential; (c) Differential pulse anodic stripping voltammogram of DA oxidation with variation of accumulation time at accumulation potential of 0V and (d) Dot-line representation of the variation of oxidation peak current of DA with deposition time. Concentration of DA is 5x10$^{-7}$M in PBS supporting electrolyte media of pH 7.

### IV. 2. 6. 5. Analytical response of the electrode for DA, UA and AA and evaluation of important analytical parameters:

Oxidation of DA produced distinguished peak at 0.2V in PBS of pH 7 (Fig. IV.30.a). Similar to DA well defined oxidation peak for UA was observed over the FCNSPE at 0.33V (Fig. IV.30.b). Voltammetric responses at varying concentration of DA showed proportional increase in the oxidation current of DA with its concentration (Inset of Fig. IV.30.a). Similar to DA the peak current for oxidation of UA was increased proportionately with the UA concentration. The calibration plot was linear in the concentration range investigated (Inset of Fig. IV.30.b).

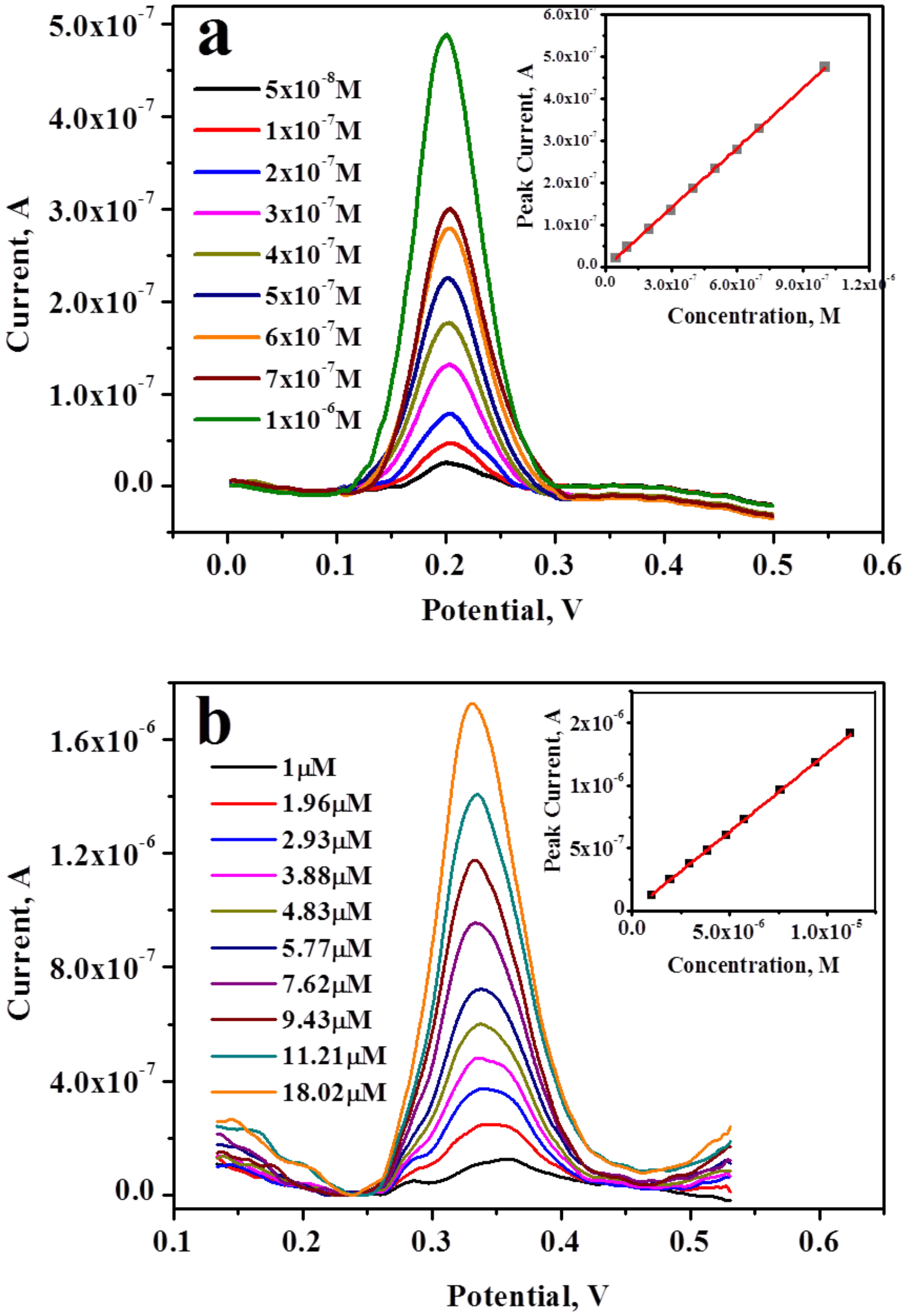

**Figure IV.30:** Differential pulse anodic stripping voltammogram of (a) DA oxidation at different concentrations, Inset: corresponding calibration plot of peak current vs. concentration and (b) Differential pulse anodic stripping voltammogram of UA oxidation at different concentrations, Inset: corresponding calibration plot of peak current vs. concentration.

The calibration plot of DA followed the regression equation $i_p$=0.499C – 0.62×$10^{-10}$, where C in M (molar) unit, the standard deviation was obtained as of 1.66×$10^{-9}$. Similarly the calibration plot of DA followed the regression equation $i_p$=0.124C + 3.49×$10^{-9}$, where C in M unit, the standard deviation was obtained as of 2.90×$10^{-9}$. The LOD of DA and UA were calculated from the slope and the intercept values and using three time of the standard deviation, the values were obtained as 10 nM and 42 nM respectively for DA and UA. The sensitivity of DA and UA are 0.499 A/M and 0.124 A/M respectively.

In order to obtain the relative dynamic response from DA and UA and AA from the modified electrode, voltammetric plots were recorded by varying the DA, UA and AA concentration in the test solution, UA and AA were added at 10 and 100 times higher than that of DA concentration respectively. Electrochemical response of both DA and UA were increasing proportionately with simultaneous addition of DA and UA in the test solution (Fig. IV.31).

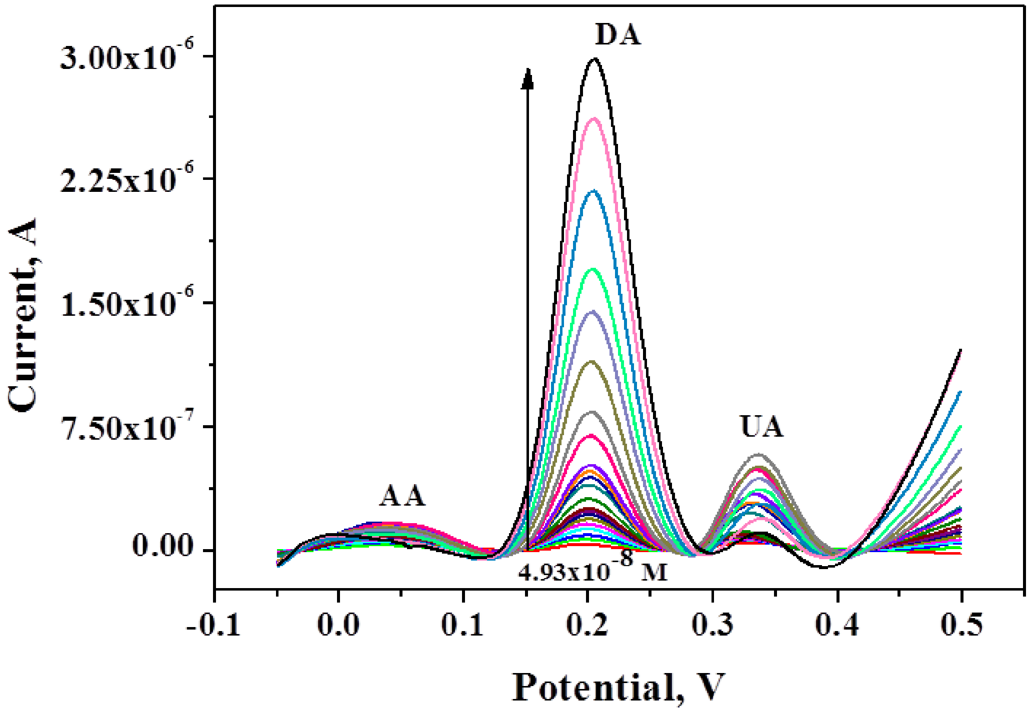

**Figure IV.31:** Differential pulse anodic stripping voltammogram of DA, UA and AA at varying concentration. AA was varied at 100 times higher and UA was varied at 10 times higher in concentration than DA. Experiments were carried out at pH 7 (PBS) accumulations at 0V for 600 sec.

The UA peak saturated at around 10x$10^{-6}$ M concentration, beyond that its oxidation peak current was not increasing. No clear peak from AA was observed. The calibration plot was linear for both DA and UA in the concentration range investigated (Fig. IV.32). The calibration plot of DA followed the regression equation $i_p$=0.489C – 0.604×$10^{-10}$, where C is concentration in M (molar) unit, the standard deviation was 1.66×$10^{-9}$. Similarly the calibration plot of UA followed the linear regression equation $i_p$=0.0357C – 5.627×$10^{-10}$, where C is concentration in M unit, the standard deviation was 1.524×$10^{-9}$. The LOD of DA and UA were calculated from the slope and the intercept values and using three time of the standard deviation, the values were obtained as 10 nM and 0.14 μM respectively for DA and UA. The sensitivity of DA and UA are 0.489 A/M and 0.0357 A/M respectively. In the dynamic presence of DA, UA and AA the linear dynamic range of DA and UA were obtained as 4.93x$10^{-8}$M to 3.98x$10^{-6}$M and 5 x $10^{-7}$ M to 9x$10^{-6}$ M respectively.

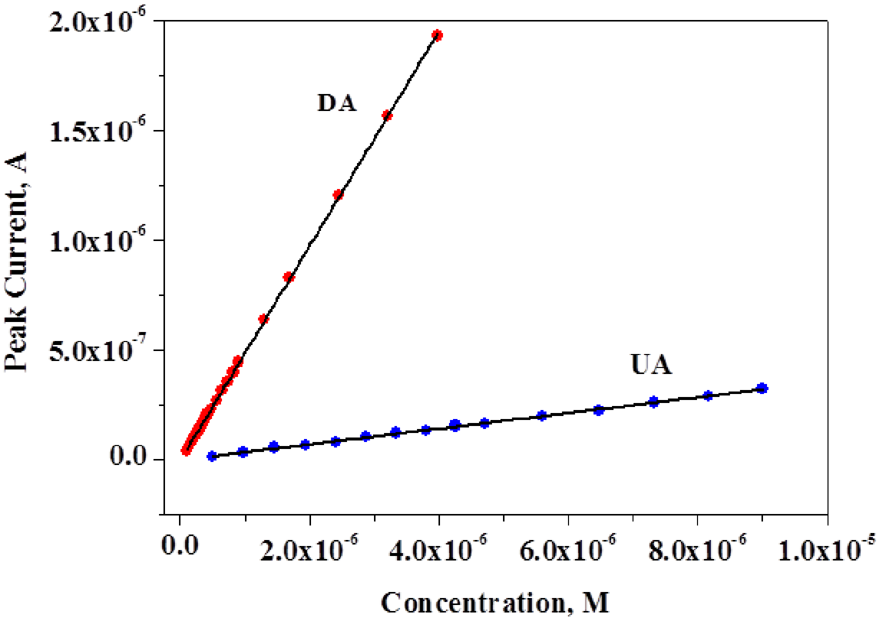

**Figure IV.32:** Calibration plot of peak current vs. concentration of DA and UA when added simultaneously in PBS of pH7.

### IV. 2. 6. 6. Result of interference study:

The method was found to tolerate interference from 100 times higher concentration of glucose and fructose and 10 times higher concentration of cysteine. Interference due to some of the commonly occurring metal ions like; $Cu^{2+}$, $Pb^{2+}$, $Cd^{2+}$, $Zn^{2+}$, $As^{3+}$, $As^{5+}$ and $Cr^{3+}$, $Cr^{5+}$ were investigated, the method was found to interference free at the presence of 10 times higher concentration of the metal ions.

### IV. 2. 6. 7. Comparison of analytical performance with reported literatures:

Analytical performance of the present method was compared along with the previously reported literatures and placed in table IV.4 [457-461, 482-485]. As seen from the comparison table present method has comparable or better analytical performance compared to the methods reported in the literature.

| **Electrode materials** | **Detection limit (µM)** | | **Linear range (µM)** | | **Reference** |
|---|---|---|---|---|---|
| | **DA** | **UA** | **DA** | **UA** | |
| $Fe_3O_4$@GNs | 0.007 | ---- | 0.02-13.0 | ---- | [457] |
| Mp-GR | 1.5 | 2.0 | 4.0-40.0 | 5.0-120.0 | [459] |
| Pdop@GR/MWCNTs | 1.0 | 15.0 | 7.0-297.0 | 20.0-320.0 | [461] |
| DNA/Pp-ABSA | 0.088 | 0.19 | 0.19-13.0 | 0.4-23.0 | [482] |
| DNA/PAMAM/MWNT-Chit/Au | 0.03 | 0.07 | 10.0-100.0 | 0.5-100.0 | [483] |
| GNP/Ch | 0.12 | 0.60 | 0.2-80.0 | 1.2-100.0 | [484] |
| Nano-Cu/PPy | 0.0008 | 0.00085 | 0.001-0.1 | 0.001-10.0 | [485] |
| FCNSPE | 0.01 | 0.042(0.14)* | 0.0493-3.98 | 0.5-9 | This work |

*Value inside the bracket corresponds to the LOD of UA when calculated in presence of DA and AA.

**Table IV.4:** Data for comparison of the analytical performance of the FCNSs modified paste electrode for determination of DA and UA with the previously reported literature.

### IV. 2. 6. 8. Interaction of molecules over the modified electrode:

As discussed in the previous section, sensitivity of the FCNSPE for the UA fell dramatically from 0.124 $AM^{-1}$ to 0.0357 $AM^{-1}$when measurement was carried out in presence of DA. On the other hand sensitivity of DA remained almost the same (from 0.499 $AM^{-1}$ to 0.489 $AM^{-1}$) even after addition of AA and UA at higher concentrations. This clearly reflected the higher selectivity of the electrode towards DA than UA and AA. It would be interesting to discuss about the difference in the electrochemical activity of DA, UA and AA over the FCNSPE electrode surface. As shown in the FTIR measurements the FCNSPE substrate was anchored with carboxylic acid groups (-COOH) along with many other active functional groups through which DA might be preconcentrated over the modified electrode surface. The possible routes of interaction of DA with the modified electrode surface can be discussed in the following way. DA is an aliphatic amine and a stronger base, the acidity constant corresponding to the protonated ethylene amine group ($-CH_2-CH_2-NH_2$) is ~10.5 and for the first and second acidity constant of the two phenolic OH groups of the catechol the values are ~9.5 and 12.5 [505].

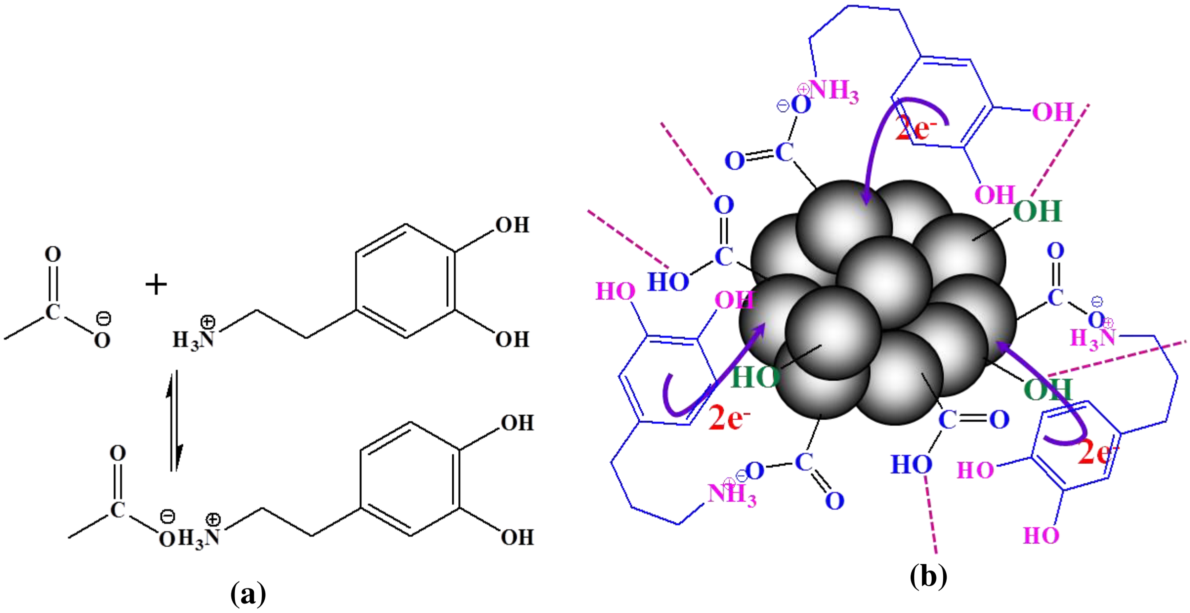

**Figure IV.33:** (a) Equation for ammonium carboxylate salt formation between carboxylate ions of FCNSs and primary amine of DA; (b) Pictorial representation of interaction pattern and the entanglement of DA with the FCNSs modified paste electrode.

Therefore at neutral pH of the experiment the amine group of DA would be in the protonated state. The protonated amine would have experienced electrostatic attraction with the carboxylate ions anchored over FCNSs and produced the ammonium carboxylate as shown in figure IV.33.a. The interaction pattern and the entanglement of DA with the functionalized carbon nano spheres modified electrode are shown in figure IV.33.b. UA and AA would have the interaction with FCNSPE through the hydrogen bonding interaction only [502], which are not so effective during pre-concentration process. Although hydrogen bonding and other adsorption processes might have some contribution to pre-concentration, however the contribution of such interaction might be equal to all these three compounds. The interaction through the formation of ammonium carboxylate was the dominating factor for stronger interaction between DA and the modified surface.

### IV. 2. 6. 9. Electrochemical Impedance Spectroscopy (EIS) on FCNSPE:

The electrochemical impedance experiments were carried out using the modified electrode in blank supporting electrolyte media and in presence of $0.5\text{x}10^{-6}$M DA; the resulted Nyquist plots are shown in figure IV.34. Corresponding equivalent circuits are shown in figure IV.35.a and IV.35.b and the corresponding fitting parameters in table IV.5 and IV.6. Impedance experiments were carried out at 0 V where the pre-concentration of DA is high. The nature of the Nyquist plot in blank supporting electrolyte media of PBS at pH 7 has shown depressed semicircular nature. In the equivalent circuit, $R_s$ corresponds to the series resistance which arises due to the resistance of the solution. $C_{dl}$ and $R_d$ correspond to the double layer capacitance and the resistance of the modified surface. $C_p$ and $R_p$ are the capacitance and resistance during the polarization process. These two components are responsible for the measure of polarization during the charge transfer processes. Upon addition of DA in the test solution the nature of the impedance plot was modified. The semicircular pattern remained depressed and the nature of the plot was modified at the low frequency region. Additional resistance and capacitance components were introduced in the equivalent circuit to fit the Nyquist plot. The resistance and capacitive components $R_{ad}$ and $C_{ad}$ corresponds to the preferential preconcentration of DA on the modified electrode surface [506-508]. Small but unavoidable contribution from Warburg component was observed at the lower frequency side of the Nyquist plot. Therefore the electrochemical oxidation process of DA over the modified electrode surface has contribution from adsorption of DA.

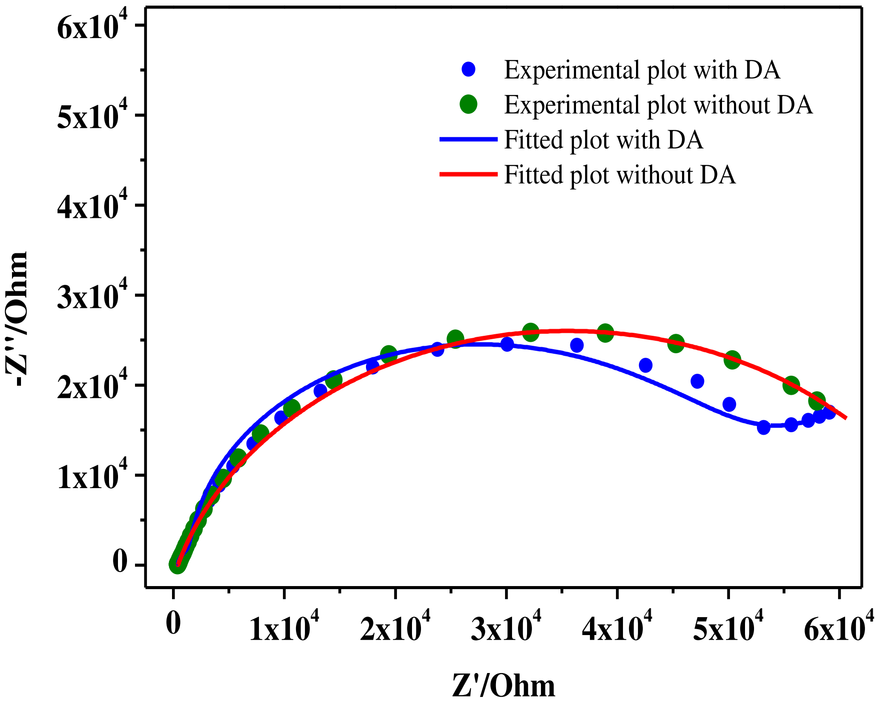

**Figure IV.34:** Nyquist plots using the FCNSs modified paste electrode in blank supporting electrolyte media and in presence of $0.5 \times 10^{-6}$M DA.

The diameter of the semicircle would have increased due to the adsorption of DA [509], however when compared with the blank supporting electrolyte solution the diameter of the semicircle remained the same. This is due to the higher oxidation current from DA containing solution at the same applied potential compared to the blank supporting electrolyte solution. Adsorption enhances the preconcentration property of DA over the electrode surface, does not foul the electrode on successive electrochemical scans when the regeneration method as specified in the beginning of this chapter was adapted. The functionalized carbon nano spheres as applied in the present case could well be applied by embedding them into polymer matrix. However preparation of carbon paste with the functionalized carbon nano spheres is one of easiest way to prepare the modified electrode.

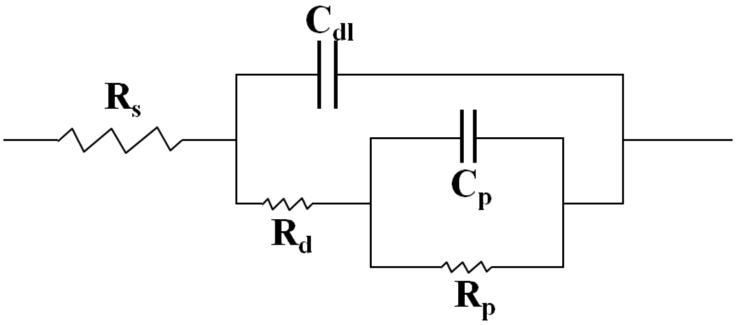

**Figure IV.35.a:** Equivalent electrical circuit for the electrochemical system having the FCNSs modified paste electrode in blank supporting electrolyte media (PBS of pH 7).

| Parameter | Value | Parameter | Value |
|---|---|---|---|
| $R_s$ | 30 Ω | $C_{dl}$ | 138 nF |
| $R_d$ | 110 Ω | $C_p$ | 22 µF |
| $R_p$ | 70 kΩ | | |

**Table IV.5:** Table showing the values of the fitting parameters of the equivalent electrical circuit represented in figure IV.35.a.

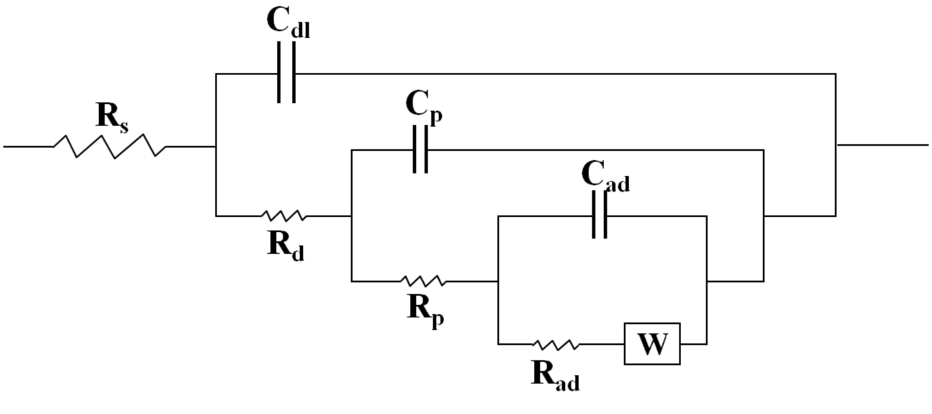

**Figure IV.35.b:** Equivalent electrical circuit for the electrochemical system having the FCNSs modified paste electrode in presence of $0.5x10^{-6}M$ DA in the supporting electrolyte media (PBS of pH 7).

| Parameter | Value | Parameter | Value |
|---|---|---|---|
| $R_s$ | 30 Ω | $C_{dl}$ | 7.6 nF |
| $R_d$ | 390 Ω | $C_p$ | 8.1 µF |
| $R_p$ | 40 kΩ | $C_{ad}$ | 11 µF |
| $R_{ad}$ | 3 kΩ | | |
| W | $0.22\ \Omega\ s^{-1/2}$ | | |

**Table IV.6:** Table showing the values of the fitting parameters of the equivalent electrical circuit represented in figure IV.35.b.

### IV. 2. 6. 10. Spike recovery test and application of the method in real blood serum analysis:

Recovery tests were performed to investigate the analytical efficiency of the electrode to recover the analyte response at low concentrations in real blood serum sample and the results with 6 repetitions are shown in table IV.7. Human blood was sample collected in a covered test tube. After collection of the blood, it was allowed to clot by leaving it undisturbed at room temperature. This usually takes around 15-30 minutes. The clot was removed by centrifuging at 15000 rpm for 10 minutes in a refrigerated centrifuge at -2°C. The resulting supernatant which is serum of the blood is collected. An aliquot of 1mL of serum was taken and diluted to 10 mL by PBS of pH 7 and used as the test solution. This solution was spiked with standard DA concentration and it was determined using the presently developed method. Corresponding voltammetric plot during the spike recovery analysis of two different concentrations (2.2 µM and 0.1µM) are shown in figure IV.36.a and IV.36.b respectively. The recovery test results have shown 100.5% and 104% recovery for DA at two different concentrations in real blood serum sample using the modified electrode. The relative standard deviations as measured from the 6 repetitive measurements at 2.2 µM and 0.1 µM concentration levels were 6.7 % and 8.6 % respectively. UA was determined directly in the real blood sample using standard addition method and the UA level in the human serum sample was obtained as 17 (±1) µM.

| Sl. No. | Concentration of Dopamine added (µM) | Measured concentration with 6 repetition (µM) | Mean ±standard deviation | Recovery |
|---|---|---|---|---|
| 1. | 2.20 | 2.3, 2.2, 2.4, 2.1, 2.0, 2.6 | 2.21±0.15 | 100.5% |
| 2. | 0.100 | 0.12, 0.098, 0.10, 0.10, 0.11, 0.095 | 0.104±0.009 | 104% |

**Table IV.7:** Results of recovery study at two different concentration levels (2.2 µM and 0.1µM) of DA in blood serum using FCNSs modified paste electrode.

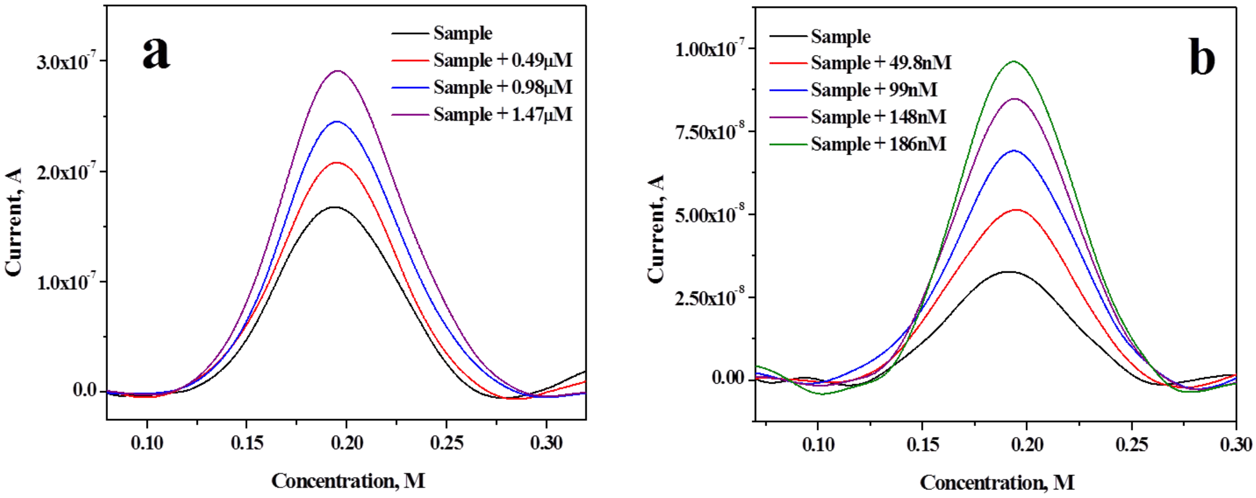

**Figure IV.36:** Differential pulse anodic stripping voltammetric plots during the spike recovery test of DA with (a) 2.2x10$^{-6}$M and (b) 1x10$^{-7}$M concentration in real blood sample.

The analytical method was also validated by measuring dopamine using HPLC technique measurements for the spike recovery test in blood serum sample. Electrochemical measurements were carried out keeping all experimental parameters same as that during calibration except a preconcentration time of 30 sec. Standard addition method was adopted for the determination. The results comparing the values obtained using the electrochemical technique and HPLC are shown in table IV.8, HPLC plots are shown as figure IV.37. The mean value obtained using two different techniques were almost similar. The statistical analysis, t test of the set of measurements was carried out and the measured t value ($t_{meas}$) of the set of measurements was obtained as 0.278. The critical t value ($t_{crit}$) was obtained by referring the t table for the degrees of freedom of 10 as 2.228. Since $t_{meas}$ is less than $t_{crit}$, the null hypothesis holds and two mean values obtained from two methods are statistically the same.

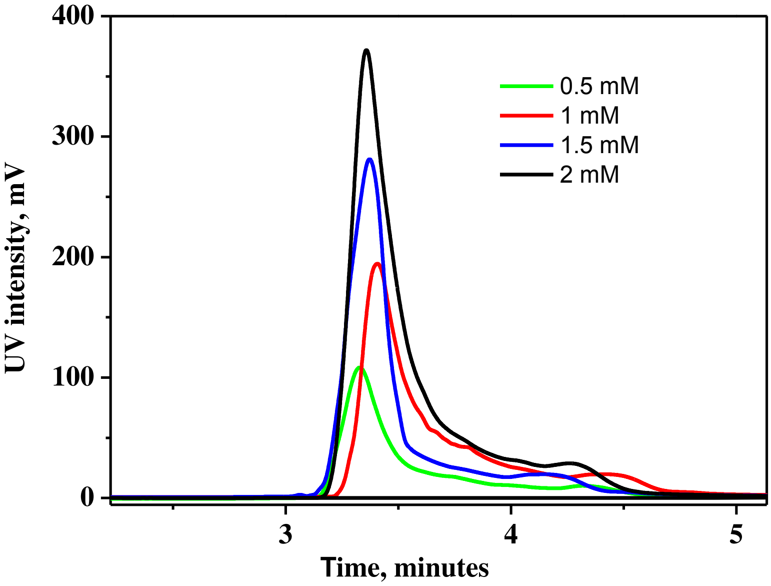

**Figure IV.37:** HPLC plots during recovery test with successive addition of dopamine.

| Dopamine added | Results using Electroanalytical technique (mM) | Mean ± standard deviation | Results of HPLC Technique (mM) | Mean ± standard deviation |
|---|---|---|---|---|
| 0.5 mM | 0.51<br>0.49<br>0.51<br>0.52<br>0.48<br>0.47 | 0.497 ± 0.019 | 0.49<br>0.53<br>0.48<br>0.46<br>0.52<br>0.51 | 0.498 ± 0.026 |

**Table IV.8:** Comparison of the results of the recovery test of DA in blood serum using the FCNSs modified paste electrode and HPLC technique.

Repeatability of the preparation of the modified electrode was investigated by recording the voltammetric scans at $2 \times 10^{-7}$ M of DA using three sets of modified electrode of same dimension, corresponding results are shown in figure IV.38. The peak current varied within 2 % from the mean current value.

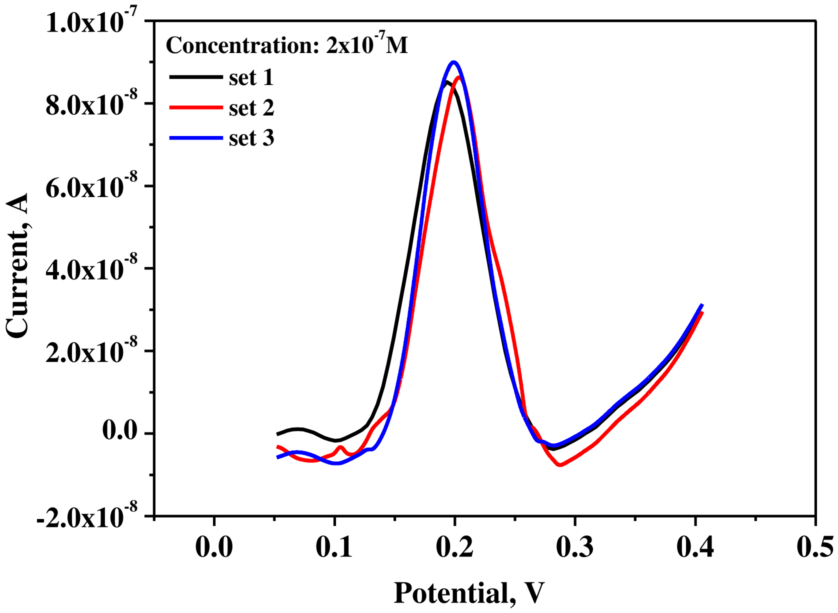

**Figure IV.38:** Differential pulse anodic stripping voltammograms of DA at $2\times10^{-7}$ M concentration with three sets of modified electrodes of same dimension.

### IV. 2. 7. Conclusion:

Functionalized carbon nano spheres were synthesised using chemical functionalization route and the functionalized materials were characterized using spectroscopic and microscopic techniques. Modified electrode was fabricated using the functionalized materials. FCNSPE showed very good activity towards the generation of electrochemical oxidation signal of DA and UA in presence of AA. The electrode was highly selective with excellent sensitivity and reproducibility of the redox signal of DA and UA. The results obtained from the spike recovery test in real blood sample were quite reliable as the results were cross validated using HPLC technique. Thus, a simple way of modification offered very good method of determination of DA and UA; the method is suitable for real application. Without having complicated modification procedure this material is a good candidate for the fabrication of ultra-microelectrode for in situ determination of DA and AA.

# Chapter IV.3

## *Investigation of electrochemical properties of L-Cysteine and method development for its determination.*

### IV. 3. 1. Abstract:

The present work is orchestrated to extract the adsorptive/desorptive electrochemical properties of biologically a very significant molecule L-cysteine on gold nanoparticles (AuNPs) modified glassy carbon electrode (GCE). Electrochemical impedance spectroscopy (IES) and scanning electrochemical microscopic (SECM) measurements are elaborated here to evident such adsorptive/desorptive behaviour of the molecule and charge transport through its dimeric oxidation product as well. The chapter also presents a voltammetric and a chronoamperometric method for the determination of the molecule using the modified electrode.

### IV. 3. 2. Introduction:

L-cysteine (CySH) is considered to be one of the most important amino acids. This amino acid has important role in biological functioning and has been used widely in the medicine and food industries. CySH (Fig. IV. 39) contains very important thiol (–SH) functional group and the formation and breaking of the disulphide bond plays important role in the biological system [510]. Activity of this functional group has important role in the biological activity of proteins and enzymes and this group is responsible for disulfide bridges in peptides and proteins. During electrochemical oxidation process CySH undergo proton coupled electron transfer and such oxidation process plays important roles in biological system to avoid any charge build up after oxidation. The proton coupled electron transfer or the concerted electron and proton transfer process has been investigated in some previous publications; the proton coupled electron transfer pathway is less energy path compared to the separate electron and proton transfer process [511-513]. Therefore from the basic aspect of the electron and proton transfer process and its electrochemical detection, the investigation of the electrochemical properties of CySH still has some important aspects to be reported. In addition to the basic electrochemical aspects it is important to have analytical method for the sensitive determination of CySH. It is difficult to determine CySH using spectrochemical technique as it does not contain any chromophoric functional group. Indirect spectrophotometric method is reported for its detection [514]. Electrochemical methods are important for its simplicity and field applicability; there are only a few literatures which reported the electrochemical method of determination of CySH based on modified electrode [515-522]. In this work a voltammetric and a potentiometric method were developed for the determination of this molecule.

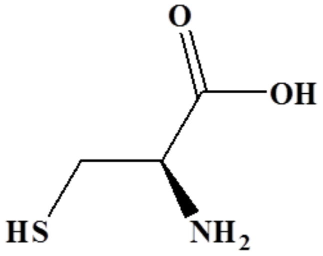

**Figure IV.39:** Chemical structure of L-Cysteine (CySH).

### IV. 3. 3. Fabrication of electrode and experimental conditions:

Glassy carbon electrode was polished using fine alumina powder (size 0.05mM) followed by sonication for 2 minutes at 20 KHz frequency. AuNPs were deposited on glassy carbon electrode by constant potential deposition at -0.8V potential (vs. Ag/AgCl/KCl (satd.) reference electrode) for 40 sec under stirring speed of 2500 rpm from 0.1mM Au(III) solution having 0.01M KCl as the supporting electrolyte (Fig. IV.52.a). Prior to each scan experimental solution was purged with high purity nitrogen gas to drive out dissolved oxygen from the aqueous solution. For the investigation of electrochemical properties of L-cysteine (CySH) pH of the phosphate buffer (PBS) was optimized at 7.5.

### IV. 3. 4. Results and Discussions:

#### IV. 3. 4. 1. Cyclic voltammetric measurements:

Cyclic voltammetry investigations were carried out using 0.1 mM of CySH using the AuNPs modified GCE. Experiments were carried out at different switching potentials and at varying pHs of the supporting electrolyte solution. A clear oxidation peak of CySH was observed at 0.69 V at pH 7.5, no reduction peak was observed during the reverse potential scan. With the shift in the switching potentials the characteristics of the oxidation peak of CySH remained the same, additional peak (at 0.85 V) due to the oxidation of gold and the corresponding reduction peak (at 0.51 V) in the reverse scan were observed (Fig. IV.40). Therefore to avoid the oxidative damage of the working electrode the suitable switching potential for this measurement was fixed at 0.78 V. The oxidation peak potential of CySH was shifted towards more negative direction with increase in pH of the solution (Fig. IV.41), this indicated an important role of the proton concentration in the supporting electrolyte solution during the oxidation process of CySH. Since the gold oxidation peak did not get shifted significantly with increase in pH, at pH 6 the oxidation of gold could not be avoided to observe the oxidation peak of CySH and the reduction peak due to the reduction of the oxidized gold electrode was also observed. The variation of the peak potential with pH of the solution was plotted in the inset of figure IV.41. A linear relationship between the peak potential and pH was observed, though the experiments were carried out within the narrow pH range to keep the CySH molecule at the similar prototropic conditions; at this pH range CySH would remain as the zwitterionic species with deprotonated carboxylic acid group and protonated amine group [523]. It was also difficult to get the oxidation peak of cysteine separated from the gold oxidation peak at lower pH of the supporting electrolyte.

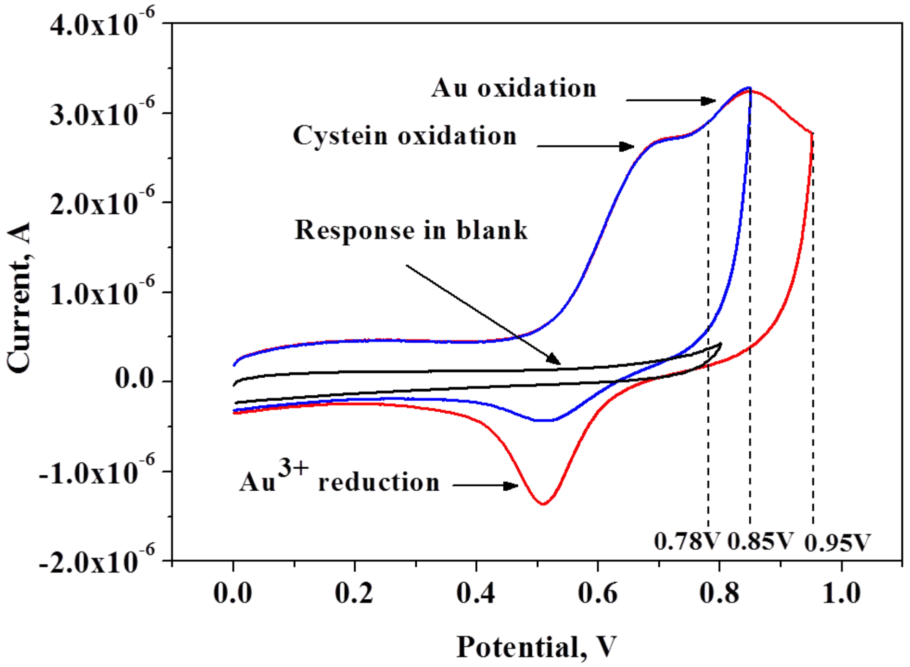

**Figure IV.40:** Effect of switching potential of CV on oxidation of CySH and gold coating.

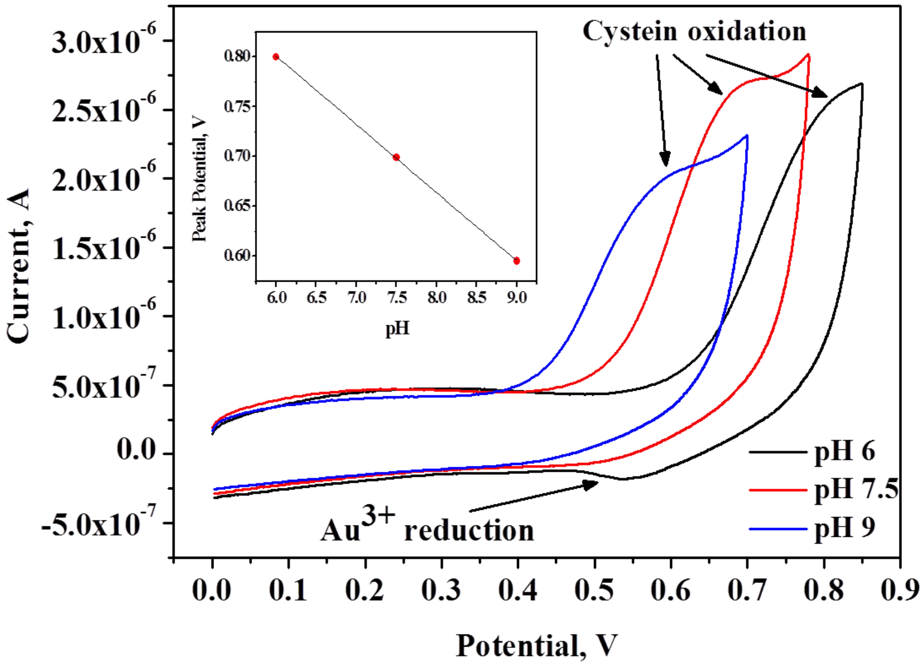

**Figure IV.41:** Cyclic voltammograms showing the effect of pH on CySH oxidation; Inset: Plot of oxidation peak potential against pH of the supporting electrolyte media.

The slope of the plot was around 68 mV/pH, which is somewhat higher than the slope corresponding to the involvement of equal number of protons and electrons in the electrochemical oxidation process. The mechanism of the electrochemical oxidation process is shown in figure IV.42. Where, CySH after one electron and one proton transfer undergo dimerization process. Thus the overall electrochemical process is characterized as the two electrons and two protons transfer process [524].

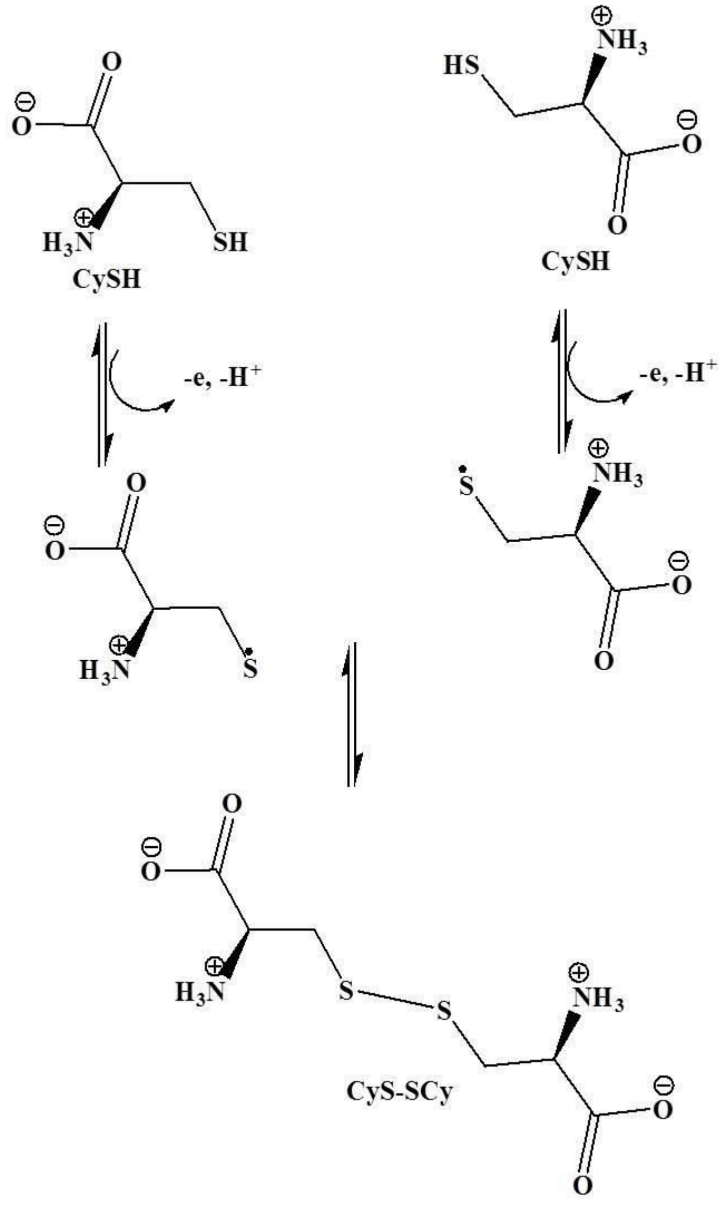

**Figure IV.42:** Schematic diagram of oxidation of L-Cysteine to Cystine (CyS-SCy).

Even higher slope (80 mV/pH) was reported previously even though the mechanism of the electrochemical oxidation process was 2 electrons and 2 protons transfer process for the formation of CyS-SCy dimeric species. Such ambiguous behavior was indicated to be due to the involvement of the oxidation of CyS-SCy dimeric species in the acidic solution where the peak potential was shifted to more positive potentials, thus sufficient for further oxidation of the dimeric species. Presently the slope is marginally higher compared to the expected slope due to the experimental pH in the narrow range of neutral to alkaline [525, 526].

Repeated cyclic voltammetry scans were recorded (Fig. IV.43); it was observed that the oxidation peak current of CySH decreased significantly on repeated scans and the peak was almost vanished at 4th scan. The drastic decrease in the oxidation peak current is due to the blockage of the electrode surface by the oxidation product.

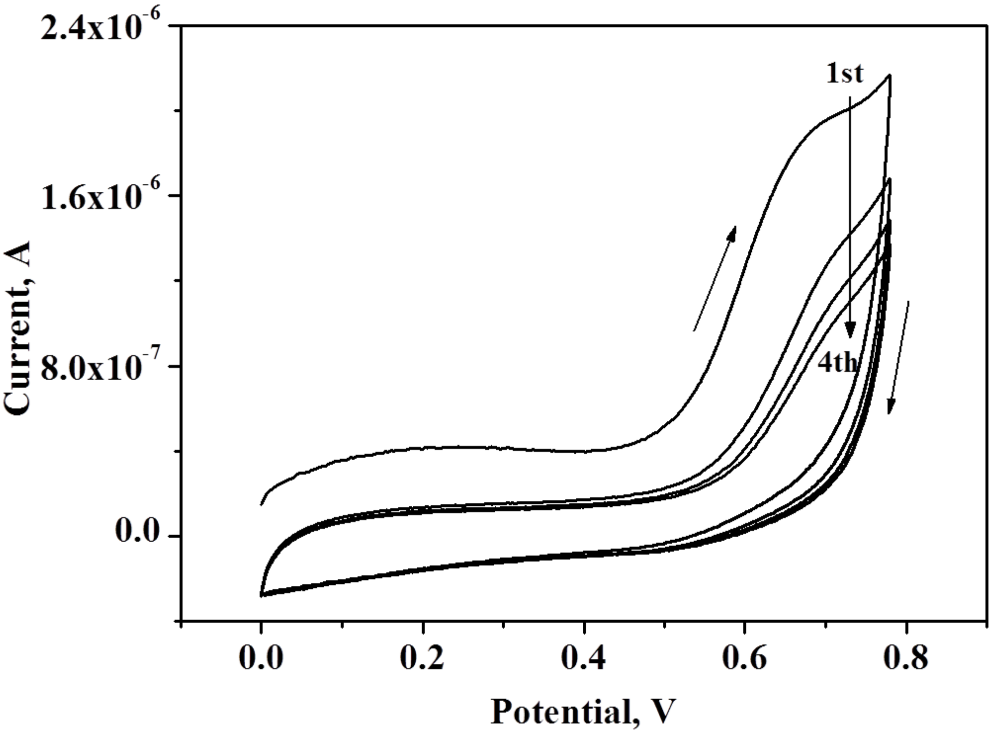

**Figure IV.43:** Cyclic voltammograms of CySH oxidation on repeated scans between 0V and 0.78V, Voltammetric response decreased substantially on successive scans.

The effect of the switching potential was further investigated by switching the potential from positive to the negative direction in the CV measurements. As seen from figure IV.44.a and IV.44.b a cathodic peak was observed at -0.57 V, when the potential was scanned towards negative direction after scanning it towards positive potential of up to 0.78 V. Effect of the switching potential was then investigated in detail and the results are shown in figure IV.44.b. As seen from the plots when the potentials were switched only in the positive potential window the oxidation peak of CySH decreased drastically (this observation is similar to what has been reported in figure IV.43), whereas upon scanning the potential first towards positive direction then scanning it up to -0.85 V, the oxidation peak was not decreased even on repeated CV scanning. CySH is known to form disulphide (cystine) on the oxidation process as shown in the oxidation mechanism in figure IV.42 and it is adsorbed over the gold electrode surface during the oxidation process. Upon cathodic potential scan the disulphide species might have undergone reductive desorption at around -0.57 V. Due to this process the electrode surface is available for further oxidation of the monomeric CySH species.

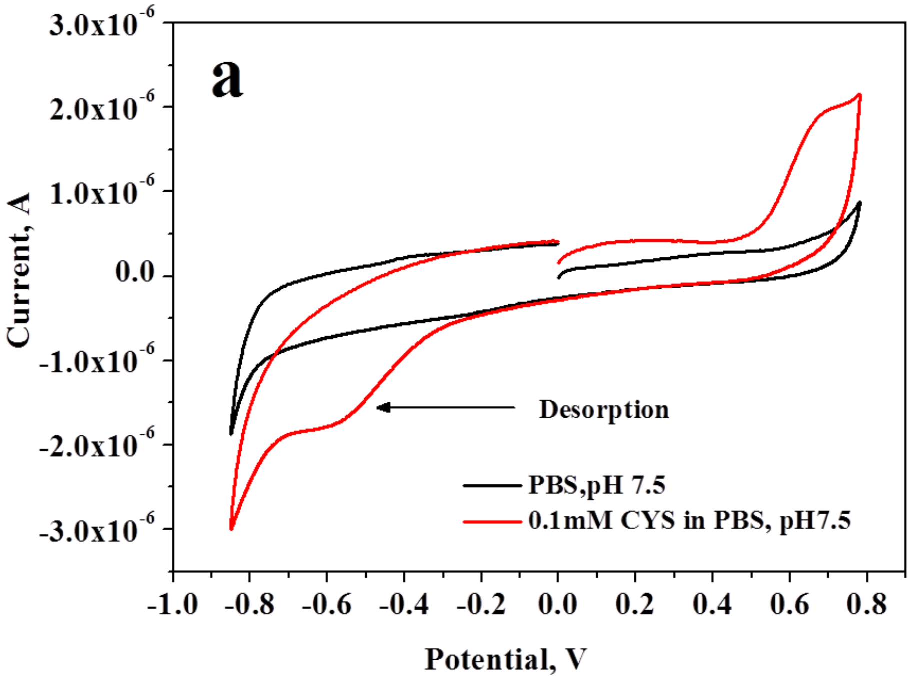

**Figure IV.44.a:** Cyclic voltammetry of CySH in phosphate buffer of pH 7.5 showing oxidation of CySH followed by desorption of oxidised species at negative potential.

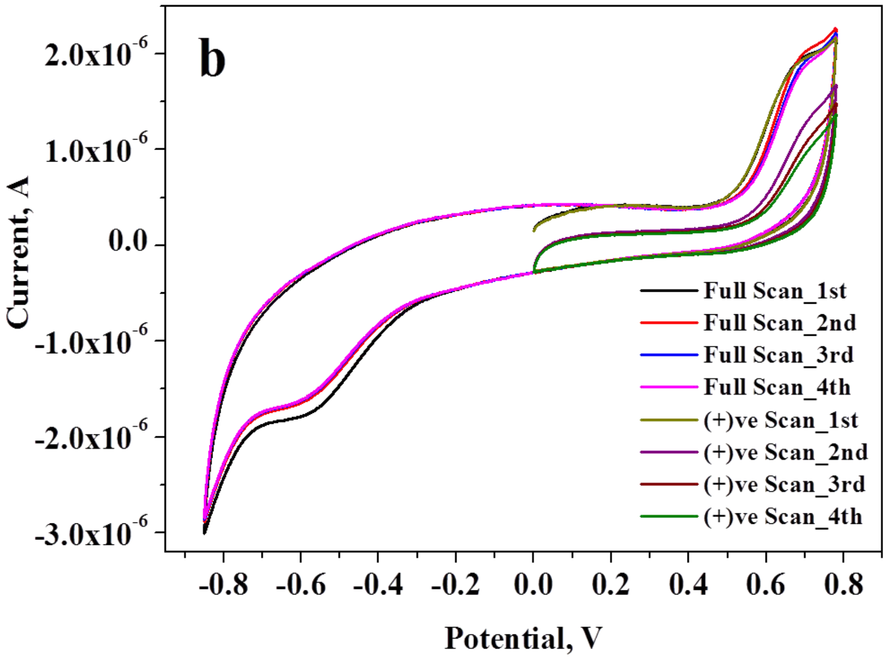

**Figure IV.44.b:** Effect of adsorption of the oxidised species upon oxidation of CySH when repeated scans were performed between 0V to 0.78V; voltammetric response due to oxidation decreased substantially due to adsorption of oxidised species of CySH; oxidation followed by desorption at negative potential (full scan) retains voltammetric response on successive scans.

Cyclic voltammetry scans were also recorded at different scan rates and for each scan freshly prepared electrodes were used, the results are shown in figure IV.45. It was observed that with the increase in the scan rates of the measurements the peak current values were increased and the peak potential was shifted towards more positive directions. The variation of the peak current was fitted linearly well with the scan rate of the measurements, indicating the deviation from the purely diffusion control nature of the electrochemical process, (inset of figure IV. 45). Adsorption process might have played some important role on the electrochemical process, which has made the deviation. The shifting of the peak potential was plotted with respect to the **logυ** where **υ** is the scan rate and the plot is shown in figure IV.46. The plot was fitted with the linear equation, $\mathbf{E_p = B + RT/(1-\alpha)nF \log\upsilon}$; where B is a constant and related to the redox potential ($E^0$) of the system. From the slope of the linear plot the (1-α) value was calculated as 0.45. The α and (1-α) parameters determine the influence of the applied potential towards the activation energy of the reduction and the oxidation process respectively. Since (1-α) was calculated as 0.45 and the value α as 0.55, it indicates that activation steps of both the cathodic and anodic processes are equally influenced by the applied potential.

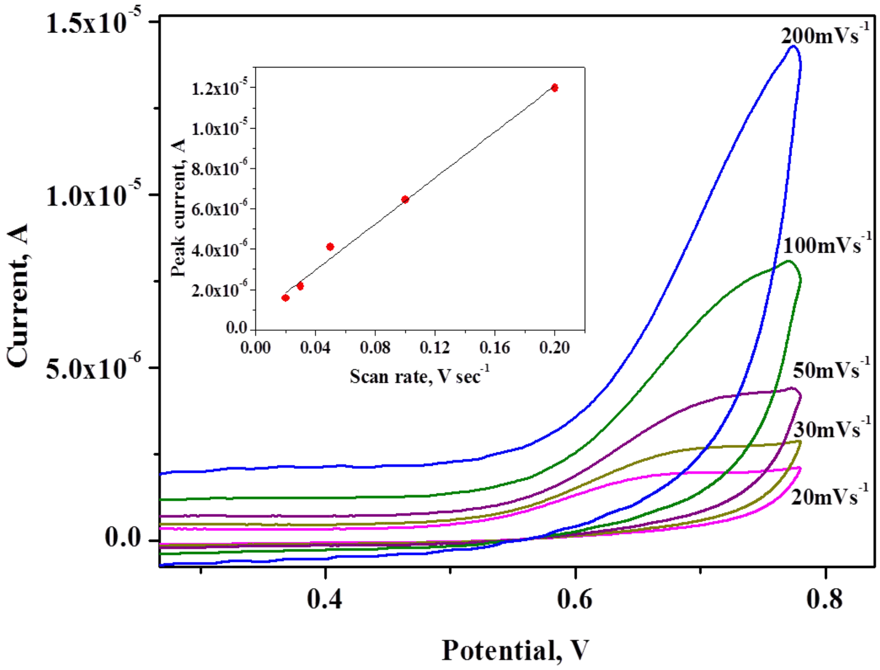

**Figure IV.45:** Effect of scan rate variation on voltammetric signal of CySH oxidation; Inset: Linear calibration plot of peak current against scan rate.

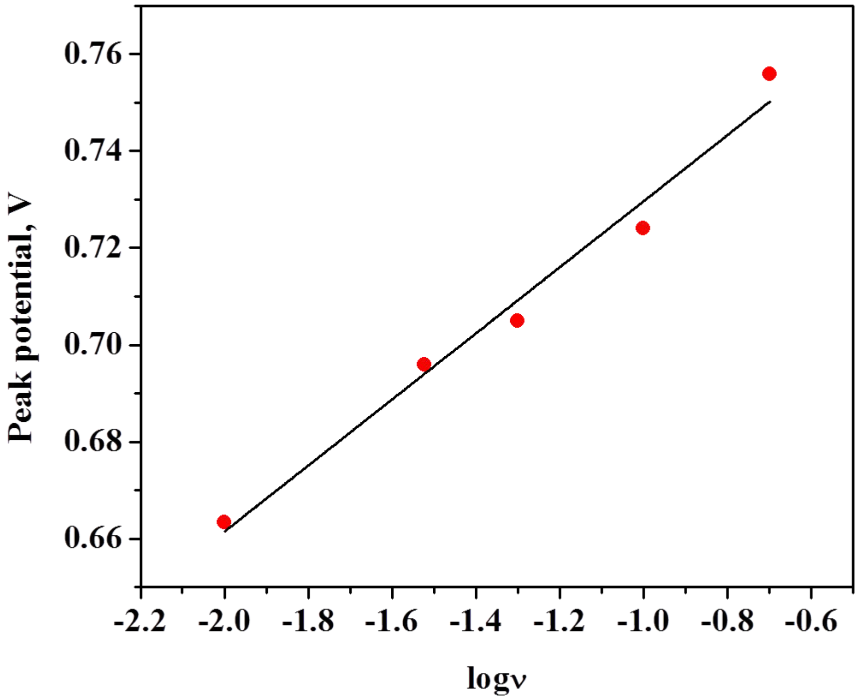

**Figure IV.46:** Variation of peak potential of CySH oxidation with log of scan rate.

### IV. 3. 4. 2. Electrochemical impedance measurement:

Electrochemical impedance measurements were carried out using the similar three electrode geometry configuration as that for the voltammetric measurements in the frequency range from 10 kHz to 0.01 Hz with the modulation amplitude of 10 mV at different applied potentials. As seen from figure IV.47 at the applied potential of 0 V the Nyquist plot has shown very high charge transfer resistance indicating non performance of any charge transfer process. At an applied potential of 0.3 V charge transfer at lower resistance and an adsorption component was observed. The corresponding equivalent circuit is shown in the inset of the figure IV.47. Deviation from simple RC circuit at an applied potential of 0.3 V indicated that CySH has started adsorbing over the electrode surface at this applied potential. At sufficiently anodic potential (0.7V) the adsorption component was more prominent, indicating the oxidative adsorption of the cystine film over the electrode surface.

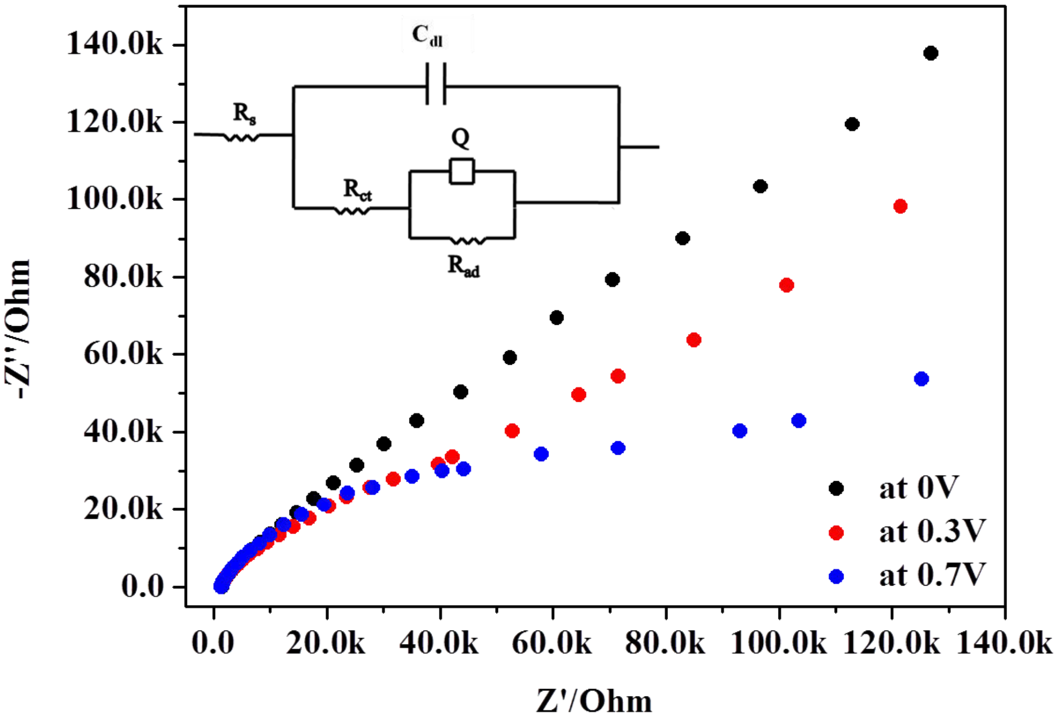

**Figure IV.47:** Nyquist plots of the electrochemical system when data were recorded by keeping the fresh AuNPs modified GCE, in the solution containing 10µM of CySH in phosphate buffer of pH 7.5, at 0V, 0.3V and 0.7V.

In order to investigate the desorption process impedance measurements were carried out at cathodic applied potentials of -0. 6V. When the electrode was pre-treated by the application of an applied potential of 0.7 V for 200 sec, where it is expected to be coated with cystine film, the Nyquist plot (Fig. IV.48) has shown to have strong contribution from the desorption component. There impedance measurements have supported the cyclic voltammetry plot of the observation of oxidative adsorption and the reductive desorption of CySH during the oxidation and reduction processes.

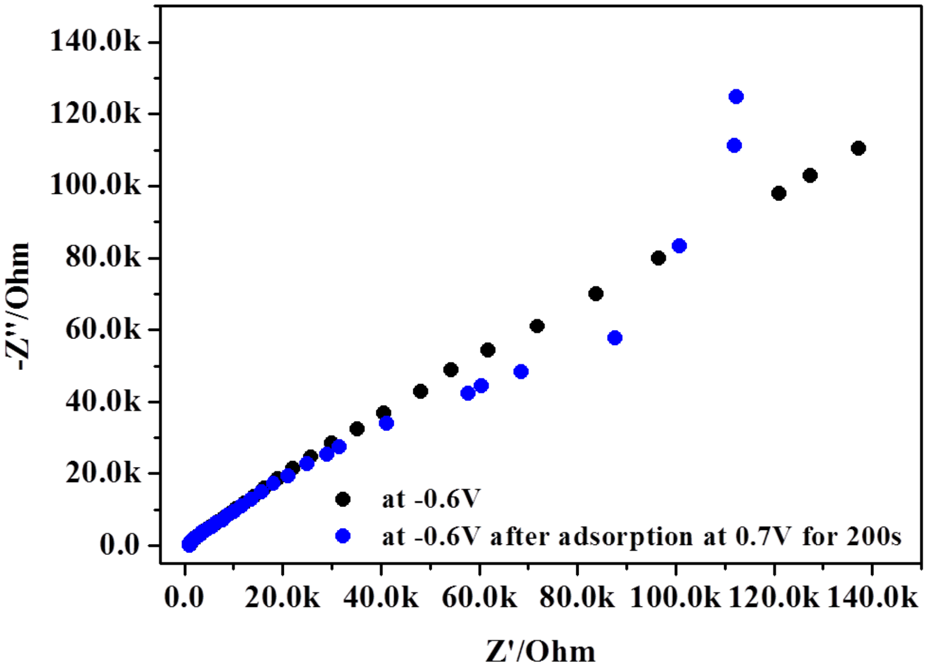

**Figure IV.48:** Nyquist plots of the electrochemical system when data were recorded by keeping the fresh AuNPs modified GCE electrode, in the solution containing 10µM of CYSH in PBS of pH 7.5, at -0.6V, and -0.6V after adsorption at 0.7V for 200 sec.

### IV. 3. 4. 3. SECM measurements:

SECM investigations were carried out using the tip and the substrate electrode of gold with diameter 10 µm and 3 mm respectively. Freshly prepared potassium ferrocyanide was used as the redox mediator to record the approach plot. Probe approach curves (PAC) were recorded by keeping the tip at 0.4 V and the substrate at -0.2 V subjected to the conditioning of the substrate by CySH at different CV cycles in the potential range from 0 to 0.78 V. In all the cases positive feedback response was observed (Fig. IV.49). Marginal improvement for the approach current was observed for the substrate used after multiple CV cycles, which were having adsorbed dimeric CyS-SCy species over the electrode surface. Therefore the adsorbed cystine improved the charge transport through its adsorbed membrane for ferrocyanide. For all the cases the approach distance was kept at 1.8 µm away from the surface of the substrate electrode.

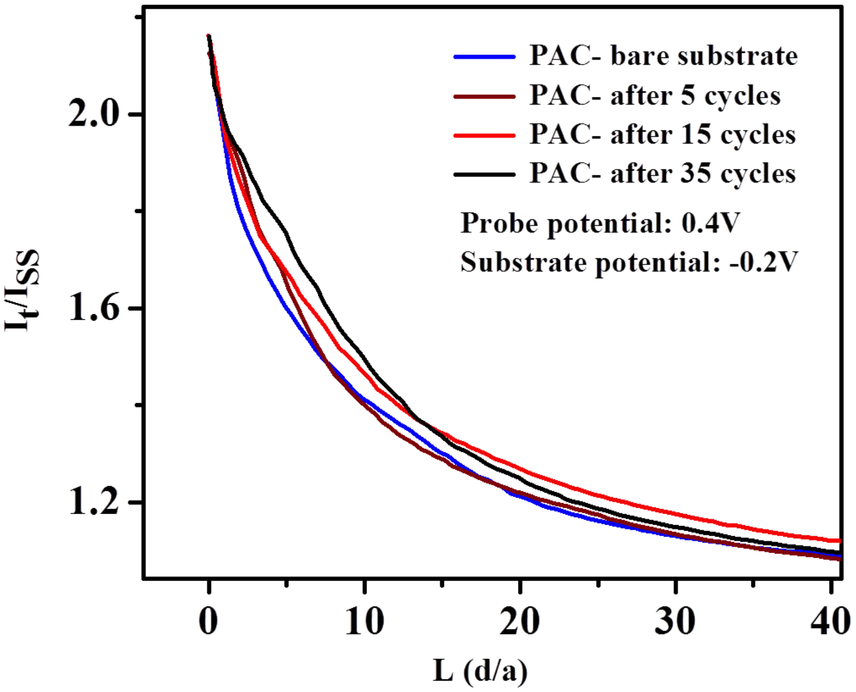

**Figure IV.49:** Probe approach plot by keeping the probe at 0.4 V and substrate at -0.2 V in 1 mM $K_4[Fe(CN)_6]$ solution.

In order to further quantify the effect of the CV cycling on the substrate for oxidation of CySH on the feedback responses, CV scans at the tip electrode for the redox probe were carried out at the approach distance and as seen from figure IV.50, the steady state current response for the redox probe ($[Fe(CN)_6]^{2+}/[Fe(CN)_6]^{3+}$ couple) from the tip was increased with increase in the CV cycling on the substrate. More CV cycling from 0V to 0.78V on the subatrate leads to more oxidation of the CySH to cystine (CyS-SCy) and thus higher is the adsorption on the electrode surface. Higher steady state tip current from the CV measurements at the approach distance indicates the enhanced transport of charge through the CyS-SCy film deposited over the electrode surface.

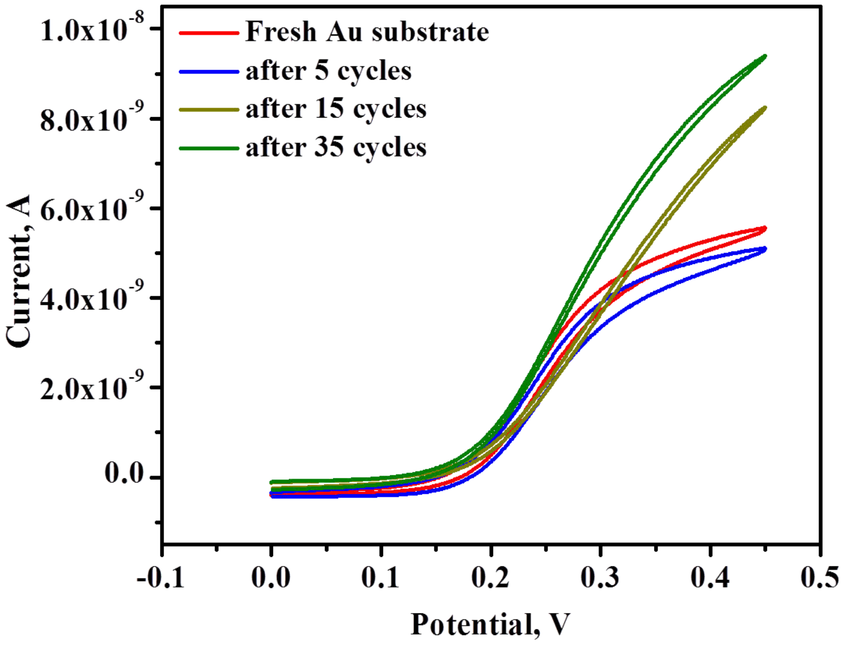

**Figure IV.50:** CV plots of the Au tip probe electrode at the approach distance after treatment of the substrate electrode by different CV cycles in CySH solution.

CV measurements were further carried out at the probe electrode at the approach distance, but, at different substrate conditions. The results are shown in figure IV.51.a and IV.51.b. In 1st case the substrate was pre-treated with cystine film formed by 15 CV cycles in the potential range of 0V to 0.78V in 0.1 mM CySH concentration and the probe was approached to this substrate. After approach the CV at the probe electrode was recorded in the potential range from -0.8V to 0V by keeping the substrate at -0.8V. During the anodic scan an oxidation peak (at -0.54V) was observed which is indicative of the oxidation of reduced product desorbed out of the substrate electrode. A reduction peak was also observed at -0.68V during the cathodic CV scan. Here the SECM measurements evident that at the positive electrochemical scanning of the substrate in CySH containing solution cystine are deposited over the substrate and with the application of negative potential it has undergone reductive desorption process which was detected by the probe electrode present at the approach distance (2 μm away from the substrate). When the similar experiments were carried out using the untreated substrate electrode no response at the tip was observed as shown in figure IV.51.b.

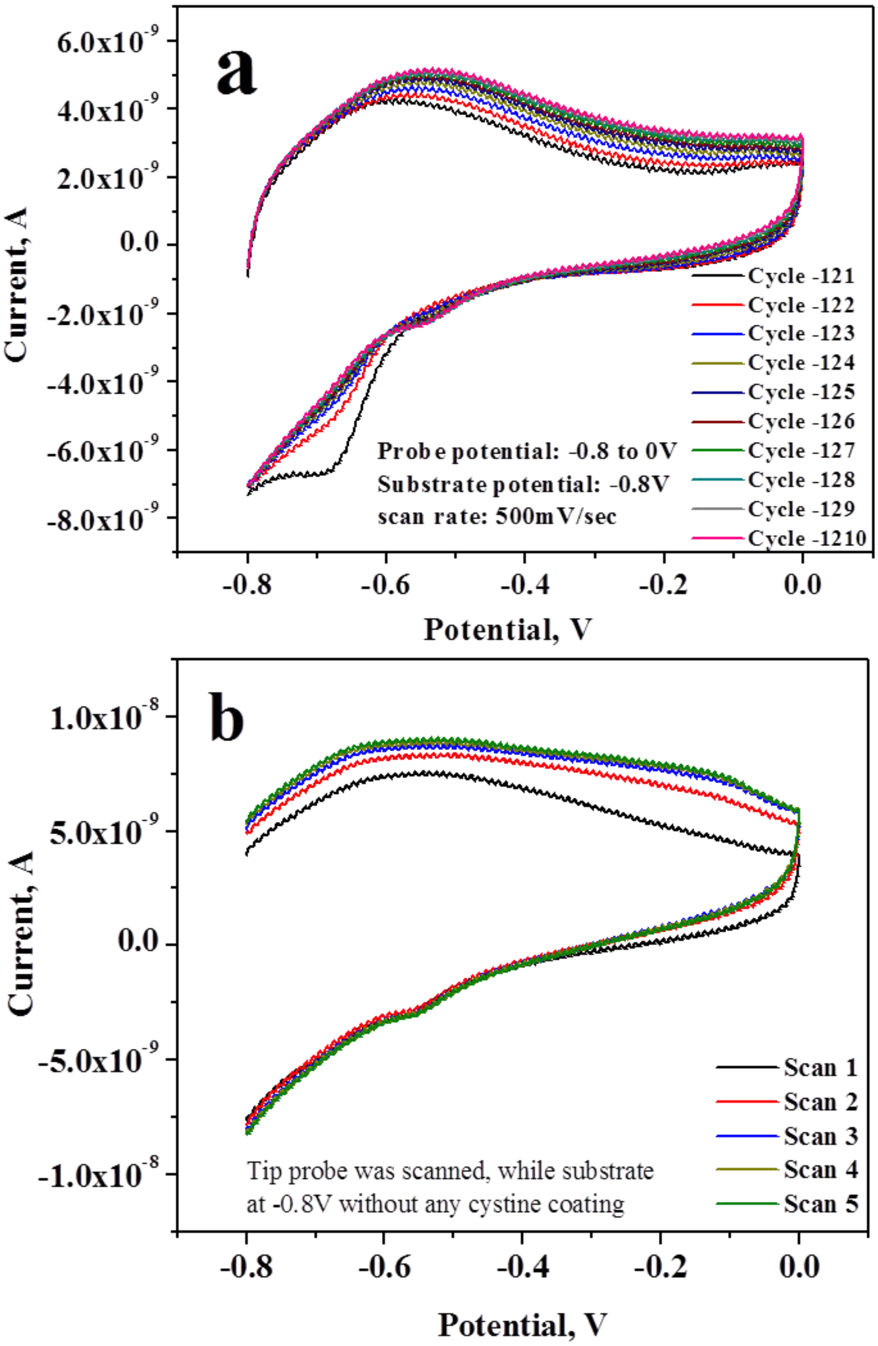

**Figure IV.51:** CV scans of the Au tip probe electrode at approach distance when a negative potential (-0.8V) was applied to the substrate (a) after coated with cystine film and (b) without having any coating of cystine film.

AFM measurements of the AuNPs modified GC substrate was recorded by fabricating the electrode holder to hold the modified GC electrode under the AFM scan head, corresponding images are shown in figure IV.52.a & IV.52.b. The AuNPs were observed to be deposited over the GC substrate. The electrode was further characterized after it was treated in CySH containing solution with the application of cyclic voltammetry scan in the potential region of 0 to 0.7 V for 50 cycles at the scan rate of 50 mVsec$^{-1}$. All the AuNPs were observed to be covered well with the thin films of cystine. In was further observed that all the films deposited on the substrate were of similar shape and sizes though there was some difference in the sizes of the deposited AuNPs. Cystine adsorbed only at the AuNP faces and the remaining part of the electrode surface remained uncovered and at 50 CV cycles all the AuNP faces were well covered by the cystine films. The mean diameter of the gold nanoparticles were increased from 38 nm to around 100 nm upon treatment of the AuNPs modified GC electrode with CySH.

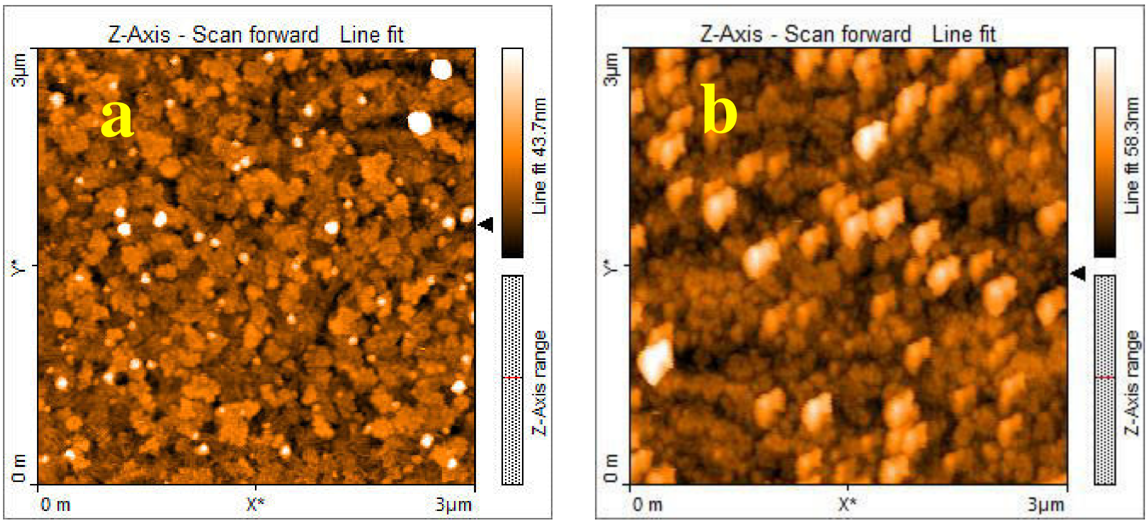

**Figure IV.52:** AFM image of (a) freshly deposited AuNPs on bare GCE (b) Cystine coated AuNPs upon 50 Cyclic Voltammetry from 0V to 0.7V in CySH solution.

### IV. 3. 4. 4. Analytical determination of CySH:

After obtaining the electrochemical behaviour of cysteine an analytical method was developed for the determination of CySH and the electrode fouling effect has been avoided by suitably choosing the desorption potential for making the successive voltammetric scans without fouling the electrode.

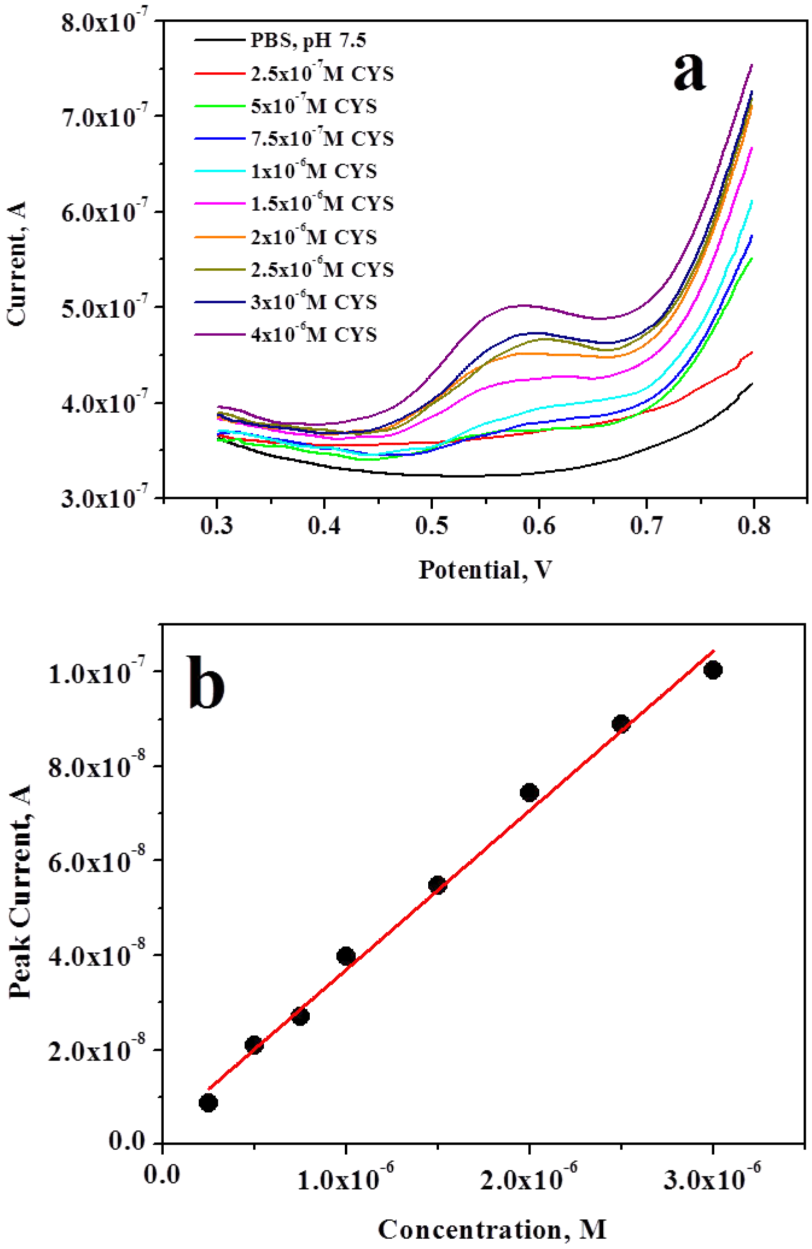

**Figure IV.53:** (a) Differential pulse anodic stripping voltammograms of different concentrations of the CySH in PBS of pH 7.5, using AuNPs modified GCE; (b) corresponding linear calibration plot of peak current and against concentration.

Differential pulse voltammetric scans were recorded in the potential region of 0.3 to 0.8 V with conditioning potential at -0.8 V for 300 s at stirring condition for the desorption of the cystine species. With the variation of the CySH concentration the voltammetric peak was increased, corresponding plots are shown in figure IV.53.a and IV.53.b. The calibration was linear and the regression equation followed $i_p = 0.0337C + 3.37\times10^{-9}$, where C in M, the standard deviation was obtained as $1.95\times10^{-9}$. The LOD was obtained as 74 nM.

Chronoamperometric measurements were also carried out at an applied potential of 0.6 V under stirring conditions and the results are shown in figure IV.54. Constant steps were observed up to 5th addition when 1 μM of CySH was added in each step in the test solution. No interference due to the tryptophan and tyrosine was observed since the chronoamperometric current response was not changed with the addition of these two chemicals.

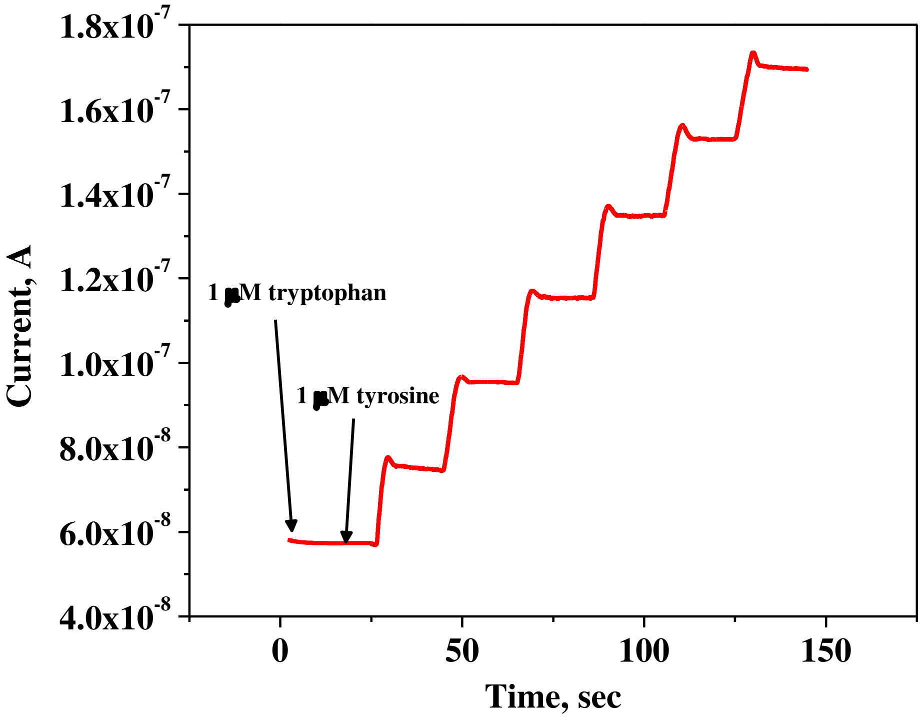

**Figure IV.54:** Chronoamperometry of CySH under stirring condition using the modified electrode.

## IV. 3. 5. Conclusion:

AuNPs modified GCE was found to be suitable for the investigation of the electrochemical property of CySH, since the electrochemical response was significantly enhanced over this modified electrode. Significant role of oxidation of monomer (CySH) and reduction of dimer (Cys-SCy) on the adsorption and desorption behaviour on the surface of the electrode were experimentally proved using EIS, AFM and SECM. SECM measurement reflected that the cystine film formed over the electrode surface has capability to improve the transport of charge from ferrocyanide compared to the gold nanoparticles modified electrode surface. Based on the electrochemical investigations an analytical method was developed for the determination CySH with the application of proper cleaning potential.

## Electrochemical investigation of 2-(o-hydroxyphenyl)benzoxazole (BNZ):

### Introduction:

Benzoxazoles are widely used as effective light protectors as well as materials in continuous lasers [527, 528]. Its different derivatives have numerous therapeutic applications where some of them act as potent anti-inflammatory, antifungal and antibacterial agents [529-533]. Other applications are in electroluminescent devices and UV-stabilization of polymers. Transition metal complexes of benzoxazoles are interestingly used as the materials for light emitting as well as for the electron transport in organic light emitting diodes (OLEDs) [534-536]. Electrochemical property and the diffusivity of the benzoxazoles are very important when it is used as the antifungal agent or as the organic dye material in OLEDs and supercapacitor applications. In the present investigation electrochemical property of 2-(o-hydroxyphenyl)benzoxazole (BNZ) (Fig. IV.55) was investigated using cyclic and voltammetric techniques. Rotating disc electrode voltammetry was carried to study the diffusivity and the charge transfer property of the compound.

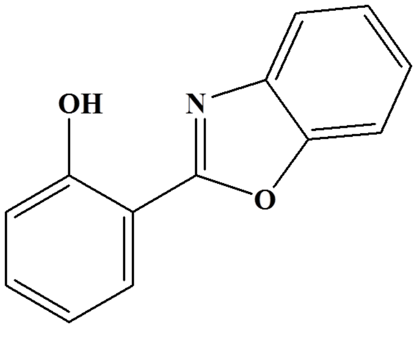

**Figure IV.55:** Chemical structure of 2-(o-hydroxyphenyl)benzoxazole

### Important findings from electrochemical investigation:

Electrochemical investigation of BNZ was carried out in 0.5 M NaOH solution owing to its application as charge storage materials when composites are formed along with other substances. Electrochemical property of BNZ over conventional electrode is poor therefore modified electrodes were searched to find electrodes with significant response from the oxidation of BNZ. Synthesis and characterisation of graphene oxide is reported in previous chapters (section II. 5. 3 and IV. 1. B. 3), it was used for the modification of glassy carbon electrode. The results are show in figure IV.56.a. Clear oxidation peak from 10µM BNZ (at a scan rate of 100 mV sec$^{-1}$) was observed at around 0.67 V (vs. Ag/AgCl/KCl (satd)), corresponding reduction peak was observed at 0.18 V, the oxidation behaviour was characterized as the quasi-reversible in nature. The inability of GC electrode to generate the electrochemical signal of BNZ is also seen from figure IV.56.a. Electrochemical scans were carried out at different scan rates and the results are shown in figure IV.56.b. The oxidation peak current was increased with increase in the scan rate of the measurements, the peak current vs. square root of scan rate has shown linear relation (plot not shown), indicating the diffusion control nature of the electrochemical oxidation process. From the rotating disc electrode measurements the diffusion coefficient of BNZ was obtained as $1.6 \times 10^{-6}$ cm$^2$/sec.

A composite with the functionalized graphitic carbon nano spheres (FCNSs, as discussed in the chapter IV.2) has been fabricated and the composite material was used for the surface modification of the glassy carbon electrode. Cyclic voltammetry scans were recorded at a scan rate of 20 mV sec$^{-1}$ in 0.5 M NaOH solution using this modified electrode at multiple cycles and the results are shown in figure IV.57. It was observed that the oxidation peak current of BNZ was increased with multiple cycles.

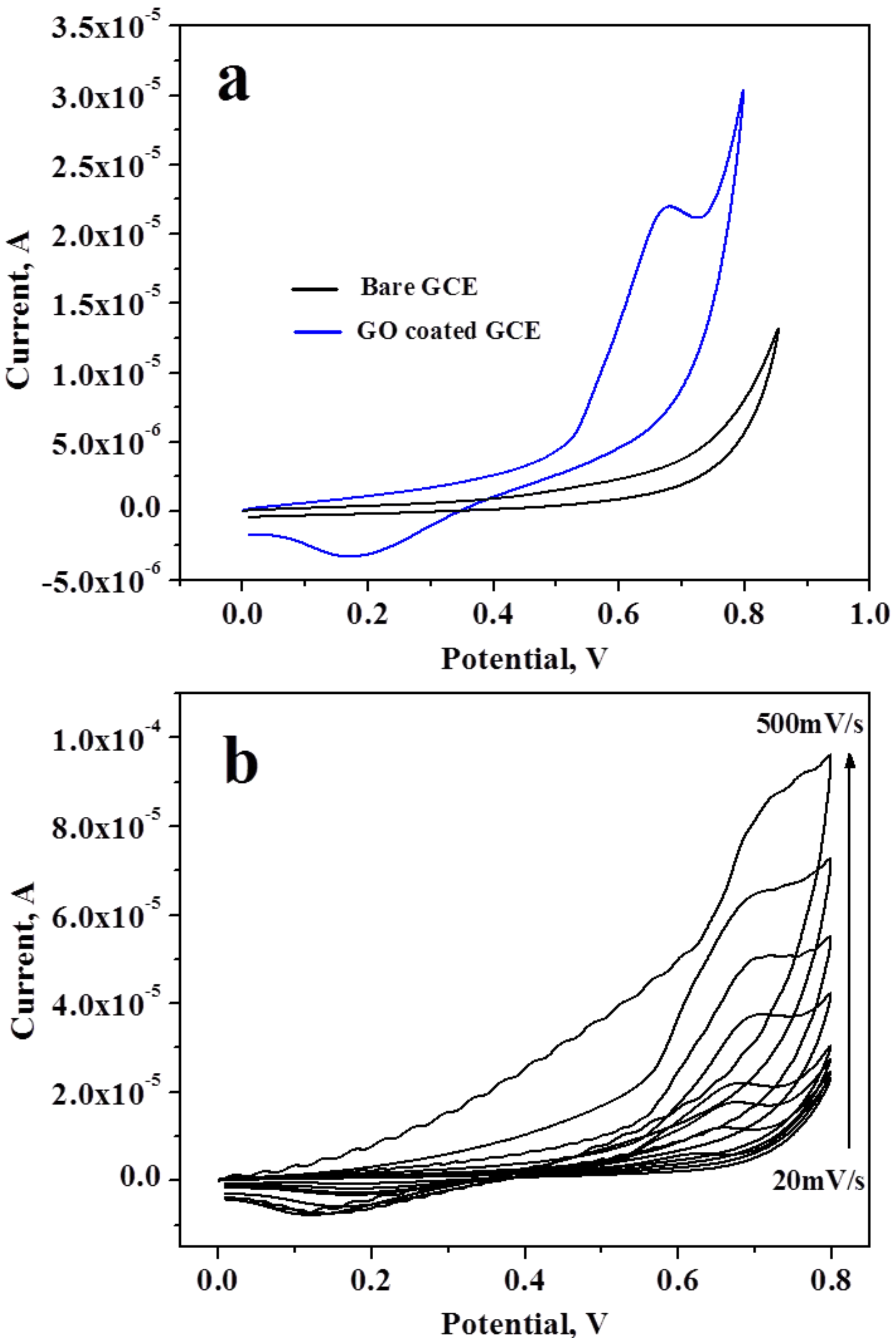

**Figure IV. 56:** (a) Electrochemical responses for the redox behaviour of BNZ on bare GCE and GO coated GCE; concentration of the compound: 10μM; medium: 0.5M NaOH and scan rate: 100mV sec$^{-1}$ ; (b) Cyclic voltammograms for the redox behaviour of BNZ in 0.5M NaOH medium, recorded at different scan rates (20 mV sec$^{-1}$, 50 mV sec$^{-1}$, 80 mv sec$^{-1}$, 100 mV sec$^{-1}$, 200 mV sec$^{-1}$, 300 mV sec$^{-1}$, 400 mV sec$^{-1}$ and 500 mV sec$^{-1}$).

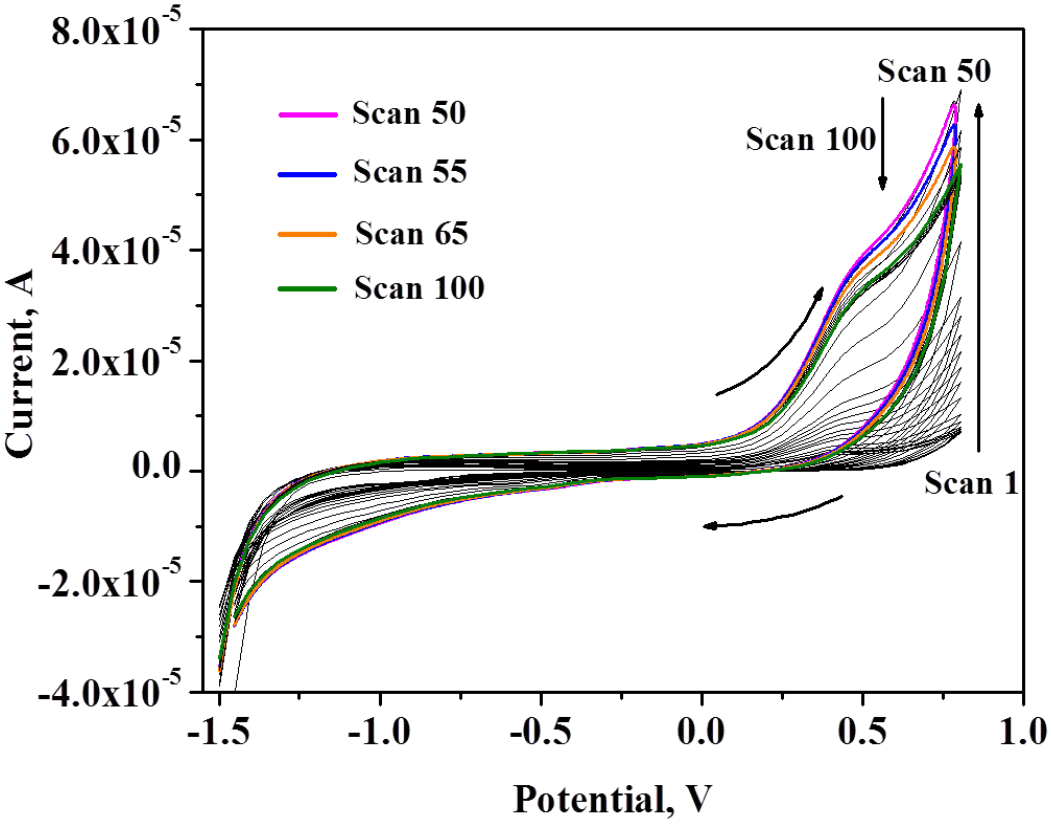

**Figure IV. 57:** Multiple scans dipping the composite electrode of FCNSs and 2-(-o-hydroxyphenyl)benzoxazole in 0.5M NaOH at a scan rate of 20mV sec$^{-1}$.

The increase in the electrochemical response is indicative of the surface activation of the composite materials. This observation also indicates the absence of any unwanted degradation of the BNZ carbon composite materials under electrochemical scanning. Present information form cyclic voltammetry scan of BNZ therefore indicates that the molecule has favourable interaction with carbonaceous materials like graphene oxide and the carbon nano sphere as investigated. Thus, the composites of BNZ with carbon could be potentially applied for the charge storage devices, such investigations on the energy storage devices are not under the scope of the present thesis, therefore the results related to such investigations are not being reported in the present thesis.

# Chapter V

## *Summary and Further Scope*

**Further scope of the thesis in line with the completed work:**

The development of chemical sensors has gathered great scientific interest in the last decades, application of chemical sensor has been extended to chemical industry, food industry, bio-industry, medicine and environmental control because of their capability to give continuously selective and fast response to the presence of a specific compound in a complex mixture of components, without perturbing the system. Chemical sensors consist of a transduction element covered with a biological or chemical recognition layer. The excellent specificity of biological recognition processes has led to the development of highly selective devices. Electrochemical sensors are the most rapidly growing class of chemical and biochemical sensors due to their capability in complex applications. Electrochemical sensors are sensitive and selective towards electroactive species; they are fast and accurate, compact, and portable. Due to its simplicity, electrochemical transduction constitutes a successful route to create low cost biosensors when coupled with biomolecules. Due to selectivity, biosensors are most powerful devices which combine the power of analytical detection techniques with the specificity of biological recognition system. Furthermore, biosensors possess many unique features such as compact size, simplicity of use, one-step reagent less analysis. Some of the reviews have reported about the recent development in the field [537-542].

Present thesis is focused on the development of the suitable substrates for the determination of metal ions and biologically important organic molecules. It has been a worldwide issue to use mercury based working electrode for the determination of heavy metal ions using stripping voltammetry. Due to the suitable conductivity soft metals, antimony and bismuth are preferred choice. Present thesis has discussed on this issue by generating analytical data on the fabrication of the modified electrode based on Sb and Bi and analytical method was developed for the determination of heavy metal ions in environmental samples.

It is a challenging task to generate the measurable electrochemical signals over conventional electrodes from the biologically active molecules investigated in the present thesis, melamine, dopamine, uric acid and cysteine. Different modification strategies were adopted for the modification of the working electrode to generate highly sensitive electrochemical signal from the organic molecules under investigations. The basic strategies are either to enhance the surface area of the substrate or to improve the charge transport of the molecules through the modified substrate. Presently both the strategies were investigated for the improvement of the analytical signals. The analytical methodologies developed under the present thesis were successfully applied in real samples. However the methodologies are based on offline instrumentation and the modified substrate developed; electrochemical sensors will be developed as the future plan of the present thesis for determining the concentration of the analyte directly from the electrochemical signal. Electrochemical signalling using ultramicro or nano electrode is very important as it can be used at very fast potential scan due to the negligible IR drop and for the generation of the steady state response on linear potential scan. In vivo analytical determination is also being targeted worldwide using the nano electrode modified with the suitable modifier for the determination of biologically active molecules. Work has been initiated already for the determination of dopamine using the modified carbon paste ultramicroelectrode inside the rat brain. A successful implication of the work will have an excellent step forward in the direction of the application of electrochemical techniques for in-vivo biochemical analysis. Electrochemical techniques based on ultramicroelectrode will be extended towards the formation of tip substrate nano gap to trap molecules at single molecular levels to detect the molecules at concentration femto-molar or less, which has application in the detection of explosives and macromolecules.

# REFERENCES:

[1]. Skoog, D. A.; West, D. M.; Holler, F. J.; Crouch, S. R. *Fundamentals of Analytical Chemistry*, 8th ed., Thomson Asia Pvt. Ltd., **2005.**

[2]. Kealey, D.; Haines, P. J. *Instant Notes: Analytical Chemistry*, 1st ed., BIOS Scientific Publishers Ltd., **2002.**

[3]. Skoog, D. A.; Holler, F. J.; Crouch, S. R. *Instrumental Analysis*, 6th ed., Cengage learning India Pvt. Ltd., **2010.**

[4]. Arikawa, Y. *Anal. Sci.*, **2001**, *17*, i571.

[5]. Murray, R. W. *Annu. Rev. Anal. Chem.*, **2010**, *3*, 1.

[6]. Bond, A. M.; Grabaric, B. S. *Anal. Chem.*, **1976**, *48*, 1624.

[7]. Bond, A. M. *Anal. Chim. Acta*, **1999**, *400*, 333.

[8]. Adams, R. N. *J. Pharm. Sci.*, **1969,** *58*, 1171.

[9]. Shrivastava, A.; Sharma, J.; Soni, V. *Bulletin of Faculty of Pharmacy, Cairo University*, **2013,** *51*, 113.

[10]. Bard, A. J.; Faulkner, L. R. *Electrochemical Methods Fundamentals and applications*, 2nd ed, John Wiley & Sons, Inc., Publication, **2004**.

[11]. Wang, J. *Analytical Electrochemistry*, 3rd ed, John Wiley & Sons, Inc., Publication, **2006**.

[12]. Brett, C. M. A.; Brett, A. M. O. *Electroanalysis*, Oxford University Press, Oxford, **1998**.

[13]. Kellner, R.; Mermet, J. M.; Otto, M.; Valcarcel, M.; Widmer, H. M. *Analytical Chemistry, A Modern Approach to Analytical Science*, 2nd ed, John Wiley & Sons, Inc., Publication, **2004**.

[14]. Mendham, J; Denney, R. C.; Barnes, J. D.; Thomas, M. *Vogel's Text Book of Quantitative Chemical Analysis*, 6th ed, Pearson Education Ltd., **2002**.

[15]. Barek, J.; Zima, J. *Electroanalysis,* **2003**, *15(5-6)*, 467.

[16]. Heyrovsky, J.; Kuta, J. *Principles of Polarography*, Academic Press, New York, **1966**.

[17]. Kalvoda, R. *Techniques of Oscillographic Polarography*, 2nd ed., Elsevier, Amsterdam **1965**.

[18]. Kalousek, M. *Collect. Czech. Chem. Commun.,* **1948**, *13*, 105.

[19]. Breyer, B.; Bauer, H. H. *Alternating Current Polarography and Tensammetry*, Interscience, New York, **1963**.

[20]. Wahlin, E.; Bresle, A. *Acta Chem. Scand.*, **1956**, *10*, 935.

[21]. Barker, G. C.; Gardner, A. W. *Z. Anal. Chem.*, **1960**, *173*, 79.

[22]. Parry, E. P.; Osteryoung, R. A. *Anal. Chem.*, **1965**, *37*, 1634.

[23]. Flato, J. B. Anal. Chem., **1972**, *44*, 75A.

[24]. Heineman, W. R.; Kissinger, P. T. *Laboratory techniques in Electroanalytical chemistry*, 2nd ed., Marcel Dekker, **1996**.

[25]. Noel, M., Vasu, K. I. *Cyclic voltammetry and the frontiers of electrochemistry*, 1st ed., Oxford and IBH publishing Co. Pvt. Ltd., **1990**.

[26]. Randles, J. E. B. *Trans. Faraday Soc.*, **1948**, *44*, 327.

[27]. Sevcik, A. Coll. Czech. Chem. Commun., **1948**, *13*, 349.

[28]. Mabbott, G. A. *J. Chem. Educ.*, **1983**, *60*, 697.

[29]. Kissinger, P. T.; Heineman, W. R. *J. Chem. Educ.*, **1983**, *60*, 702.

[30]. Barker, G. C.; Jenkins, I. L. *Analyst*, **1952**, *77*, 685.

[31]. Compton, R. G.; Banks, C. E., *Understanding voltammetry*, 2nd ed., World scientific publication Co. Pvt. Ltd., **2011.**

[32]. Ramaley, L.; Krause, Jr., M. S. *Anal. Chem.*, **1969**, *41*, 1362.

[33]. Osteryoung, J. *Accts. Chem. Res.*, **1993**, *26*, 77.

[34]. Osteryoung, R. A.; Osteryoung, J. *Phil. Trans. Roy. Soc. London, Ser. A*, **1981**, *302*, 315.

[35]. Osteryoung, J; O'Dea, J. J. *Electroanal. Chem.*, **1986**, *14*, 209.

[36]. Matsuda, H.; Ayabe, Y. *Z. Elektrochem.,* **1955**, *59*, 494.

[37]. Stetter, J. R.; Penrose, W. R.; Yao S. *J. Electrochem. Soc.,* **2003**, *150*, S11.

[38]. Stradiotto, N. R.; Yamanaka, H.; Zanoni, M. V. B. *J. Braz. Chem. Soc.,* **2003**, *14*, 159.

[39]. Bakker, E.; Diaz, M. T. *Anal.Chem.,* **2002**, *74*, 2781.

[40]. Privett, B. J.; Shin, J. H.; Schoenfisch, M. H. *Anal. Chem.,* **2010**, *82*, 4723.

[41]. Edwards, P. P.; Porch, A.; Jones, M. O.; Morgan, D. V.; Perks, R. M. *Dalton Trans.* **2004**, 2995.

[42]. Perednis, D.; Gauckler, L. J.; *J. Electroceram*. **2005**, *14*, 103.

[43]. Skotheim, T. A.; Elsenbaumer, R. L.; Reynolds, J. R. *Handbook of conducting polymers*, 2nd ed., Marcel Decker, Inc., **1998**.

[44]. Moretto, L. M.; Kalcher, K. *Environmental analysis by electrochemical sensors and biosensors fundamentals*, Vol. 1, Spinger, **2014**.

[45]. Rice, M. E.; Galus, Z.; Adams, R. N. *J. Electroanal. Chem.*, **1983**, *143*, 89.

[46]. Wang, J.; Deshmukh, B. K.; Bonakdar, M. *J. Electroanal. Chem.*, **1985**, *194*, 339.

[47]. Kissinger, P. T.; Heineman, W. R. *Laboratory techniques in electroanalytical chemistry*, 2nd ed, Marcel Dekker, Newyork, **1996**.

[48]. Apetrei, C.; Apetrei, I. M.; Saja, J. A. D.; Rodriguez-Mendez, M. L. *Sensors*, **2011**, *11*, 1328.

[49]. Adams, R. N. *Anal. Chem.*, **1958**, *30*, 1576.

[50]. Olson, C.; Adams, R. N. *Anal. Chim. Acta*, **1960**, *22*, 582.

[51]. Adams, R. N. *Electrochemistry at solid electrodes*, Marcel Dekker, Newyork, **1969**.

[52]. Kuwana, T. *Personal Communication*, **2002**.

[53]. Kalcher, K. *Electroanalysis*, **1990**, *2*, 419.

[54]. Olson, C.; Adams, R. N. *Anal. Chim. Acta*, **1963**, *29*, 358.

[55]. Svancara, I.; Vytras, K.; Kalcher, K.; Walcarius, A.; Wang, J. *Electroanalysis*, **2009**, *21*, 7.

[56]. Kalcher, K.; Cai, X.; Kclbl, G.; Svancara, I.; Vytras, K.; *Sb. Ved. Pr., Vys. Sk. Chemickotechnol., Pardubice,* **1994**, *57*, 5.

[57]. Kalcher, K.; Svancara, I.; Metelka, R.; Vytras, K.; Walcarius, A. *The Encyclopedia of Sensors*, *Vol. 4*, American Scientific, Stevenson Ranch, **2006**.

[58]. Adams, R. N.; *Rev. Polarog. (Kyoto)*, **1963**, *11*, 71.

[59]. Li, G.; Wan, C. D.; Ji, Z. M.; Wu, K. B. *Sens. Actuators B*, **2007**, *124*, 1.

[60]. Svancara, I.; Hvzdalova, M. K.; Vytras, K.; Kalcher, K.; Novotny, R. *Electroanalysis,* **1996**, *8*, 61.

[61]. Wang, J.; Kirgcz, U. A.; Mo, J. W.; Lu, J. M.; Kawde, A. N.; Muck, A. *Electrochem. Commun.,* **2001**, *3*, 203.

[62]. Stefan, R. I.; Bairu, S. G. *Anal. Chem.,* **2005**, *75*, 5394.

[63]. Nossol, E.; Zarbin, A. J. G. *Qim. Nova,* **2007**, *30*, 1469.

[64]. Hernandez, A. M.; Gonzalez I. *Carbon,* **2005**, *43*, 1961.

[65]. He, J. B.; Lin, X. Q.; Pan, J. *Electroanalysis,* **2005**, *17*, 1681.

[66]. Rivas, G. A.; Rubianes, M. D.; Pedano, M. L.; Ferreyra, N. F.; Luque, G. L.; Rodriguez, M. C.; Miscoria, S. A. *,* **2007**, *19*, 823.

[67]. Ricci, F.; Amine, A.; Moscone, D.; Palleschi, G. *Anal. Lett.*, **2003**, *36*, 1921.

[68]. Antiochia, R.; Lavagnini, I.; Magno, F.; Valentini, F.; Palleschi, G. *Electroanalysis*, **2004**, *16*, 1451.

[69]. Lawrence, N. S.; Deo, R. P.; Wang, J. *Talanta*, **2004**, *63*, 443.

[70]. Chicharro, M.; Bermejo, E.; Moreno, M.; Sanchez, A.; Zapardiel, A.; Rivas, G. A. *Electroanalysis*, **2005**, *17*, 476.

[71]. Pungor, E.; Szepesvary, E. *Anal. Chim. Acta*, **1968**, *43*, 289.

[72]. Svancara, I.; Vytras, K. *Anal. Chim. Acta*, **1993**, *273*, 195.

[73]. Rumirez, M. T.; Pulomur, M. E.; Gonzalez, I.; Rojus-Hernandez, A. *Electroanalysis*, **1995**, *7*, 184.

[74]. Liu, H. T.; He, P.; Li, Z. Y.; Sun, C. Y.; Shi, L. H.; Liu, Y.; Zhu, G. Y.; Li, J. H. *Electrochem. Commun.,* **2005**, *7*, 1357.

[75]. Svancara I., Vytras K. *Chem. Listy*, **1994**, *88,* 138.

[76]. Lindquist, J. *Anal. Chem.*, **1973**, *45*, 1006.

[77]. Kalcher, K.; Kauffmann, J. M.; Wang, J.; Svancara, I.; Vytras, K.; Neuhold, C.; Yang, Z. *Electroanalysis*, **1995**, *7*, 5.

[78]. Svancara, I.; Schachl, K. *Chem. Listy*, **1999**, *93*, 490.

[79]. Cermakova I. *MSc Thesis.* University of Pardubice, Pardubice, **1998**.

[80]. Gorton, L. *Electroanalysis.,* **1995**, 7, 23.

[81]. Zhang, Z. Q.; Liu, H.; Zhang, H.; Li Y. F. *Anal. Chim. Acta.,* **1996**, *333*, 119.

[82]. Kuwana, T.; French, W. *G. Anal Chem.,* **1964***,* *36*, 241.

[83]. Schultz F. A.; Kuwana, T. *J. Electrmnal. Chem.*, **1965**, *10*, 95.

[84]. Marcoux, L. S.; Prater, K. G.; Prater, B. G.; Adams, R. N. *Anal. Chem.*, **1965**, *37*, 1446.

[85]. Cheek, G. T.; Nelson, R. R. *Anal. Lett.*, **1978**, *11*, 393.

[86]. Ravichandran, K.; Baldwin, R. P. *J. Eiectroanal. Chem.,* **1981**, *126*, 293.

[87]. Yao, T.; Musha, S. *Anal. Chim. Acta*, **1979**, *110*, 203.

[88]. Svancara, I.; Pravda, M.; Hvzdalova, M.; Vytras, K.; Kalcher, K. *Electroanalysis*, **1994**, *6*, 663.

[89]. Dey, M. K.; Satpati, A. K.; Sahoo, S.; Kameswaran, R.; Reddy, A. V. R.; Mukherjee, T. *Anal. Methods*, **2011**, *3*, 2540.

[90]. Hocevar, S. B.; Svancara, I.; Ogorevc, B.; Vytras, K. *Electrochim. Acta*, **2005**, *51*, 706.

[91]. Dey, M. K.; Satpati, A. K.; Reddy, A. V. R. *Anal. Methods*, **2014**, *6*, 5207.

[92]. Svancara, I.; Hocevar, S. B.; Baldrianova, L.; Tesarova, E.; Vytras, K. *Sci. Pap. Univ. Pardubice A*, **2007**, *13*, 5.

[93]. Metelka, R.; Vytras, K.; Bobrowski, A. *J.Solid State Electrochem.*, **2000**, *4*, 348.

[94]. Svobodova, E.; Baldrianova, L.; Hocevar, S. B.; Svancara, I. *Int. J. Electrochem. Sci.*, **2012**, *7*, 197.

[95]. Qui, D. F.; Zhao, Q.; Liu, K. Z. *Huaxue Yanjiu.* **1997**, *8*, 41.

[96]. Cai, Q.T.; Khoo, S. B. *Electroanalysis.,* **1995**, *7*, 379.

[97]. Cai, Q.-T.; Khoo, S. B. *Analyst.,* **1995**, *120*, 1047.

[98]. Kalcher, K.; *Fresenius Z. Anal. Chem.*, 1986, *325*, 181.

[99]. Holgado, T. M.; Pinilla-Macias, J. M.; Hernandez-Hernandez, L. *Anal. Chim. Acta*, **1995**, *309*, 117.

[100]. Navratilova, Z. *Electroanalysis,* **1991**, *3*, 799.

[101]. Paniagua, A. R.; Vazquez, M. D.; Tascon, M. L.; Sanchez Batanero, P. *Electroanalysis*, **1993**, *5*, 155.

[102]. Wang, J.; Zadeii, J. M. *Talanta*, **1986**, *33*, 321.

[103]. Cai, Q.; Khoo, S. B. *Bull. Singapore Natl. Inst. Chem.*, **1993**, *21*, 157.

[104]. Qiao, W. J.; Ding, H. *J. Tongji Med. Univ.,* **1993**, *13*, 190.

[105]. Bae, Z. U.; Jun, H. S.; Chang, H. Y. *J. Korean Chem. Soc.*, **1993**, *37*, 723.

[106]. Khoo, S. B.; Soh, M. K.; Cai, Q.; Khan, M. R.; Guo, S. X. *Electroanalysis*, **1997**, *9*, 45.

[107]. Guo, H. S.; Li, Y. H. *Fenxi Huaxue*, **2000**, *28*, 1527.

[108]. Khan, M. R. *Analyst.,* **1998**, *123*, 1351.

[109]. Walcarius, A. *Anal. Chim. Acta.,* **1999**, *338*, 79.

[110]. Walcarius, A.; Mariaaulle, P.; Lamberts, L. *J. Electroanal. Chem.,* **1999**, *4653*, 100.

[111]. Kula, P.; Navratilova, Z. *Fresenius J. Anal. Chem.,* **1996**, *354*, 692.

[112]. Raber, G.; Kalcher, K.; Stadlober, M. *Sci. Pap.Univ. Pardubice, Ser. A.,* **1997**, *3*, 163.

[113]. Kalcher, K.; Grabec, I.; Raber, G.; Cai, X. H; Tavcar, G.; Ogorevc, B. *J. Electroanal. Chem.*, **1995**, *386*, 149.

[114]. Cai, X. H.; Kalcher, K.; Diewald, W.; Neuhold, C. G.; Magee, R. J. *Fresenius J. Anal. Chem.*, **1993**, *345*, 25.

[115]. Neuhold, C.; Kalcher, K.; Diewald, W.; Cai, X.; Raber, G. *Electroanalysis*, **1994**, *6*, 227.

[116]. Svancara, I.; Ogorevc, B.; Novic, M.; Vytras, K. *Anal. Bioanal. Chem.*, **2002**, *372*, 795.

[117]. Svancara, I.; Foret, P.; Vytras, K. *Talanta*, **2004**, *64*, 844.

[118]. Svancara, I.; Kalcher, K.; Diewald, W.; Vytras, K. *Electroanalysis,* **1996**, *8*, 336.

[119]. Posac, J. R.; Vazquez, M. D.; Tascon, M. L.; Acuna, J. A.; dela Fuente, C.; Velasco, E.; Sanchez Batanero, P. *Talanta*, **1995**, *42*, 293.

[120]. Wang, J.; Bonakdar, M. *Talanta*, **1988**, *35*, 277.

[121]. Ferancova, A.; Labuda, J. *Fresenius J. Anal. Chem.*, **2001**, *370*, 1.

[122]. Arrigan, D. W. M.; Svehla, G.; Harris, S. J.; McKervey, M. A. *Electroanalysis*, **1994**, *6*, 97.

[123]. Nawutiloua, Z.; Kula, P. *Electroanalysis*, **1992**, *4*, 683.

[124]. Soreta, T. R.; Gojeh, M.; Moses, Y.; Yakubu1, Y.; Bahago, N. *IOSR J. Appl. Chem.,* **2015**, *8,* 19.

[125]. Rodriguez-Bravo1, L. A.; Palomar-Pardave1, M.; Corona-Avendano, S.; Romero-Romo M.; Herrera-Hernandez, H.; Ramirez-Silva, M. T.; Escarela-Perez, R. *Int. J. Electrochem. Sci.*, **2011**, *6*, 2730.

[126]. Csokaa, B.; Mekhalif, Z. *Croat. Chem. Acta*, **2011**, *84*, 407.

[127]. Raoof, J. B.; Ojani, R.; Kolbadinezhad, M. *J. Solid State Electrochem.*, **2009**, *13*, 1411.

[128]. Raoof, J. B.; Ojani, R.; Kiani, A. *J. Electroanal. Chem.*, **2001**, *515*, 45.

[129]. Oni, J.; Nyokong, T. *Anal. Chim. Acta*, **2001**, *434*, 9.

[130]. Rezaei, B., Ghiaci, M.; Sedaghat, M. E. *Sensors and Actuators B,* **2008***, 131*, 439.

[131]. Saby, C.; Mizutani, F.; Yabuki, S. *Anal. Chim. Acta*, **1995**, *304*, 33.

[132]. Varga, G. M.; Burestedt, E.; Svensson, C. J.; Emneus, J.; Gorton, L.; Ruzgas, T.; Lutz, M.; Unger, K. K. *Electrounalysis*, **1996**, *8*, 1121.

[133]. Rodrıiguez, M. C.; Rivas, G. A. *Anal. Chim. Acta*, **2002**, *459*, 43.

[134]. Varma, S. *Bioelectrochemistry*, **2002**, *56*, 107.

[135]. Yao1, Q.; Yabuki, S.; Mizutani, F. *Sensors and Actuators B*, **2000**, *65*, 147.

[136]. Wang, Y.; Xiong, H.; Zhang, X.; Wang, S. *Microchimica Acta*, **2010**, *170*, 27.

[137]. Thomas, T.; Mascarenhas, R. J.; D'Souza, O. J.; Martis, P.; Dalhalle, J.; Kumara Swamy, B. E. *J. Colloid and Interface Sci.*, **2013**, *402*, 223.

[138]. Stojanovic, Z. S.; Mehmeti, E.; Kalcher, K.; Guzsvany, V.; Stankovic, D. M. *Food Anal. Methods*, **2016**, *9*, 2701.

[139]. Zheng, D.; Liu, X.; Zhu, S.; Cao, H.; Chen, Y.; Hu, S. *Microchimica Acta*, **2015**, *182*, 2403.

[140]. Vidya, H.; Kumara Swamy, B. E. *Sci. Lett. J.*, **2015**, *4*, 77.

[141]. Hamidi-Asl, E.; Raoof, J. B.; Naghizadeh, N.; Akhavan-Niaki, H.; Ojani, R.; Banihashemi, A. *Int. J. Biol. Macromol.*, **2016**, *91*, 400.

[142]. Shahrokhian, S.; Rastgar, S. *Analyst*, **2012**, *137*, 2706.

[143]. Behpour, M.; Ghoreishi, S. M.; Honarmand, E. *Int. J. Electrochem. Sci.*, **2010**, *5*, 1922.

[144]. Ardakani, M. M.; Talebi, A.; Naeimi, H.; Barzoky, M. N.; Taghavinia, N. *J. Solid State Electrochem.*, **2009**, *13*, 1433.

[145]. Rahbar, N.; Parham, H. *Jundishapur J Nat Pharm Prod.*, **2013**, *8*, 118.

[146]. Berber, M. R.; Hafez, I. H. *Carbon Nanotubes - Current Progress of their Polymer Composites*, InTech, **2016.**

[147]. Sanghavi, B. J.; Wolfbeis, O. S.; Hirsch, T.; Swami, N. S. *Microchim. Acta*, **2015**, *182*, 1.

[148]. Wang, L.; Jiang, M.; Wang, E. B.; Lian, S. Y.; Xu, L.; Li, Z. *Mater. Lett.*, **2004**, *58*, 683.

[149]. Han, Z. G.; Zhao, Y. L.; Peng, J.; Liu, Q.; Wang, E. B. *Electrochim. Acta*, **2005**, *51*, 218.

[150]. Ulakhovich, N. A.; Medyanceva, E. P.; Budnikov, G. K. *Zh. Anal. Khim.*, **1993**, *48*, 980.

[151]. Mikysek, T.; Svancara, I.; Vytras, K.; Banica, F. G. *Electrochem. Commun.*, **2008**, *10*, 242.

[152]. Baldwin, R. P.; Christensen, J. K.; Kryger, L. *Anal. Chem.*, **1986**, *58*, 1790.

[153]. Thenmozhi, K.; Narayanan, S. *Int. J. ChemTech Research*, **2014**, *6*, 1760.

[154]. Ma, L.; Wang, Z.; Li, Q. *Analyst*, **2012**, *137*, 432.

[155]. Rondeau, A.; Larsson, N.; Boujtita, M.; Gorton, L.; El Murr, N. *Analusis*, **1999**, *27*, 649.

[156]. Ban, F. Y.; Majid, S. R.; Huang, N. M.; Lim, H. N. *Int. J. Electrochem. Sci.*, **2012**, *7*, 4345.

[157]. Geim, K.; Novoselov, K. S. *Nat. Mater.*, **2007**, *6*, 183.

[158]. Stoller, M. D.; Park, S.; Zhu, Y. W.; An, J.; Ruoff, R. S. *Nano Lett.*, **2008**, *8*, 3498.

[159]. Park, S.; Ruoff, R. S. *Nat. Nanotechnol.*, **2009**, *4*, 217.

[160]. Novoselov, K. S.; Geim, A. K.; Morozov, S. V.; Jiang, D.; Katsnelson, M. I.; Grigorieva, I. V.; Dubonos, S. V.; Firsov, A. A. *Nature*, **2005**, *438*, 197.

[161]. Zhang, Y. B.; Tan, Y. W.; Stormer, H. L.; Kim, P. *Nature*, **2005**, *438*, 201.

[162]. Novoselov, K. S.; Jiang, Z.; Zhang, Y.; Morozov, S. V.; Stormer, H. L.; Zeitler, U.; Maan, J. C.; Boebinger, G. S.; Kim, P.; Geim, A. K. *Science*, **2007**, *315*, 1379.

[163]. Bunch, J. S.; Verbridge, S. S.; Alden, J. S.; van der Zande, A. M.; Parpia, J. M.; Craighead, H. G.; McEuen, P. L. *Nano Lett.*, **2008**, *8*, 2458.

[164]. Lee, C.; Wei, X.; Kysar, J. W.; Hone, J. *Science*, **2008**, *321*, 385.

[165]. Balandin, A. A.; Ghosh, S.; Bao, W. Z.; Calizo, I.; Teweldebrhan, D.; Miao, F.; Lau, C. N. *Nano Lett.*, **2008**, *8*, 902.

[166]. Bolotin, K. I.; Sikes, K. J.; Jiang, Z.; Klima, M.; Fudenberg, G.; Hone, J.; Kim, P.; Stormer, H. L. *Solid State Commun.*, **2008**, *146*, 351.

[167]. Geim, A. K. *Science*, **2009**, *324*, 1530.

[168]. Srivastava, S. K.; Shukla, A. K.; Vankar, V. D.; Kumar, V. *Thin Solid Films*, **2005**, *492*, 124.

[169]. Hamilton, C. E.; Lomeda, J. R.; Sun, Z.; Tour, J. M.; Barron, A. R. *Nano Letters*, **2009**, *9*, 3460.

[170]. Jiang, H. *Small*, **2011**, *7*, 2413.

[171]. Dikin, D. A.; Stankovich, S.; Zimney, E. J.; Piner, R. D.; Dommett, G. H.; Evmenenko, G; Nguyen, S. T.; Ruoff, R. S.; *Nature*, **2007**, *448*, 457.

[172]. Hummers Jr., W. S.; Offeman, R. E. *J. Am. Chem. Soc.*, **1958**, *80*, 1339.

[173]. Guo, S.; Dong, S. *Chem. Soc. Rev.*, **2011**, *40*, 2644.

[174]. Zhu, C.; Guo, S.; Fang, Y.; Dong, S. *ACS Nano*, **2010**, *4*, 2429.

[175]. Rao, C. N. R.; Subrahmanyam, K. S.; RamakrishnaMatte, H. S. S.; Maitra, U.; Moses, K.; Govindaraj, A. *Int. J. Mod. Phys. B*, **2011**, *25*, 4107.

[176]. Ruoff, R. S. *Nat. Nanotechnol.*, **2008**, *3*, 10.

[177]. Dreyer, D. R.; Park, S.; Bielawski, C. W.; Ruoff, R. S. *Chem. Soc. Rev.*, **2010**, *39*, 228.

[178]. Zhu, P.; Shen, M.; Xiao, S.; Zhang, D. *Physica B: Condensed Matter*, **2011**, *406*, 498.

[179]. Compton, O. C.; Nguyen, S. T. *Small*, **2010**, *6*, 711.

[180]. Becerill, H. A.; Mao, J.; Liu, Z. F.; Stoltenberg, R. M.; Bao, Z. N.; Chen, Y. S. *ACS Nano*, **2008**, *2*, 463.

[181]. Eda, G.; Chhowalla, M. *Adv. Mater.*, **2010**, *22*, 2392.

[182]. Mattevi, C.; Eda, G.; Agnoli, S.; Miller, S.; Mkhoyan, K. A.; Celik, O.; Mastrogiovanni, D.; Granozzi, G.; Garfunkel, E.; Chhowalla, M. *Adv. Funct. Mater.*, **2009**, *19*, 2577.

[183]. Eda, G.; Mattevi, C.; Yamaguchi, H.; Kim, H.; Chhowalla, M. *J. Phys. Chem. C*, **2009**, *113*, 15768.

[184]. Gómez-Navarro, C.; Weitz, R. T.; Bittner, A. M.; Scolari, M.; Mews, A.; Burghard, M.; Kern, K. *Nano Lett.*, **2007**, *7*, 3499.

[185]. Si, Y.; Samulski, E. T. *Nano Lett.*, **2008**, *8*, 1679.

[186]. Li, D.; Müller, M. B.; Gilje, S.; Kaner, R. B.; Wallace, G. G. *Nat. Nanotechnol.*, **2008**, *3*, 101.

[187]. Brodie, B. C. *Philos. Trans. R. Soc. Lond.*, **1859**, *149*, 249.

[188]. Young, R. J.; Kinloch, I. A.; Gong, L.; Novoselov, K. S. *Compos. Sci. Technol.*, **2012**, *72*, 1459.

[189]. Staudenmaier, L. *Ber. Dtsch. Chem. Ges.*, **1898**, *31*, 1481.

[190]. Ulrich, H.; Rudolf, H. *Ber. Dtsch. Chem. Ges.*, **1939**, *72*, 754.

[191]. Ruess, G. *Monatsch. Chem.*, **1946**, *76*, 381.

[192]. Kovtyukhova, N. I.; Ollivier, P. J.; Martin, B. R.; Mallouk, T. E.; Chizhik, S. A.; Buzaneva, E.V.; Gorchinskiy, A. D. *Chem. Mater.*, **1999**, *11*, 771.

[193]. Ma, C.; Liu, W.; Shi, M.; Lang, X.; Chu, Y.; Chen, Z.; Zhao, D.; Lin, W.; Hardacre, C. *Electrochim. Acta*, **2013**, *114*, 133.

[194]. Nikolakopoulou, A.; Tasis, D.; Sygellou, L.; Dracopoulos, V.; Galiotis, C.; Lianos, P *Electrochim. Acta*, **2013**, *111*, 698.

[195]. Yu, Y; Kang, B.; Lee, Y.; Lee, S.; Ju, B. *Appl. Surf. Sci.*, **2013**, *287*, 91.

[196]. Marcano, D. C.; Kosynkin, D. V.; Berlin, J. M.; Sinitskii, A.; Sun, Z.; Slesarev, A.; Alemany, L. B.; Lu, W.; Tour, J. M. *ACS Nano*, **2010**, *4*, 4806.

[197]. Higginbotham, A. L.; Kosynkin, D. V.; Sinitskii, A.; Sun, Z.; Tour, J. M. *ACS Nano*, **2010**, *4*, 2059.

[198]. Li, W.; Xu, Z.; Chen, L.; Shan, M.; Tian, X.; Yang, C.; Lv, H.; Qian, X. *Chem. Eng. J.*, **2014**, *237*, 291.

[199]. Stankovich, S.; Dikin, D. A.; Dommett, G. H. B.; Kohlhaas, K. M.; Zimney, E. J.; Stach, E. A.; Piner, R. D.; Nguyen, S. T.; Ruoff, R. S. *Nature*, **2006**, *442*, 282.

[200]. Gao, W.; Alemany, L. B.; Ci, L.; Ajayan, P. M. *Nat. Chem.*, **2009**, *1*, 403.

[201]. Stankovich, S.; Dikin, D. A.; Piner, R. D.; Kohlhaas, K. A.; Kleinhammes, A.; Jia, Y.; Wu, Y.; Nguyen, S. T.; Ruoff, R. S. *Carbon*, **2007**, *45*, 1558.

[202]. Wang, L.; Ye, Y.; Lu, X.; Wu, Y.; Sun, L.; Tan, H.; Xu, F.; Song, Y. *Electrochim. Acta*, **2013**, *114*, 223.

[203]. Song, P; Zhang, X; Sun, M; Cui, X; Lin, Y. *RSC Adv.*, **2012,** *2*, 1168.

[204]. Wang, G.; Yang, J.; Park, J.; Gou, X.; Wang, B.; Liu, H.; Yao, J. *J. Phys. Chem. C*, **2008**, *112*, 8192.

[205]. Zhou, T.; Chen, F.; Tang, C.; Bai, H.; Zhang, Q.; Deng, H.; Fu, Q. *Compos. Sci. Technol.*, **2011**, *71,* 1266.

[206]. Fernandez-Merino, M. J.; Guardia, L.; Paredes, J. I.; Villar-Rodil, S.; Solis-Fernandez, P.; Martínez-Alonso, A; Tascon, J. M. D. *J. Chem. Phys.*, **2010**; *114*, 6426.

[207]. Xing, Z.; Chu, Q.; Ren, X.; Tian, J.; Asiri, A. M.; Alamry, K. A.; Al-Youbi, A. O.; Sun, X. *Electrochem. Commun.*, **2013**, *32*, 9.

[208]. Wang, Y.; Shi, Z.; Yin, J. *ACS Appl. Mater. Interfaces,* **2011,** *3*, 1127.

[209]. Muszynski, R.; Seger, B.; Kamat, P. V. *J. Phys. Chem. C*, **2008**, *112*, 5263.

[210]. Schniepp, H. C.; Li, J.; McAllister, M. J.; Sai, H.; Herrera-Alonso, M.; Adamson, D. H.; Prudhomme, R. K.; Car, R.; Saville, D. A.; Aksay, I. A. *J. Phys. Chem. B*, **2006**, *110*, 8535.

[211]. Jang, H.; Yun, J.; Kim, D. Y.; Park, D. W.; Na, S. I.; Kim, S. S. *Electrochim. Acta*, **2012**, *81*, 301.

[212]. Williams, G.; Serger, B.; Kamat, P. V. *ACS Nano*, **2008**, *2*, 1487.

[213]. Liu, X.; Pan, L.; Zhao, Q.; Lv, T.; Zhu, G.; Chen, T.; Lu, T.; Sun, Z.; Sun, C. *Chem. Eng. J.*, **2012**, *183*, 238.

[214]. Choobtashani, M.; Akhavan, O. *Appl. Surf. Sci.*, **2013**, *276*, 628.

[215]. Akhavan, O.; Ghaderi, E.; Abouei, E.; Hatamie, S.; Ghasemi, E. *Carbon*, **2014**, *66*, 395.

[216]. Ghorbani, M.; Abdizadeh, H.; Golobostanfard, M. R. *Proc. Mater. Sci.*, **2015**, *11*, 326.

[217]. Mei, X.; Meng, X.; Wu, F. *Physica E*, **2015**, *68*, 81.

[218]. Kong, C.; Song, W.; Meziani, M. J.; Tackett, K. N.; Cao, L.; Farr, A. J.; Anderson, A.; Sun, Y. *J. Supercrit. Fluids*, **2012**, *61*, 206.

[219]. Miller, J. N.; Miller, J. C. *Statistics and Chemometrics for Analytical Chemistry*, *6th ed.*, Pearson Education Limited, England, **2010**.

[220]. Randviir, E. P.; Banks, C. E. *Anal. Methods*, **2013**, *5*, 1098.

[221]. Barsoukov, E.; Macdonald, J. R. *Impedance Spectroscopy: Theory, Experiment, and Applications*, Wiley, **2005**.

[222]. Lisdat, F.; Schafer, D. *Anal. Bioanal. Chem.*, **2008**, *391*, 1555.

[223]. Randles, J. E. B. *Trans. Faraday Soc.*, **1948**, *44*, 327.

[224]. Fayyad, E. M.; Almaadeed, M. A.; Jones, A.; Abdullah, A. M. *Int. J. Electrochem. Sci.*, **2014**, *9*, 4989.

[225]. Nagiub, A. M. *Portugal. Electrocim. Acta*, **2005**, *22*, 301.

[226]. Hamdy, A. S.; El-Shenawy, E.; El-Bitar, T. *Int. J. Electrochem. Sci.*, **2006**, *1*, 171.

[227]. Barón, A.; Valenzuela, E.; Sanchez, R.; Gonzalez-Gutierrez, A. G.; Sebastian, P. J. *Int. J. Electrochem. Sci.*, **2016**, *11*, 8057.

[228]. Malevich, D.; Halliop, E.; Peppley, B. A.; Pharoah, J. G.; Karan, K. *J. Electrochem. Soc.,* **2009**, *156*, B216.

[229]. Hu, C.; Hu, S. *Electrochim. Acta*, **2004**, *49*, 405.

[230] Zhou, Y.; Tang, W.; Dang, F.; Chai, S.; Zhang, L. *Colloids and Surfaces B: Biointerfaces,* **2014,** *118*, 148.

[231]. Zaidi, S. A. *Int. J. Electrochem. Sci.*, **2013**, *8*, 11337.

[232] El-Kady, M. F.; Strong, V.; Dubin, S.; Kaner, R. B. *Science,* **2012**, *335*, 1326.

[233]. Chatterjee, K.; Shankar, R.; Kumar, A. *J. Fuel Cell Sci. Technol.,***2014**, *11*, 051004.

[234]. Bard, A. J.; Fan, F. R. F.; Kwak, J.; Lev, O. *Anal. Chem.*, **1989**, *61*, 132.

[235]. Engstrom, R. C.; Pharr, C. M. *Anal. Chem.* **1989**, *61*, 1099A.

[236]. Lefrou, C.; Cornut, R. *Chem. Phys. Chem.* **2010**, *11*, 547.

[237]. Bard, A. J.; Mirkin, M. V.; Unwin, P. R.; Wipf, D. O. *J. Phys. Chem.*, **1992**, *96*, 186.

[238]. Wei, C.; Bard, A. J.; Mirkin, M. V. *J. Phys. Chem.*, **1995**, *99*, 16033.

[239]. Zhou, J.; Zu, Y.; Bard, A. J. *J. Electroanal. Chem.*, **2000**, *491*, 22.

[240]. Zoski, C. G. *J. Phys. Chem. B*, **2003**, *107*, 6401.

[241]. Zoski, C. G. in *Encyclopedia of Analytical Chemistry*, editor: Meyers, R. A.; Supplementary Volumes S1-S3, John Wiley & Sons, Ltd, Chichester, UK, **2011**.

[242]. Zhou, F.; Unwin, P. R.; Bard, A. J. *J. Phys. Chem.*, **1992,** *96*, 4917.

[243]. Bard, A. J.; Mirkin, M. V. *Scanning Electrochemical Microscopy*, 2nd ed., Taylor and Francis, New York, **2012**.

[244]. Eckhard, K.; Chen, X.; Turcu, F.; Schuhmann, W. *Phys. Chem. Chem. Phys.*, **2006**, *8*, 5359.

[245] Santana, J. J.; González-Guzmán, J.; Fernández-Mérida, L.; González, S.; Souto, R. M. Electrochim. Acta, **2010**, *55*, 4488.

[246]. Wittstock, G.; Schuhmann, W. *Anal. Chem.*, **1997**, *69*, 5059.

[247]. Meltzer, S.; Mandler, D. *J. Electrochem. Soc.*, **1995**, *142*, L82.

[248]. Wuu, Y. M.; Fan, F. R. F.; Bard, A. J. *J. Electrochem. Soc.*, **1989**, *136*, 885.

[249]. Bard, A. J.; Denuault, G.; Friesner, R. A.; Dornblaser, B. C.; Tuckerman, L. S. *Anal. Chem.*, **1991**, *63*, 1282.

[250]. Denuault, G.; Mirkin, M. V.; Bard, A. J. *J. Electroanal. Chem. Interfac. Electrochem.*, **1991**, *308*, 27.

[251]. El-Giar, E. E. D. M.; Wipf, D. O. *J. Electroanal. Chem.*, **2007**, *609*, 147.

[252]. Fergusson, J. E. *The Heavy Elements: Chemistry, Environmental Impact and Health Effects*, Oxford: Pergamon Press, **1990**.

[253]. He, Z. L.; Yang, X. E.; Stoffella, P. J. J. *Trace Elem. Med. Biol.*, **2005,** *19*, 125.

[254]. Goyer, R. A.; Clarkson, T. W., *Toxic effects of metals in Cassarett and Doull's Toxicology: The Basic Science of Poisons*, 6th ed., McGraw-Hill Publisher, New York, **2001**.

[255]. Herawati, N.; Suzuki, S.; Hayashi, K.; Rivai, I. F.; Koyoma, H., *Bull. Env. Contam. Toxicol.*, **2000**, *64*, 33.

[256]. Shallari, S.; Schwartz, C.; Hasko, A.; Morel, J. L. *Sci. Total Environ.*, **1998,** *19209*, 133.

[257]. WHO/FAO/IAEA, *Trace elements in human nutrition and health*, World Health Organization. Switzerland: Geneva, **1996**.

[258]. Chang, L. W.; Magos, L.; Suzuki, T. *Toxicology of Metals*, Boca Raton. FL, USA: CRC

Press, **1996**.

[259]. Singh, R.; Gautam, N.; Mishra, A.; Gupta, R. *Indian J. Pharmacol.*, **2011**, *43*, 246.

[260]. Yedjou, C. G.; Tchounwou, P. B. *Metal Ions Biol. Med.*, **2006**, *9*, 298.

[261]. Yedjou, C. G., Tchounwou, P. B. *Mol. Cell Biochem.*, **2007**, *301*, 123.

[262]. Tchounwou, P. B.; Centeno, J.A.; Patlolla, A. K. *Mol.Cell Biochem.*, **2004**, *255*, 47.

[263] Tchounwou, P. B.; Ishaque, A.; Schneider, J. *Mol. Cell Biochem.*, **2001,** *222*, 21.

[264] Patlolla, A.; Barnes, C.; Field, J.; Hackett, D.; Tchounwou, P. B. *Int. J. Environ. Res. Public Health*, **2009**, *6*, 643.

[265]. Patlolla, A.; Barnes, C.; Yedjou, C.; Velma, V.; Tchounwou, P. B. *Environ. Toxicol.*, **2009**, *24*, 66.

[266] Yedjou, G. C.; Tchounwou, P. B. *Intl. J. Environ. Res. Public Health,* **2008**, *4*, 132.

[267]. Tchounwou, P. B.; Yedjou, C. G.; Foxx, D.; Ishaque, A.; Shen, E. *Mol. Cell Biochem.*, **2004**, *255*, 161.

[268]. Sutton, D. J.; Tchounwou, P. B. *Intl. J. Environ. Res. Public Health*, **2007**, *4*, 138.

[269]. Sutton, D. J.; Tchounwou, P. B.; Ninashvili, N.; Shen, E. *Intl. J. Mol. Sci.*, **2002**, *3*, 965.

[270]. Kenawy, I. M. M.; Hafez, M. A. H.; Akl, M. A.; Lashein, R. R. *Anal. Sci.*, **2000**, *16*, 493.

[271]. Caroli, S.; Forte, G.; Lamiceli, A. L.; Galoppi, B. *Talanta,* **1999**, *50*, 327.

[272]. Feldmann, J.; Salaun, P.; Lombi, E. *Environ. Chem.,* **2009**, *6*, 275.

[273]. Wang, J.; Lu, J.; Hocevar, S. B.; Farias, P. A. M.; Ogorevc, B. *Anal. Chem.*, **2000**, *72*, 3218.

[274]. Wang, J.; Lu, J. M.; Kirgoz, U. A.; Hocevar, S. B.; Ogorevc, B. *Anal. Chim. Acta*, **2001**, *434*, 29.

[275]. Wang, J. *Electroanalysis*, **2005**, *17*, 1341.

[276]. Wang, J.; Deo, R. P.; Thongngamade, S.; Ogorevc, B. *Electroanalysis*, **2001**, *13*, 1153.

[277]. Economou, A. *TrAC, Trends Anal. Chem.*, **2005**, *24*, 334.

[278]. Krolicka, A.; Bobrowski, A. *Electrochem. Commun.*, **2004**, *6*, 99.

[279]. Svancara, I.; Vytras, K. *Chem. Listy*, **2006**, *100*, 90.

[280]. Krolicka, A.; Pauliukaite, R.; Svancara, I.; Metelka, R.; Bobrowski, A.; Norkus, E.; Kalcher, K.; Vytras, K. *Electrochem. Commun.*, **2002**, *4*, 193.

[281]. Hocevar, S. B.; Ogorevc, B.; Wang, J.; Pihlar, B. *Electroanalysis*, **2002**, *14*, 1707.

[282]. Long, G. G.; Freedman, L. D.; Doak, G. O. *Bismuth and bismuth alloys, in Kirk-Othmer Encyclopedia of Chemical Technology* , editor: Grayson, M. John Wiley and Sons, New York, **1978**.

[283]. Krueger, J.; Winkler, P.; Luederitz, E. L.; Lueck, M. *Bismuth Alloys and Bismuth Compounds,in Ullman's Encyclopedia of Industrial Chemistry* , editor: Gerhartz, W. , 5th ed, VCH, Weinheim, **1985**.

[284]. Wang, J.; Kirgoz, U. A.; Lu, J. M. *Electrochem. Commun.*, **2001**, *3*, 703.

[285]. Hocevar, S. B.; Wang, J.; Deo, R. P.; Ogorevec, B. *Electroanalysis*, **2002**, *14*, 112.

[286]. Wang, J.; Lu, J. *Electrochem. Commun.*, **2000**, *2*, 390.

[287]. Kefala, G.; Economou, A.; Voulgaropoulos, A.; Sofoniou, M. *Talanta*, **2003**, *61*, 603.

[288]. Alberich, A.; Serrano, N.; Arino, C.; Diaz-Cruz, J. M.; Esteban, M. *Talanta*, **2009**, *78*, 1017.

[289]. Flechsig, G. U.; Kienbaum, M.; Grundler, P. *Electrochem.Commun.*, **2005**, *7*, 1091.

[290]. Vytras, K.; Svancara, I.; Metelka, R. *Electroanalysis*, **2002**, *14*, 1359.

[291]. Economou, A.; Fielden, P. R. *Analyst*, **1993**, *118*, 1399.

[292]. Christensen, M. K.; Hoyer, *Electroanalysis*, **2000**, *12*, 35.

[293]. Brett, C. M. A.; Fungaro, D. A. *Talanta*, **2000**, *50*, 1223.

[294]. Wang, Z.; Galal, A.; Zimmer, H.; Mark, H. B. *Electroanalysis*, **1992**, *4*, 77.

[295]. Arrigan, D. W. M.; Lowens, M. J. *Anal. Commun.*, **1998**, *35*, 61.

[296]. Lu, T. H.; Huang, J. F.; Sun, I. W. *Anal. Chim. Acta*, **2002**, *454*, 93.

[297]. Mogensen, L.; Kryger, L. *Electroanalysis*, **1998**, *10*, 1285.

[298]. Campanella, L.; Ferri, T.; Petronio, B. *Analusis*, **1996**, *24*, 35.

[299]. Kelly, M. J.; Heineman, W. R. *J. Electroanal. Chem. Interfacial Electrochem.*, **1987**, *222*, 243.

[300]. Turyan, I.; Mandler, D. *Anal. Chem.*, **1994**, *66*, 58.

[301]. Hoyer, B.; Florence, T. M.; Batley, G. *Anal. Chem.*, **1987**, *59*, 1608.

[302]. Kefala, G.; Economou, A.; Voulgaropoulos, A. *Analyst*, **2004**, *129*, 1082.

[303]. Torma, F.; Kadar, M.; Toth, K.; Tatar, E. *Anal. Chim. Acta*, **2008**, *619*, 173.

[304]. Xu, H.; Zeng, L. -P.; Xing, S. -J.; Xian, Y. -Z.; Jin, L. -T. *Chin. J. Chem.*, **2008**, *26*, 847.

[305]. Xu, H.; Zeng, L.; Huang, D.; Xian, Y.; Jin, L. *Food Chem.*, **2008**, *109*, 834.

[306]. Abbaspour, A.; Izadyar, A. *Talanta*, **2007**, *71*, 887.

[307]. Hwang, G. H.; Hana, W. K.; Park, J. S.; Kang, S. G. *Talanta*, **2008**, *76*, 301.

[308]. Liu, G.; Lin, Y.; Tu, Y.; Ren, Z. *Analyst*, **2005**, *130*, 1098.

[309]. Deng, W.; Tan, Y.; Fang, Z.; Xie, Q.; Li, Y.; Liang, X.; Yao, S. *Electroanalysis*, **2009**, *21*, 2477.

[310]. Kubiak, W.; Wang, J. *J. Electroanal. Chem.*, **1989**, *258*, 41.

[311]. Kirgoz, U. A.; Marin, S.; Pumera, M.; Merkoci, A.; Alegret, S. *Electroanalysis*, **2005**, *17*, 881.

[312]. Zhu, W. W.; Li, N. B.; Luo, H. Q. *Anal. Lett.*, **2006**, *39*, 2273.

[313]. Uhl, A.; Kestranek, W. *Monatsh.* **1923**, *44*, 29.

[314]. Brinkman, R.; Buytendiyk, F. J. J. *Biochem. Z.* **1928**, *199*, 387.

[315]. Brown, D. H.; Gould, C. T.; Tatevossian, A. *Arch. Oral Biol.* **1974**, *19*, 601.

[316]. Alexander, P. W.; Joseph, J. P. *Anal. Chim. Acta* **1981**, *131*, 103.

[317]. Kinoshita, E.; Ingman, F.; Edwall, G.; Thulin, S.; Glab, S. *Talanta* **1986**, *33*, 125.

[318]. Wang, M.; Ha, Y. *Biosens. Bioelectron.* **2007**, *22*, 2718.

[319]. Hocevar, S. B.; Syvancara, I.; Ogorevc, B.; Vytras, K. *Anal. Chem.*, **2007,** 79, 8639.

[320]. Guzsvany, V.; Nakajima, H.; Soh, N.; Nakano, K.; Svancara, I.; Vytras, K.; Bjelica, L.; Imato, T. *Electroanalysis*, **2011**, *23*, 1593.

[321]. Xu, H.; Yang, P.; Zheng, Q.; Liu, J.; Jin, L. *Chin. J. Chem.*, **2010**, *28*, 2287.

[322]. Jovanovski, V.; Hocevar, S. B.; Ogorevc, B. *Electroanalysis*, **2009**, *21*, 2321.

[323]. Sopha, H.; Jovanovski, V.; Hocevar, S. B.; Ogorevc, B. *Electrochem. Commun.*, **2012**, *20*, 23.

[324]. Nigovica, B.; Hocevar, S. B. *Electrochim. Acta*, **2011**, *58*, 523.

[325]. Pauliukaite, R.; Metelka, R.; Svancara, I.; Krolicka, A.; Bobrowski, A.; Vytras, K.; Norkus, E.; Kalcher, K. *Sci. Pap. Univ. Pardubice, Ser. A*, **2004**, *10*, 47.

[326]. Dal Borgo, S.; Jovanovski, V.; Hocevar, S. B. *Electrochim. Acta*, **2013**, *88*, 713.

[327]. Tesarova, E. S.; Baldrianova, L.; Hocevar, S. B.; Svancara, I.; Vytras, K.; Ogorevc, B. *Electrochim. Acta*, **2009**, *54*, 1506.

[328]. Yi, W.-J.; Li, Y.; Ran, G. Luo, H.-Q.; Li, N.-B. *Mikrochim. Acta*, **2012**, *179*, 171.

[329]. Tesarova, E. S.; Baldrianova, L.; Stoces, M.; Svancara, I.; Vytras, K.; Hocevar, S. B.; Ogorevc, B. *Electrochim. Acta*, **2011**, *56*, 6673.

[330]. Sopha, H.; Baldrianova, L.; Tesarova, E.; Hocevar, S. B.; Svancara, I.; Ogorevc, B.; Vytras, K. *Electrochim. Acta*, **2010**, *55*, 7929.

[331]. Tesarova, E.; Vytras, K. *Electroanalysis*, **2009**, *21*, 1075.

[332]. Svancara, I.; Bartos, K.; Stoces, M. *Sci. Pap. Univ. Pardubice, Ser A*, **2011**, *17*, 5.

[333]. Ashrafi, A. M.; Vytras, K. *Electrochim. Acta*, **2012**, *73*, 112.

[334]. Ashrafi, A. M.; Vytras, K. *Int. J. Electrochem. Sci.*, **2012**, *7*, 68.

[335]. Ashrafi, A. M.; Vytras, K. *Talanta*, **2011**, *85*, 2700.

[336]. Toghill, K.; Xiao, L.; Wildgoose, G.; Compton, R. *Electroanalysis*, **2009**, *21*, 1113.

[337]. Kokkinos, C.; Economou, A.; Raptis, I.; Speliotis, T. *Electrochem. Commun.*, **2009**, *11*, 250.

[338]. Niu, X.; Zhao, H.; Lan, M. *Electrochim. Acta*, **2011**, *56*, 9921.

[339]. Slavec, M.; Hocevar, S. B.; Baldrianova, L.; Tesarova, E.; Svancara, I.; Ogorevc, B.; Vytras, K. *Electroanalysis*, **2010**, *22*, 1617.

[340]. Svancara, I.; Kalcher, K.; Walcarius, A.; Vytras, K. *Electroanalysis with Carbon Paste Electrodes, within Analytical Chemistry Series; CRC Press*, Boca Raton (Fl, USA), **2012**.

[341]. Ordeig, O.; Banks, C. E.; del Campo, J.; Munoz, F. X.; Compton, R. G. *Electroanalysis*, **2006**, *18*, 573.

[342]. Bonfil, Y.; Brand, M.; Kirowa-Eisner, E. *Anal. Chim. Acta*, **2000**, *424*, 65.

[343]. Ermakov, S. S.; Borzhitskaya, A. V.; Moskvin, L. N. *J. Anal. Chem.*, **2001**, *56*, 542.

[344]. Augelli, M. A.; Munoz, R. A. A.; Richter, E. M.; Canta-gallo, M. I.; Angnes, L., *Food Chem.*, **2007**, *101*, 579.

[345]. Okcu, F.; Ertas, F. N.; Gokcel, H. I.; Tural, H. *Turk. J. Chem.*, **2005**, *29*, 355.

[346]. Widmann, A.; van den Berg, C. M. G. *Electroanalysis*, **2005**, *17*, 825.

[347]. Salaun, P.; van den Berg, C. M. G. *Anal. Chem.*, **2006**, *78*, 5052.

[348]. Wang, J.; Gründler, P.; Flechsig, G. U.; Jasinski, M.; Lu, J.; Wang, J.; Tian, Z. Z. B. *Anal. Chim. Acta*, **1999**, *396*, 33.

[349]. Huiliang, H.; Jagner, D.; Renman, L. *Anal. Chim. Acta*, **1987**, *202*, 117.

[350]. Xiao, L.; Dietze, W.; Nyasulu, F.; Mibeck, B. A. F. *Anal. Chem.*, **2006**, *78*, 5172.

[351]. Gao, X.; Wei, W.; Yang, L.; Yin, T.; Wang, Y. *Anal. Lett.*, **2005**, *38*, 2327.

[352]. Abollino, O.; Giacomino, A.; Malandrino, M.; Piscionieri, G.; Mentasti, E. *Electroanalysis*, **2008**, *20*, 75.

[353]. Bernalte, E.; Sanchez, C. M.; Gil, E. P. *Sensors and Actuators B*, **2012**, *161*, 669.

[354]. S. Sahoo, A. K. Satpati and A. V. R. Reddy, Electrochemically Deposited Gold Nanoparticles on Carbon Paste Electrode Surface for the Determination of Mercury, *J. AOAC Int.* (manuscript id 13–0355, in press).

[355]. Ashrafi, A. M.; Vytras, K. *Int. J. Electrochem. Sci.*, **2013**, *8*, 2095.

[356]. Linarez Perez, O. E.; Perez, M. A.; Teijelo, M. L. *J. Electroanal. Chem.*, **2009**, *632*, 64.

[357]. Grieshaber, D.; MacKenzie, R.; Voros, J.; Reimhult, E. *Sensors*, **2008**, *8*, 1400.

[358]. Eggins, B. *Chemical sensors and biosensors* in *Analytical Techniques in the Sciences*, editor: Ando, D. J., John Wiley & Sons, West Sussex, **2002**.

[359]. Sivanesan, A.; John, S. A. *Gold nanoparticles modified electrodes for biosensors* in *Nanostructured Materials for Electrochemical Biosensors*, editors: Yogeswaran, U.; Kumar, S.; Chen, S., chapter 4, Nova Science Publishers, **2009**.

[360]. Xia, L.; Xu, L.; Song, J.; Xu, R.; Liu, D.; Dong, B.; Song, H. *Scientific Reports*, **2015**, *5*, 10838.

[361]. Frasco, M. F.; Chaniotakis, N. *Sensors*, **2009**, *9*, 7266.

[362]. Amelia, M.; Credi, A.; Silvi, S., *Electrochemical properties of semiconductor quantum dots in Quantum Dot Sensors: Technology and Commercial Applications*, editors: Callan, J. F.; Raymo, F. M., chapter 3, CRC press, Boca Raton (Fl, USA), **2013**.

[363]. Prakash, S.; Chakrabarty, T.; Singh, A. K.; Shahi, V. K. *Biosensors and Bioelectronics*, **2013**, *41*, 43.

[364]. Sołoducho, J.; Cabaj, J. *J. Anal. Bioanal. Tech.*, **2013**, *4(S7:005)*, 1.

[365]. Liu, F. L.; Xiao, P.; Fang, H. L.; Dai, H. F.; Qiao, L.; Zhang, Y. H. *Physica E*, **2011**, *44*, 367.

[366]. Balasubramanian, K.; Burghard, M. *Anal. Bioanal. Chem.*, **2006**, *385*, 452.

[367]. Ramoni, R.; Staiano, M.; Bellucci, S.; Grycznyski, I.; Grycznyski, Z.; Crescenzo, R.; Iozzino, L.; Bharill, S.; Conti, V.; Grolli, S.; D'Auria, S. *J. Phys.: Condens. Matter*, **2008**, *20*, 474201.

[368]. Jia, J.; Guan, W.; Sim, M.; Li, Y.; Li, H. *Sensors*, **2008**, *8*, 1712.

[369]. Zhang, W.; Patel, K.; Schexnider, A.; Banu, S.; Radadia, A. D. *ACS Nano*, **2014**, *8*, 1419.

[370]. Chan, C. Y.; Guo, J.; Sun, C.; Tsang, M. K.; Tian, F.; Hao, J.; Chen, S.; Yang, M. *Sens. Act. B*, **2015**, *220*, 131.

[371]. Wei, J.; Qiu, J.; Li, L.; Ren, L.; Zhang, X.; Chaudhuri, J.; Wang, S. *Nanotech.*, **2012**, *23*, 335707.

[372]. Zhou, M.; Zhai, Y.; Dong, S. *Anal. Chem.*, **2009**, *81*, 5603.

[373]. Zhang, Y.; Shen, J.; Li, H.; Wang, L.; Cao, D.; Feng, X.; Liu, Y.; Ma, Y.; Wang, L. *Chem. Rec.*, **2016**, *16*, 273.

[374]. Yu, L.; Wu, H.; Wu, B.; Wang, Z.; Cao, H.; Fu, C.; Jia, N. *Nano-Micro Lett.*, **2014**, *6*, 258.

[375]. Yang, J.; Deng, S.; Lei, J.; Ju, H.; Gunasekaran, S. *Biosens. Bioelectron.*, **2011**, *29*, 159.

[376]. Tiwari, J. N.; Vij, V.; Kemp, K. C.; Kim, K. S. *ACS Nano*, **2016**, *10*, 46.

[377]. Yang, C.; Denno, M. E.; Pyakurel, P.; Venton, B. J. *Anal. Chim. Acta*, **2015**, *887*, 17.

[378]. Brown, C. A.; Jeong, K. S.; Poppenga, R. H.; Puschner, B.; Miller, D. M.; Ellis, A. E.; Kang, K. I.; Sum, S.; Cistola, A. M.; Brown, S. A. *J. Vet. Diagn. Invest.*, **2007**, *19*, 525.

[379]. *US Food and Drug Administration (2008) Pet food recall (melamine)/tainted animal feed. US Food and Drug Administration, Rockville, MD*. (http://www.fda.gov/oc/opacom/hottopics/petfood.html), accessed February 25, **2009**.

[380]. *US Food and Drug Administration (2007) FDA's ongoing pet food investigation. US Food and Drug Administration, Rockville, MD*, April 16, 2007. (http://www.fda.gov/consumer/updates/petfoodrecallup.html), accessed February 25, **2009**.

[381]. Reimschuessel, R.; Gieseker, C. M.; Miller, R. A.; Ward, J.; Boehmer, J.; Rummel, N. et al *Am. J. Vet. Res.*, **2008**, *69*, 1217.

[382]. Puschner, B.; Poppenga, R. H.; Lowenstine, L. J.; Filigenzi, M. S.; Pesavento, P. A. *J. Vet. Diagn. Invest.*, **2007**, *19*, 616.

[383]. *US Food and Drug Administration (2009) Melamine contamination in China. US Food and Drug Administration, Rockville, MD*, April 5, 2009. http://www.fda.gov/oc/opacom/hottopics/melamine.html, accessed February 25, **2009**.

[384]. *World Health Organization (2008) Melamine-contamination event. World Health Organization, Geneva, Switzerland*, December 8, 2008. (http://www.who.int/foodsafety/fs_management/infosan_events/en/index.html), accessed February 25, **2009**.

[385]. *World Health Organization (2008) Expert meeting to review toxicological aspects of melamine and cyanuric acid,* in collaboration with FAO, supported by Health Canada, Ottawa, Canada, December 1–4, 2008, *overall conclusions and recommendations,* World Health Organization, Geneva, Switzerland. (http://www.who.int/foodsafety/fs_management/conclusions_recommendations.pdf), accessed February 25, **2009**.

[386]. *Workshop on Melamine*, *Beijing, People's Republic of China*, November 18–19, **2008**.

[387]. Ranganathan, A.; Pedireddi, V. R.; Rao, C. N. R. *J. Am. Chem. Soc.*, **1999**, *121*, 1752.

[388]. Archer, E. A.; Gong, H.; Krische, M. J. *Tetrahedron*, **2001**, 57, 1139.

[389]. Perdigao, L. M.; Champness, N. R.; Beton, P. H. *Chem. Commun.*, **2006**, *5*, 538.

[390]. Whitesides, G. M.; Mathias, J. P.; Seto, C. T. *Science*, **1991**, *254*, 1312.

[391]. Whitesides, G. M.; Simanek, E. E.; Mathias, J. P.; Seto, C. T.; Chin, D.; Mammen, M. et. al. *Acc. Chem. Res.*, **1995**, *28*, 37.

[392]. Melnick, R. L.; Boorman, G. A.; Haseman, J. K.; Montali, R. J.; Huff, J. *Toxicol. Appl. Pharmacol.*, **1984**, *72*, 292.

[393]. *IUCLID dataset substance ID: 108-78-1. Melamine*. in *18 Feb ed: European Commission, European Chemicals Bureau*, **2000**.

[394]. *Natl. Toxicol. Program. Tech. Rep. Ser.*, **1983,** *245*, 1.

[395]. Ogasawara, H.; Imaida, K.; Ishiwata, H.; Toyoda, K.; Kawanishi, T.; Uneyama, C. et. al. *Carcinogenesis*, **1995**, *16*, 2773.

[396]. Okumura, M.; Hasegawa, R.; Shirai, T.; Ito, M.; Yamada, S.; Fukushima, S. *Carcinogenesis*, **1992**, *13*, 1043.

[397]. Cremonezzi, D. C.; Diaz, M. P.; Valentich, M. A.; Eynard, A. R. *Food Chem. Toxicol.*, **2004**, *42*, 1999.

[398]. Heck, H. D.; Tyl, R. W. *Regul. Toxicol. Pharmacol.*, **1985**, *5*, 294.

[399]. Filigenzi, M. S.; Puschner, B.; Aston, L. S.; Poppenga, R. H. *J. Agric. Food Chem.*, **2008**, *56*, 7593.

[400]. Wang, H.; Liu, Y. Q.; Cao, H.; Yang, H. M.; Liu, X. L.; Yan, L. B. *Chin. J. Anal. Chem.*, **2008**, *36*, 273.

[401]. Andersen, W. C.; Turnipseed, S. B.; Karbiwnyk, C. M.; Clark, S. B.; Madson, M. R.; Gieseker, C. M.; Miller, R. A.; Rummel, N. G.; Reimschuessel, R. *J. Agric.Food Chem.*, **2008**, *56*, 4340.

[402]. Wei, F.; Lam, R.; Cheng, S.; Lu, S.; Ho, D.; Li, N. *Appl. Phys. Lett.*, **2010**, *96*, 133702.

[403]. Bera, R. K.; Raj, C. R. *Analyst*, **2011**, *136*, 1644.

[404]. Cao, Q.; Zhao, H.; Zeng, L.; Wang, J.; Wang, R.; Qiu, X.; He, Y. *Talanta*, **2009**, *80*, 484.

[405]. Liao, C. W.; Chen, Y. R.; Chang, J. L.; Zen, J. M. *Electroanalysis*, **2011**, *23*, 573.

[406]. Fotouhi, L.; Farzinnegad, N.; Heravi, M. M.; Khaleghi, Sh. (2003) *Bull. K. Chem. Soc.*, **2003**, *24*, 1751.

[407]. Zhu, H.; Zhang, S.; Li, M.; Shao, Y.; Zhu, Z. *Chem. Commun.*, **2010**, *46*, 2259.

[408] Zhu, Y.; Zhang, Y.; Li, J.; Han, Y.; Dong, G.; Zhang, H. *Am. J. Anal. Chem.*, **2011**, *2*, 612.

[409] Kong, Y.; Wei, C.; Wang, Z.; Hou, Z.; Li, H.; Yu, J.; Yuan, J.; Zhao, Y.; Long, J.; Tang, Y.; Gao, M. *Am.J. Anal. Chem.*, **2014**, *5*, 258.

[410] Akter, H.; Shaikh, A. A.; Chowdhury, T. R.; Rahman, M. S.; Bakshi, P. K.; Ahammad, A. J. S. *ECS Electrochem. Lett.*, **2013**, *2*, B13.

[411]. Yue, J.; Jiang, X.; Kaneti, Y. V.; Yu, A. *J. Colloid Interface Sci.*, **2012**, *367*, 204.

[412]. Bai, L. Y.; Dong, C. X.; Zhang, Y. P.; Li, W.; Chen, J. *J. Chin. Chem. Soc.*, **2011**, *58*, 846.

[413]. Guo, Z., Xu, X. F.; Li, J.; Liu, Y. W.; Zhang, J.; Yang, C. *Sensors and Actuators B*, **2014**, *200*, 101.

[414]. Ping, J. G.; Yu, B.; Xin, C. Z.; Yu, C. X.; Ming, Z.; Chang, Z. *J. Solid State Electrochem.,* **2010**, *15*, 2653.

[415]. Hajian, R.; Yusof, N. A.; Faragi, T.; Shams, N. *PLoS One*, **2014**, *9*, e96686.

[416]. Han, M. S.; Lytton-Jean, A. K. R.; Oh, B. K.; Heo, J.; Mirkin, C. A.; *Angewandte Chemie*, **2006**, *118*, 1839.

[417]. Yang, W.; Gooding, J. J.; He, Z.; Li, Q.; Chen., G. *J. Nanosci. Nanotechnol.*, **2007**, *7*, 712.

[418]. Zhao, W.; Chiuman, W.; Lam, J. C.; Brook, M. A.; Li, Y. *Chem. Commun.*, **2007**, *36*, 3729.

[419]. Aili, D.; Enander, K.; Rydberg, J.; Nesterenko, I.; Bjorefors, F.; Baltzer, L.; Liedberg, B. 2008. *J. Am. Chem. Soc.*, **2008**, *130*, 5780.

[420]. Welch, C. W.; Compton, R. G. *Anal. Bioanal. Chem.*, **2006**, *384*, 601.

[421]. Roy-Mayhew, J.; Bozym, D. D. J.; Punckt, C.; Aksay, I. A. *ACS Nano*, **2010**, *4*, 6203.

[422]. Alwarappan, S.; Boyapalle, S.; Kumar, A.; Li, C. Z.; Mohapatra, S. *J. Phys. Chem. C*, **2012**, *116*, 6556.

[423]. Govindhan, M.; Amiri, M.; Chen, A. *Biosens. Bioelectron.*, **2015**, *66*, 474.

[424]. Song, J.; Xu, L.; Xing, R.; Li, Q.; Zhou, C.; Liu, D.; Song, H. *Scientific Reports*, **2014**, *4*, 7515.

[425]. Dharuman, V.; Hahn, J. H.; Jayakumar, K.; Teng, W. *Electrochim. Acta*, **2013**, *114*, 590.

[426]. Li, J.; Feng, H.; Li, J.; Feng, Y.; Zhang, Y.; Jiang, J.; Qian, D. *Electrochim. Acta*, **2015**, *167*, 226.

[427]. Wuesta, J.; Rochefort, D. A. *Chem. Commun.*, **2010**, *46*, 2923.

[428]. Zeng, S.; Cai, M.; Liang, H.; Hao, J. *Anal. Methods*, **2012**, *4*, 2499.

[429]. Chi, H.; Liu, B.; Guan, G.; Zhang, Z.; Han, M. Y. *Analyst*, **2010**, *135*, 1070.

[430]. Chen, N.; Cheng, Y.; Li, C.; Zhang, C.; Zhao, K.; Xian, Y. *Microchim. Acta*, **2015**, *182*, 1967.

[431]. Mirkin, M. V.; Bard, A. J. *Anal. Chem.*, **1992**, *64*, 2293.

[432]. Venkatasami, G.; Sowa, J. R. Jr. *Anal. Chim. Acta*, **2010**, *665*, 227.

[433]. Montague, P. R.; Hyman, S. E.; Cohen, J. D. *Nature*, **2004**, *431*, 760.

[434]. Seeman, P. *Historical overview: Introduction to the dopamine receptors* In *The Dopamine Receptors*, ed. 2nd, editor: Neve, K., chapter 1, Springer, **2010**.

[435]. Shizgal, P.; Arvanitogiannis, A. *Science*, **2003**, *299*, 1856.

[436]. Benes, F. M. *Trends pharmacol. Sci.*, **2001**, *22*, 46.

[437]. Ndamanisha, J. C.; Guo, L. *Biosens. Bioelectron.*, **2004**, *23*, 1680.

[438]. Saha, S.; Sarkar, P.; Turner, A. *Electroanalysis*, **2014**, *26*, 2197.

[439]. Wang, C.; Yuan, R.; Chai, Y.; Chen, S.; Zhang, Y.; Hu, F.; Zhang, M. *Electrochim. Acta*, **2012**, *62*, 109.

[440]. Xie, S. H.; Liu, Y. Y.; Li, J. Y. *Appl. Phys. Lett.*, **2008**, *92*, 243121-1.

[441]. Zhang, H.; Gai, P.; Cheng, R.; Wu, L.; Zhang, X.; Chen, J. *Anal. Methods*, **2013**, *5*, 3591.

[442]. Beitollahi, H.; Karimi-Maleh, H.; Khabazzadeh, H. *Anal. Chem.*, **2008**, *80*, 9848.

[443]. Beitollahi, H.; Ebadinejad, F.; Shojaiec, F.; Torkzadeh-Mahanid, M. *Anal. Methods*, **2016**, *8*, 6185.

[444]. Molaakbari, E.; Mostafavi, A.; Beitollahi, H.; Alizadehd, R. *Analyst*, **2014**, *139*, 4356.

[445]. Moghaddam, H. M.; Beitollahi, H.; Tajik, S.; Soltani, H. *Electroanalysis*, **2015**, *27*, 2620.

[446]. Beitollahi, H.; Nekooei, S. *Electroanalysis*, **2016**, *28*, 645.

[447]. Beitollahi, H.; Tajik, S.; Jahani, S. *Electroanalysis*, **2016**, *28*, 1093.

[448]. Jahani, S.; Beitollahi, H. *Electroanalysis*, **2016**, *28*, 2022.

[449]. Beitollahi, H.; Nejad, F. G. *Electroanalysis*, **2016**, *28*, 2237.

[450]. Beitollahi, H.; Gholami, A.; Reza Ganjali, M. *Mater. Sci. Engin. C*, **2015**, *57*, 107.

[451]. Beitollahi, H.; Ivari, S. G.; Torkzadeh-Mahani, M. *Mater. Sci. Engin. C*, **2016**, *69*, 128.

[452]. Beitollahi, H.; Hamzavi, M.; Mahani, M. T.; Shanesaz, M.; Maleh, H. K. *Electroanalysis*, **2015**, *27*, 524.

[453]. Pan, D.; Rong, S.; Zhang, G.; Zhang, Y.; Zhou, Q.; Liu, F.; Li, Chang, D.; Pan, H. *Electrochemistry*, **2015**, *83*, 725.

[454]. Noroozifar, M.; Motlagh, M. K.; Akbari, R.; Bemanadi, M. P. *Biosens. Bioelectron.*, **2011**, *28*, 56.

[455]. Sun, C. L.; Lee, H. H.; Yang, J. M.; Wu, C. C. *Biosens. Bioelectron.*, **2011**, *26*, 3450.

[456]. Cheemalapati, S.; Palanisamy, S.; Mani, V.; Chen, S. M. *Talanta*, **2013**, *117*, 297.

[457]. Zhang, W. X.; Zheng, J. Z.; Shi, J. G.; Lin, Z. Q.; Huang, Q. T.; Zhang, H. Q.; Wei, C.; Chen, J. H.; Hua, S.; Hao, A. *Anal. Chim. Acta*, **2015**, *853*, 285.

[458]. Li, H.; Wang, Y.; Ye, D.; Luo, J.; Su, B.; Zhang, S.; Kong, J. *Talanta*, **2014**, *127*, 255.

[459]. Zhu, X. H.; Liang, Y.; Zuo, X. X.; Hu, R. P.; Xiao, X.; Nan, J. *Electrochim. Acta*, **2014**, *143*, 366.

[460]. Canevari, T. C.; Raymundo-Pereira, P. A.; Landers, R.; Benvenutti, E. V.; Machado, S. A. S. *Talanta*, **2013**, *116*, 726.

[461]. Wang, C.; Li, J.; Shi, K.; Wanga, Q.; Zhao, X.; Xiong, Z.; Zou, X.; Wang, Y. *J. Electroanal. Chem.*, **2016**, *770*, 56.

[462]. Liu, B.; Ouyang, X.; Ding, Y.; Luo, L.; Xu, D.; Ning, Y. *Talanta*, **2016**, *146*, 114.

[463]. Bahrami, S.; Abbasi, A. R.; Roushani, M.; Derikvand, Z.; Azadbakht, A. *Talanta*, **2016**, *159*, 307.

[464]. Yang, L.; Liu, S.; Zhang, Q.; Li, F. *Talanta*, **2012**, *89*, 136.

[465]. Tian, X.; Cheng, C.; Yuan, H.; Du, J.; Xiao, D.; Xie, S.; Choi, M. M. F. *Talanta*, **2012**, *93*, 79.

[466]. Niu, X.; Yang, W.; Guo, H.; Ren, J.; Yang, F.; Gao, J. Talanta, **2012**, *99*, 984.

[467]. Weng, X.; Cao, Q.; Liang, L.; Chen, J.; You, C.; Ruan, Y.; Lin, H.; Wu, L. *Talanta*, **2013**, *117*, 359.

[468]. Ponnusamy, V. K.; Mani, V.; Chen, S. M.; Huang, W. T.; Jen, J. F. *Talanta*, **2014**, *120*, 148.

[469]. Sathisha, T. V.; Kumara Swamy, B. E.; Schell, M.; Eswarappa, B. *J. Electroanal. Chem.*, **2014**, *720*, 1.

[470]. Oh, J. W.; Yoon, Y. W.; Heo, J.; Yu, J.; Kim, H.; Kim, T. H. *Talanta*, **2016**, *147*, 453.

[471]. Zhang, D. D.; Hu, L. L.; Chen, Q.; Chen, X. W.; Wang, J. H. *Talanta*, **2016**, *159*, 23.

[472]. Li, J.; Zhang, N.; Sun, Q.; Bai, Z.; Zheng, J. *Talanta*, **2016**, *159*, 379.

[473]. Sheng, Z. H.; Zheng, X. Q.; Xu, J. Y.; Bao, W. J.; Wang, F. B.; Xia, X. H. *Biosens. & Bioelectron.*, **2012**, *34*, 125.

[474]. Deshmukh, A. A.; Mhlanga, S. D.; Coville, N. J. *Mater. Sci. Eng.: R: Reports*, **2010**, *70*, 1.

[475]. Du, H.; Li, B.; Kang, F.; Fu, R.; Zeng, Y. *Carbon*, **2007**, *45*, 429.

[476]. Alcantara, R.; Madrigal, F. J. F.; Lavela, P.; Tirado, J. L.; Mateos, J. M. J.; de Salazar, C. G.; Stoyanova, R.; Zhecheva, E. *Carbon*, **2000**, *38*, 1031.

[477]. Bibby, A.; Mercier, L. *Chem. Mater.*, **2002**, *14*, 1591.

[478]. Pol, V. G.; Thackeray, M. M. *Energy Environ. Sci.*, **2011**, *4*, 1904.

[479]. Chen, J.; Xia, N.; Zhou, T.; Tan, S.; Jiang, F.; Yuan, D. *Int. J. Electrochem. Sci.*, **2009**, *4*, 1063.

[480]. Xu, C.; Cheng, L.; Shen, P.; Liu, Y. *Electrochem. Commun.*, **2007**, *9*, 997.

[481]. Liu, Y. C.; Qiu, X. P.; Huang, Y. Q.; Zhu, W. T. *Carbon*, **2002**, *40*, 2375.

[482]. Lin, X. Q.; Kang, G. F.; Lu, L. P. *Bioelectrochemistry*, **2007**, *70*, 235.

[483]. Liu, X. G.; Peng, Y. H.; Qu, X. J.; Ai, S. Y.; Han, R. X.; Zhu, X. B. *J. Electroanal. Chem.*, **2011**, *654*, 72.

[484]. Wang, P.; Li, Y. X.; Huang, X.; Wang, L. *Talanta*, **2007**, *73*, 431.

[485]. Ulubay, S. U.; Dursun, Z. *Talanta*, **2010**, *80*, 1461.

[486]. Zhang, J.; Zhu, Z.; Zhu, J.; Hua, K. L. S. *Int. J. Electrochem. Sci.*, **2014**, *9*, 1264.

[487]. Shankar, S. S.; Swamy, B. E. K.; Chandra, U.; Manjunatha, J. G.; Sherigara, B. S. *Int. J. Electrochem. Sci.*, **2009**, *4*, 592.

[488]. Ye, F.; Wen, Z.; Wu, H.; Wang, C.; Qian, Y. *Int. J. Electrochem. Sci.*, **2015**, *10*, 1136.

[489]. Ku, S.; Palanisamy, S.; Chen, S. M. *J. Col. Interface Sci.*, **2013**, *411*, 182.

[490]. Kuzmanya, H.; Kukovecz, A.; Simon, F.; Holzweber, M.; Kramberger, C.; Pichler, T. *Synthetic Metals*, **2004**, *41*, 113.

[491]. Balasubramanian, K.; Burghard, M. *Small*, **2005**, *1*, 180.

[492]. Darmstadt, H.; Roy, C.; Kaliaguine, S.; Xu, G.; Auger, M.; Tuel, A.; Ramaswamy, V. *Carbon*, **2000**, *38*, 1279.

[493]. Kumar, M.; Ando, Y. *Diamond and Related Materials*, **2003**, *12*, 1845.

[494]. Ungar, T.; Gubicza, J.; Ribarik, G.; Pantea, C.; Zerda, T. W. *Carbon*, **2002**, *40*, 929.

[495]. Manoj, B.; Kunjomana, A. G. *Int. J. Electrochem. Sci.*, **2012**, *7*, 3127.

[496]. Zhou, Q.; Zhao, Z.; Zhang, Y.; Meng, B.; Zhou, A.; Qiu, J. *Energy and fuels*, **2012**, *26*, 5186.

[497]. Marquez, A. N.; Romero, R.; Romero, A.; Valverde, J. L. *J. Mater. Chem.*, **2011**, *21*, 1664.

[498]. Ramya, K.; John, J.; Manoj, B. *Int. J. Electrochem. Sci.*, **2013**, *8*, 9421.

[499]. Abbaspour, A.; Noori, A. *Biosens. Bioelectron.*, **2011**, *26*, 4674.

[500]. Palanisamy, S.; Thirumalraj, B.; Chen, S. M.; Ali, M. A.; Muthupandi, K.; Emmanuel, R.; Prakash, P.; Al-Hemaid, F. M. A. *Electroanalysis*, **2015**, *27*, 1998.

[501]. Corona-Avendano, S.; Alarcon-Angeles, G.; Ramırez-Silva, M. T.; Rosquete-Pina, G.; Romero-Romo, M.; Palomar-Pardave, M. *J. Electroanal. Chem.*, **2007**, *609*, 17.

[502]. Aldana-González, J.; Palomar-Pardavé, M.; Corona-Avendaño, S.; Montes de Oca, M. G.; Ramírez-Silva, M. G.; Romero-Romo, M. *J. Electroanal. Chem.*, **2013**, *706*, 69.

[503]. Colín-Orozco, E.; Ramírez-Silva, M. T.; Corona-Avendano, S.; Romero-Romo, M.; Palomar-Pardavé, M. *Electrochim. Acta*, **2012**, *85*, 307.

[504]. Struck, W. A.; Elving, P. J. *Biochemistry*, **1965**, *4*, 1343.

[505]. Corona-Avendano, S.; Alarcon-Angeles, G.; Rosquete-Pina, G. A.; Rojas-Hernandez, A.; Gutierrez, A.; Ramırez-Silva, M. T.; Romero-Romo, M.; Palomar-Pardave, M. *J. Phys. Chem. B*, **2007**, *111*, 1640.

[506]. Oliveira-Brett, A. M.; Brett, C. M. A.; Silva, L. A. *Bioelectrochemistry*, **2002**, *56*, 33.

[507]. Adekunle, A. S.; Ayenimo, J. G.; Fang, X. Y.; Doherty, W. O.; Arotiba, O. A.; Mamba, B. B. *Int. J. Electrochem. Sci.*, **2011**, *6*, 2826.

[508]. Mohsen, Q.; Fadl-allah, S. A.; El-Shenawy, N. S. *Int. J. Electrochem. Sci.*, **2012**, *7*, 4510.

[509]. Oliveira-Brett, A. M.; da Silva, L. A.; Brett, C. M. A. *Langmuir*, **2002**, *18*, 2326.

[510]. Burtis, C.A.; Ashwood, E.R. *Tietz Fundamental of Clinical Chemistry*, 4th ed.; W.S. Saunders company: A Division of Horcount Brace & Company: Philadelphia, PA, USA, **1996**.

[511]. Gagliardi, C. J.; Murphy, C. F.; Binstead, R. A.; Thorp, H. H.; Meyer, T. J. *J. Phys. Chem. C*, **2015**, *119*, 7028.

[512]. Sjodin, M.; Irebo, T.; Utas, J. E.; Lind, J.; Merenyi, G.; Åkermark, B.; Hammarstrom, L. *J. Am. Chem. Soc.*, **2006**, *128*, 13076.

[513]. Costentin, C.; Louault, C.; Robert, M.; Saveant, J.-M. *Proc. Natl. Acad. Sci. U.S.A.*, **2009**, *106*, 18143.

[514]. Fornazari, A. L. deTo.; Suarez, W. T.; Vieira, H. J.; Fatibello, F. O. *Acta Chim. Slov.*, **2005**, *52*, 164.

[515]. Zhong, Y. W.; Lin, M. H.; Zhou, J. D.; Liu, Y. J. *Fenxi Huaxue*, **2010**, *38*, 229.

[516]. Ensafi, A. A.; Shirin, B. *Sens. Actuat. B*, **2007**, *122*, 282.

[517]. Nezamzadeh-Ejhieh, A.; Hashemi, H. S. *Talanta*, **2012**, *88*, 201.

[518]. Johll, M. E.; Williams, D. G.; Johnson, D. C. *Electroanalysis*, **1997**, *9*, 1397.

[519]. Donga, Y. P.; Peib, L. Z.; Chua, X. F.; Zhanga, W. B.; Zhang, Q. F. *Electrochim. Acta*, **2010**, *55*, 5135.

[520]. Fei, S.; Chen, J.; Yao, S.; Deng, G.; He, D.; Kuang, Y. *Anal. Biochem.*, **2005**, *339*, 29.

[521]. Wang, L.-H.; Huang, W.-S. *Sensors*, **2012**, *12*, 3562.

[522]. Hager, G.; Brolo, A. G. *J. Electroanal. Chem.*, **2003**, *550-551*, 291.

[523]. Yakobke, H. D.; Jeschkert, H. *Amino Acids, Peptides and Proteins: an Introduction*, Akademie Verlag, Berlin, **1977.**

[524]. Spataru, N.; Sarada, B. V.; Popa, E.; Tryk, D. A.; Fujishima**,** A. *Anal. Chem.*, **2001,** *73*, 514.

[525]. Davis, D. G.; Bianco, E. *J. Electroanal. Chem.* **1966**, *12*, 254.

[526]. Koryta, J.; Pradac, J. *J. Electroanal. Chem.* **1968**, *17*, 185.

[527]. Rullière, C.; Joussot-Dubien, J. *Optics Commun.*, **1978**, *24*, 38.

[528]. Fayed, T. A.; Etaiw Sel,-D. *Spectrochim. Acta A Mol. Biomol. Spectrosc.*, **2006**, *65*, 366.

[529]. Turker, L.; Sener, E.; Yalcin, I.; Akbulut, U.; Kayalidere, I. *Sci. Pharm.*, **1990**, *58*, 107.

[530]. Singh, L. P.; Chawla, V.; Chawla, P.; Saraf, S. K. *Der Pharma Chemica*, **2010**, *2*, 206.

[531]. Liu, Y. K.; Lou, D. J.; Qian, J. Q.; Xu, Z. Y. *J. Zhejiang Univ. Sci.*, **2009**, *10*, 472.

[532]. Srinivas, A.; Vidyasagar, J.; Sarangapani, M. *J. Chem. Pharm. Res.*, **2010**, *2*, 319.

[533]. Srinivas, A.; Vidyasagar, J.; Swathi, K.; Sarangapani, M. *J. Chem. Pharm. Res.*, **2010**, *2*, 213.

[534]. Son, S. -H.; Yun, J. -J.; Oh, G. -C.; Jung, S. -Y.; Kim, Y. -K.; Kuhta, A. V.; Olkhovik, V. K.; Sasnouski, G.; Han, E. -M. *Curr. Appl. Phys.*, **2005**, *5*, 75.

[535]. Jo, H.; Kim, K.; Kim, D. -E.; Shin, H. -K.; Lee, B. -J. *Mol. Cryst. Liq. Cryst.*, **2016**, *636*, 60.

[536]. Ai, W.; Zhou, W.; Du, Z.; Du, Y.; Zhang, H.; Jia, X.; Xie, L.; Yi, M.; Yu, T.; Huang, W. *J. Mater. Chem.*, **2012**, *22*, 23439.

[537]. March, G.; Nguyen, T. D.; Piro, B. *Biosensors*, **2015**, *5*, 241.

[538]. Sajid, M.; Nazal, M. K.; Mansha, M.; Alsharaa, A.; Jillani, S. M. S.; Basheer, C. *Trends Anal. Chem.*, **2016**, *76*, 15.

[539]. Zen, J. -M.; Kumar, A. S.; Tsai, D. -M. *Electroanalysis*, **2003**, *15*, 1073.

[540]. Ramachandran, R.; Mani, V.; Chen, S. -M.; kumar, G. G.; Govindasamy, M. *Int. J. Electrochem. Sci.*, **2015**, *10*, 859.

[541]. Turner, A. P. F. *Chem. Soc. Rev.*, **2013**, *42*, 3184.

[542]. Rocchitta, G. ; Spanu, A.; Babudieri, S.; Latte, G.; Madeddu, G.; Galleri, G.; Nuvoli, S.; Bagella, P.; Demartis, M.; Fiore, V.; Manetti, R.; Serra, P. A. *Sensors*, **2016**, *16*, 780.